# DEVELOPMENT OF METAL-LIGAND COOPERATION IN BIS(PHOSPHINIMINE)PYRROLIDE COMPLEXES OF RHODIUM

**CONNOR STEWART MACNEIL**
**Bachelor of Science, Mount Allison University, 2014**

A thesis submitted
in partial fulfilment of the requirements for the degree of

**DOCTOR OF PHILOSOPHY**

in

**EARTH, SPACE, AND PHYSICAL SCIENCE**

Department of Chemistry and Biochemistry
University of Lethbridge
LETHBRIDGE, ALBERTA, CANADA

DEVELOPMENT OF METAL-LIGAND COOPERATION IN BIS(PHOSPHINIMINE)PYRROLIDE COMPLEXES OF RHODIUM

CONNOR MACNEIL

Date of defence: August 20, 2021

| | | |
|---|---|---|
| Dr. P. Hayes<br>Thesis Supervisor | Professor | Ph.D. |
| Dr. M. Gerken<br>Thesis Examination Committee Member | Professor | Ph.D. |
| Dr. J.-D. Hamel<br>Thesis Examination Committee Member | Assistant Professor | Ph.D. |
| Dr. L. Spencer<br>Internal Examiner | Associate Professor | Ph.D. |
| Dr. T. D. Tilley<br>External Examiner<br>University of California, Berkeley | Professor | Ph.D. |
| Dr. R. T. Boeré<br>Chair, Thesis Examination Committee | Professor | Ph.D. |

## Abstract

The synthesis and characterization of bis(phosphinimine)pyrrolide complexes of rhodium is described. A combination of solution and solid-state spectroscopies, X-ray crystallography, and computational analyses were used to characterize relevant compounds. Crystallographic analysis of phosphinimine fragments in the reported rhodium complexes showed significant P–N bond elongation relative to uncoordinated phosphinimines in both the parent ligand scaffold and partially-coordinated ($\kappa^2$-*N*,*N*) species, emphasizing the ylidic structure of the P–N linkage.

In the rhodium complexes surveyed, hemilabile phosphinimines were shown to engage small molecule substrates leading to heterolytic cleavage of $H_2$, CO deoxygenation, dehydrogenation of hydrosilanes, and the reversible activation of B–H bonds. Catalytic hydrogenation of alkenes and alkynes could be initiated from well-defined mononuclear complexes of the bis(phosphinimine)pyrrolido ligand. Taken together, the incorporation of phosphinimines in a monoanionic ligand scaffold paired with rhodium enabled new reactivities, representing an advancement in metal-ligand cooperation.

## Contributions of Authors

The following thesis chapters containing original research are based on the following publications, the contents of which are reproduced with permissions from the corresponding publishers:

**Chapter 2** – Hänninen. M. M.; Zamora, M. T.; MacNeil, C. S.; Knott, J. P.; Hayes, P. G. Elucidation of the resting state of a rhodium NNN-pincer hydrogenation catalyst that features a remarkably upfield hydride $^{1}$H NMR chemical shift. *Chem. Commun.* **2016**, *52*, 586–589.

**Chapter 3** – MacNeil, C. S.; Glynn, K. E.; Hayes, P. G. Facile Activation and Deoxygenative Metathesis of CO. *Organometallics* **2018**, *37*, 3248–3252.

**Chapter 4** – MacNeil, C. S.; Hayes, P. G. An H-Substituted Rhodium Silylene. *Chem. Eur. J.* **2019**, *25*, 8203–8207.

**Chapter 5** – MacNeil, C. S.; Hsiang, S.-J.; Hayes, P. G. Reversible dehydrogenation of a primary aryl borane. *Chem. Commun.* **2020**, *56*, 12323–12326.

I am responsible for the experimental and computational research reported in this thesis. In Chapter 1, M. M. H. and M. T. Z. isolated and characterized compounds which I have not described in this thesis. M. M. H. initially developed the procedure to isolate **2-Rh$_2$** which I reproduced and used to isolate the isotopologue **2-Rh$_2$-*d*$_2$**. I am responsible for the preparation and characterization of the compounds discussed in Chapter 2, as well as all catalytic chemistry conducted using **1-COE**. In Chapter 3, K. E. G. and I developed the synthesis of $^{iPr}$NNN, which I reproduced, isolated, and characterized by X-ray crystallography. In Chapter 5, S.-J. H. initially prepared the trifluoromethylated borane $H_2BAr^F$; ($Ar^F$ = 3,5-$(CF_3)_2C_6H_3$) which I reproduced for subsequent studies involving

reversible B–H activation. Following the same procedure used to isolated **5-BMes** as single-crystals suitable for X-ray diffraction studies, S.-J. H. was successful in recrystallizing the sample of **5-CO·$H_2$BAr$^F$** that was ultimately used in my X-ray diffraction analysis.

**Acknowledgements**

To my supervisor, Paul, who throughout this degree has been a constant source of encouragement, especially in the final stretches, I extend my most sincere gratitude. His work ethic, attention to detail, and uncompromising belief in only delivering the highest quality of work has made me a better scientist and will forever be a source of inspiration in my life as I pursue my own career. I thank him especially for his comments on this manuscript, and for orchestrating a thesis defence with so many moving pieces. I thank him for his unwavering support in the final years of my degree, especially for allowing me to pursue opportunities away from Lethbridge. I found my way to Paul's group because of Prof. Stephen Westcott, and I am indebted to him for making one of the most important connections of my life. A kindred spirit, a fellow Allisonian and Maritimer, with an unwavering enthusiasm for chemistry is more than anyone could hope to find in a mentor. Thank you, Paul.

For five years, the Hayes group was my home away from home, and I will be forever grateful to the friends and colleagues who made it such a memorable place to study chemistry. To Dr. Matt Zamora and Dr. Mikko Hänninen for sharing their considerable knowledge and experience of synthetic chemistry, spectroscopy, and X-ray crystallography, and for being such gracious hosts during my first weeks in Lethbridge. To Tara Dickie: for her fierce friendship, and for being a constant supporter and critic of my work – I was most excited to share new results with her and cherished the discussions that would follow. I wish her the best as she wraps up her own work. To Jackson Knott, Kayla Glynn, Edward Hsiang, Ashraf Aborawi, and Eric Bowes: thank you for being wonderful collaborators and for your contributions to this work. To the new school – Dylan Webb,

Desmond Chisholm, Sam Drescher, and Daisy Cruz-Milette: thank you for being great colleagues and friends, I know the group is in great hands. To my departmental colleagues and friends: David McWatters, Nathan Kostiuk, Dylan Girodat, Rhys Hakstol, Justin Vigar, Doug Turnbull, Felix O'Donnell, Daniel Stuart, and Nils Schopper – it was a privilege to have crossed paths with you all. To Luc, Jennifer, Hudson, and Blue: thank you for welcoming me into your lives – I will always think of you as family.

I am deeply indebted to my Princeton colleagues, and the Chirik group for providing some consistency and comfort when the world seemed at its most chaotic. I wish to thank Prof. Paul Chirik and Dr. Jonathan Darmon for their guidance and support, I am lucky to know you both. There have been many exceptional chemists who have trained in the Chirik group, and I was fortunate to work alongside Aaron Zhong, a mentor and friend who shared so much of his knowledge and experience with me. I owe a great deal of my success at Princeton to him. To Jacob Ludwig, Carli Kovel, William Whitehurst, Jose Roque, Tyler Pabst, Samantha Yruegas, and L. Reginald Mills: you have all profoundly shaped my experience in America for the better. Your friendships have redeemed, for me, much of what is broken in academia and has been a silver-lining in my life in so many ways. To Lauren Mendelsohn and Yoonsu Park: thank you for sharing your knowledge of all things photo-driven, and for the many enlightening discussions that have made the Monday subgroup a highlight of every week. To Megan Mohadjer Beromi and Brian Koronkiewicz: thank you for our Sunday morning pick-up games, and for introducing the group to the greatest bar in the world.

For administrative and technical support, I wish to thank Susan Hill, Tony Montina, Michael Opyr, Prof. René Boeré, and Kris Fischer. I am deeply grateful to the University

of Lethbridge, the Government of Alberta, and the Natural Sciences and Engineering Research Council of Canada (NSERC CGS - Alexander Graham Bell and Michael Smith Fellowship programs) for their generous financial support in the form of teaching assistantships and scholarships throughout my graduate studies.

I am grateful to my Ph.D. supervisory committee for their encouragement and guidance over the years. To Prof. Michael Gerken and Prof. Peter Dibble, for spirited discussions during my transfer and candidacy exams, and to Prof. Jean-Denys Hamel, Prof. René Boeré, Prof. Locke Spencer, and Prof. T. Don Tilley for attending my Ph.D. defence. Thank you all for your contributions.

To Zachary Sweet, Michael Ford, Ryan Clarke, and Kirsten Weagle: for seeing me through the ups and downs and for giving the very best of yourselves in every phone call, weekend trip, and summer adventure. I owe you all more than I can ever repay in this lifetime.

To my sister, Zoë, who has been a constant source of inspiration, especially in the final year of my studies – you are the very best of us, never change. To my family, Karolyn, Yvon and Jeannine, Elliot and Noah, Merrily and Don, Pierre and Cathy, Gregory and Janina, and Colin: thank you all for your love and support. Finally, to my parents, Jac and Sylvia: I am proud to be your son every day of my life. You are my greatest teachers, and all the good in me comes from you. I'll love you forever, I'll like you for always.

*Dedicated to the memory of Charles Myron Paynter*

## Table of Contents

## List of Compounds

| | |
|---|---|
| 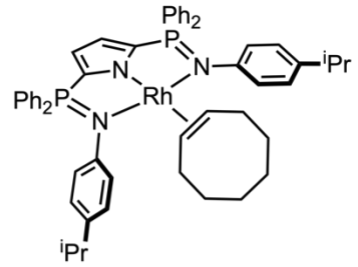 | 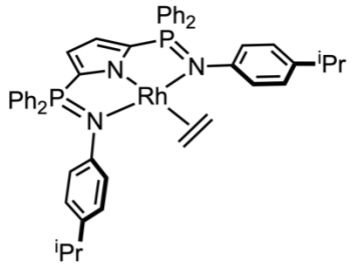 |
| **1-COE** | **2-$C_2H_4$** |
| 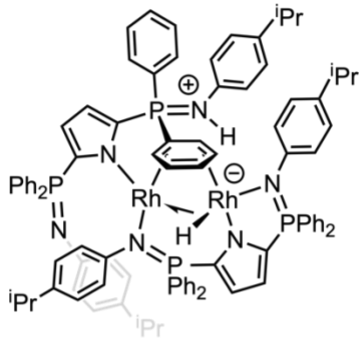 | 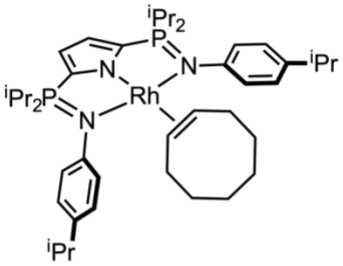 |
| **2-$Rh_2$** | **2-COE** |
| 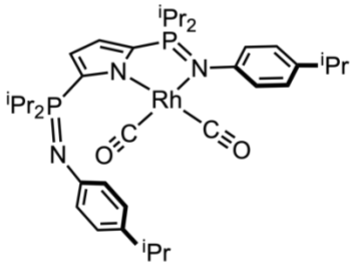 | 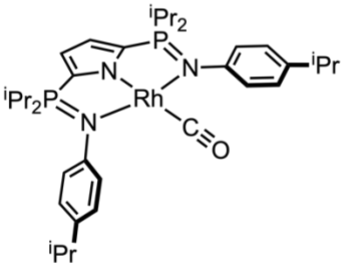 |
| **3-$(CO)_2$** | **3-CO** |
| 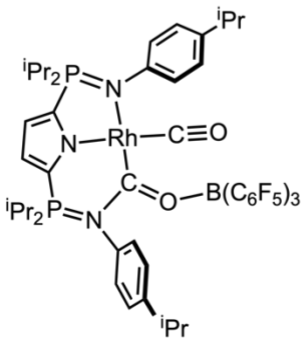 | 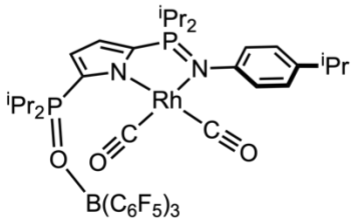 |
| **3-$(CO)_2$·BCF** | **3-$(CO)_2$PO·BCF** |

| | |
|---|---|
| 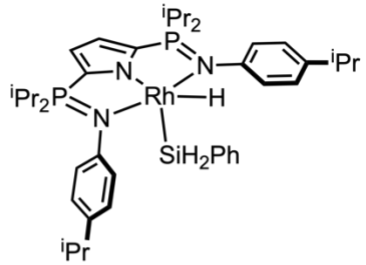 | 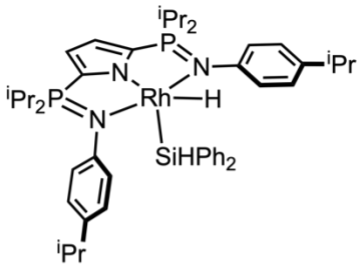 |
| **4-$SiH_2Ph$** | **4-$SiHPh_2$** |
| 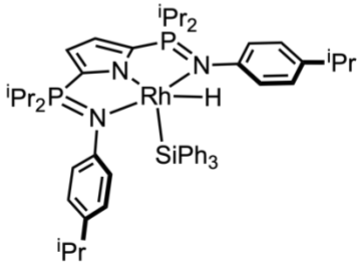 | 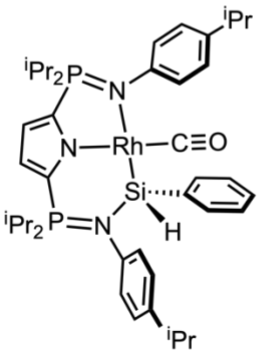 |
| **4-$SiPh_3$** | **4-SiHPh** |
| 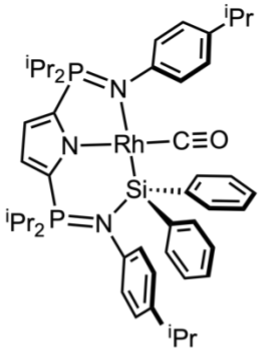 | 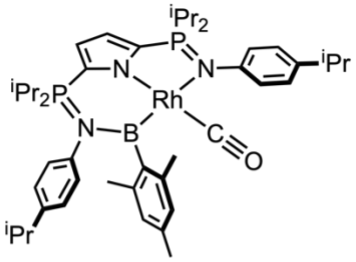 |
| **4-$SiPh_2$** | **5-BMes** |
| 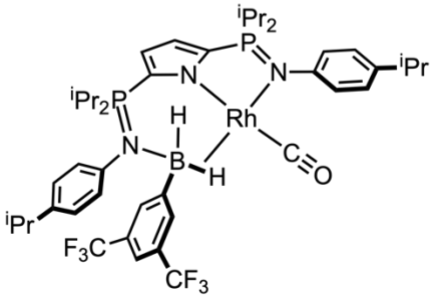 | 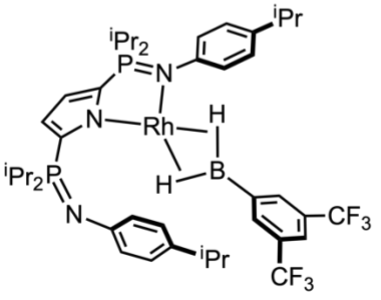 |
| **5-CO·$H_2BAr^F$** | **5-$H_2BAr^F$** |

## List of Tables

## List of Figures

## List of Schemes

## List of Abbreviations and Symbols

| | |
|---|---|
| Å | angstrom |
| Anal Calcd | calculated (elemental analysis) |
| Ar | aryl |
| atm | atmosphere |
| bpy | (2,2’-bipyridine) |
| br | broad |
| BCF | tris(pentafluorophenyl)borane |
| C | Celsius |
| CCDC | Cambridge Crystallographic Data Centre |
| CN | coordination number |
| COE | cyclooctene |
| Cp | cyclopentadienyl |
| Cp* | pentamethylcyclopentadienyl |
| Cy | cyclohexylk |
| d | doublet |
| deg | degree (temperature) |
| Dipp | (2,6-diisopropylphenyl) |
| DFT | Density Functional Theory |
| dmpe | 1,2-bis(dimethylphosphino)ethane |
| η | eta (coordination) |
| FLP | frustrated Lewis pair |
| g | gram(s) |

| | |
|---|---|
| h | hour(s) |
| Hz | hertz |
| *I* | nuclear spin quantum number |
| $^{i}$Pr | isopropyl |
| IMes | 1,3-bis(2,4,6-trimethylphenyl)-1,3-dihydro-2*H*-imidazol-2-ylidene |
| ImMes | 1-mesitylimidazole |
| *J* | symbol for coupling constant |
| K | Kelvin |
| κ | kappa (coordination) |
| $L_n$ | ligand(s) |
| m | multiplet |
| Me | methyl |
| Mes | mesityl |
| *m*-F | *meta*-fluorine |
| MHz | megahertz |
| mL | millilitre(s) |
| MLMB | metal-ligand multiple bond |
| min | minute(s) |
| mmol | millimole(s) |
| NIR | near-infrared |
| NMR | nuclear magnetic resonance |
| *o*-F | *ortho*-fluorine |
| ov | overlapping |

| | |
|---|---|
| *p*-F | *para*-fluorine |
| Ph | phenyl |
| Pipp | *p*-isopropylphenyl |
| PNP | amido-diphosphine |
| ppm | parts per million |
| q | quartet |
| R | alkyl or aryl group |
| s | singlet |
| S/Sol | solvent |
| sp | septet |
| t | triplet |
| THF | tetrahydrofuran |
| tol | toluene |
| δ | chemical shift (parts per million) |
| $^{o}$ | degree (angle) |
| $^{n}J_{XY}$ | *n*-bond coupling constant between X and Y |
| 1D | one dimensional |
| {$^{1}$H} | proton decoupled |
| 2D | two dimensional |
| λ | wavelength |
| xs | excess |
| WBI | Wiberg bond index |

# Chapter 1: Introduction

## 1.1. Coordination and Organometallic Chemistry of Transition Metals

A sustained focus on the development of transition metal-catalyzed technologies that increase access to commodity chemicals from simple building blocks has been a defining feature of synthetic chemistry in the last century.[1] To this end, industrial processes often rely on transition metal catalysts to accelerate selective chemical transformations by virtue of reductive and oxidative processes that transfer the electrons required to break and forge new chemical bonds. Often, these reactive metal ions are stabilized (coordinated) by molecules called ligands, performing ancillary (spectator) or cooperative roles.[2]

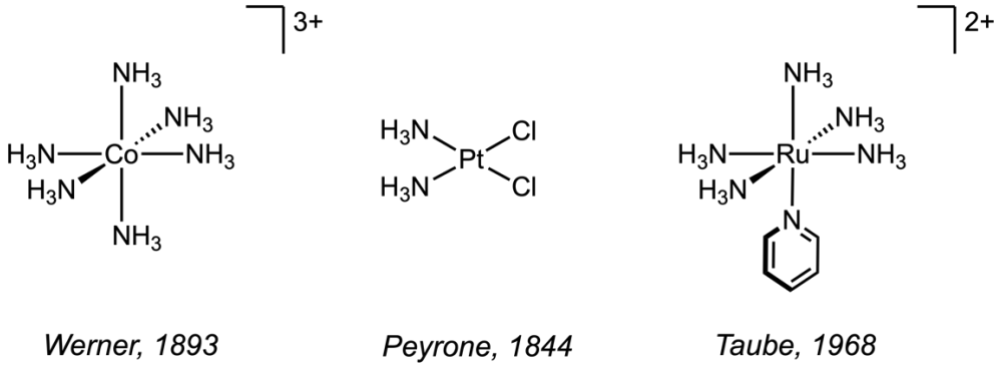


**Figure 1.1.** Coordination complexes of some late transition metals.

Transition metal coordination complexes (Figure 1.1) of mono- and bidentate ligands, including ammine, halides, pyridine, bipyridine (bpy), and a variety of phosphines ($PR_3$) and bis(phosphines), largely define the study of inorganic chemistry.[2] By extension, organometallic chemistry, dealing with those complexes containing metal–carbon bonds, places a focus on carbon-based ligands of varying complexity and reactivity.[1] Carbocyclic ligands (Figure 1.2) have contributed substantially to the development of organometallic chemistry leading to the 1973 Nobel Prize in Chemistry[3] (Fischer and Wilkinson) for "…

pioneering work on the chemistry of the organometallic, so called sandwich compounds." Metallocene complexes (e.g., ferrocene) bearing cyclopentadienyl ligands (Cp = $\eta^5$-$C_5H_5$), provide exceptional stability to a transition metal ion ($M^{n+}$) by virtue of the $\eta^5$ coordination mode (i.e., bonding equally to a metal centre through all carbon atoms in the π-system of the ring),[2] and are still employed in the design of organometallic catalysts for a variety of applications including, but not limited to, olefin polymerization,[4] C–H amination,[5] hydrogenation,[6] and proton-coupled electron-transfer (PCET) reactions.[7] The permethylated Cp* ligand (Cp* = $\eta^5$-$C_5Me_5$), along with the 'tethered' *ansa*-metallocenes build on the Cp framework, enabling modular tuning of electronic and steric parameters that ultimately translate into distinct reactivities.[1]

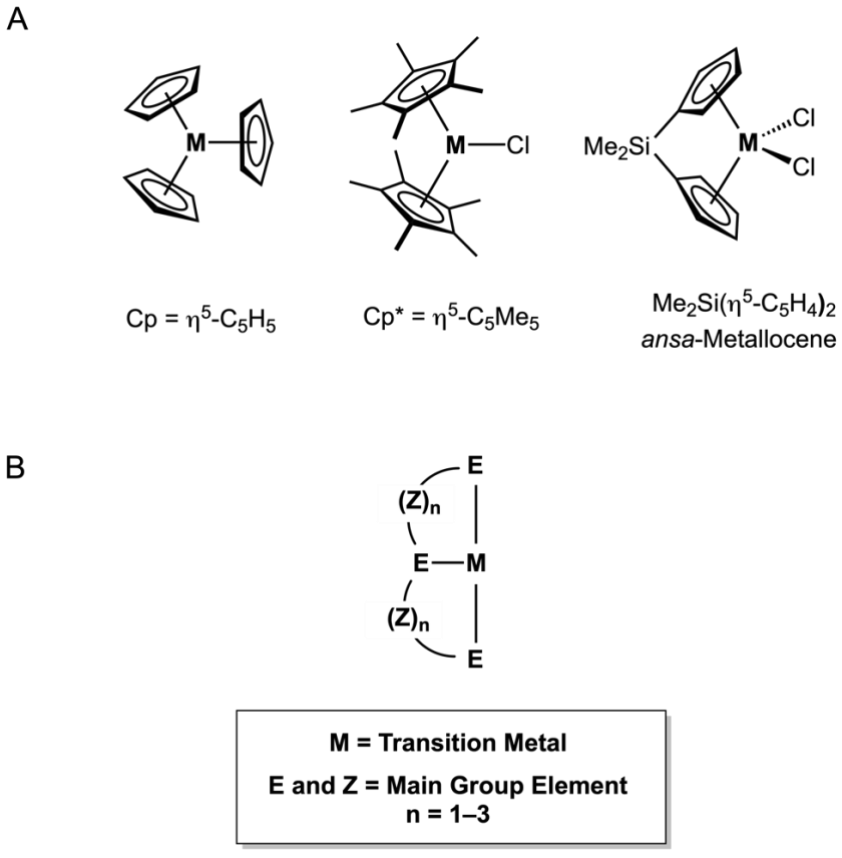


**Figure 1.2.** (A) Metallocene complexes. (B) Generic representation of a transition metal complex stabilized by a pincer ligand coordinated in a meridional geometry.

While metallocene chemistry continues to be prevalent in the chemical literature, the elaboration of Cp-based frameworks is largely limited to addition of varying substituents to the core carbocyclic structure. The adoption of tridentate ligands that coordinate to the metal in a meridional fashion has thus led to a renaissance of organometallic chemistry. These 'pincer' ligands (Figure 1.2), first reported by Shaw in 1976,[8] have since become ubiquitous in coordination chemistry and catalysis. In the post-metallocene era of organometallic chemistry, reactive metals are continuously worked into carefully designed ligands (PNP, PCP, NCN), providing catalysts for a plethora of useful reactions in both synthetic organic and inorganic chemistry. Some pioneers of this area include van Koten,[9] Fryzuk,[10] Milstein,[11] and Goldman.[12] Notably, the use of monoanionic multidentate 'hybrid' PNP ligands by Fryzuk inspired some of the chemistry discussed in Chapter 2 (PNP = $[N(SiMe_2CH_2PPh_2)_2]^-$). In this example, both 'hard' amido nitrogen, and 'soft' phosphine donors are components in the same tridentate ligand, providing a flexibility that would otherwise be unavailable to Cp-based ligands.

With the notable exception of variable coordination (i.e., $\eta^5$-$\eta^3$ 'ring-slipping') in metal indenyl complexes,[13] carbocyclic ligands bind strongly to transition metals and are generally considered inert to substitution. The formation of metallocene complexes bearing multiple Cp-based ligands (CN $\geq$ 6) forces the metal to engage with substrates in a specific way, which can be advantageous for promoting specific chemical transformations (e.g., alkene insertion), but limiting in other respects. Monodentate phosphines and amines are ligands that are often referred to as 'spectators' given their role in the stabilization of metal centers during a catalytic reaction without modification or substitution.[2] These ligands

provide increased access to the metal center, but often at the cost of lower selectivity and catalyst stability as a consequence of irreversible ligand loss.

The incorporation of main group element (e.g., N, O, P) donors into tridentate ligand scaffolds has enabled the synthesis of diverse catalysts that profoundly impact various areas of chemical science.[14] The adoption of pincer ligands (Figure 1.2) in catalysis both complements, and in many ways, improves upon well-established methods based on metallocene systems.[15] For example, tridentate ligands allow for careful manipulation of steric and electronic parameters that ultimately control the reactivity of the metal center with target substrates.[15] Like metallocenes, pincer ligands impart marked thermal stability to transition metal complexes with the added benefit of increased access to the metal center by forming complexes with lower coordination numbers. Tridentate ligands conceivably provide a platform for the generation of reactive metal centers and will be the focus of the discussion moving forward.

### 1.2. Metal-Ligand Cooperation

Milstein's seminal 2015 review on metal-ligand cooperation has provided a framework for understanding how the activation of small molecules can be targeted by leveraging reactivities within specially designed transition metal complexes.[14] The following section is not meant to be a comprehensive review, but rather, a summary of key aspects of metal-ligand cooperation, particularly those involving pincer-type ligands in late transition metal systems, to contextualize the work contained in this thesis for rhodium complexes of bis(phosphinimine)pyrrolide ligands. An emphasis on reversible, stoichiometric transformations is made to highlight the reactivity of these rhodium

complexes with representative small molecules, including $H_2$ (Chapter 2), CO (Chapter 3), hydrosilanes (Chapter 4), and hydroboranes (Chapter 5).

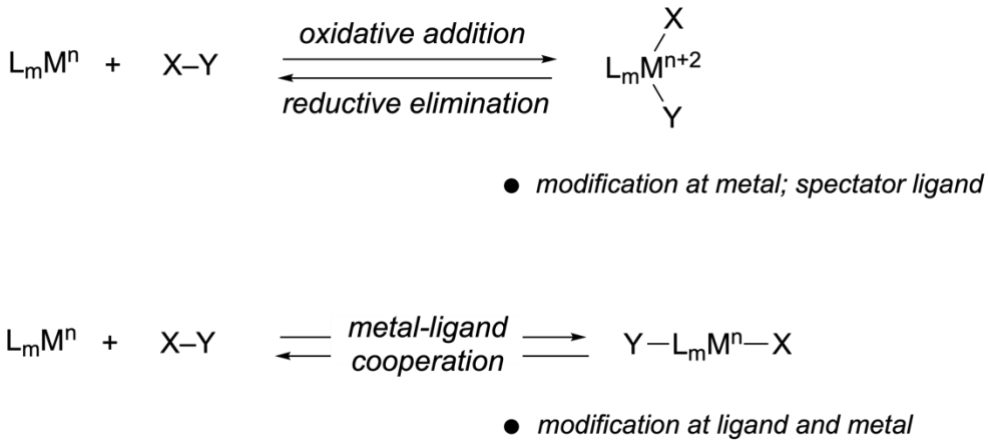


**Scheme 1.1.** Reversible bond activation by oxidative addition/reductive elimination (top) and metal-ligand cooperation (bottom).

In the generic reaction outlined in Scheme 1.1, oxidative addition of an X–Y bond to a transition metal complex results in the formal oxidation of the metal center and increases the coordination number by 2.[16] Alternatively, the hypothetical molecule X–Y could be activated and result in the functionalization of both the ligand ($L_m$) and transition metal center in an overall redox-neutral process (no change in metal oxidation state). Whereas the reactive species are the same in both cases, metal-ligand cooperation results in complementary reactivity to well-established oxidative addition/reductive elimination. An example of this type of reactivity from Milstein and co-workers described the activation of N–H bonds in electron-deficient anilines by a ruthenium complex bearing a PNP pincer ligand (Scheme 1.2).[17] An example of metal-ligand cooperation involving aromatization/dearomatization of the PNP pincer promotes proton-transfer to the unsaturated fragment in the ligand backbone, causing aromatization of the central pyridine

ring.[14] Fryzuk showed related ligand "non-innocence" in the addition of $H_2$ across a monoanionic PNP complex of iridium.[18]

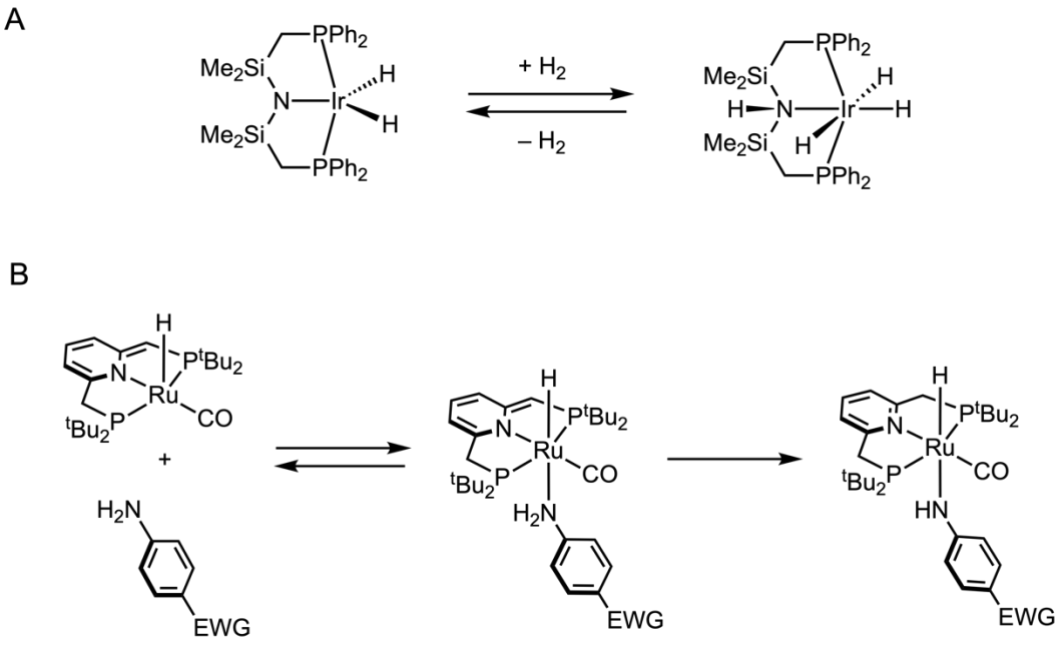


**Scheme 1.2.** (A) Activation of $H_2$ by hybrid PNP ligand. (B) Redox-neutral N–H activation enabled by metal-ligand cooperation.[15]

Specific ligand-based reactivities that are highlighted include hemilabile P/N-donors and the formation of metal-ligand multiple bonds (MLMBs). Following a brief introductory section on these topics, a monoanionic NNN-pincer ligand bearing phosphinimines will be described. The resulting stoichiometric and catalytic reaction chemistry of the corresponding rhodium complexes will lay the groundwork for the remainder of the thesis.

### 1.3. Hemilabile P/N donors

Activity in homogeneous transition metal catalyzed reactions is often associated with the availability of open coordination sites on the metal to bind substrates.[2] A delicate

balance needs to be achieved in order for productive catalysis to occur insofar as to not saturate the metal center of all available coordination.[2]

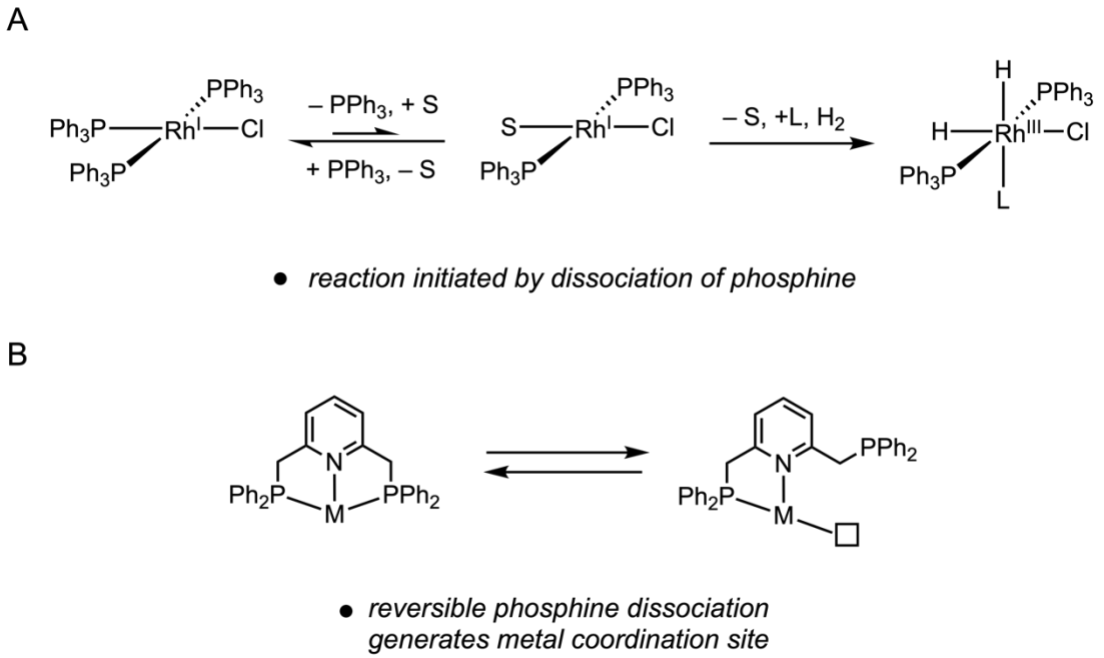


**Scheme 1.3.** (A) Loss of triphenylphosphine ($PPh_3$) from Wilkinson's catalyst initiates oxidative addition of $H_2$ and substrate binding. (B) A generic PNP pincer ligand bound $\kappa^3$ (left) and $\kappa^2$ (right) highlights the 'hemilability' of the phosphine.

To initiate catalysis from stable precatalyst species, the dissociation of a phosphine or amine is often required to generate a vacant coordination site that enables substrate binding. For example, loss of a triphenylphosphine ligand from $(PPh_3)_3RhCl$ (Wilkinson's catalyst) is required to promote a diversity of reactions including hydrogenation and hydrosilation (Scheme 1.3).[19] Thus, the development of ligand scaffolds comprising L-type (neutral) donors capable of reversible dissociation, termed 'hemilability', has inspired new catalyst designs to exploit reactivity patterns between metal and main group elements for the purpose of designing catalyst systems that generate less waste.[14]

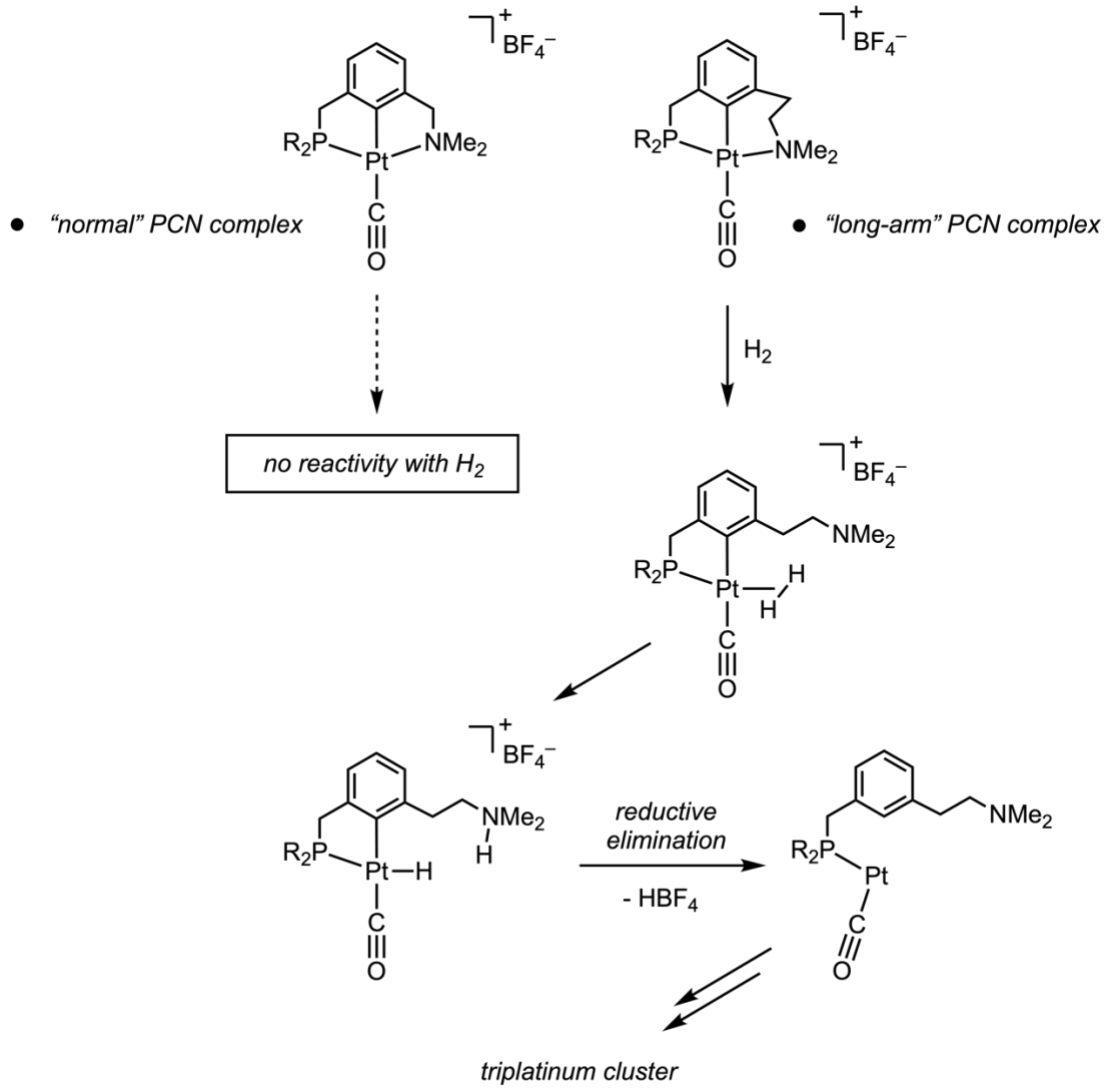


**Scheme 1.4.** Demonstration of the pincer 'hemilabile' effect using Milstein's "normal" and "long arm" PCN ligands.[20]

Milstein's PCN ligands, bearing "normal" $C_6H_4[CH_2P(^tBu)_2](CH_2)N(CH_2CH_3)_2$ and "long-arm" $C_6H_4[CH_2P(^tBu)_2](CH_2)_2N(CH_2CH_3)_2$ amino donors, (Scheme 1.4), served as a platform to exploit the ligand hemilability concept in the activation of $H_2$.[20] Under hydrogen pressure, the tertiary amine donors of the "normal" and "long arm" complexes demonstrated divergent reactivity patterns. In an early display of metal-ligand cooperation, the hemilabile dimethylamine donor in the "long arm" complex deprotonates a dihydrogen ligand, leading to reductive elimination of the aryl group from the relatively electron-

deficient metal center and formation of the triplatinum cluster coordinated by the phosphine component of the original ligand (Scheme 1.4).[20] By varying the length of the amine donor through addition or removal of a methylene (–$CH_2$–) spacer, Milstein showed that 5-membered chelates within the "normal" PCN complex are sufficiently stable, to prevent reactivity with $H_2$. This important contribution has inspired a broader consideration of hemilability within well-defined pincer scaffolds.

An application of pincer ligand hemilability that extends beyond the transition metal series was disclosed in a landmark report from Kiplinger and co-workers,[21] detailing the synthesis and characterization of tri- and tetravalent uranium halide complexes with the monoanionic bis[2-(diisopropylphosphino)-4-methylphenyl]amido (PNP) ligand originally developed by Ozerov.[22] Notably, both $\kappa^2$-(*P*,*N*) and $\kappa^3$-(*P*,*N*,*P*) coordination modes were observed for the PNP ligand with the latter adopting either pseudo-meridional or pseudo-facial geometries (Scheme 1.5).[21] Permethylated cyclopentadienide ($Cp^*$; $C_5Me_5^-$) ligands, in contrast, adopt only one mode of coordination ($\eta^5$) leading to divergent reactivity and strikingly different electronic structures between U(III) and U(IV) halide complexes bearing bis($Cp^*$) and bis(PNP) ligand scaffolds as determined by electron absorption and NIR spectroscopies.[21]

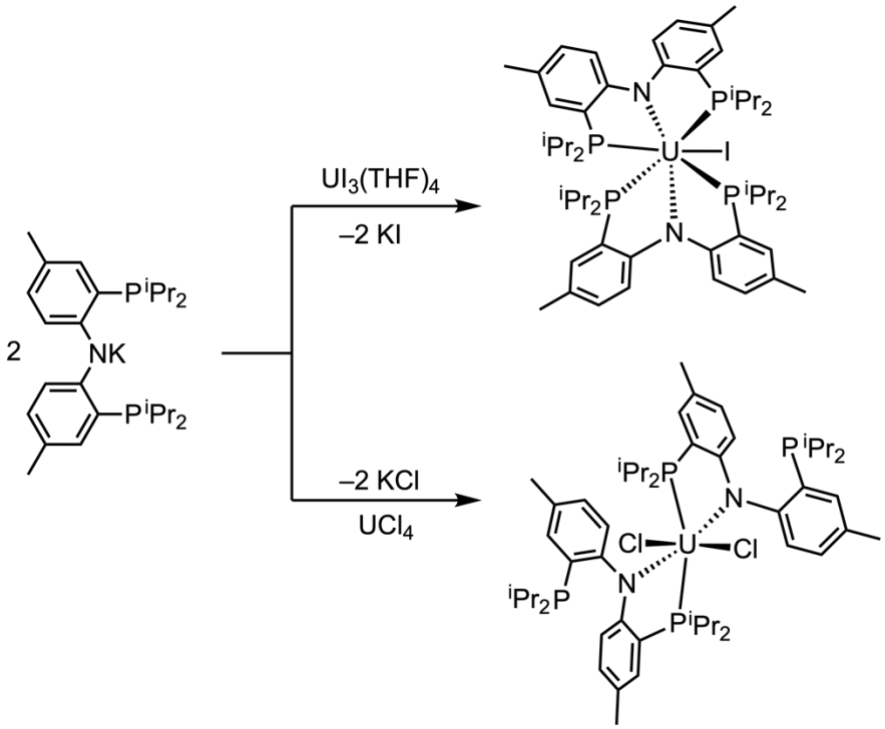


**Scheme 1.5.** Varying coordination modes of the PNP ligand in uranium(III) and uranium(IV) halides.

In related work by the same group, both $\kappa^3$-(*P*,*N*,*P*) and $\kappa^2$-(*P*,*N*) coordination modes were observed in the remarkable uranyl complex, $(PNP)_2U(O)_2$. Starting from trivalent $(PNP)_2UI$, the uranyl complex was generated by chemical oxidation using 2 equivalents of pyridine-*N*-oxide and $KC_8$ (Scheme 1.6). Notably, $(PNP)_2U(O)_2$ represents the first example of a uranyl phosphine complex.[21b] Given that the pairing of soft ligands with the hard $[UO_2]^{2+}$ fragment is generally thought of as disfavored, this result illustrates the flexibility of the PNP ligand in accommodating the highest oxidation state of uranium (6+). Chemical oxidation of $Cp^*_2UI(THF)$ gave only mixtures of uranium oxides, along with the Cp* dimer, $(C_5Me_5)_2$ as the sole organic product. Evidently, under these conditions the PNP pincer scaffold, likely due in part to its hemilability, is better suited than $Cp^*$ to supporting complexes of both low- and high-valent uranium (3+ and 6+), thus providing opportunity to harness redox chemistry in bond activation strategies.[21]

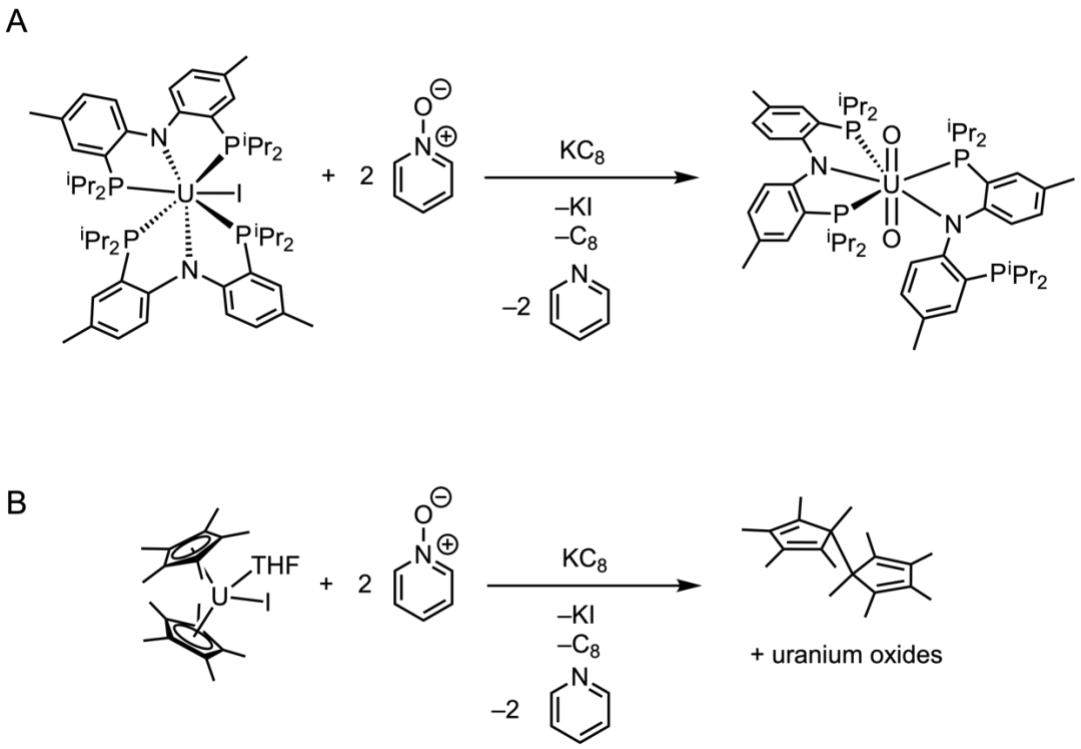


**Scheme 1.6.** (A) Formation of uranyl complexes supported by a hemilabile PNP ligand. (B) Decomposition of a uranium(III) metallocene complex into uranium oxides and bis(Cp*).

### 1.4. Ligand Hemilability in Catalysis

In 2020, Milstein and co-workers shared a detailed mechanistic study of PNP zinc systems capable of base-free hydrogenation and dehydrogenation.[23] Their work exploited key aspects of metal-ligand cooperation and was noteworthy for the utilizations of zinc as an abundant, non-precious metal in catalysis. Both N–H and H–H bond activations were shown to be reversible and driven by a combination of aromatization/dearomatization and phosphorus donor hemilability within a PNP scaffold.[14] Computational analyses of imine and ketone hydrogenation suggest a phosphine donor within the $^{tBu}$PNPZnMe complex dissociates from the metal, leading to heterolytic cleavage of dihydrogen by metal-ligand cooperation (Scheme 1.7).[23]

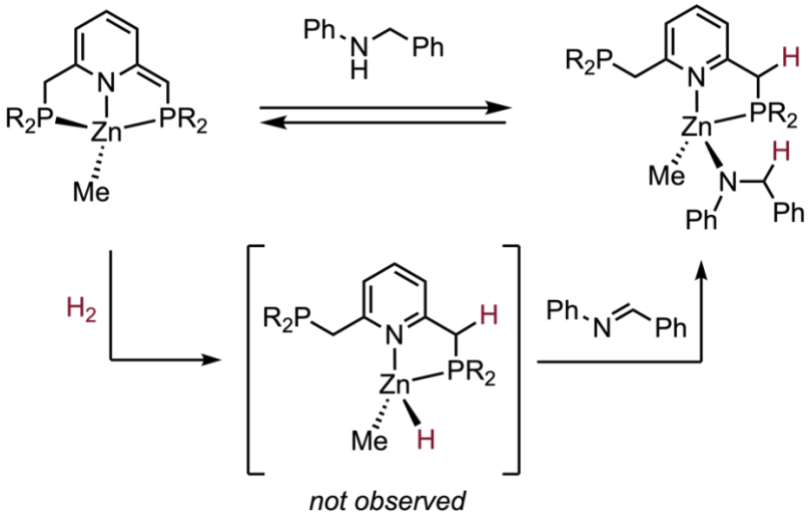


**Scheme 1.7.** $H_2$ activation by aromatization/dearomatization metal-ligand cooperation.

Isotopic-labelling studies showed incorporation of the deuterium label into both methylene sites of the PNP ligand upon exposure of $^{t\text{Bu}}$PNPZnMe to $D_2$ pressure (Scheme 1.8). Notably, no incorporation of the deuterium label was observed in reactions of $D_2$ with the PNP ligand, suggesting that metal-ligand cooperation is operative (Scheme 1.8). Ketones and imines were hydrogenated at relatively low pressures (5-7 bar) of $H_2$ with catalyst loadings between 2.5 and 5 mol%, a notable achievement considering the low cost and accessibility of zinc compared to precious metals employed in well-established hydrogenation catalysis.[23]

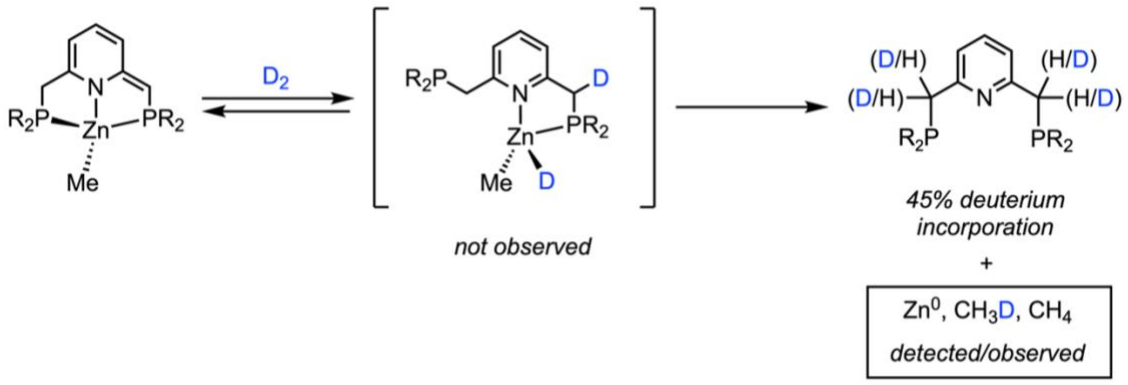


**Scheme 1.8.** Isotopic ($D_2$) labelling studies of the Milstein Zn-PNP system.

### 1.5. Metal-Ligand Multiple Bonds

Another strategy for the activation of small molecules deals with the reactivity of ligands bound to transition metals through multiple bonds.[14] Historically, MLMBs aided in the development of chemical bonding theory, later becoming instrumental in the realization of catalytic olefin metathesis, for which the Nobel Prize in Chemistry was awarded in 2005 (Schrock, Chauvin, and Grubbs).[24] Moreover, MLMBs can serve as highly reactive components of transition metal complexes capable of transferring heteroatom functionality to substrates containing, for example, unreactive C–C or C–H bonds. More generally, the activation of small molecules across MLMBs is of interest in considering metal-ligand cooperation (Scheme 1.9).[14]

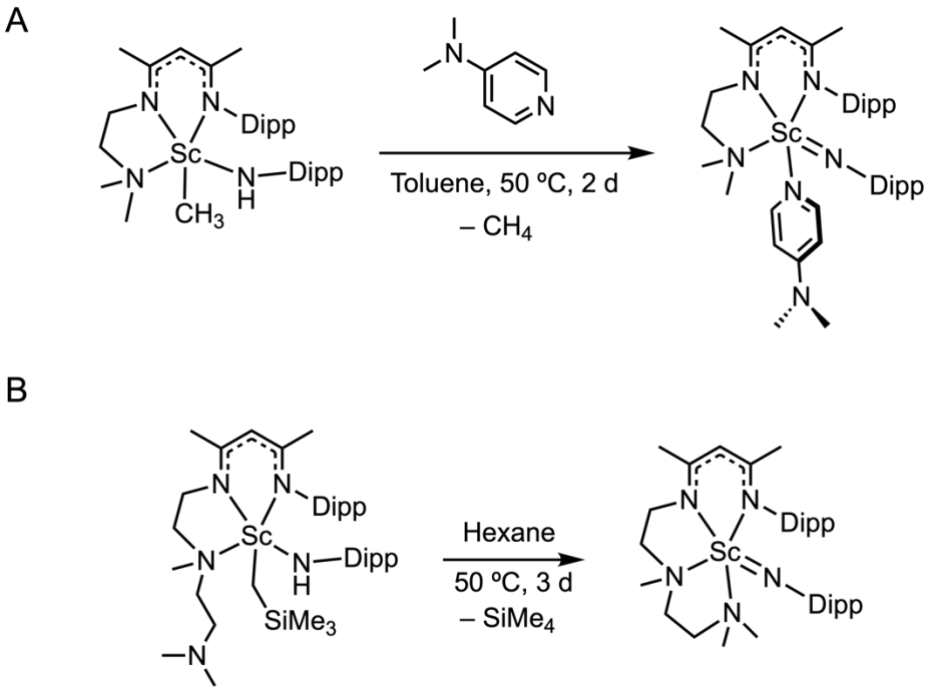


**Scheme 1.9.** (A) Synthesis of a terminal scandium imido complex by addition of exogenous DMAP. (B) Synthesis of terminal scandium imido enabled by metal-ligand cooperation.

In a report from Chen in 2011, metal-ligand cooperation was exploited using a monoanionic Nacnac$^-$ (β-diketiminato) with a tethered amine donor to stabilize a terminal scandium imido ($L_n$Sc=NR) complex formed by alkane elimination.[25] This example followed previous work from the same group which required addition of exogenous DMAP to promote the desired reactivity.[26] These reports demonstrate how ligand design, and specifically, ligand hemilability, can be successfully exploited to access unique and reactive functionalities. Moreover, these works from Chen highlight two aspects of metal-ligand cooperation, namely ligand hemilability, and reactivity of MLMBs, that are central to this thesis work.

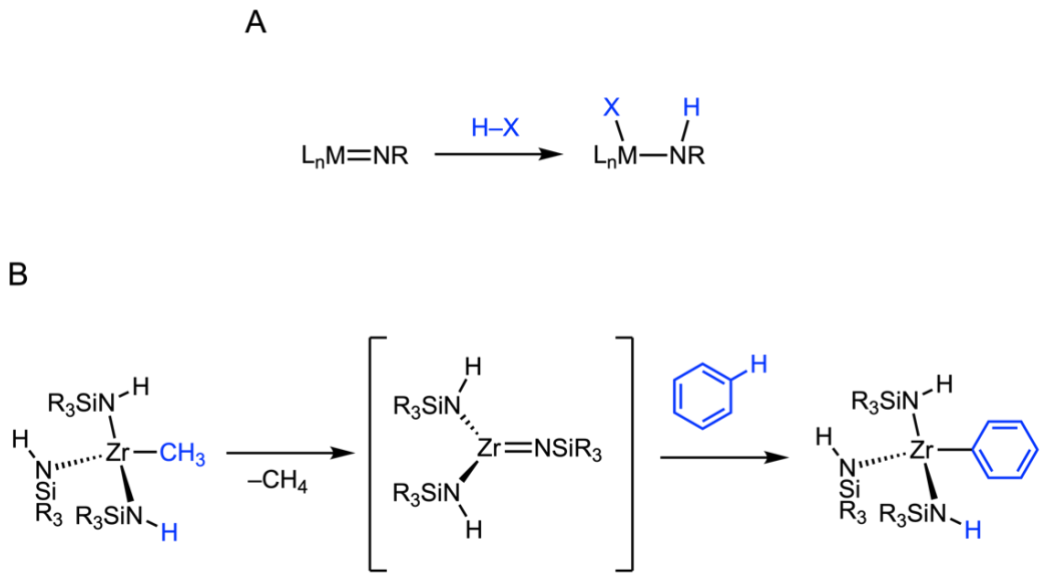


**Scheme 1.10.** (A) Activation of small molecule HX across a generic transition metal imido complex. (B) C–H bond activation across a transient zirconium imido complex.

The reactivity of MLMBs in the transition series is well-established for early, intermediate, and late metals. For example, early 3d metals contain MLMBs that are highly polarized, whereas late transition metals exhibit MLMBs that are more covalent as a result of metal valence orbitals being closer in energy to main group element energies.[27] Cooperative bond activation in mononuclear imido complexes is well-established (Scheme 1.10), as can be seen in the formal 1,2-addition of benzene across a zirconium–nitrogen double bond reported by Wolczanski.[28] Specifically, a transient zirconium(IV) imido complex, formed by methane elimination, reacts with benzene giving a stable phenyl amido complex (Scheme 1.10). Incorporating reactivity of this type in a catalytic cycle, however, is challenging due to the thermodynamics of the reverse reaction. The focus herein is to highlight examples of well-defined MLMBs in the context of homogeneous catalysis pertaining to the work contained in this thesis.

### 1.5.1. Metal–Silicon Multiple Bonds in Catalytic Hydrosilation[1]

The synthesis of late transition metal silylenes ($L_nM{=}SiR_2$), pioneered by Tilley and co-workers,[29] has provided fascinating insight into metal-ligand cooperation in homogenous hydrosilation catalysis. Notably, the isolation of ruthenium silylenes of the general form $Cp^*(PR_3)Ru{=}SiR_2$ by Glaser and Tilley in 2003 led to the development of a new alkene hydrosilation mechanism.[30] In this work, a hydrogen-substituted ruthenium silylene [$Cp^*(P^iPr_3)Ru{=}SiHPh$] was combined with alkenes (e.g. 1-hexene), resulting in direct addition of the Si–H bond to the alkene to produce the terminal hydrosilated alkane product (e.g. $PhSi(H)_2Hex$) with exclusive anti-Markovnikov selectivity (Scheme 1.11).

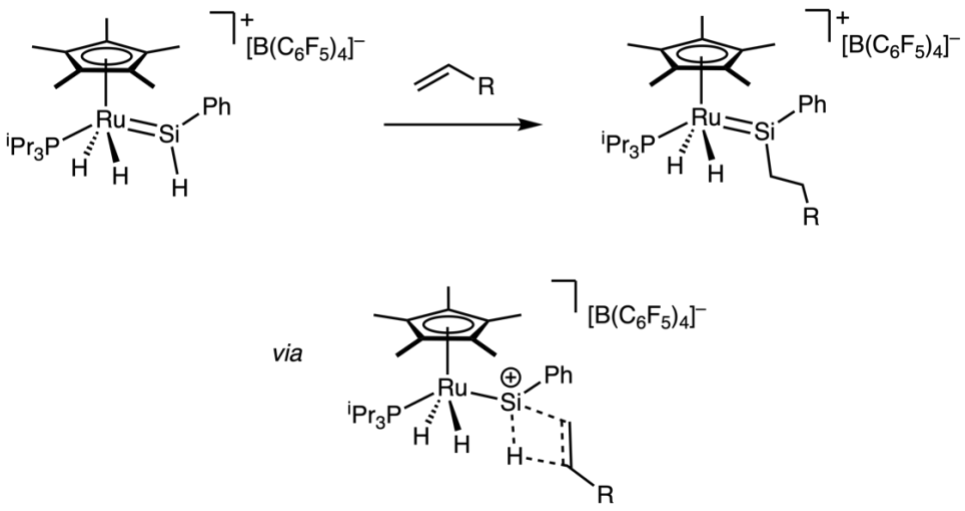


**Scheme 1.11.** Key Si–C bond-forming step in Tilley-Glaser hydrosilation mediated by ruthenium silylene.[30]

The observed selectivity towards primary silanes ($RSiH_3$) is not compatible with a Chalk-Harrod mechanism and led the authors to propose a key Si–C bond-forming step following

[1]In Chapter 4, the involvement of metal–silicon multiple-bonds in catalytic ketone hydrosilation are discussed in greater detail, along with a thorough description of metal–silicon bonding in the context of MLMB reactivity.

concerted addition of the Si–H bond of the silylene across the alkene C=C bond (Scheme 1.11). Moreover, direct addition of alkenes to metal silylene Si–H bonds represents a redox-neutral process that avoids the intermediacy of a metal alkene complex, and does not, therefore, require a coordinatively unsaturated metal center to promote the bond-forming elementary step. Sequential 1,2-H migration, followed by reductive elimination, releases the silylated product (Scheme 1.12). The interconversion of a ruthenium silylene dihydride and ruthenium silyl hydride by 1,2-H migration is central to the discussion of base-stabilized rhodium silylenes (Chapter 4) and borylenes (Chapter 5) and illustrates a key aspect of metal-ligand cooperation in catalysis.

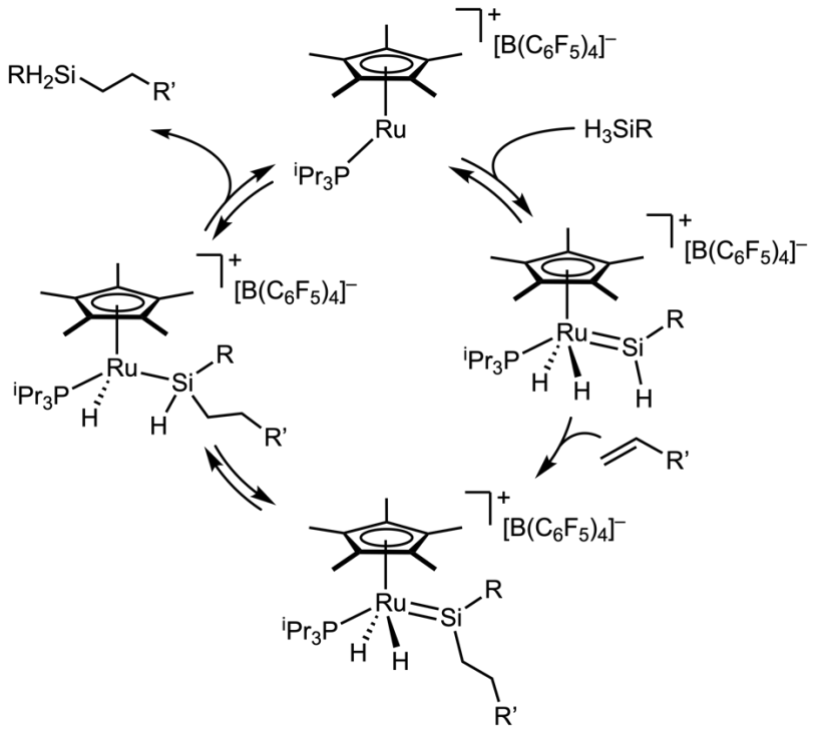


**Scheme 1.12.** Proposed catalytic cycle for the hydrosilation of alkenes by a ruthenium silylene complex.[30]

### 1.6. Thesis Goals and Outcomes

The evolution of metal-ligand cooperation into a major area of focus within coordination chemistry and catalysis has been enabled by the synthesis of new pincer ligands bearing reactive fragments. Specifically, the design of pincer ligands that can change coordination number by virtue of hemilability is a viable strategy to low-valent, and therefore reactive transition metals. Recognizing that monoanionic NNN-pincer ligands are historically underdeveloped for late transition metals, it was the goal of this thesis research to evaluate a class of monoanionic bis(phosphinimine)pyrrolide ligands in the preparation of low-valent rhodium complexes. With these complexes in hand, well-defined examples of metal-ligand cooperation in bond-activation reactions would be surveyed.

First, the evaluation of isolated rhodium alkene and alkyne complexes in hydrogenation catalysis is discussed in Chapter 2. An explicit aim was to identify novel pathways for $H_2$ activation in the context of metal-ligand cooperation. Moreover, the isolation and characterization of catalyst resting states resulting from ligand-based reactivity was of interest, specifically pathways that exploited phosphinimine hemilability.

Chapter 3 describes the synthesis of rhodium carbonyl complexes and places an emphasis on the pairing of a Lewis acid activator with a hemilabile phosphinimine. Ligand modifications are described, highlighting the extent to which phosphinimines can be tuned to promote or suppress specific reactivities. Exploratory chemistry with $B(C_6F_5)_3$ is discussed, in which the concepts of Frustrated Lewis Pair (FLP) chemistry are exploited for C–O, $H_2$, and $H_2O$ activation.

Chapters 4 and 5 are conceptually-related and seek to exploit the reactivity of a rhodium monocarbonyl (described in Chapter 3) in the activation of Si–H and B–H bonds, respectively. Consecutive Si–H activation leading to dehydrogenation of hydrosilanes is discussed in the context of hydrosilation catalysis, specifically in reference to historical routes to transition metal silylene complexes. The reversibility of such bond activation processes are described in Chapter 5. A specific aim was to understand how the bis(phosphinimine)pyrrolido ligand promotes B–H bond activation by attempting to isolate an 'encounter' complex comprised of an NNN-rhodium monocarbonyl and a borane substrate.

Chapter 6 provides preliminary results of attempts to access cationic variants of the rhodium silylene complexes described in Chapter 4. These data suggest that such species are indeed obtainable and encourage further development of their reaction chemistry. Lastly, proposals are presented that would exploit the well-defined carbonyl complexes described in Chapter 3 in visible light-driven catalysis. More detailed introductory material is presented at the beginning of each chapter where it was felt to be more pertinent, and thereby more beneficial, to the reader.

### 1.7. References

**1.** Housecraft, C. E.; Sharpe, A. G. Inorganic Chemistry, 4th ed.; Pearson Education Ltd: London, 2012.

**2.** Hartwig, J. Organotransition Metal Chemistry: From Bonding to Catalysis, University Science Books, New York, 2009.

**3.** The Nobel Prize in Chemistry 1973. NobelPrize.org. Nobel Prize Outreach AB 2021. <https://www.nobelprize.org/prizes/chemistry/1973/summary/>

**4.** Chirik, P. J.; Zubris, D. L.; Ackerman, L. J.; Henling, L. M.; Day, M. W.; Bercaw, J. E. Preparation of *ansa*-Niobocene and *ansa*-Tantalocene Olefin Hydride Complexes as Transition State Analogues in Metallocene-Catalyzed Olefin Polymerization. *Organometallics* **2003**, *22*, 172–187.

**5.** Park, Y.; Park, K. T.; Kim, J. G.; Chang, S. Mechanistic Studies on the Rh(III)-Mediated Amido Transfer Process Leading to Robust C–H Amination with a New Type of Amidating Reagent. *J. Am. Chem. Soc.* **2015**, *137*, 4534–4542.

**6.** Gu, Y.; Norton, J. R.; Salahi, F.; Lisnyak, V. G.; Zhou, Z.; Snyder, S. A. Highly Selective Hydrogenation of C═C Bonds Catalyzed by a Rhodium Hydride. *J. Am. Chem. Soc.* **2021**, *143*, 9657–9663.

**7.** Kim, S.; Zhong, H.; Park, Y.; Loose, F.; Chirik, P. J. Catalytic Hydrogenation of a Manganese(V) Nitride to Ammonia. *J. Am. Chem. Soc.* **2020**, *142*, 9518–9524.

**8.** Moulton, C. J.; Shaw, B. L. Transition Metal-Carbon Bonds. Part XLII. Complexes of Nickel, Palladium, Platinum, Rhodium and Iridium with the Tridentate Ligand 2,6- Bis[(di-t-butylphosphino)methyl]phenyl. *J. Chem. Soc., Dalton Trans.* **1976**, *11*, 1020–1024.

**9.** van Koten, G.; Klein Gebbink, R. J. M. (Bert). The monoanionic pincer-metal platform: a scaffold for meeting challenges in catalysis and materials research. *Dalton Trans.* **2011**, *40*, 8731–8732.

**10.** Fryzuk, M. D.; Haddad, T. S. Phosphine complexes of yttrium(III). Synthesis, reactivity and fluxional behavior of YCl[N(SiMe2CH2PMe2)2]2. *J. Am. Chem. Soc.* **1988**, *110*, 8263–8265.

**11.** Zhang, J.; Leitus, G.; Ben-David, Y.; Milstein, D. Facile Conversion of Alcohols into Esters and Dihydrogen Catalyzed by New Ruthenium Complexes. *J. Am. Chem. Soc.* **2005**, *127*, 10840−10841.

**12.** Kumar, A.; Bhatti, T. M.; Goldman, A. S. Dehydrogenation of Alkanes and Aliphatic Groups by Pincer-Ligated Metal Complexes. *Chem. Rev.* **2017**, *117*, 12357–12384.

**13.** (a) Faller, J. W.; Crabtree, R. H.; Habib, A. Control of Slippage and Conformation in Indenyl Complexes. *Organometallics*, **1985**, *4*, 929–935. (b) O'Connor, J. M.; Casey, C. P. Ring-slippage chemistry of transition metal cyclopentadienyl and indenyl complexes. *Chem. Rev.* **1987**, 87, 307–318.

**14.** Khusnutdinova, J. R.; Milstein, D. Metal–Ligand Cooperation. *Angew. Chem. Int. Ed.* **2015**, *54*, 12236–12273.

**15.** (a) Van koten, G.; Milstein, D. Organometallic Pincer Chemistry, Springer, Berlin, Heidelberg, **2013**. (b) Morales-Morales, D.; Jensen, C. M. The Chemistry of Pincer Compounds, Elsevier, 1st edn, **2007**.

**16.** Labinger, J. A. Tutorial on Oxidative Addition. *Organometallics* **2015**, *34*, 4784–4795.

**17.** Khaskin, E.; Iron, M. A.; Shimon, L. J. W.; Zhang, J.; Milstein, D. N−H Activation of Amines and Ammonia by Ru via Metal−Ligand Cooperation. *J. Am. Chem. Soc.* **2010**, *132*, 8542–8543.

**18.** Fryzuk, M. D.; MacNeil, P. A. Stereoselective formation of iridium (III) amides and ligand-assisted heterolytic splitting of dihydrogen. *Organometallics* **1983**, *2*, 682–684.

**19.** Osborn, J. A.; Jardine, F. H.; Young, J. F.; Wilkinson, G. The preparation and properties of tris(triphenylphosphine)halogenorhodium(I) and some reactions thereof including catalytic homogeneous hydrogenation of olefins and acetylenes and their derivatives. *J. Chem. Soc. A*, **1966**, *0*, 1711–1732.

**20.** Poverenov, E.; Gandelman, M.; Shimon, L. J. W.; Rozenberg, H.; Ben-David, Y.; Milstein, D. Pincer "Hemilabile" Effect. PCN Platinum(II) Complexes with Different Amine "Arm Length". *Organometallics*, **2005**, *24*, 1082–1090.

**21.** (a) Cantat, T.; Scott, B. L.; Morris, D. E.; Kiplinger, J. L. What a Difference a 5f Element Makes: Trivalent and Tetravalent Uranium Halide Complexes Supported by One and Two Bis[2-(diisopropylphosphino)-4-methylphenyl]amido (PNP) Ligands. *Inorg. Chem.* **2009**, *48*, 2114–2127. (b) Cantat, T.; Graves, C. R.; Scott, B. L.; Kiplinger, J. L. Challenging the Metallocene Dominance in Actinide Chemistry with a Soft PNP Pincer Ligand: New Uranium Structures and Reactivity Patterns. *Angew. Chem. Int. Ed.* **2009**, *48*, 3681–3684.

**22.** Fan, L.; Foxman, B. M.; Ozerov, O. V. N−H Cleavage as a Route to Palladium Complexes of a New PNP Pincer Ligand. *Organometallics*, **2004**, *23*, 326–328.

**23.** Rauch, M.; Kar, S.; Kumar, A.; Avram, L.; Shimon, L. J. W.; Milstein, D. Metal–Ligand Cooperation Facilitates Bond Activation and Catalytic Hydrogenation with Zinc Pincer Complexes. *J. Am. Chem. Soc.* **2020**, *142*, 14513–14521.

**24.** The Nobel Prize in Chemistry 2005. NobelPrize.org. Nobel Prize Outreach AB 2021. <https://www.nobelprize.org/prizes/chemistry/2005/summary/>

**25.** Chen, Y.; Chu, J.; Lu. E. Scandium Terminal Imido Chemistry. *Acc. Chem. Res.* **2018**, *51*, 557–566.

**26.** Lu, E.; Li, Y.; Chen, Y. A scandium terminal imido complex: synthesis, structure and DFT studies. *Chem. Commun.* **2010**, *46*, 4469–4471.

**27.** Mindiola, D. J. Oxidatively Induced Abstraction Reactions. A Synthetic Approach to Low-Coordinate and Reactive Early Transition Metal Complexes Containing Metal−Ligand Multiple Bonds. *Acc. Chem. Res.* **2006**, *39*, 813–821.

**28.** Cummins, C. C.; Baxter, S. M.; Wolczanski, P. T. Methane and benzene activation via transient (tert-$Bu_3SiNH)_2Zr$:NSi-tert-$Bu_3$. *J. Am. Chem. Soc.* **1988**, *110*, 8731–8733.

**29.** Waterman, R.; Hayes, P. G.; Tilley, T. D. Synthetic Development and Chemical Reactivity of Transition-Metal Silylene Complexes. *Acc. Chem. Res.* **2007**, *40*, 712–719.

**30.** Glaser, P. B.; Tilley, T. D. Catalytic Hydrosilylation of Alkenes by a Ruthenium Silylene Complex. Evidence for a New Hydrosilylation Mechanism. *J. Am. Chem. Soc*. **2003**, *125*, 13640–13641.

## Chapter 2: Evaluation of Bis(phosphinimine)pyrrolido Rhodium Alkene and Alkyne Complexes in Catalytic Hydrogenation*

### 2.1. Abstract

Rhodium(I) alkene complexes of an NNN-pincer ligand catalyze the hydrogenation of alkenes, including ethylene, as well as the partial hydrogenation of alkynes. The terminal or resting state of the catalyst, which exhibits a remarkably upfield rhodium hydride $^{1}H$ NMR chemical shift, has been isolated and a synthetic cycle for regenerating the catalytically active species has been established. The work reported in this Chapter highlights metal-ligand cooperation in the context of small molecule activation ($H_2$), specifically phosphinimine hemilability, which will be discussed throughout the thesis.

*****Adapted from: 'Hänninen, M. H.; Zamora, M. T.; MacNeil, C. S.; Knott, J. P.; Hayes, P. G. *Chem. Commun.* **2016**, *52*, 586–589.' with permission from The Royal Society of Chemistry.

## 2.2. Introduction

Although pincer ligands have garnered ever-increasing attention in recent years,[1] the sub-class of monoanionic NNN-scaffolds (Figure 2.1) has been less studied than other variants, especially in the chemistry of late transition metals.[2] A diverse grouping of these nitrogen-based pincer ligands have been assembled, primarily for the stabilization of electrophilic rare earth metal complexes.[3–5]

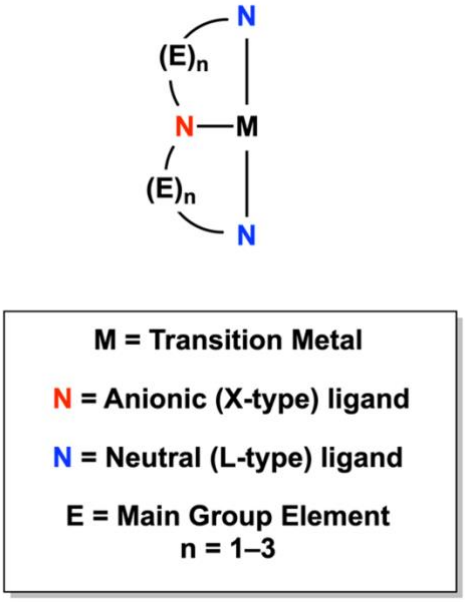


**Figure 2.1.** Generic representation of a monoanionic NNN-pincer ligand.

The utility of these species has thus far been limited to a narrow catalytic scope, inspiring more rigorous examination of monoanionic NNN-ligands with late transition metals given their exceptional utility in catalysis,[6] and the novel chemistry often induced by hard nitrogen-based ligands bound to soft metals.[2,7,8] Furthermore, the propensity for ubiquitous phosphorus-containing pincer ligands to succumb to oxidative degradation[9] inspired a broader consideration of nitrogen-containing variants, which are much less prone to such

decomposition pathways, and could prove particularly useful in stabilizing both robust and unusual late transition metal complexes.

More specifically, a goal of this thesis work was to utilize monoanionic, bis(phosphinimine)pyrrolide pincer ligands developed in the Hayes group[3] with transition metals that typically form four-coordinate complexes. As discussed in Chapter 1, pincer systems adopt a meridional geometry that can promote access to low-coordinate, 14-electron transition metal species that participate in various bond activation processes relevant to a plethora of industrially relevant catalytic transformations, including hydrogenation.[10,11] Accordingly, square planar rhodium(I) complexes bearing labile alkene ligands were identified as appropriate targets for these studies. Moreover, placement of an ylidic phosphinimine within the primary coordination sphere of low-valent Rh(I) had not been explored. Although Rh(I) complexes bearing NNN-pincer ligands are relatively scarce,[2,12–16] those that are known have consistently demonstrated intriguing chemical reactivity. For example, a Rh(I) species bearing a 2,2′:6′,2″-terpyridine (Terpy) ligand was reported to activate $O_2$ in $H_2O$ upon addition of $H_2$,[17] a reaction that would have been impossible if traditional phosphine-containing pincers had been utilized. The following sections describe the evaluation of a monoanionic bis(phosphinimine)pyrrolide ligand in the synthesis of alkene and alkyne Rh(I) complexes relevant to catalytic hydrogenation. The following results will be presented in the context of original thesis work, with co-author contributions addressed explicitly.

### 2.3. Results and Discussion

Reaction between the THF-solvated sodiated ligand Na-$^{Ph}$NNN·THF, ($^{Ph}$NNN = 2,5-[$Ph_2P$=N(4-$^{i}$Pr$C_6H_4$)]$_2$N($C_4H_2$)$^-$), and 0.5 equivalents of [RhCl(COE)$_2$]$_2$ (COE =

cyclooctene) at 50 °C in toluene cleanly afforded ($^{Ph}$NNN)Rh(COE), **1-COE** (Scheme 2.1), after 1 hour, as seen by complete disappearance of the $^{31}P\{^{1}H\}$ NMR resonance for Na-$^{Ph}$NNN·THF (δ 8.8), along with concomitant emergence of a new signal at δ 33.8 that features diagnostic coupling to $^{103}$Rh ($^{2}J_{PRh}$ = 6.0 Hz; $^{103}$Rh = 100%, $I$ = ½).

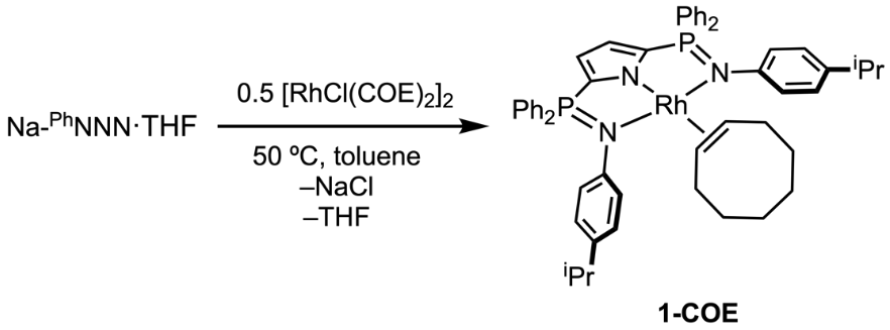


**Scheme 2.13.** Preparation of **1-COE** by salt metathesis.

In addition, resonances corresponding to free COE in benzene-$d_6$, as well as a dramatic upfield shift and broadening of the resonance attributed to the bound olefin (δ 3.52, $^{2}J_{HRh}$ = 7.8 Hz, cf. δ 5.65 for corresponding protons in non-coordinated COE) were apparent in the $^{1}$H NMR spectrum. Finally, the $^{13}C\{^{1}H\}$ NMR spectrum exhibits properties similar to published rare earth complexes ligated by the $^{Ph}$NNN ligand.[3,18]

Next, the substitutional lability of cyclooctene was surveyed. Over the course of 45 minutes at ambient temperature in benzene-$d_6$ solution, **1-COE** readily reacted with excess ethylene to form ($^{Ph}$NNN)Rh($C_2H_4$), **2-$C_2H_4$**, as evidenced by the disappearance of the coordinated COE signals in the $^{1}$H NMR spectrum, along with materialization of resonances corresponding to a rhodium-coordinated $C_2H_4$ ligand (δ 3.14, cf. δ 5.22 for free ethylene in benzene-$d_6$). In addition, a frequency change (from δ 33.8 to δ 33.9) was observed for the $^{103}$Rh coupled doublet in the corresponding $^{31}P\{^{1}H\}$ NMR spectrum. Recrystallization of **2-$C_2H_4$** from pentane at –35 ºC gave single crystals suitable for X-ray

diffraction analysis (Figure 2.2). The structure was confirmed as the planar rhodium ethylene complex, with an olefinic C–C bond distance of 1.40(2) Å suggesting some degree of metallacyclopropane character. The elongated P–N bond distances (Table 2.1) emphasize single-bond character consistent with an ylidic phosphinimine.

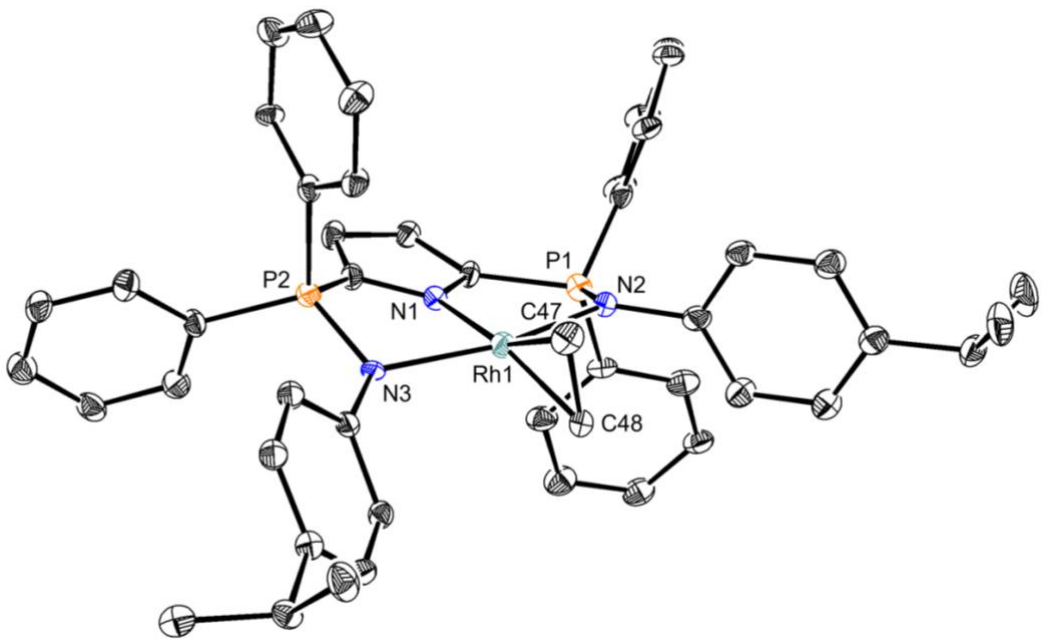


**Figure 2.2.** X-ray crystal structure of **2-$C_2H_4$** at 30% probability ellipsoids. Hydrogen atoms have been omitted for clarity.

**Table 2.1.** Selected bond distances (Å) and angles (º) for **2-$C_2H_4$**.

| **Parameter** | **2-$C_2H_4$** |
|---|---|
| Bond distance (Å) | |
| Rh1–N1 | 2.005(9) |
| Rh1–N2 | 2.11(1) |
| Rh1–N3 | 2.13(1) |
| Rh1–C47 | 2.09(1) |
| Rh1–C48 | 2.10(1) |
| Rh2–C83 | 2.130(3) |
| P1–N2 | 1.624(9) |
| P2–N3 | 1.63(1) |
| C47–C48 | 1.40(2) |
| Bond angle (º) | |
| N1–Rh1–N3 | 81.7(4) |
| N1–Rh1–N2 | 81.2(4) |
| N2–Rh1–N3 | 162.9(4) |

Similarly, **1-COE** reacted with a stoichiometric amount of diphenylacetylene to give the anticipated alkyne complex ($^{Ph}$NNN)Rh(PhCCPh), **1-PhCCPh**, and liberated cyclooctene (Scheme 2.2). Diagnostic resonances attributed to coordinated diphenylacetylene were found at δ 8.34, 7.24 and 7.12 in the $^1$H NMR spectrum of complex **1-PhCCPh**. Independent preparation of **1-PhCCPh** was also achieved by addition of 1 equivalent of diphenylacetylene to the ethylene complex **2-C$_2$H$_4$**.

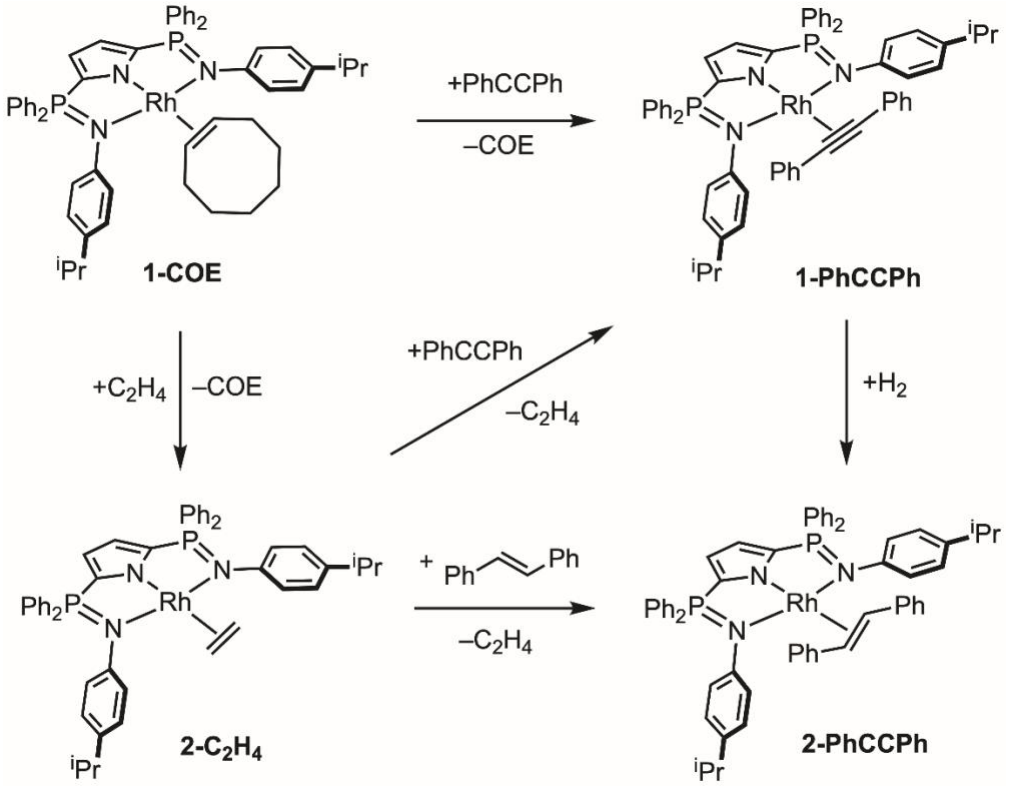


**Scheme 2.14.** Interconversion of rhodium alkene and alkyne species relevant to Chapter 2.

The ability of complex 1-COE to activate $H_2$ and potentially hydrogenate unsaturated fragments was probed by introducing 1 atm of dihydrogen to an ambient temperature benzene-$d_6$ solution of the complex. Under these conditions, consumption of $H_2$ and hydrogenation of COE, as indicated by the appearance of a signal consistent with

free cyclooctane (COA, δ 1.51) in the $^{1}$H NMR spectrum, was observed. Likewise, all COE resonances gradually vanished. Over the course of the reaction, four new resonances emerged at δ 31.1 (s), 23.5 (s), 11.8 (d, $^{2}J_{PRh}$ = 6.2 Hz) and −1.9 (s) in the $^{31}$P{$^{1}$H} NMR spectrum in a 1:1:1:1 ratio. This spectroscopic signature suggested that an asymmetric dirhodium complex **2-Rh$_2$** (Scheme 2.3), likely the product of self-reaction of a putative 14-electron intermediate, was forming upon ejection of COA from the coordination sphere of the metal. Under the same conditions, 1 atm of $D_2$ yielded **2-Rh-*d*$_2$**, along with labelled cyclooctane-*d*$_2$ (broad resonance centered at δ 1.43 in the $^{2}$H NMR spectrum), with identical $^{1}$H and $^{31}$P{$^{1}$H} spectroscopic signatures as complex **2-Rh$_2$**.

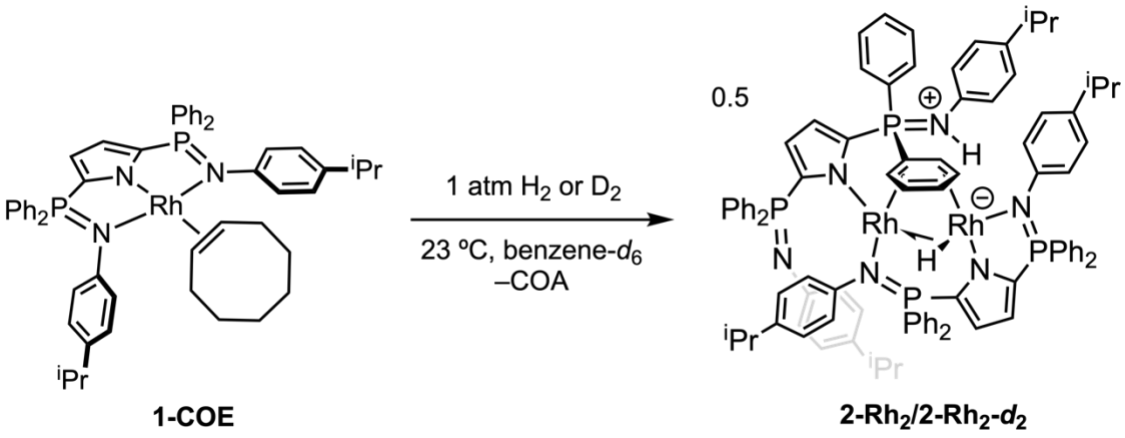


**1-COE** **2-Rh$_2$/2-Rh$_2$-*d*$_2$**

**Scheme 2.15.** Hydrogenation of **1-COE** generated the dirhodium complex **2-Rh$_2$**.

After 19 h at ambient temperature, complex 1-COE was completely converted to the **2-Rh$_2$**. The $^{1}$H NMR spectrum, while complicated, exhibits diagnostic spectral features, including four separate $^{i}$Pr methine and eight distinct $^{i}$Pr methyl signals, which are consistent with formation of an asymmetric dirhodium complex. Intriguingly, the $^{1}$H NMR spectrum contained an unusually upfield virtual triplet centered at δ −35.8 ($^{1}J_{HRh(1)} = {}^{1}J_{HRh(2)}$ = 19.8 Hz), suggesting a remarkably shielded rhodium hydride ligand. This signal represented the most upfield chemical shift hitherto reported for any rhodium

hydride species at the time of publication.[19,20] A deshielded singlet (δ 11.40), attributed to an NH moiety, was also present. As expected, Rh–H and NH resonances are absent in the $^1$H NMR spectrum of **2-Rh$_2$-*d*$_2$**; no evidence of H/D exchange was observed after subjecting either **2-Rh$_2$** to 1 atm of $D_2$ or **2-Rh$_2$-*d*$_2$** to $H_2$ gas.

The identity of **2-Rh$_2$** was unambiguously established by an X-ray diffraction study of high-quality crystals grown from a benzene solution layered with pentane at ambient temperature. Dr. Mikko Hänninen, a former postdoctoral fellow in the Hayes group, performed the X-ray diffraction analysis, solved the structure, and completed the data refinement. The zwitterionic species, **2-Rh$_2$**, can be confidently assigned as a dirhodium complex resulting from the twofold cleavage of $H_2$ and hydrogenation of COE. This product features a Rh–H–Rh interaction, as well as an unusual μ-η$^2$:η$^2$-bridging phenyl group (Scheme 2.3). Hence, in addition to the shielding effects imparted by two directly-bonded Rh centers, the cause of the low-frequency hydride $^1$H NMR chemical shift is presumably a consequence of shielding imparted by ring current anisotropy of the bridging phenyl group, which is locked into position directly above the hydride ligand (H1–phenyl centroid = 2.318 Å; average H1–centroid–C(aryl) angle = 90.0º, Figure 2.3). Although the NH proton is located near the deshielding vicinity of the aryl ring, its downfield $^1$H chemical shift most likely originates largely from the positive charge of the phosphiniminium group; comparable protonated phosphinimine benzofuran ligands and zwitterionic 2-phosphiniminium-arenesulfonates exhibit resonances with similar chemical shifts.[21,22]

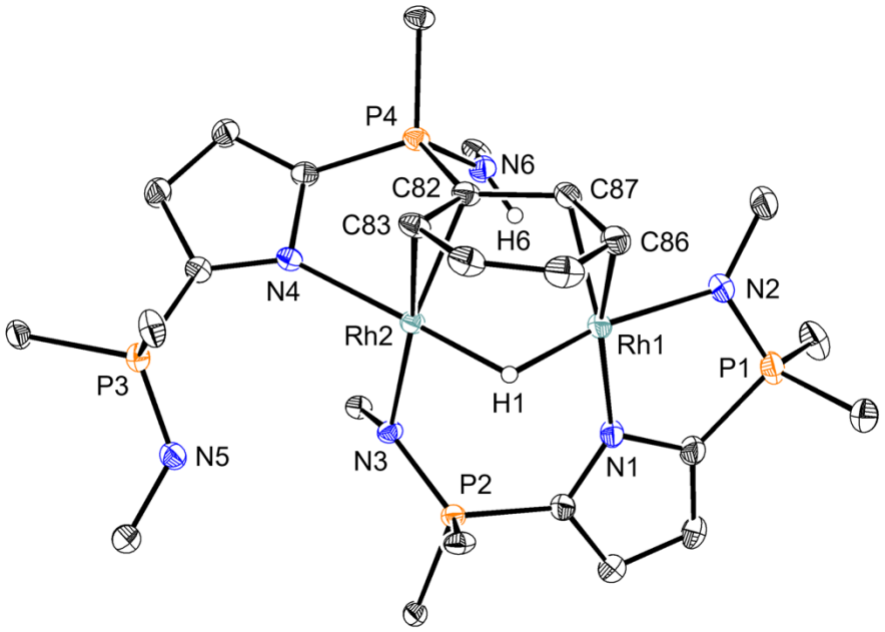


**Figure 2.3.** X-ray crystal structure of **2-Rh$_2$** at 30% probability ellipsoids. Hydrogens atoms except for Rh–H–Rh and N–H, as well as $^{i}$Pr groups, and non-ipso aryl carbon atoms have been omitted for clarity.

**Table 2.2.** Selected bond distances (Å) and angles (º) for **2-Rh$_2$**.

| **Parameter** | **2-Rh$_2$** |
|---|---|
| Bond distance (Å) | |
| Rh1–N1 | 2.060(3) |
| Rh1–N6 | 2.120(3) |
| Rh1–C86 | 2.170(4) |
| Rh1–C87 | 2.091(3) |
| Rh2–C82 | 2.086(3) |
| Rh2–C83 | 2.130(3) |
| Rh1–H1 | 1.70(3) |
| Rh2–H1 | 1.69(3) |
| Rh1---Rh2 | 2.7689(7) |
| Rh2–N3 | 2.118(3) |
| Rh2–N4 | 2.103(3) |
| P1–N2 | 1.598(3) |
| P2–N3 | 1.600(3) |
| P3–N5 | 1.567(3) |
| P4–N6 | 1.654(3) |
| Bond angle (º) | |
| N1–Rh1–C86 | 158.23(12) |
| N1–Rh1–C87 | 163.22(12) |
| N3–Rh2–C83 | 165.14(11) |

Complex **2-Rh$_2$** crystallized as dinuclear neutral units in a monoclinic C2/c space group. The Rh–H bond lengths are identical, which implies resonance forms of alternating agostic interactions. However, the coordination sphere about each rhodium center is slightly different which explains the chemically inequivalent ligand environments apparent in solution-state NMR studies. In addition to the rhodium–hydride (H1) bond, Rh1 is ligated by the pyrrole (N1) and phosphinimine (N2) nitrogens of one bis(phosphinimine)pyrrolide ligand, $^{Ph}$NNN-1; the second phosphinimine nitrogen (N3) is coordinated to Rh2. Since N3 is bound to the adjacent rhodium center, the remaining coordination site on Rh1 is occupied by the π system of a C=C moiety (C86=C87) from a P–Ph group of a second bis(phosphinimine)pyrrolide ligand, $^{Ph}$NNN-2, which is bound to Rh2 via only the pyrrole nitrogen (N4) and another C=C (C82=C83) donor from the aforementioned phenyl substituent. The coordination sphere on Rh2 is completed with an agostic interaction from the adjacent Rh–H bond. The absence of coordination by N5 or N6 is supported by the fact that both atoms are more than 3 Å away from either of the metal centers. Interestingly, as a result of protonation of N6, one of the phosphinimine functionalities was transformed into a phosphiniminium (or aminophosphonium) group. Accordingly, the P–N bond distance (P4–N6 = 1.654(3) Å) has been elongated by almost 0.1 Å compared to the free phosphinimine (P3–N5 = 1.567(3) Å, Table 2.1). Both the hydride and the NH hydrogen were located in the Fourier difference map and refined isotropically. The bonding in 2-Rh$_2$ can be envisioned several ways. A 16e–16e system is most consistent with the diamagnetic NMR spectra obtained in the solution state. Owing to the proximity of both Rh atoms, there is likely some degree of overlap between metal d-orbitals; however, addition of a formal metal–metal bond would imply a 17e–17e system,

which was ultimately not considered. Taken together, the formation of 2-$Rh_2$ highlights cooperative activation of $H_2$ by the $^{Ph}$NNN ligand scaffold and Rh centers and illustrates the extent to which the $^{Ph}$NNN ligand undergoes structural change to accommodate the storage of a hydride and proton by way of heterolytic cleavage of $H_2$.

Since complex 2-$Rh_2$ appeared to be the terminal, or resting state of hydrogenation, the reactivity of this complex was of special interest. Notably, complex 2-$Rh_2$ could not be converted back to 1-COE even in the presence of excess COE, or with prolonged heating at 70 °C. Harsher experimental conditions caused decomposition. Likewise, introduction of $H_2$ in the presence of additional COE did not result in any observable reaction. Attempts to generate monomeric species by adding σ-donors ($PPh_3$, $PEt_3$, CO) to 2-$Rh_2$ yielded no change. By contrast, when an atmosphere of $C_2H_4$ was added to a benzene-$d_6$ solution of 2-$Rh_2$, near quantitative conversion to the mononuclear complex **2-$C_2H_4$** was observed after 96 h at ambient temperature. Intriguingly, ethane formation was also evident, indicating that the bridging hydride and phosphiniminium proton of **2-$Rh_2$** were either extruded as $H_2$, or directly transformed 2-$Rh_2$ into a transient rhodium hydride species that ultimately led to complex **2-$C_2H_4$**. Finally, addition of COE to 2-$C_2H_4$ quantitatively regenerated complex **1-COE** (Scheme 2.4), thus completing the synthetic cycle for the interconversion of relevant species.

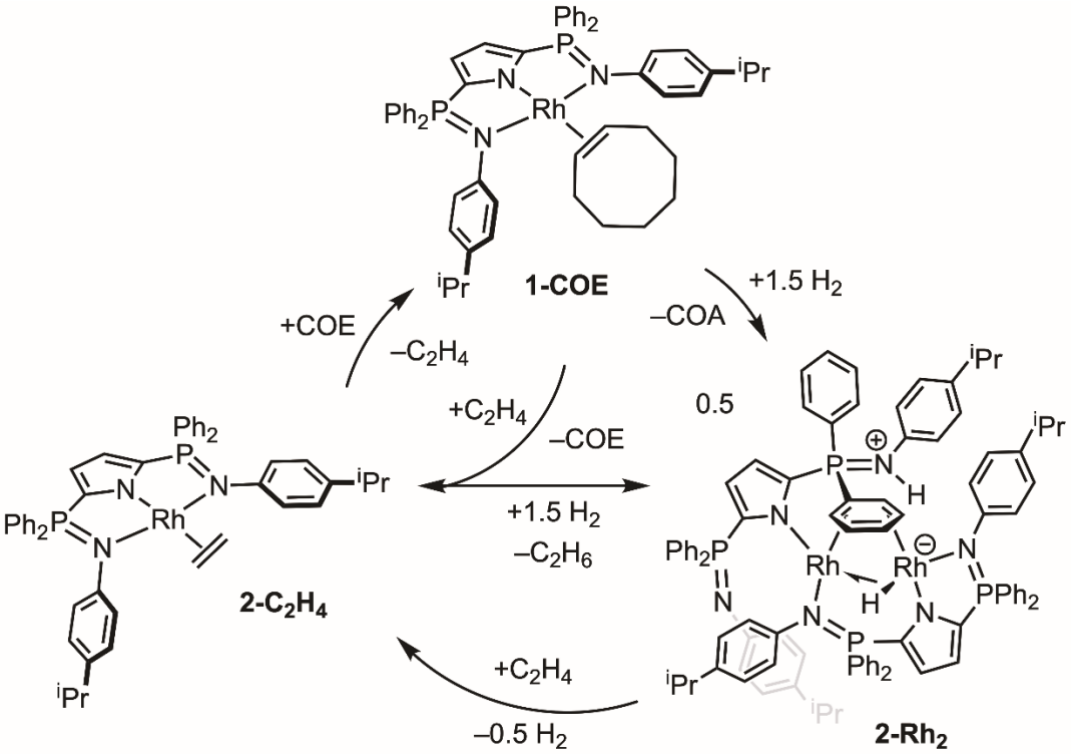


**Scheme 2.16.** Synthetic cycle for the interconversion of rhodium alkene complexes **1-COE** and **2-$C_2H_4$** with **2-$Rh_2$**.

Although hydrogenation of $C_2H_4$ can be challenging,[5] the ethylene complex 2-$C_2H_4$ gratifyingly reacts under 1 atm of $H_2$ at ambient temperature to produce ethane. Thus, rhodium(I) complexes bearing the $^{Ph}$NNN-pincer are capable of hydrogenating even the smallest alkenes. In addition, the alkyne complex **1-PhCCPh** can undergo hydrogenation of its diphenylacetylene ligand to form the *trans*-1,2-diphenylethylene complex ($^{Ph}$NNN)Rh((*E*)-PhHC=CPhH), **2-PhCCPh**, exclusively (Scheme 2.2). Notably, **2-PhCCPh** was independently prepared following the addition of *trans*-1,2-diphenylethylene to either 1-COE or 2-$C_2H_4$. Finally, the catalytic hydrogenation of COE was investigated with 30–60 equiv. of COE consumed under ambient conditions. When compared to Wilkinson's catalyst $RhCl(PPh_3)_3$, 1-COE showed comparable activity in turnover frequency at >95% conversion (TOF = 12 $h^{-1}$ for Wilkinson's catalyst, 20

$h^{-1}$ for 1-COE). These exploratory experiments clearly demonstrate the potential of these Rh complexes to serve as hydrogenation catalysts. This display of metal-ligand cooperation encouraged further study by systematic ligand modification.

### 2.4. Conclusions

In addition to facilitating the catalytic hydrogenation of COE using $H_2$, the Rh NNN-pincer framework in **1-COE** can exchange COE for other unsaturated hydrocarbons, including ethylene and alkynes. As a result, the catalyst system tolerates a range of π-donating species, and by virtue of **2-Rh$_2$** storing both hydridic and protic hydrogen, a synthetic route has been established to regenerate active Rh–alkene species **1-COE**. Beyond hydrogenation, this Rh NNN-pincer system serves as a modular platform to explore a variety of small-molecule activation by leveraging the reactivity of a low-valent transition metal complex supported by electron-donating bis(phosphinimine)pyrrolide ligands. Moreover, the observation of net heterolytic, rather than homolytic cleavage of $H_2$ suggests that element–hydrogen bonds may be activated in analogy to Frustrated Lewis Pairs,[23] where a hemilabile phosphinimine Lewis base and suitable Lewis acid could access promising reaction chemistry.

### 2.5. References

**1.** (a) Van koten, G.; Milstein, D. Organometallic Pincer Chemistry, Springer, Berlin, Heidelberg, **2013**. (b) Morales-Morales, D.; Jensen, C. M. The Chemistry of Pincer Compounds, Elsevier, 1st edn, **2007**.

**2.** (a) Wanniarachchi, S.; Liddle, B. J.; Lindeman, S. V.; Gardinier, J. R. Preparation, properties, and reactivity of carbonylrhodium(I) complexes of di(2-pyrazolylaryl)amido-pincer ligands. *J. Organomet. Chem*. **2011**, *696*, 3623–3636. (b) Melen, R. L.; Gade, New Chemistry with Anionic NNN Pincer Ligands. *Top. Organomet. Chem*. **2016**, *54*, 179–208.

**3.** Johnson, K. R. D.; Hayes, P. G. Synthesis and Reactivity of Dialkyl Lutetium Complexes Supported by a Novel Bis(phosphinimine)carbazole Pincer Ligand. *Organometallics* **2009**, *28*, 6352–6361.
**4.** Johnson, K. R. D.; Hannon, M. A.; Ritch, J. S.; Hayes, P. G. Thermally stable rare earth dialkyl complexes supported by a novel bis(phosphinimine)pyrrole ligand. *Dalton Trans.* **2012**, *41*, 7873–7875.

**5.** Johnson, K. R. D.; Kamenz, B. L.; Hayes, P. G. Bis(pyrazolyl)carbazole as a Versatile Ligand for Supporting Lutetium Alkyl and Hydride Complexes. *Organometallics*, **2014**, *33*, 3005–3011.

**6.** Evans, P. A. Modern Rhodium-Catalyzed Organic Reactions, Wiley-VCH Verlag GmbH & Co. KGaA, Weinheim, **2005**.

**7.** McBee, J. L.; Escalada, J.; Tilley, T. D. High Oxidation State Rhodium and Iridium Bis(silyl)dihydride Complexes Supported by a Chelating Pyridyl-Pyrrolide Ligand. *J. Am. Chem. Soc.* **2009**, *131*, 12703–12713.

**8.** Scheuermann, M. L.; Luedtke, A. T.; Hanson, S. K.; Fekl, U.; Kaminsky, W.; Goldberg, K. I. *Organometallics* **2013**, *32*, 4752–4758.

**9.** Edwards, P. G.; Haigh, R.; Li, D.; Newman, P. D. Template Synthesis of 1,4,7-Triphosphacyclononanes. *J. Am. Chem. Soc.*, **2006**, *128*, 3818–3830.

**10.** C. Gunanathan and D. Milstein. Applications of acceptorless dehydrogenation and related transformations in chemical synthesis. *Science* **2013**, *341*, 249–260.

**11.** van der Boom, M. E.; Milstein, D. Cyclometalated Phosphine-Based Pincer Complexes: Mechanistic Insight in Catalysis, Coordination, and Bond Activation. *Chem. Rev*. **2003**, *103*, 1759–1792.

**12.** Dzik, W. I.; Creusen, C.; de Gelder, R.; Peters, T. P. J.; Smits, J. M. M.; de Bruin, B. Carbonyl Complexes of Rhodium with N-Donor Ligands: Factors Determining the Formation of Terminal versus Bridging Carbonyls. *Organometallics* **2010**, *29*, 1629–1641.

**13.** Tejel, C.; Ciriano, M. A.; del Rio, M. P.; van den Bruele, F. J.; Hetterscheid, D. G. H.; Tsichlis i Spithas, N.; de Bruin, B. Deprotonation Induced Ligand-to-Metal Electron Transfer: Synthesis of a Mixed-Valence Rh(−I,I) Dinuclear Compound and Its Reaction with Dioxygen. *J. Am. Chem. Soc*. **2008**, *130*, 5844–5845.

**14.** Wanniarachchi, S.; Liddle, B. J.; Kizer, B.; Hewage, J. S.; Lindeman, S. V.; Gardinier, J. R. Syntheses and Electronic Properties of Rhodium(III) Complexes Bearing a Redox-Active Ligand. *Inorg. Chem.* **2012**, *51*, 10572–10580.

**15.** Hetterscheid, D G. H.; Klop, M.; Kicken, R. J. N. A. M.; Smits, J. M. M.; Reijerse, E. J.; de Bruin, B. Hydrogen-Atom Transfer in Open-Shell Organometallic Chemistry: The Reactivity of $Rh^{II}$(cod) and $Ir^{II}$(cod) Radicals. *Chem. Eur. J.* **2007**, *13*, 3386–3405.

**16.** Dzik, W. I.; Fuente Arruga, L.; Siegler, M. A.; Spek, A. L.; Reek, J. N. H.; de Bruin, B. Open-Shell Organometallic $[M^{II}$(dbcot(bislutidylamine)$]^{2+}$ Complexes (M = Rh, Ir): Unexpected Base-Assisted Reduction of the Metal Instead of Amine Ligand Deprotonation. *Organometallics* **2011**, *30*, 1902–1913.

**17.** Inoki, D.; Matsumoto, T.; Hayashi, H.; Takashita, K.; Nakai, H.; Ogo, S. Establishing the mechanism of Rh-catalysed activation of $O_2$ by $H_2$. *Dalton Trans*. **2012**, *41*, 4328–4334.

**18.** Zamora, M. T.; Johnson, K. R. D.; Hänninen, M. M.; Hayes, P. G. Differences in the cyclometalation reactivity of bisphosphinimine-supported organo-rare earth complexes. *Dalton Trans.* **2014**, *43*, 10739–10750.

**19.** Brayshaw, S. K.; Ingleson, M. J.; Green, J. C.; Raithby, P. R.; Kociok-Köhn, G.; McIndoe, J. S.; Weller, A. S. Holding onto Lots of Hydrogen: A 12-Hydride Rhodium Cluster That Reversibly Adds Two Molecules of $H_2$. *Angew. Chem. Int. Ed*. 2005, 44, 6875–6878.

**20.** Kohrt, C.; Hansen, S.; Drexler, H.-J.; Rosenthal, U.; A. Schulz, A.; Heller, D. Molecular Vibration Spectroscopy Studies on Novel Trinuclear Rhodium-7-Hydride Complexes of the General Type $\{[Rh(PP^*)X]_3(\mu_2\text{-}X)_3(\mu_3\text{-}X)\}(BF_4)_2$ (X = H, D). *Inorg. Chem.* **2012**, *51*, 7377–7383.

**21.** Wheaton, C. A.; Ireland, B. J.; Hayes, P. G. Activated Zinc Complexes Supported by a Neutral, Phosphinimine-Containing Ligand: Synthesis and Efficacy for the Polymerization of Lactide. *Organometallics* **2009**, *28*, 1282–1285.

**22.** Burns, C. T.; Shang, S.; Thapa, R.; Mashuta, M. S. Synthesis of air-stable zwitterionic 2-phosphiniminium-arenesulfonates. *Tetrahedron Lett.* **2012**, *53*, 4832–4835.

**23.** Stephan, D. W. Frustrated Lewis Pairs: From Concept to Catalysis. *Acc. Chem. Res.* **2015**, *48*, 306–316.

## Chapter 3: Metal-Ligand Cooperation Enables Activation and Deoxygenation of CO*

### 3.1. Abstract

The rhodium dicarbonyl complex ($^{iPr}$NNN)Rh(CO)$_2$ (**3-(CO)$_2$**), $^{iPr}$NNN = 2,5-[$^{i}$Pr$_2$P = N(4-$^{i}$PrC$_6$H$_4$)]$_2$N(C$_4$H$_2$)$^-$), which bears a monoanionic NNN-pincer ligand, effectively promotes the complete C–O bond cleavage of a carbonyl ligand with the addition of B(C$_6$F$_5$)$_3$. Solid-state characterization of the encounter complex ($^{iPr}$NNN)Rh(CO)$_2$·B(C$_6$F$_5$)$_3$ (**3-(CO)$_2$·BCF**) by X-ray crystallography provided evidence to suggest a hemilabile phosphinimine acts cooperatively with B(C$_6$F$_5$)$_3$ to activate CO. Mechanistic studies using the $^{13}$CO-labelled complex **3-($^{13}$CO)$_2$·BCF** revealed that a deoxygenative metathesis reaction between P–N and C–O atoms is operative, affording the CO-derived organic product (C$_6$F$_5$)$_3$B←:C≡N(4-$^{i}$PrC$_6$H$_4$) along with modification of the $^{iPr}$NNN ligand to include a phosphine oxide capped by B(C$_6$F$_5$)$_3$.

*****Adapted from: MacNeil, C. S.; Glynn, K. E.; Hayes, P. G. *Organometallics* **2018**, *37*, 3248-3252. with permission from the American Chemical Society.

## 3.2. Introduction

The chemistry of C1 oxygenates (CO, $CO_2$, $CO_3^{2-}$) defines the global carbon cycle and is intrinsically tied to energy production and consumption. Processes capable of converting $CO_2$ into value-added chemicals, specifically liquid hydrocarbon fuels ($C_nH_{2n+2}$), present an ongoing challenge in organometallic chemistry and industrial catalysis. Electrocatalytic reduction of $CO_2$ has been achieved,[1] providing an efficient route to CO; however, further deoxygenative transformations are rarely observed outside of cluster complexes relevant to heterogeneous catalysis (Figure 3.1).[2] Overcoming the oxophilicity of carbon presents an ongoing challenge in realizing a general strategy that enables complete deoxygenation of $CO_2$. The first example of a single-component mononuclear complex facilitating the deoxygenation of CO was reported in 2016 by Braunschweig and co-workers (Figure 3.1B).[3] Given the considerable strength (257 kcal $mol^{-1}$) of the C≡O triple bond,[4] reactions that result in deoxygenation are understandably limited under mild conditions.

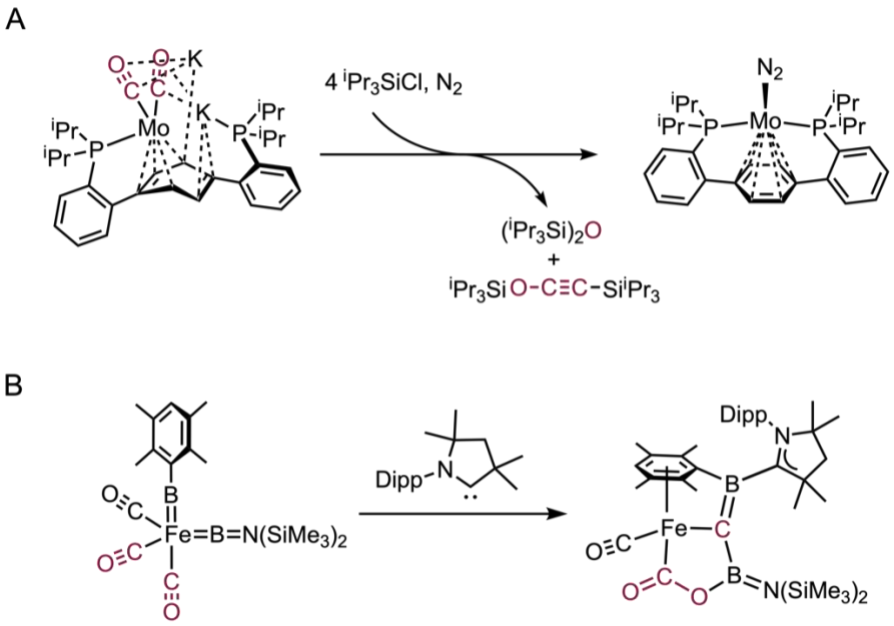


**Figure 3.1.** (A) CO deoxygenation on a reduced molybdenum platform.[6] (B) CO deoxygenation by a well-defined iron borylene.[3]

The complete scission of carbonyl ligands at molybdenum under reducing conditions has been known for decades.[5] Eight electron equivalents are required to fully reduce $CO_2$, six for CO. A representative example reported by Cummins and co-workers described the addition of electron equivalents (e.g. Na/Hg) to (CO)Mo{N(R)Ar}$_3$ followed by pivaloyl chloride, resulting in the formation of a carbyne pivalate.[5] With the addition of Na metal in THF, C–O bond scission gave a molybdenum methylidyne H(C)Mo{N(R)Ar}$_3$ complex. In conceptually related work, $KC_8$ and oxophilic silyl cations ($R_3Si^+$) were combined to enact the deoxygenative coupling of CO leading to the generation of C2 products. In their study, Agapie and Buss described the activation and cleavage of CO, leading to the formation of the terminal molybdenum carbide L$_n$Mo(C)(CO) (L$_n$ = 1,4-bis(2-(diisopropylphosphino)phenyl)benzene).[6] Subsequent C–C coupling generated metal-free ethynol derivatives $R_3SiOC{\equiv}CSiR_3$, (R = Me, $^i$Pr), providing an analogy to the synthesis of multiple carbon atom containing products from CO and $H_2$.[7]

Isoelectronic with $SiR_3^+$, borane electrophiles ($BR_3$; R = Et, $C_6F_5$), introduced externally, or as the Lewis acidic component of phosphinoborane ligands (Re–$Ph_2P(CH_2)_nB(C_8H_{14})$; *n* = 1, 2), have shown a propensity to activate metal–carbonyl ligands.[8] From their initial findings in this area, Bercaw and co-workers developed a working model for the reductive coupling of CO, demonstrating that a pendant borane directs the transfer of a nucleophilic hydride from $[HPt(dmpe)_2]^+$ to $[(Ph_2P(CH_2)_2B(C_8H_{14}))_2Re(CO)_4]^+$ by activating the oxygen atom of the CO ligand.[9–11] Braunschweig reported that two Lewis acidic borylene boron atoms can cooperatively activate and cleave a CO multiple bond (Figure 3.1B).[3] This work marked the first example of a well-defined, single-site transition-metal complex facilitating complete CO bond scission. Notably, a distinguishing feature of the system is the fact that the deoxygenation reaction proceeds in the absence of explicit reducing agents (e.g. Na/Hg or $KC_8$). In addition, the authors claim that the zerovalent iron center exerts minimal influence on the observed chemistry.[3]

Combinations of transition metals with reactive ligand environments capable of stabilizing CO in atypical bonding modes might promote deoxygenation. Interest in the fundamental transformations of CO and other diatomics was piqued after observing effective metal-ligand cooperation in the heterolytic cleavage and storage of $H_2$, described in Chapter 2. Addition of $H_2$ to the rhodium cyclooctene complex **1-COE** resulted in hydrogenation of the alkene and formation of the dirhodium complex **2-Rh$_2$** bearing a protonated phosphinimine and a bridging hydride (Scheme 3.1).[12] In this system, $H_2$ could be liberated following addition of ethylene to **2-Rh$_2$**. Realizing the capacity of hemilabile phosphinimines to act cooperatively with Rh in activating $H_2$, it was questioned whether

similar reactivities could be translated to CO activation. Work from Stephan's group has demonstrated the ability of phosphinimine–borane combinations to be effective in activating $CO_2$, alkynes, and $H_2$.[13] Rhodium carbonyl complexes of the bis(phosphinimine)pyrrolide ligand paired with a suitable borane might very well mediate the activation of CO, in analogy to well-established Frustrated Lewis Pair (FLP) reactivity.[14–18]

### 3.3. Results and Discussion

Recognizing that the $^{Ph}$NNN ligand scaffold described in Chapter 2 participates in cooperative chemistry insofar as stabilizing a dirhodium complex through a unique μ-$\eta^2$:$\eta^2$-bridging phenyl group (Scheme 3.1), a modified NNN ligand was employed which substitutes phenyl groups for isopropyl on the P atom of the phosphinimines. This ligand modification renders the phosphinimines more electron-donating while suppressing formation of the dirhodium species in the presence of $H_2$. In developing a strategy for CO activation and ultimately, reduction to ($C_nH_{2n+2}$), $H_2$ is the ideal terminal reductant as a source of protons and electrons, obviating the chemical overpotentials associated with strong reductants (e.g. Na/Hg or $KC_8$) and acids (e.g. $HBF_4$).

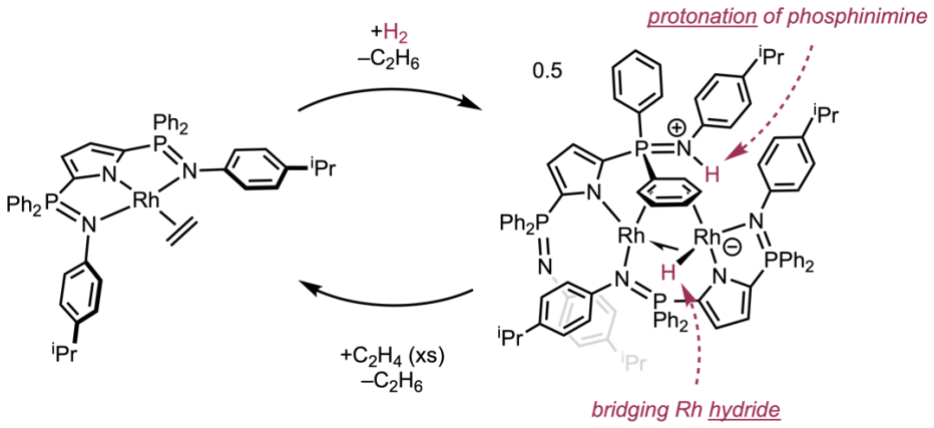


**Scheme 3.17.** Metal-ligand cooperation in the heterolytic cleavage of $H_2$ (the aryl component of an uncoordinated phosphinimine was made transparent for clarity).

Accordingly, addition of the sodiated pincer ligand Na-$^{iPr}$NNN ($^{iPr}$NNN = 2,5-[$^{i}$Pr$_2$P = N(4-$^{i}$PrC$_6$H$_4$)]$_2$N(C$_4$H$_2$)$^-$) to a toluene solution of 0.5 equivalents of [Rh$_2$(μ-Cl)(CO)$_2$]$_2$ resulted in the formation of the rhodium dicarbonyl complex ($^{iPr}$NNN)Rh(CO)$_2$ (**3-(CO)$_2$**), wherein the $^{iPr}$NNN ligand showcases $\kappa^2$-*N,N* bonding to the metal center through pyrrole and phosphinimine nitrogens (Scheme 3.2). Alternatively, **3-(CO)$_2$** could be prepared by condensation of CO gas onto a toluene solution of **2-COE**, the analogous rhodium cyclooctene complex bearing $^{iPr}$NNN.

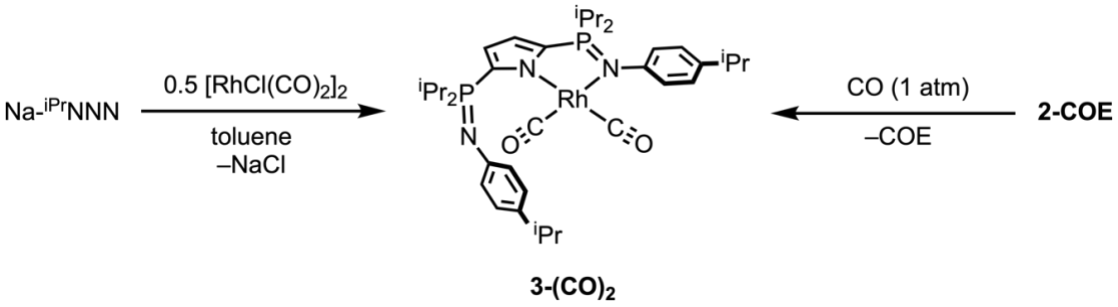


**Scheme 3.18.** Syntheses of **3-(CO)$_2$** by salt metathesis (left to right) or condensation of CO (right to left).

The $^{31}$P NMR spectrum of complex **3-(CO)$_2$** exhibits two resonances at δ 57.9 and 13.8 for the bound and free phosphinimine donors, respectively (Figure 3.3).[19] Two unique downfield $^{13}$C NMR resonances for the CO ligands in **3-(CO)$_2$** were observed at δ 185.9 (dd, $^1J_{CRh}$ = 68.5 Hz, $^2J_{CC}$ = 9.5 Hz) and 184.4 (dd, $^1J_{CRh}$ = 69.3 Hz, $^2J_{CC}$ = 9.5 Hz) (Figure 3.2). This assignment was made possible by preparing the $^{13}$C-labelled complex **3-($^{13}$CO)$_2$** using $^{13}$C-enriched CO gas.

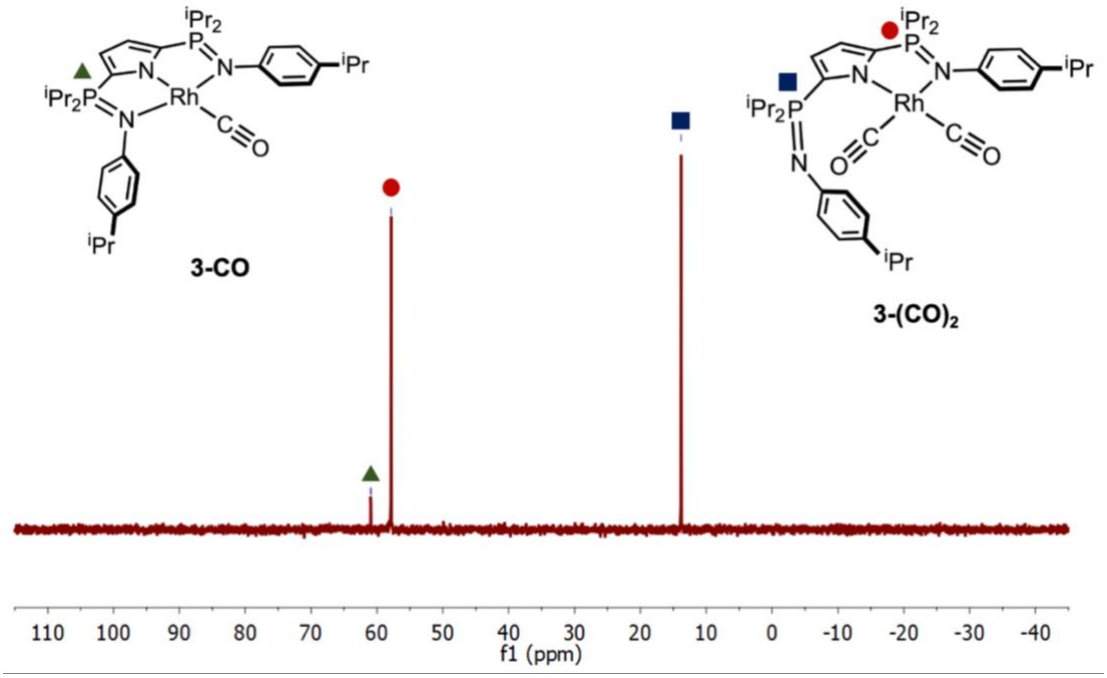


**Figure 3.2.** $^{31}$P NMR (125 MHz) spectrum of **3-(CO)$_2$** in benzene-$d_6$ at 23 ºC. A small amount (< 5%) of **3-CO** is observed.

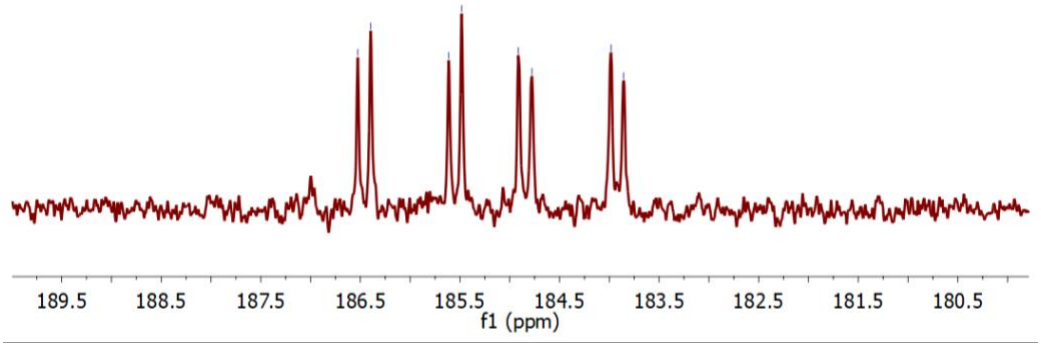


**Figure 3.3.** Downfield region of $^{13}$C NMR (75 MHZ) spectrum of **3-($^{13}$CO)$_2$** ($^{13}$CO ligands enriched with 99% $^{13}$CO) in benzene-$d_6$ at 23 ºC.

Single crystals of **3-(CO)$_2$** suitable for X-ray diffraction studies were grown from a concentrated pentane solution at –35 ºC. The structure of **3-(CO)$_2$** was fully consistent with $^{31}$P NMR spectroscopy, and confirmed the $\kappa^2$-*N*,*N* ligand bonding (Figure 3.4).

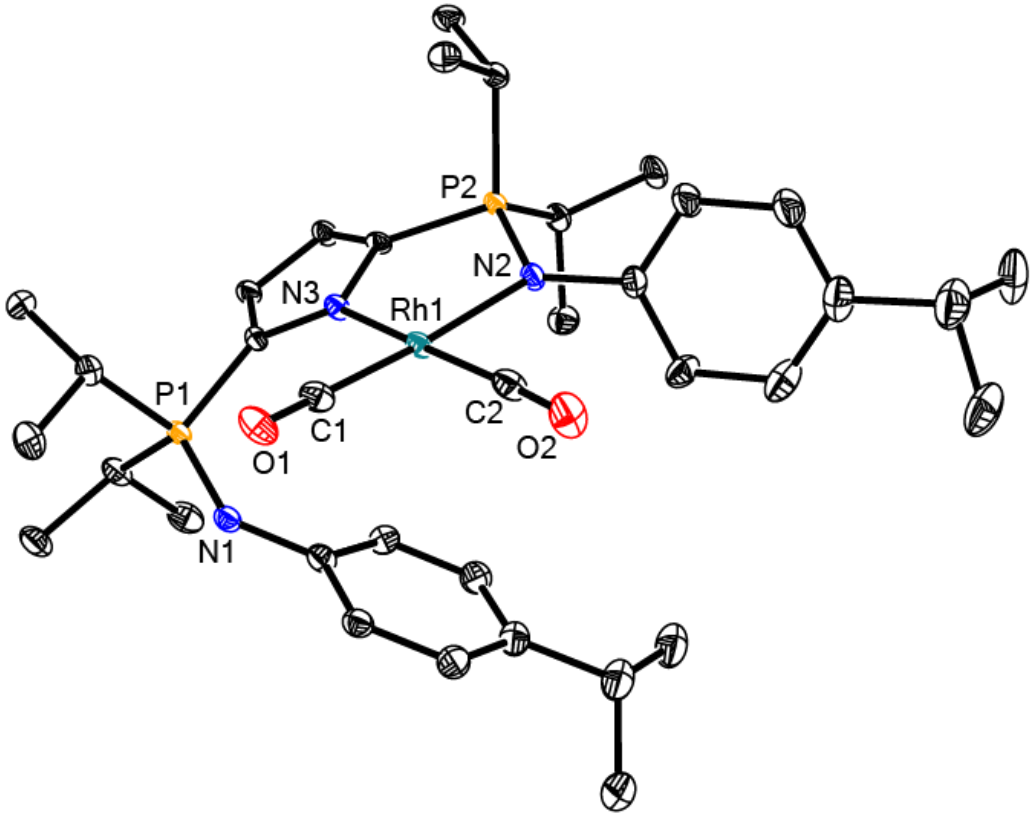


**Figure 3.4.** X-ray crystal structure of **3-(CO)$_2$** at 30% probability ellipsoids. Hydrogen atoms have been omitted for clarity.

**Table 3.1.** Selected bond distances (Å) for **3-(CO)$_2$**.

| **Parameter** | **3-(CO)$_2$** |
|---|---|
| Bond distance (Å) | |
| P1–N1 | 1.562(2) |
| P2–N2 | 1.612(2) |
| C1–O1 | 1.149(4) |
| C2–O2 | 1.139(4) |
| Rh1–C1 | 1.848(3) |
| Rh1–C2 | 1.847(4) |
| Rh1–N2 | 2.090(2) |
| Rh1–N3 | 2.094(2) |

The crystallographic data for **3-(CO)$_2$** illustrates the extent to which P–N bonds compress or elongate to accommodate various bonding situations. An elongated P–N bond reflects a more pronounced ylidic character, where a formal positive charge is located on P and N

bears a formal negative charge. In the case of **3-(CO)$_2$**, one phosphinimine coordinates directly to a Rh center, with a P–N bond distance of 1.613(3) Å, reflecting this ylidic character when compared directly to the non-interacting phosphinimine with a compressed P–N bond distance of 1.562(2) Å. This crystallographic feature appears throughout the thesis and will be discussed when relevant.

Recognizing that in forming **3-(CO)$_2$**, a small amount (< 5% based on $^{31}$P NMR spectroscopy) of the monocarbonyl complex **3-CO** was also generated, a direct synthesis of **3-CO** was targeted. Initially, conversion of **3-(CO)$_2$** to **3-CO** was achieved by prolonged exposure of a stirring toluene solution of **3-(CO)$_2$** to vacuum at 323 K, typically in modest yield (< 70 %). Notably, the rhodium dicarbonyl complex **3-(CO)$_2$** can be regenerated by addition of CO gas onto a toluene solution of **3-CO** in aromatic solvents, accompanied by a color change from red to bright yellow. Following the initial synthesis of **3-CO**, an improved method was developed which exploits an intermetallic CO transfer reaction between **2-COE** and **3-(CO)$_2$**. When 1 equivalent of rhodium dicarbonyl **3-(CO)$_2$** was combined with the cyclooctene complex **2-COE**, a comproportionation reaction occurred, rapidly generating 2 equivalents of **3-CO**. This method was found to be reproducible and gave substantially better yields of the desired monocarbonyl product (> 95%). Moreover, a reliable method of interconverting rhodium carbonyl complexes was established, being crucial to studies involving **3-CO** in Chapters 4 and 5. Moving forward, **3-CO** was prepared following the revised procedure (Scheme 3.3). Analysis by multinuclear NMR spectroscopy showed that complex **3-CO** contains 7 $^{1}$H and 11 $^{13}$C NMR resonances, consistent with a complex of $C_{2v}$ symmetry. The $^{31}$P NMR spectrum of **3-CO** in benzene-$d_6$ contained a single resonance centered at δ 60.9 (d, $^{2}J_{PRh}$ = 5.6 Hz). In pentane at –35 ºC,

**3-CO** crystallized as large red blocks suitable for X-ray diffraction analysis (Figure 3.5). The crystallographic data confirm the $\kappa^3$-*N*,*N*,*N* bonding arrangement of the bis(phosphinimine)pyrrolide ligand.

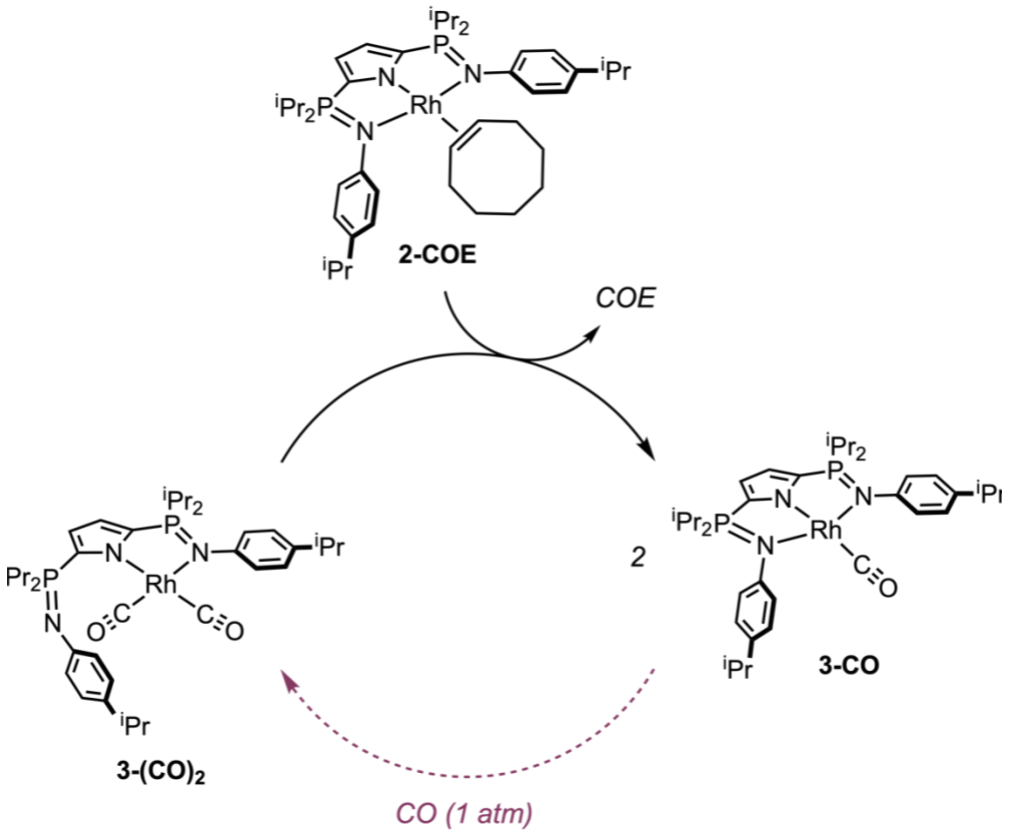


**Scheme 3.19.** Interconversion of rhodium carbonyls and **3-(CO)$_2$** by intermetallic CO transfer from **3-(CO)$_2$** to **2-COE** and CO addition to **3-CO**.

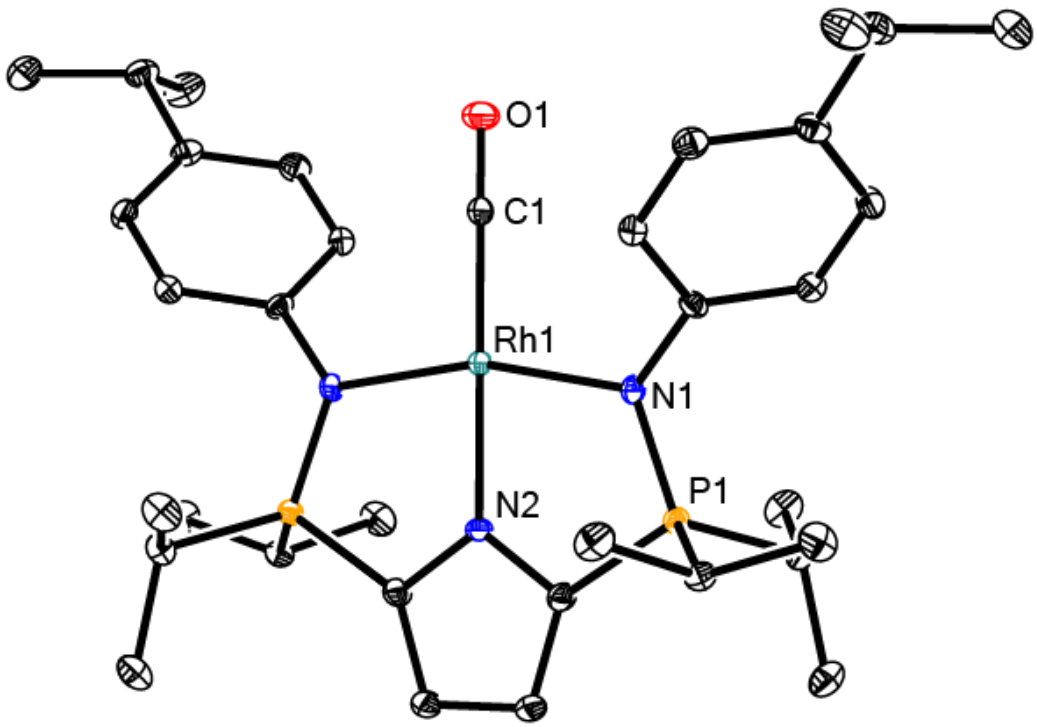


**Figure 3.5.** X-ray crystal structure of **3-CO** at 30% probability ellipsoids. Hydrogen atoms have been omitted for clarity.

**Table 3.2.** Selected bond distances (Å) for **3-CO**.

| Parameter | 3-CO |
|---|---|
| Bond distance (Å) | |
| P1–N1 | 1.629(3) |
| C1–O1 | 1.149(6) |
| Rh1–C1 | 1.828(4) |
| Rh1–N1 | 2.007(3) |
| Rh1–N2 | 2.111(2) |

Next, the reactivity of **3-(CO)$_2$** with the prototypical Lewis acid B($C_6F_5$)$_3$ was evaluated to determine whether the uncoordinated phosphinimine could participate in the activation of a CO ligand. Combining B($C_6F_5$)$_3$ with **3-(CO)$_2$** in benzene-$d_6$ resulted in quantitative formation of a new product in 15 minutes. The $^{31}$P NMR spectrum (Figure 3.6)

of this compound showed two equal-intensity resonances at δ 58.8 and 54.2 (cf. δ 57.9 and δ 13.8 for **3-(CO)$_2$**).

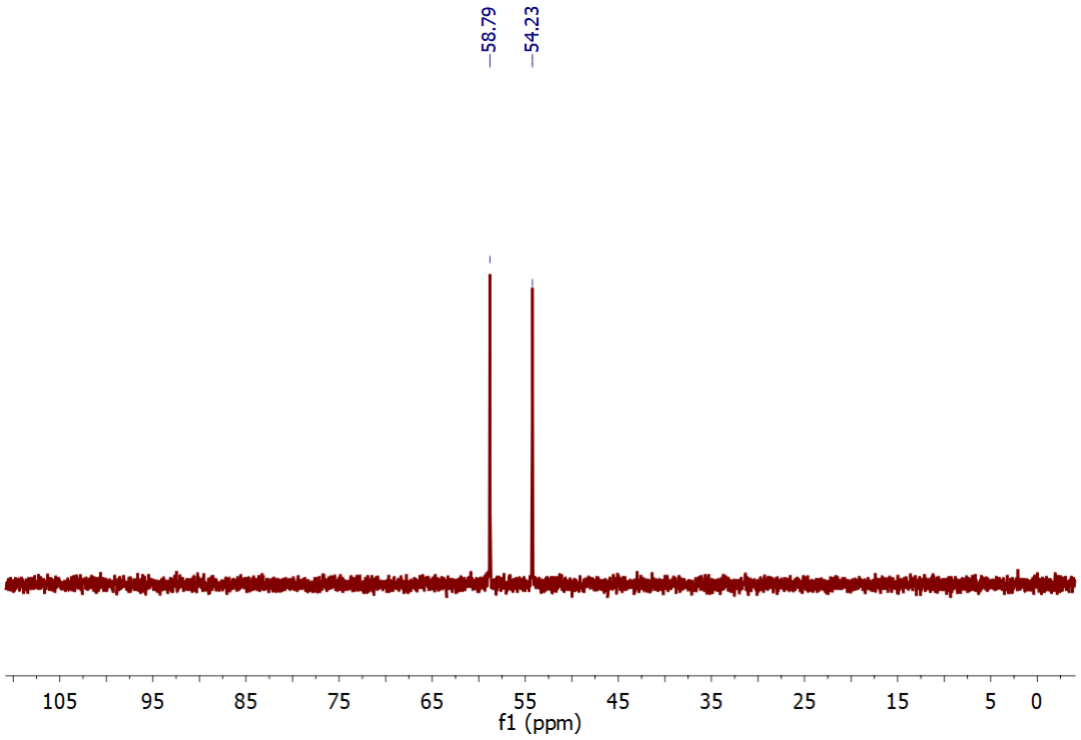


**Figure 3.6.** $^{31}$P NMR (125 MHz) spectrum from the reaction of **3-(CO)$_2$** + B(C$_6$F$_5$)$_3$ in benzene-$d_6$ at 23 ºC.

Attempts to locate the $^{13}$C signals associated with the CO ligands were initially unsuccessful, although a broad $^{11}$B resonance was located at δ −3.1. Together with $\Delta\delta_{m,p}$ = 3.8 ppm in the $^{19}$F NMR spectrum, these data suggest the presence of a neutral four-coordinate borane.[20] Notably, at 243 K, the $^{19}$F NMR spectrum contained 15 unique resonances, implying that B–C$_{aryl}$ bond rotation is slower than the NMR time scale.[21]

It could be reasoned that CO abstraction would give rise to the Lewis acid–base adduct (OC)B(C$_6$F$_5$)$_3$ and the monocarbonyl species **3-CO**. In a report from Berke and Erker, the free energy change for the reaction B(C$_6$F$_5$)$_3$ + CO → (OC)B(C$_6$F$_5$)$_3$ was assigned a value of $\Delta G \approx +40$ kJ mol$^{-1}$ at 298 K in the gas phase.[22] Furthermore, $^{31}$P and

$^{19}$F NMR spectra are not consistent with the formation of **3-CO** and (OC)B($C_6F_5$)$_3$. Thus, CO abstraction from the metal was ruled out on the basis of the available spectroscopic evidence. Intriguingly, comparing the IR spectra of **3-(CO)$_2$** and the product of **3-(CO)$_2$** + B($C_6F_5$)$_3$ showed a dramatic attenuation of one of the two CO absorption bands upon addition of the Lewis acid (Figure 3.7).

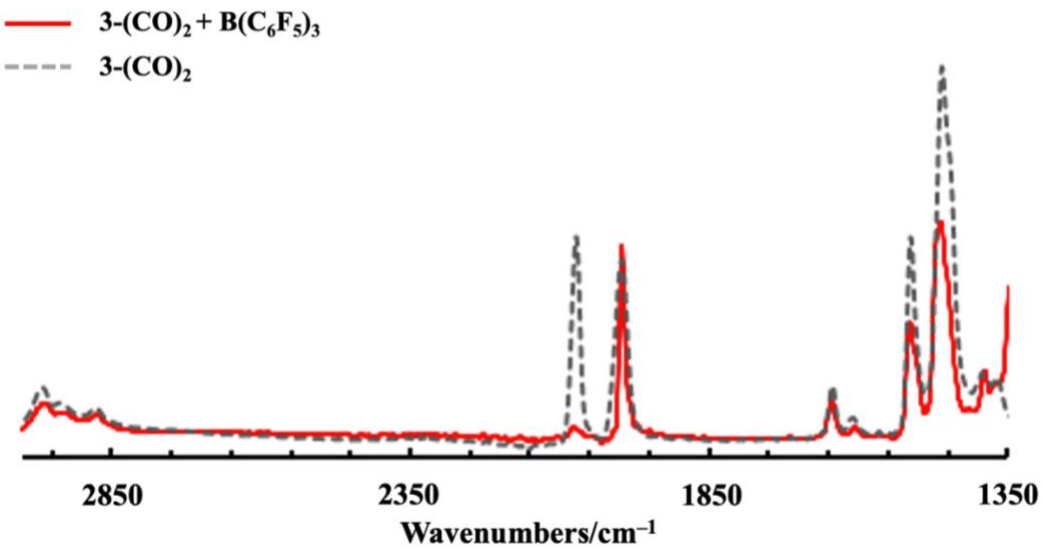


**Figure 3.7.** Overlay of the IR spectra of **3-(CO)$_2$** (gray hashed trace) and **3-(CO)$_2$** + B($C_6F_5$)$_3$ (red trace).

Recrystallization of product from a 1:1 pentane:toluene solution at 238 K gave bright yellow crystals suitable for X-ray diffraction studies. The structure confirmed the identity of the product as **3-(CO)$_2$·BCF**, a phosphinimine-stabilized metalated formamide ($^{iPr}$NNN)Rh(CO)$_2$·B($C_6F_5$)$_3$, an 'O–B encounter complex' between a carbonyl ligand oxygen atom and B($C_6F_5$)$_3$ boron atom. CO activation is accompanied by formation of a new C–N bond (1.420(3) Å), completing a six-membered metallaheterocycle (Figure 3.8).

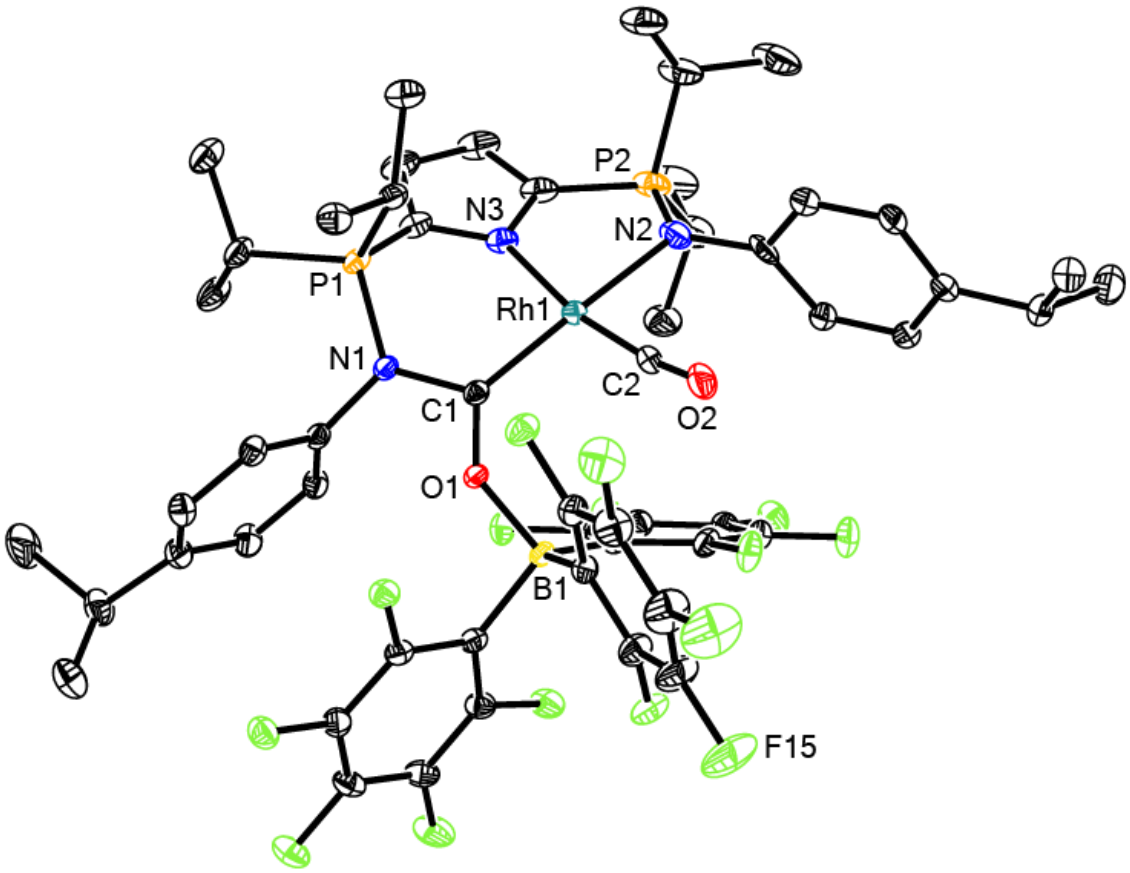


**Figure 3.8.** X-ray crystal structure of **3-(CO)$_2$·BCF** at 30% probability ellipsoids. Hydrogen atoms and solvent molecules of recrystallization have been omitted for clarity.

**Table 3.3.** Selected bond distances (Å) and angles (º) for **3-(CO)$_2$·BCF**.

| **Parameter** | **3-(CO)$_2$·BCF** |
|---|---|
| Bond distance (Å) | |
| P1–N1 | 1.693(2) |
| P2–N2 | 1.606(3) |
| C1–O1 | 1.291(3) |
| C2–O2 | 1.144(3) |
| Rh1–C1 | 1.958(2) |
| Rh1–C2 | 1.829(3) |
| Rh1–N2 | 2.131(2) |
| Rh1–N3 | 2.055(2) |
| C1–N1 | 1.420(3) |
| O1–B1 | 1.520(3) |

| Bond angle (º) | |
|---|---|
| N1–C1–O1 | 106.2(2) |
| Rh1–C1–O1 | 130.9(2) |
| N1–C1–Rh1 | 122.7(2) |

This formulation was maintained as a benzene-$d_6$ solution based on spectroscopic evidence, with $^{2}J_{PC}$ = 17.2 Hz in the $^{31}$P NMR spectrum of the $^{13}$CO-labeled sample **3-($^{13}$CO)$_2$·BCF**. Unambiguous characterization of both CO ligands in the product was made possible by $^{13}$C NMR spectroscopy of **3-($^{13}$CO)$_2$·BCF**, revealing a doublet of doublets for the activated CO ligand (dd, $^{1}J_{CRh}$ = 57.1 Hz, $^{2}J_{CP}$ = 17.2 Hz) centered at δ 227.1, and a doublet of doublets (dd, $^{1}J_{CRh}$ = 79.9 Hz, $^{3}J_{CP}$ = 4.8 Hz) centered at δ 190.4 for the unactivated CO ligand (Figure 3.9). Comparing the product IR spectra of **3-(CO)$_2$** + B($C_6F_5$)$_3$ and **3-($^{13}$CO)$_2$** + B($C_6F_5$)$_3$ showed $\nu$($^{12}$C≡O) and $\nu$($^{13}$C≡O) vibrations at 1993 and 1950 cm$^{-1}$, respectively. The isotopically labeled product **3-($^{13}$CO)$_2$·BCF** moves to lower frequency by 43 cm$^{-1}$, consistent with the predicted shift (44 cm$^{-1}$) from the reduced mass calculation for a simple harmonic oscillator model (Figure 3.10).

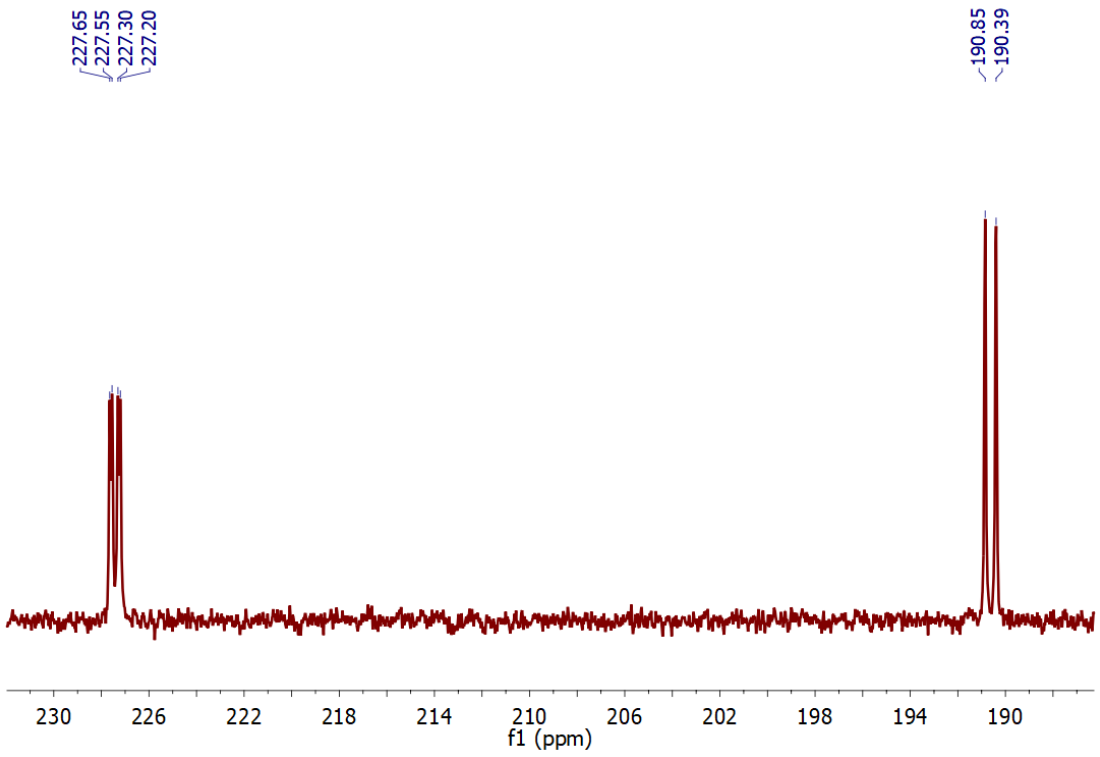


**Figure 3.9.** Downfield region of $^{13}C$ NMR (175 MHz) spectrum of **3-($^{13}CO)_2$·BCF** in benzene-$d_6$ at 23 ºC.

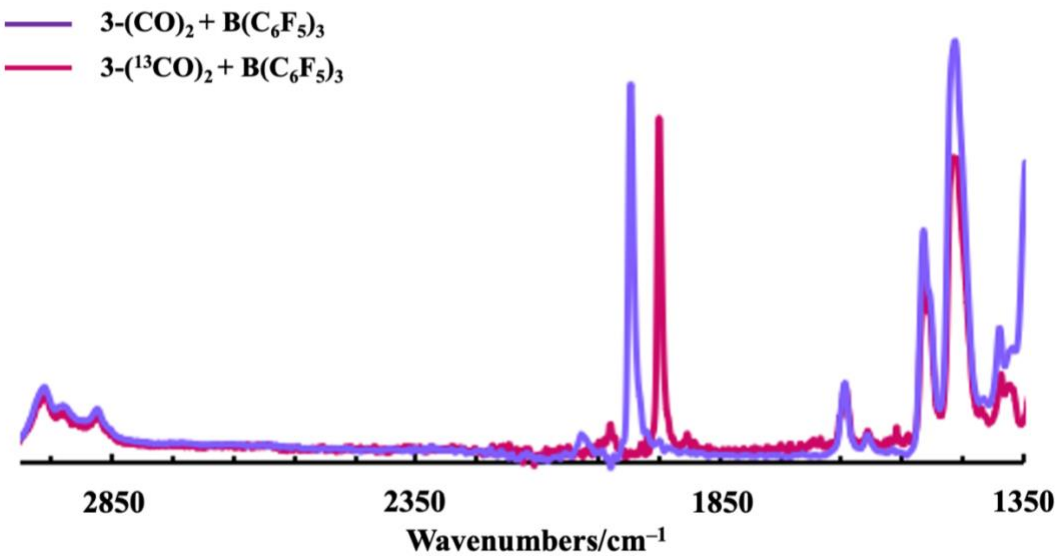


**Figure 3.10.** Overlay of the IR spectra of **3-$(CO)_2$** + $B(C_6F_5)_3$ (purple trace) and **3-($^{13}CO)_2$** + $B(C_6F_5)_3$ (magenta trace).

Isolation of **3-(CO)$_2$·BCF** in the solid state allowed comparison with a variety of organometallic complexes with activated carbonyl ligands in atypical bonding modes. For example, **3-(CO)$_2$·BCF** resembles the $\eta^2$-formyl complex Zr($\eta^5$-$C_5H_5$)($BH_4$)(HCOP$^i$Pr$_2$SiMe$_2$)N(SiMe$_2$CH$_2$P$^i$Pr$_2$$BH_3$), reported by Fryzuk, wherein a labile phosphine stabilizes a formyl ligand.[23] Moreover, the rhodium–carbon bond in **3-(CO)$_2$·BCF** (Rh1–C1 = 1.958(2) Å, Table 3.3) compares well with the Fe–$C_{carboxyl}$ bond (1.959(3) Å) in the Braunschweig CO bond scission product (Figure 3.1).[3] A report from Oestreich and co-workers re-examined Bullock's cationic tungsten(II) catalyst [CpW(CO)$_2$(IMes)][B($C_6F_5$)$_4$][24] and found that the active species in ionic outer-sphere hydrosilation using triethylsilane was a tungsten hydride complex bearing a silyl cation-functionalized CO ligand (Scheme 3.4A).[25] Successful crystallization of this CO-activated complex adduct from neat $Et_3SiH$ confirmed the W–CO–$SiEt_3$ arrangement. Examination of the X-ray crystal structure reveals important similarities between the $Et_3Si^+$ adduct and **3-(CO)$_2$·BCF**, specifically the activation of carbonyl ligands by the valence-isoelectronic silylium cation ($Et_3Si^+$; C–O = 1.25(2) Å) and B($C_6F_5$)$_3$ Lewis acid (Scheme 3.4B). The C1–O1 distance of 1.291(3) Å in **3-(CO)$_2$·BCF** is significantly lengthened relative to the unactivated C–O bond (C2–O2 = 1.144(3) Å) in the neighboring CO ligand, as well as the C–O bond *trans* to the phosphinimine nitrogen donor in **3-(CO)$_2$** (C1–O1 = 1.149(4) Å, Table 3.1) suggesting the complex bears some boroxycarbene character (**3-(CO)$_2$·BCF-1** depicted in Scheme 3.4B). Formation of **3-(CO)$_2$·BCF** also results in significant elongation of the P–N bond of the phosphinimine bound to the activated CO (P1–N1 = 1.693(2) Å; cf. P1–N1 = 1.562(2) Å in complex **3-(CO)$_2$**).[26] In the solid state, boron adopts a near-tetrahedral geometry (average O–B–$C_{aryl}$ angle 107.3°). Further examination of the crystal

structure of **3-(CO)$_2$·BCF** revealed a π-stacking interaction between one −$C_6F_5$ group and a proximal N-aryl ring.

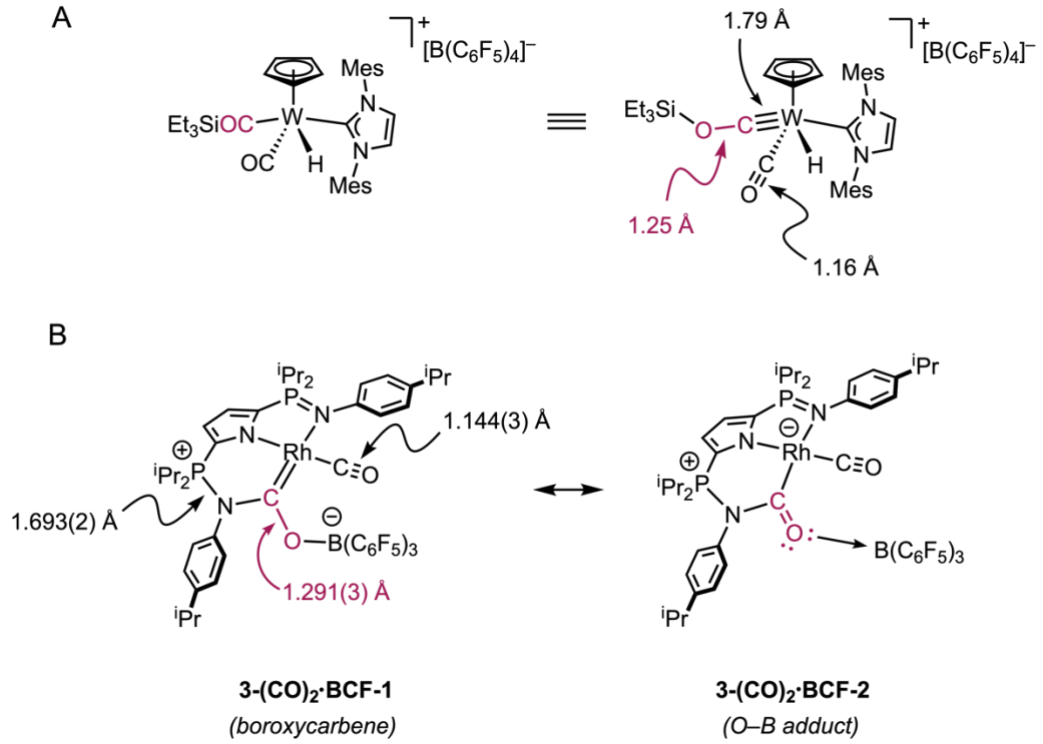


**Scheme 3.20.** (A) Product of $Et_3SiH$ activation by Bullock's cationic tungsten(II) catalyst. (B) Possible resonance structures of **3-(CO)$_2$·BCF**, illustrating both the boroxycarbene (**3-(CO)$_2$·BCF-1**) and coordinating adduct (**3-(CO)$_2$·BCF-2**) structures. Relevant bond distances shown for comparison.

With **3-(CO)$_2$·BCF** in hand, the stability of the O–B interaction was investigated. Addition of 1 equivalent of THF to a benzene-$d_6$ solution of **3-(CO)$_2$·BCF** resulted in the immediate formation of **3-(CO)$_2$**, suggesting that the B–O interaction in **3-(CO)$_2$·BCF** is weak, with $B(C_6F_5)_3$ being readily coordinated by exogenous donors. Moreover, an equilibrium mixture between **3-(CO)$_2$·BCF** + THF and **3-(CO)$_2$** + (THF)$B(C_6F_5)_3$ was not observed by NMR spectroscopy. The $^{31}$P NMR spectrum of **3-(CO)$_2$·BCF** in benzene-$d_6$ was monitored over time, revealing gradual consumption of the rhodium complex at ambient temperature ($t_{1/2} \approx 3$ h) even in the absence of THF or other coordinating species.

Heating a benzene-$d_6$ solution of **3-(CO)$_2$·BCF** at 323 K for 18 h resulted in complete conversion of starting material into three new products observed by multinuclear NMR spectroscopy. The $^{31}$P NMR spectrum of the product mixture exhibited resonances at δ 61.0 and δ 59.9 in a 1:1 ratio that were correlated by two-dimensional NMR experiments. In addition, a resonance was observed at δ 60.9, resembling the $^{31}$P NMR spectrum of an authentic sample of **3-CO** (Figure 3.11).

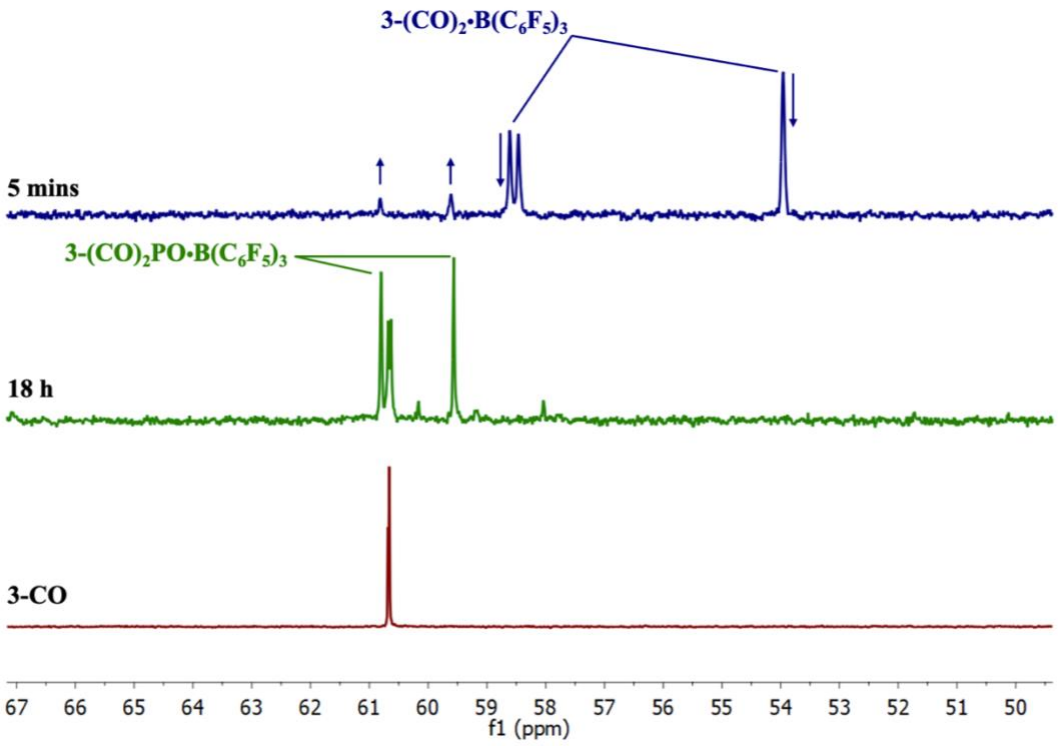


**Figure 3.11.** $^{31}$P NMR spectra of **3-(CO)$_2$·BCF** in benzene-$d_6$ after 5 minutes (top, blue trace) after 18 h (middle, green trace) and the $^{31}$P NMR spectrum of an authentic sample of monocarbonyl **3-CO** (bottom) in benzene-$d_6$.

The $^{19}$F NMR spectrum of the product mixture contained two sets of $C_6F_5$ resonances in approximately 1:1 ratio, suggesting the presence of two unique $B(C_6F_5)_3$-containing products. Notably, though, only one broad $^{11}$B signal was observed (δ −21.2). These findings are consistent with a report by Stephan that describes phosphine oxide adducts of $B(C_6F_5)_3$.[27] Thus, a rhodium center bearing two CO ligands and a

phosphinimine/phosphine oxide-borane adduct scaffold was the presumed fate of complex **3-(CO)$_2$·BCF**.

By monitoring the thermal decay of the $^{13}$C-labelled complex **3-($^{13}$CO)$_2$·BCF** in benzene-$d_6$, unambiguous assignment of the relevant products in the apparent deoxygenation pathway was possible by $^{13}$C NMR spectroscopy. The $^{13}$C{$^{31}$P} NMR spectrum of the product mixture revealed four unique $^{13}$CO resonances in an approximate 1:1:1:1 ratio, attributed to three separate $^{13}$CO-containing products, one of which appeared to possess two chemically inequivalent Rh–$^{13}$CO ligands. Specifically, two multiplets were observed at δ 184.5 (dd, $^1J_{CRh}$ = 69.7 Hz, $^2J_{CC}$ = 9.2 Hz) and 183.6 (dd, $^1J_{CRh}$ = 66.5 Hz, $^2J_{CC}$ = 9.2 Hz). In addition, a doublet was observed at δ 195.6 ($^1J_{CRh}$ = 74.5 Hz), assigned as **3-$^{13}$CO** by comparing the spectrum with that of an authentic sample of **3-CO**.

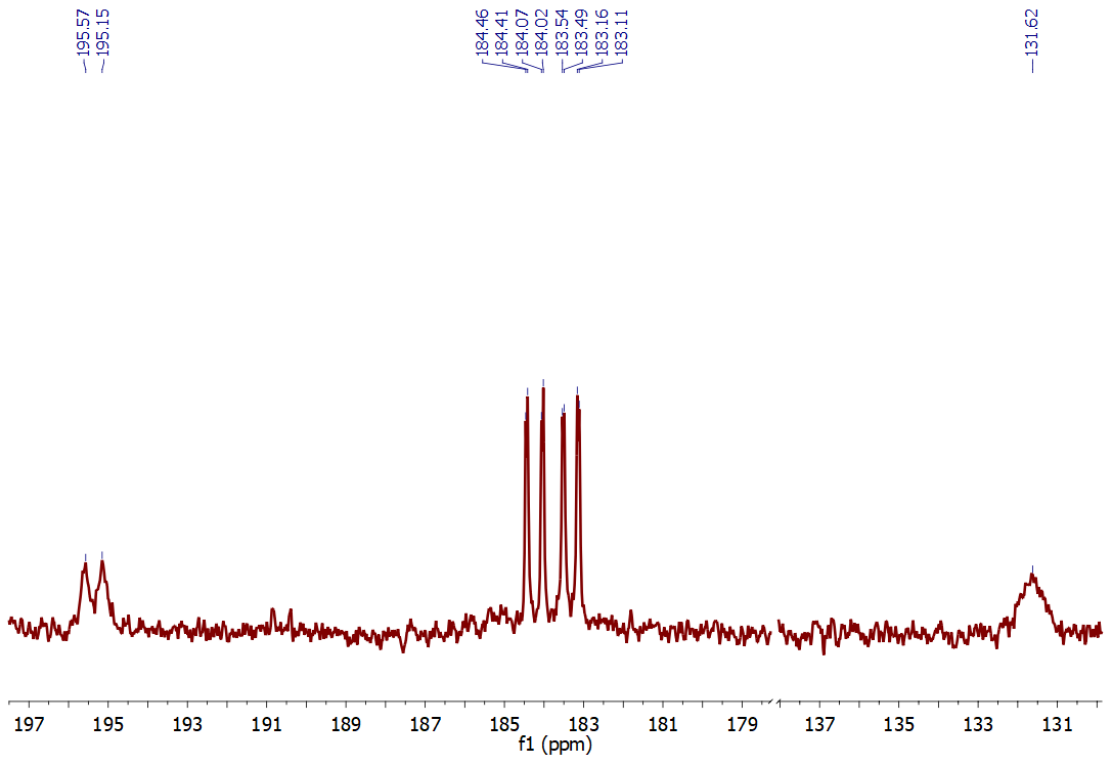


**Figure 3.12.** $^{13}$C NMR (74 MHz) spectrum of products resulting from deoxygenative metathesis. **3-($^{13}$CO)$_2$PO·BCF**, **3-$^{13}$CO**, and $^{13}$C-labelled isocyanide-B($C_6F_5$)$_3$ adduct in benzene-$d_6$ at 23 ºC.

The final $^{13}$C-labeled resonance appears as a broad singlet centered at δ 131.9, consistent with isocyanide-borane adducts described by Erker and Berke,[22] thus implying the formation of ($C_6F_5$)$_3$B←:$^{13}$C≡N(4-$^{i}$Pr$C_6H_4$) from P–N fragmentation of the phosphinimine group. The organic product of the reaction was isolated and characterized by X-ray crystallography (Figure 3.13).

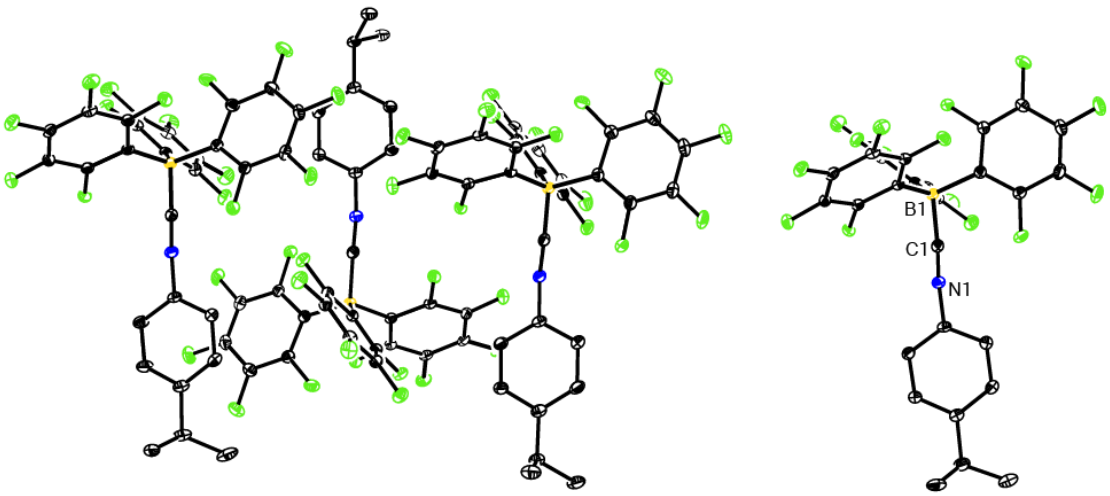


**Figure 3.13.** X-ray crystal structure of **$(C_6F_5)_3B{\cdot}CN(4\text{-}^iPrC_6H_4)$** at 30% probability ellipsoids. Hydrogen atoms and solvent molecules of recrystallization have been omitted for clarity. Four crystallographically-unique molecules (Z = 4) were found in the unit cell; metrical data correspond to the labelled molecule.

**Table 3.4.** Selected bond distances (Å) and angles (º) for $(C_6F_5)_3B{\cdot}CN(4\text{-}^iPrC_6H_4)$.

| **Parameter** | **$(C_6F_5)_3B{\cdot}CN(4\text{-}^iPrC_6H_4)$** |
|---|---|
| Bond distance (Å) | |
| B1–C1 | 1.627(3) |
| C1–N1 | 1.143(2) |
| Bond angle (º) | |
| B1–C1–N1 | 174.6(2) |

Extraction and recrystallization from pentane confirmed the identity of the rhodium carbonyl complex **3-$(CO)_2$PO·BCF** (Figure 3.14). The bonding in **3-$(CO)_2$PO·BCF** highlights the differences between phosphine oxide and phosphinimine donors insofar as no interaction was observed between the newly formed phosphine oxide and CO ligand in the presence of $B(C_6F_5)_3$. This observation may be a result of the steric inaccessibility of a hemilabile phosphinimine relative to phosphine oxide. Nevertheless, the pronounced ylidic nature of the P–N bond facilitates C–O activation as well as deoxygenative metathesis akin to aza-Wittig reactions between carbonyl substrates and P–N bonds.[27] Examination of the $^{31}$P NMR spectrum of isolated **3-$(CO)_2$PO·BCF** (Figure 3.15) matched closely with the

$^{31}$P NMR spectrum of the product mixture obtained from heating **3-(CO)$_2$·BCF** (Figure 3.11).

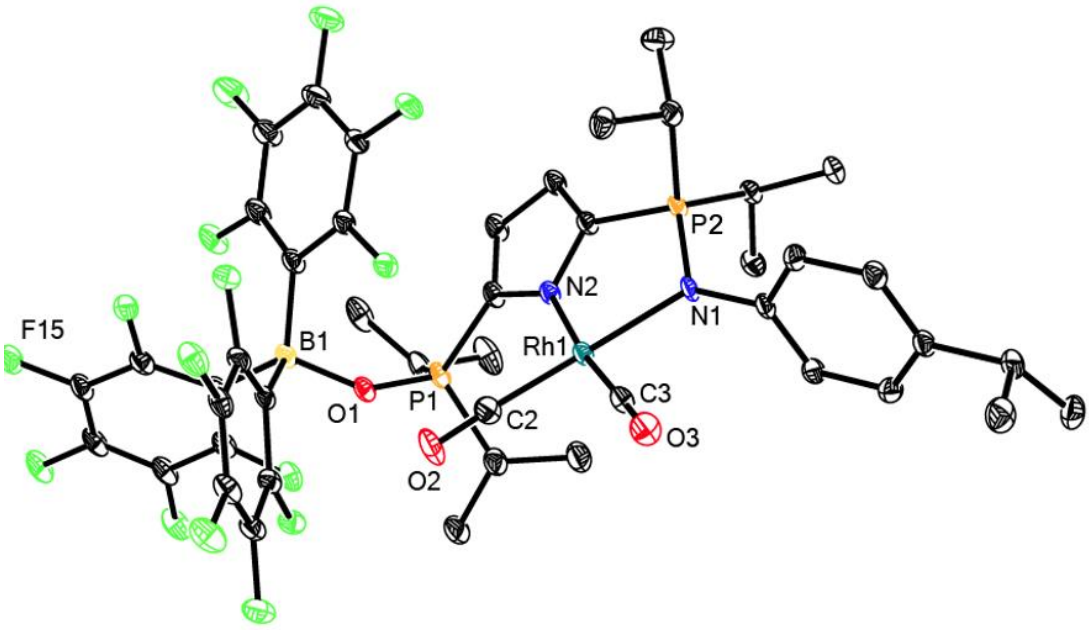


**Figure 3.14.** X-ray crystal structure of **3-(CO)$_2$PO·BCF** at 30% probability ellipsoids. Hydrogen atoms and solvent molecules of recrystallization have been omitted for clarity.

**Table 3.5.** Selected bond distances (Å) and angles (º) for **3-(CO)$_2$PO·BCF**.

| **Parameter** | **3-(CO)$_2$PO·BCF** |
|---|---|
| Bond distance (Å) | |
| P1–O1 | 1.532(2) |
| P2–N1 | 1.613(2) |
| C3–O3 | 1.127(3) |
| C2–O2 | 1.135(4) |
| Rh1–C2 | 1.850(3) |
| Rh1–C3 | 1.865(3) |
| Rh1–N1 | 2.070(2) |
| Rh1–N2 | 2.110(2) |
| O1–B1 | 1.535(3) |
| Bond angle (º) | |
| P1–O1–B1 | 147.3(2) |

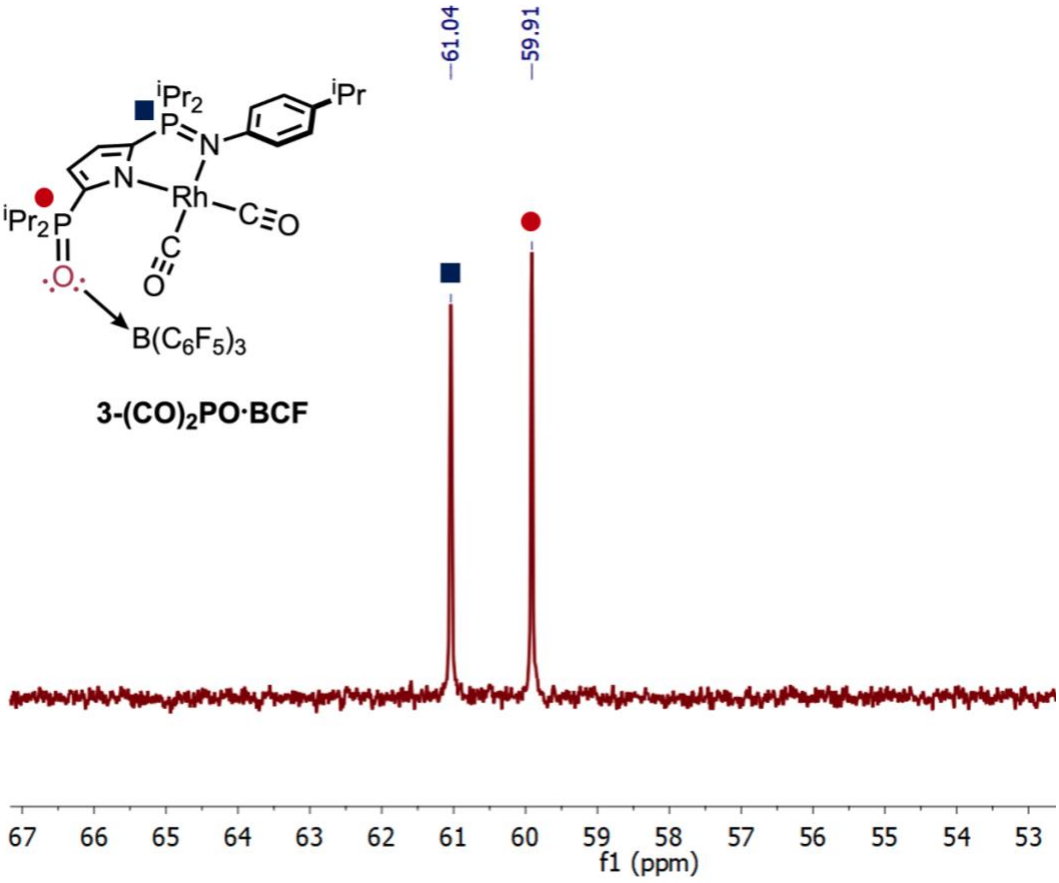


**Figure 3.15.** $^{31}$P NMR (125 MHz) spectrum of **3-(CO)$_2$PO·BCF** in benzene-$d_6$ at 23 ºC.

The distribution of products are reasonably explained by a deoxygenative metathesis reaction between CO and the phosphinimine in complex **3-(CO)$_2$·BCF** to liberate $(C_6F_5)_3B{\leftarrow}$:CN(4-$^i$Pr$C_6H_4$) and the putative 14-electron intermediate [$^i$Pr$_2$P═N(4-$^i$Pr$C_6H_4$)$C_4H_2$NiPr$_2$P═O]Rh(CO), which could react rapidly with a second equivalent of **3-(CO)$_2$·BCF** by intermetallic CO transfer (*vide supra*) to afford the phosphine oxide–borane adduct **3-(CO)$_2$PO·BCF** and **3-CO** in a 1:1 ratio (Scheme 3.5). Notably, the same distribution of products was observed after repeating the reaction multiple times in either benzene-$d_6$ or toluene-$d_8$.

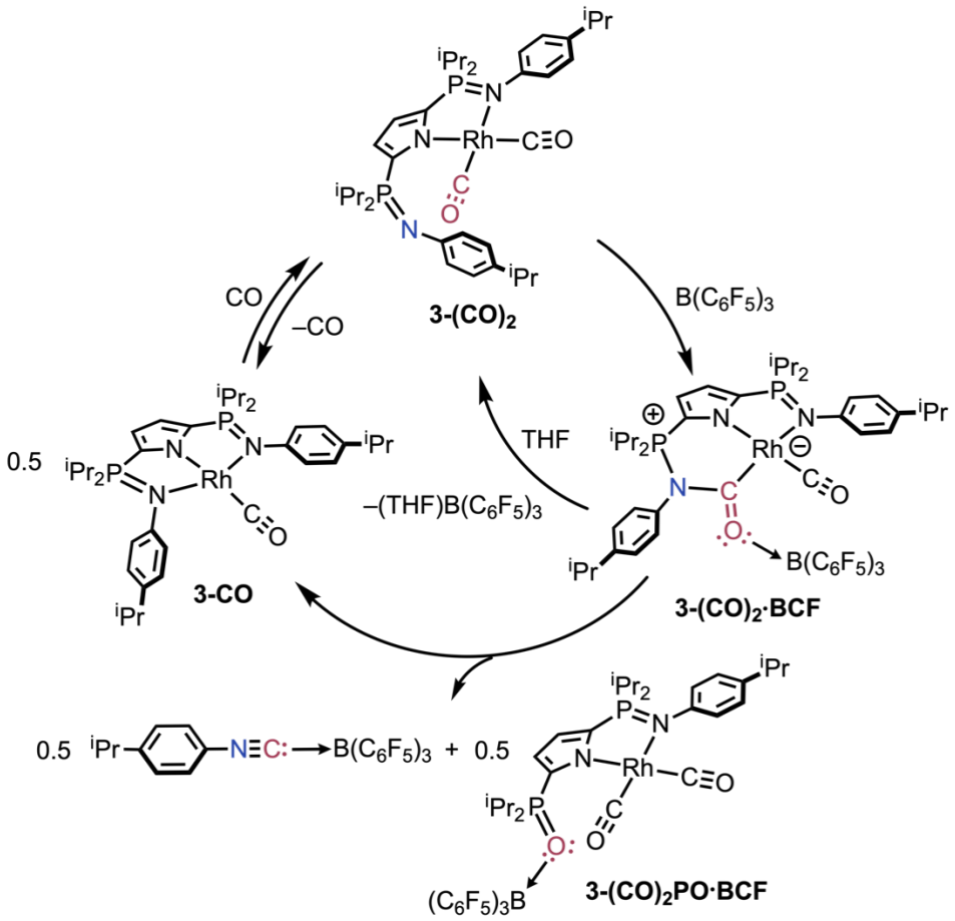


**Scheme 3.21.** Proposed mechanism for the deoxygenative metathesis of CO and synthetic cycle for the interconversion of relevant species.

Recognizing that deoxygenative metathesis proceeds gradually at ambient temperature, the reactivity of **3-(CO)$_2$·BCF** was evaluated to better understand the relative rates of metathesis compared with small molecule activation. Recognizing that THF rapidly displaces B(C$_6$F$_5$)$_3$ from the carbonyl oxygen atom in **3-(CO)$_2$·BCF**, it was reasoned that other oxygen-containing molecules might lead to sequestration of B(C$_6$F$_5$)$_3$. An NMR tube was charged with **3-(CO)$_2$·BCF** and dissolved in benzene-$d_6$. A small excess (5 equivalents) of distilled H$_2$O was then added, accompanied by an immediate color change from dark yellow to orange. In the downfield region of the $^1$H NMR spectrum, a

doublet was observed ($^2J_{HP}$ = 10.5 Hz) at δ 9.25, assigned as a protonated phosphinimine similar to that observed in **2-Rh$_2$** (Chapter 2). When the $^{31}$P nucleus was decoupled from $^1$H the doublet collapsed to a singlet, further supporting this assignment. The downfield chemical shift can be reasonably explained by a hydrogen bonding interaction between the protonated phosphinimine –P=N*H*$^+$ and either free $H_2O$ or the *O*H group of the putative anion (HO)B($C_6F_5$)$_3^-$. Notably, water did not displace the borane but was instead deprotonated in a reaction that resembles FLP chemistry. Cooperative activation of the O–H bond in water by the phosphinimine/borane pair inspired additional bond activation reactions.

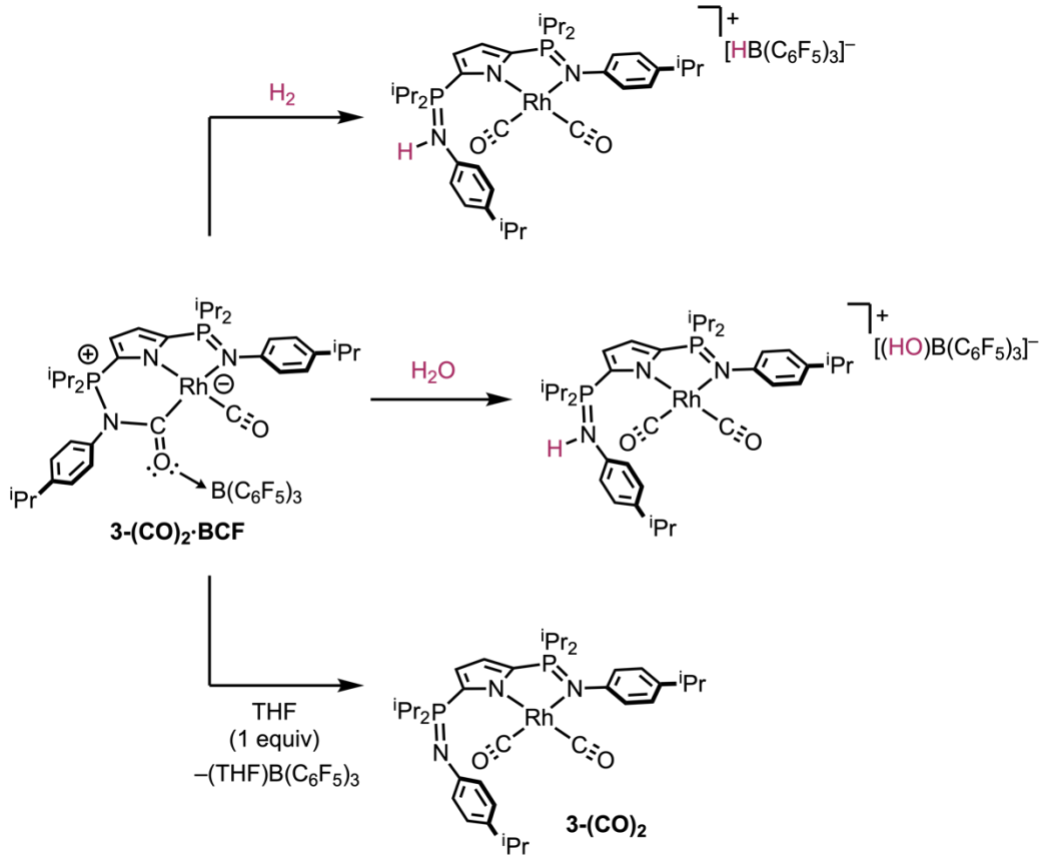


**Scheme 3.22.** Reaction of **3-(CO)$_2$·BCF** with $H_2$ (top), $H_2O$ (middle), and THF (bottom).

When a benzene-$d_6$ solution of **3-(CO)$_2$·BCF** in a J. Young NMR tube was pressurized with 4 atm of $H_2$, the solution turned rose-gold over the course of 16 h. Examination of the $^{31}$P NMR spectrum showed clean conversion of **3-(CO)$_2$·BCF** to an asymmetric product with inequivalent phosphinimines (Figure 3.16) with resonances at δ 62.7 and δ 47.4. The $^1$H NMR spectrum revealed a well-defined doublet at δ 4.58 ($^2J_{HP}$ = 8.5 Hz) which, when decoupled from $^{31}$P, collapsed to a broad singlet (Figure 3.17). Multinuclear NMR spectroscopy ($^{19}$F, $^{11}$B) suggested formation of the hydridoborate anion $HB(C_6F_5)_3^-$ consistent with FLP reactivity between phosphinimine and borane partners. Presumably, dihydrogen was heterolytically cleaved, delivering a proton ($H^+$) to the phosphinimine nitrogen and a hydride ($H^-$) to $B(C_6F_5)_3$. The chemical shift of the proton assigned to the protonated phosphinimine is markedly upfield from the reaction of **3-(CO)$_2$·BCF** with $H_2O$. The foregoing results indicate that spectroscopic assignments of protonated phosphinimines are sensitive to hydrogen-bonding interactions between the solvent or the counter anion generated in the reaction.

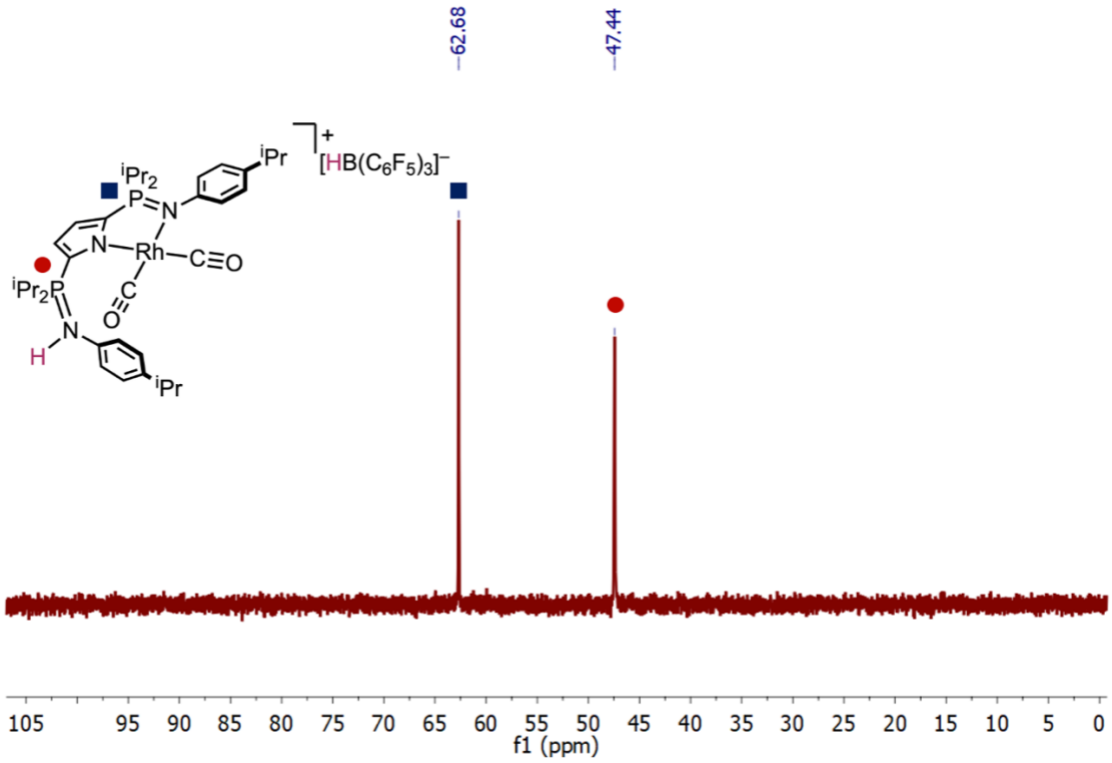


**Figure 3.16.** $^{31}$P NMR (124 MHz) spectrum of the reaction between **3-(CO)$_2$·BCF** and 4 atm $H_2$ in benzene-$d_6$ at 23 ºC and proposed structure of the product.

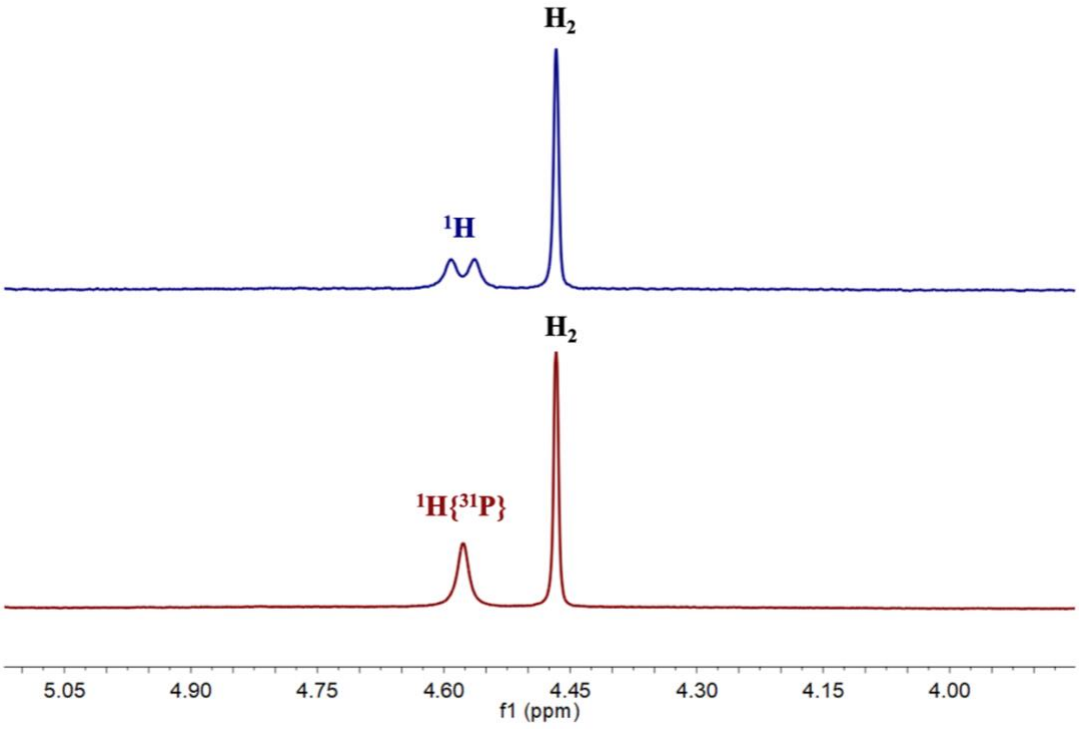


**Figure 3.17.** $^{1}H$ (top) and $^{1}H\{^{31}P\}$(bottom) NMR (300 MHz) spectra of the reaction between **3-(CO)$_2$·BCF** and 4 atm $H_2$ in benzene-$d_6$ at 23 ºC.

### 3.4. Conclusions

The $^{iPr}$NNN ligand reported herein serves as a platform to study the activation and deoxygenative metathesis of CO at ambient temperature. The metathetical reaction between the phosphinimine P–N ylide and the CO multiple bond was confirmed by isotopic labeling with $^{13}CO$, along with characterization of the labeled isocyanide $(C_6F_5)_3B\leftarrow:^{13}C\equiv N(4\text{-}^{i}PrC_6H_4)$. Cooperative action of the phosphinimine and borane Lewis acid appear to promote the deoxygenation reaction with minimal influence from the metal center. The foregoing hypothesis involves the cooperative engagement of CO by a dissociated phosphinimine and Lewis acid, raising questions as to whether an external additive is required to promote metal-ligand cooperation in the context of small molecule

activation. The remaining chapters of this thesis will focus on leveraging the aforementioned metal-ligand cooperation in the absence of activators.

### 3.5. References


**1.** Lu, Q.; Rosen, J.; Zhou, Y.; Hutchings, G. S.; Kimmel, Y. C.; Chen, J. G.; Jiao, F. A selective and efficient electrocatalyst for carbon dioxide reduction. *Nat. Commun.* **2014**, *5*, 3242.

**2.** (a) Muetterties, E. L.; Stein, J. Mechanistic Features of Catalytic Carbon Monoxide Hydrogenation Reactions. *Chem. Rev.* **1979**, *79*, 479–490. (b) Shriver, D. F.; Sailor, M. J. Transformations of Carbon Monoxide and Related Ligands on Metal Ensembles. *Acc. Chem. Res.* **1988**, *21*, 374–379. (c) Neithamer, D. R.; LaPointe, R. E.; Wheeler, T. A.; Richeson, D. S.; VanDuyne, G. D.; Wolczanski, P. T. Carbon Monoxide Cleavage by (silox)3Ta (silox = tert-Bu3SiO-): physical, theoretical, and mechanistic Investigations. *J. Am. Chem. Soc.* **1989**, *111*, 9056–9072. (d) Bailey, P. J. The cleavage of a cluster carbonyl C≡O bond by trifluoromethanesulphonic anhydride. *J. Organomet. Chem.* **1991**, *420*, C21–C23. (e) Chisholm, M. H.; Hammond, C. E.; Johnston, V. J.; Streib, W. E.; Huffman, J. C. Metal alkoxides: models for metal oxides. 17. Reductive cleavage of carbon monoxide to carbide and oxide by ditungsten and tetratungsten alkoxides. Crystal and molecular structures of W4(.mu.4-C)(OCH2-c-Pen)14, W4(.mu.4-C)(O)(OCH2-tert-Bu)12 and W4(.mu.4-C)(O)(O-i-Pr)12. *J. Am. Chem. Soc.* **1992**, *114*, 7056–7065. (f) Miller, R. L.; Wolczanski, P. T. Carbide formation via carbon monoxide dissociation across a tungsten-tungsten triple bond. *J. Am. Chem. Soc.* **1993**, *115*, 10422–10423. (g) Miller, R. L.; Toreki, R.; LaPointe, R. E.; Wolczanski, P. T.; Van Duyne, G. D.; Roe, C. Syntheses, carbonylations, and dihydrogen exchange studies of monomeric and dimeric silox (tert-Bu3SiO-) hydrides of tantalum: structure of [(silox)2TaH2]2. *J. Am. Chem. Soc.* **1993**, *115*, 5570–5588. (h) Calderazzo, F.; Englert, U.; Guarini, A.; Marchetti, F.; Pampaloni, G.; Segre, A. [$Zr_3Cp_2(O_2CN{i}Pr_2)_6(\mu\text{-}O)(\mu\text{-}CCO)$], the First Crystallographically Established Ketenylidene Complex; A Model for CO Reductive Cleavage on Metal Surfaces. *Angew. Chem., Int. Ed. Engl.* **1994**, *33* (11), 1188–1189. (i) Busetto, L.; Marchetti, F.; Zacchini, S.; Zanotti, V. CO Cleavage Promoted by Acetylide Addition to Vinyliminium Diiron Complexes. *Eur. J. Inorg. Chem.* **2006**, *2006*, 285–289.

**3.** Braunschweig, H.; Celik, M. A.; Dewhurst, R. D.; Kachel, S.; Wennemann, B. Mild and Complete Carbonyl Ligand Scission on a Mononuclear Transition Metal Complex. *Angew. Chem., Int. Ed.* **2016**, *55*, 5076–5080.

**4.** 1076.38 ± 0.67 kJ $mol^{-1}$ (257.26 ± 0.16 kcal $mol^{-1}$): Luo, Y.-R. *Comprehensive Handbook of Chemical Bond Energies*; Taylor and Francis: Boca Raton, FL, **2007**.

**5.** Peters, J. C.; Odom, A. L.; Cummins, C. C. A terminal molybdenum carbide prepared by methylidyne deprotonation. *Chem. Commun.* **1997**, 1995–1996.

**6.** Buss, J. A.; Agapie, T. Four-electron deoxygenative reductive coupling of carbon at a single metal site. *Nature* **2016**, *529*, 72–75.

**7.** Buss, J. A.; Agapie, T. Mechanism of Molybdenum-Mediated Carbon Monoxide Deoxygenation and Coupling: Mono- and Dicarbyne Complexes Precede C−O Bond Cleavage and C−C Bond Formation. *J. Am. Chem. Soc.* **2016**, *138*, 16466–16477.

**8.** West, N. M.; Miller, A. J. M.; Labinger, J. A.; Bercaw, J. E. Homogeneous syngas conversion. *Coord. Chem. Rev.* **2011**, *255*, 881–898.

**9.** Miller, A. J. M.; Labinger, J. A.; Bercaw, J. E. Homogeneous CO Hydrogenation: Dihydrogen Activation Involves a Frustrated Lewis Pair Instead of a Platinum Complex. *J. Am. Chem. Soc.* **2010**, *132*, 3301–3303.

**10.** Miller, A. J. M.; Labinger, J. A.; Bercaw, J. E. Homogeneous CO Hydrogenation: Ligand Effects on the Lewis Acid-Assisted Reductive Coupling of Carbon Monoxide. *Organometallics* **2010**, *29*, 4499–4516.

**11.** Miller, A. J. M.; Labinger, J. A.; Bercaw, J. E. Reductive Coupling of Carbon Monoxide in a Rhenium Carbonyl Complex with Pendant Lewis Acids. *J. Am. Chem. Soc.* **2008**, *130*, 11874–11875.

**12.** Haňninen, M.M.; Zamora, M.T.; MacNeil, C.S.; Knott, J.P.; Hayes, P. G. Elucidation of the resting state of a rhodium NNN-pincer hydrogenation catalyst that features a remarkably upfield hydride $^{1}$H NMR chemical shift. *Chem. Commun.* **2016**, *52*, 586–589.

**13.** Jiang, C.; Stephan, D. W. Phosphinimine−borane combinations in frustrated Lewis pair chemistry. *Dalton Trans.* **2013**, *42*, 630–637.

**14.** Stephan, D. W. The broadening reach of frustrated Lewis pair chemistry. *Science* **2016**, 354, aaf7229.

**15.** Boone, M. P.; Stephan, D. W. Ancillary Metal Centers in Frustrated Lewis Pair Chemistry: Ruthenium Acetylide as a Lewis Base in the Activation of $CO_2$, Aldehyde, and Alkyne. *Organometallics* **2014**, *33*, 387–393.

**16.** Boone, M. P.; Stephan, D. W. A Ru−$\eta^6$-Arene Complex as a C-Based Lewis Acid in the Activation of Hydrogen and Hydrogenation Catalysis. *J. Am. Chem. Soc*. **2013**, *135*, 8508–8511.

**17.** Tutusaus, O.; Ni, C.; Szymczak, N. K. A Transition Metal Lewis Acid/Base Triad System for Cooperative Substrate Binding. *J. Am. Chem. Soc*. **2013**, *135*, 3403–3406.

**18.** Lambic, N. S.; Sommer, R. D.; Ison, E. A. Transition-Metal Oxos as the Lewis Basic Component of Frustrated Lewis Pairs. *J. Am. Chem. Soc.* **2016**, *138*, 4832–4842.

**19.** The previously reported complex ($^{Ph}$NNN)Rh(CO)$_2$ features similar $^{31}$P chemical shifts for coordinated (δ 32.3) and free (δ −2.9) phosphinimine donors.

**20.** Horton, A. D. Direct Observation of β-Methyl Elimination in Cationic Neopentyl Complexes: Ligand Effects on the Reversible Elimination of Isobutene. *Organometallics* **1996**, *15*, 2675–2677.

**21.** Blackwell, J. M.; Piers, W. E.; Parvez, M.; McDonald, R. Solution and Solid-State Characteristics of Imine Adducts with Tris(pentafluorophenyl)borane. *Organometallics* **2002**, *21*, 1400–1407.

**22.** Jacobsen, H.; Berke, H.; Döring, S.; Kehr, G.; Erker, G.; Fröhlich, R.; Meyer, O. Lewis Acid Properties of Tris- (pentafluorophenyl)borane. Structure and Bonding in L–B($C_6F_5$)$_3$ Complexes. *Organometallics* **1999**, *18*, 1724–1735.

**23.** Fryzuk, M. D.; Mylvaganam, M.; Zaworotko, M. J.; MacGillivray, L. R. Reduction of Carbon Monoxide by Tandem Electron Transfer and Migratory Insertion of a Masked Zirconium- (IV) Hydride. Formation of a Zirconium Formyl−Ylide Complex. *Organometallics* **1996**, *15*, 1134–1138.

**24.** (a) Dioumaev, V. K.; Szalda, D. J.; Hanson, J.; Franz, J. A.; Bullock, R. M. An N-heterocyclic carbene as a bidentate hemilabile ligand: a synchrotron X-ray diffraction and density functional theory study. *Chem. Commun*. **2003**, 1670−1671. (b) Wu, F.; Dioumaev, V. K.; Szalda, D. J.; Hanson, J.; Bullock, R. M. A Tungsten Complex with a Bidentate, Hemilabile N-Heterocyclic Carbene Ligand, Facile Displacement of the Weakly Bound W−(C=C) Bond, and the Vulnerability of the NHC Ligand toward Catalyst Deactivation during Ketone Hydrogenation. *Organometallics* **2007**, *26*, 5079−5090.

**25.** Fuchs, J.; Irran, E.; Hrobárik, P.; Klare, H. F. T.; Oestreich, M. Si–H Bond Activation with Bullock's Cationic Tungsten(II) Catalyst: CO as Cooperating Ligand. *J. Am. Chem. Soc.* **2019**, *141*, 18845–18850.

**26.** The P1−N1 bond distance (1.693(2) Å) in complex 3 was compared to 410 related structures in the Cambridge Structural Database using Mogul: mean 1.58(3) Å, minimum 1.506(5) Å, maximum 1.687(7) Å. Bruno, I. J.; Cole, J. C.; Kessler, M.; Luo, J.; Motherwell, W. D. S.; Purkis, L. H.; Smith, B. R.; Taylor, R.; Cooper, R. I.; Harris, S. E.; Orpen, A. G. Retrieval of Crystallographically- Derived Molecular Geometry Information. *J. Chem. Inf. Comput. Sci.* **2004**, *44*, 2133–2144.

**27.** Neu, R. C.; Otten, E.; Lough, A.; Stephan, D. W. The synthesis and exchange chemistry of frustrated Lewis pair−nitrous oxide complexes. *Chem. Sci.* **2011**, *2*, 170–176.

## Chapter 4: Accessing Neutral Base-stabilized Rhodium Silylenes by Metal-Ligand Cooperation*

### 4.1. Abstract

Divergent reactivity of organometallic rhodium complexes is reported, leading to the isolation of neutral rhodium silylenes obtained by dehydrogenation of the corresponding hydrosilane. Addition of $PhRSiH_2$ (R = H, Ph) or $Ph_3SiH$ to the rhodium cyclooctene complex ($^{iPr}$NNN)Rh(COE) (**2-COE**; $^{iPr}$NNN = 2,5-[$^{i}Pr_2P$=N(4-$^{i}PrC_6H_4$)]$_2$N($C_6H_2$)$^-$, COE = cyclooctene) resulted in the oxidative addition of an Si–H bond, providing rhodium silyl hydride complexes ($^{iPr}$NNN)Rh(H)SiHRPh (R = H, **4-SiH$_2$Ph**; Ph, **4-SiHPh$_2$**) or ($^{iPr}$NNN)Rh(H)$SiPh_3$ (**4-SiPh$_3$**) along with loss of cyclooctene. When the carbonyl complex ($^{iPr}$NNN)Rh(CO) (**3-CO**) was treated with hydrosilanes, base-stabilized rhodium silylenes κ$^2$-*N*,*N*-($^{iPr}$NNN)(CO)RhSiRPh (R = H, **4-SiHPh**; Ph, **4-SiPh$_2$**) were isolated and characterized by multinuclear NMR spectroscopy ($^1$H, $^{31}$P, $^{13}$C, $^{29}$Si) and X-ray crystallography. Both silylene species feature short Rh–Si bonds [2.262(1), **4-SiHPh**; 2.2702(7), **4-SiPh$_2$**] that agree well with the gas-phase DFT-computed structures. Examination of the natural bonding orbitals (NBOs) in **4-SiHPh** and **4-SiPh$_2$**, together with second-order perturbation theory analysis, suggest Si-based acceptor orbitals are stabilized by delocalization of electron density from phosphinimine lone pairs along with Rh-based d-orbitals of π-symmetry. The overall reaction led to a change in the $^{iPr}$NNN ligand bonding mode (κ$^3$→κ$^2$) with deuterium labelling experiments supporting loss of $D_2$ from the deuterosilane $PhSiRD_2$.

*Adapted from: MacNeil, C. S.; Hayes, P. G. *Chem. Eur. J.* **2019**, *25*, 8203-8207. with permission from John Wiley and Sons.

## 4.2. Introduction

Essential to the production of organosilicon compounds $R_nSiH_{4-n}$ (n = 1, 2, 3), hydrosilation (HS) of carbon-element multiple bonds is a principal application of platinum group metal catalysis.[1] Homogeneous catalysts based on rhodium provide high stereo-, regio-, and enantioselectivities, particularly in the HS of ketones.[2] Oxidative addition of a Si–H bond to well-defined complexes of Rh is a common feature of such processes; for example, Ojima demonstrated it to be the first step in the HS of ketones using Wilkinson's catalyst, $(PPh_3)_3RhCl$ (**I**, Scheme 4.1).[3] According to Ojima, *O*-coordination of the ketone (or aldehyde) substrate to the rhodium center (**II**) led to insertion of the carbonyl functionality into the Rh–Si bond (**III**). Reductive elimination produces a silyl ether and the active rhodium catalyst is regenerated (**IV**). Inconsistencies associated with the Ojima cycle have been highlighted in several follow-up mechanistic studies on Rh-catalyzed HS of ketones; most notably perhaps is that the mechanism does not account for the observed rate increase on going from mono- to dihydrosilanes (e.g. $R_2SiH_2 > R_3SiH$). Zheng and Chan proposed an alternative mechanism wherein the ketone oxygen binds selectively to the silyl silicon atom instead of the Rh center.[2c] In both cases, loss of ligand (*e.g.* $PPh_3$) and oxidative addition of the Si–H bond occur before the ketone substrate interacts with the active catalyst. Insertion of the incipient carbonyl group into the Si–H generates an alkoxysilylrhodium intermediate which undergoes reductive elimination with the rhodium hydride (Scheme 4.2).

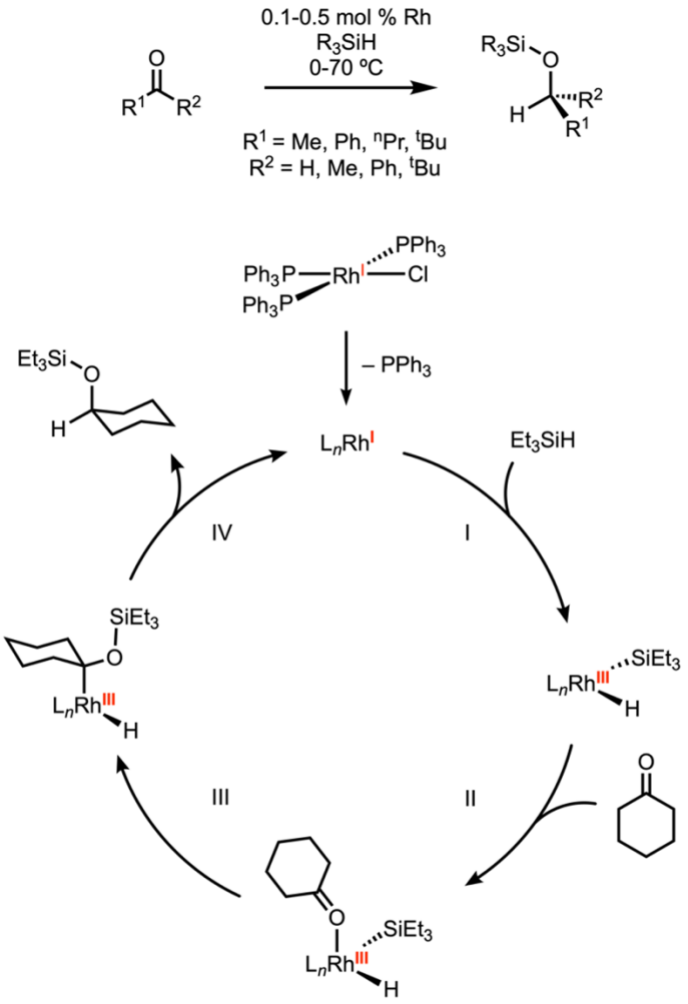


**Scheme 4.23.** Rh-catalyzed hydrosilation of cyclohexanone proposed by Ojima.[3] Step I: oxidative addition of triethylsilane. Step II: *O*-coordination of cyclohexanone to the Rh(III) center. Step III: Insertion of the C=O double bond into the Rh–Si bond. Step IV: reductive elimination and regeneration of the active catalyst.

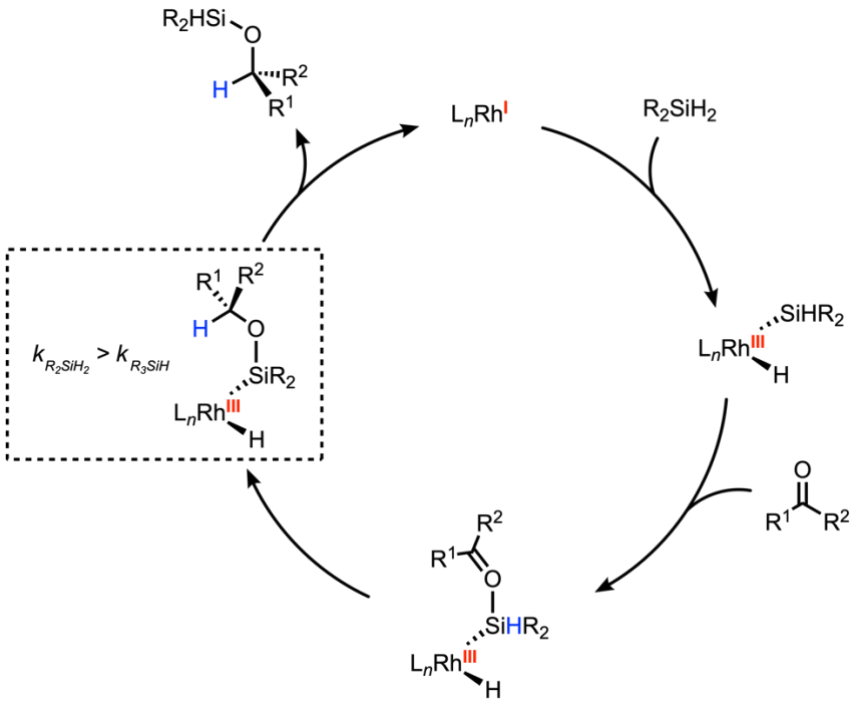


**Scheme 4.24.** Rh-catalyzed hydrosilation of ketones proposed by Zheng and Chan.[2c] This mechanism deviates from the Ojima mechanism in the locus of ketone coordination (Si vs. Rh). Secondary hydrosilanes ($R_2SiH_2$) translated to higher rates of reaction compared to tertiary hydrosilanes ($R_3SiH$).

Building on these early reports from Ojima, Zheng, and Chan,[2,3] additional mechanisms have been proposed for ketone HS wherein the general form of the hydrosilane is either $R_2SiH_2$ or $RSiH_3$ (a *secondary* or *primary* silane). Specifically, the HS of acetophenone catalyzed by cationic rhodium oxazoline-*N*-heterocyclic carbene chelates showed an inverse KIE ($k_H/k_D$ = 0.8) for $Ph_2SiH_2$ and $Ph_2SiD_2$.[4] For an inverse KIE to be observed, a rate-determining C–H/D forming step must take place *before* reductive elimination and catalyst regeneration. Accordingly, the authors proposed a pathway that invokes a transient, but key, rhodium silylene dihydride $[L_nRh(H)_2{=}SiR_2]^+$ intermediate, resulting from consecutive Si–H activation or "double silicon–hydrogen activation" (Scheme 4.3). Following oxidative addition of the first Si–H bond to the Rh center, the second Si–H bond is cleaved by α-H migration from Si to Rh. DFT studies by Gade and

Hofmann were in accord with experiment, supporting this silylene-based mechanism over the established mechanisms of Ojima, Zheng and Chan.[5] Following the disclosure of Gade's proposed mechanism in 2009, experimental work by Kühn, Herrmann, and co-workers provided supporting evidence that rhodium silylenes are key intermediates in ketone HS catalysis.[6] Despite mounting evidence supporting the intermediacy of rhodium silylenes, a structurally characterized example remained elusive at the outset of this thesis work, inspiring the following studies.

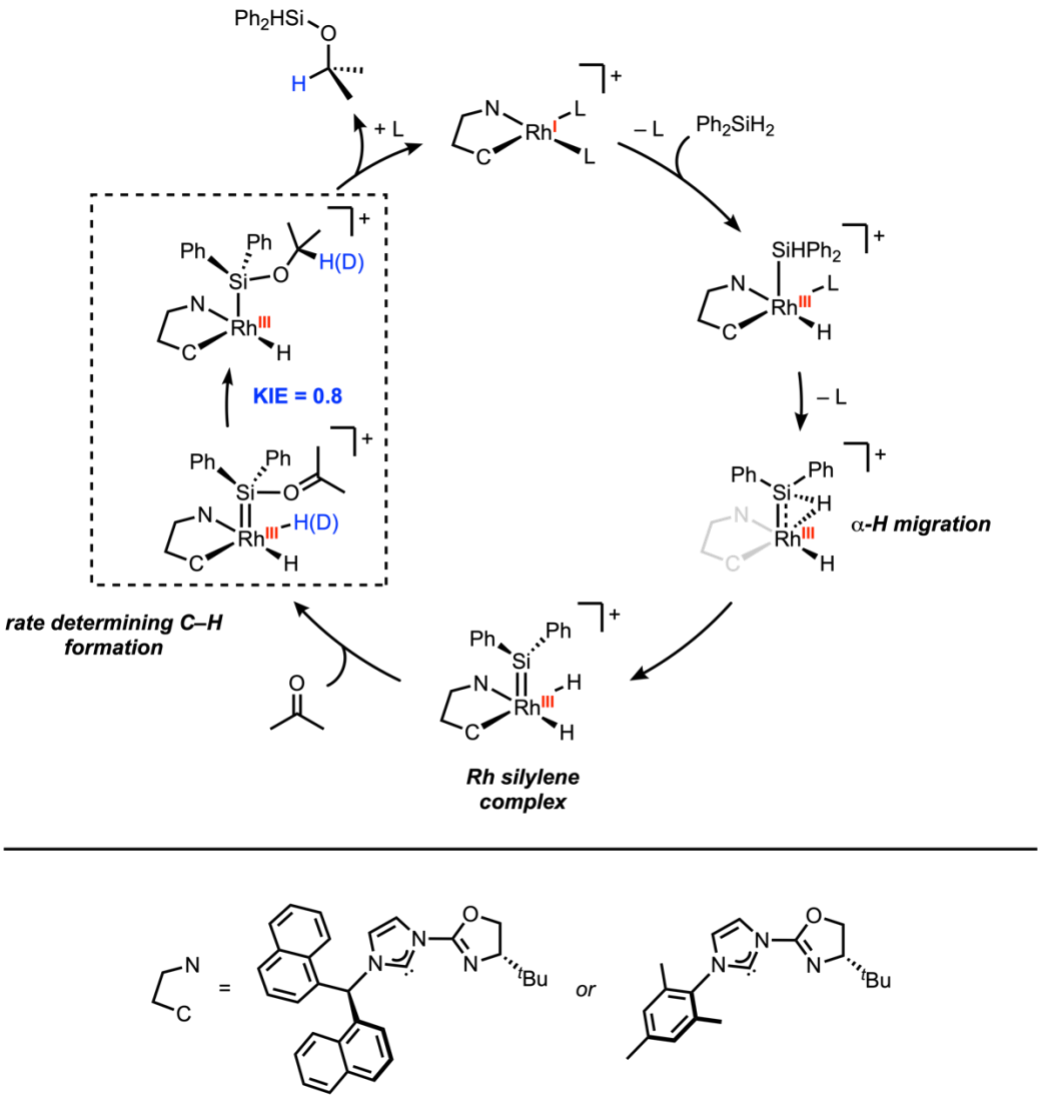


**Scheme 4.25.** Rh-catalyzed hydrosilation of ketones proposed by Gade.[4,5] A rhodium silylene dihydride species is formed by α-H migration from Si to Rh. The rate-determining step is C–H bond formation, supported experimentally by an inverse KIE of 0.8.

Beyond the relevance to HS catalysis, the reactivity, structure, and bonding of an isolable rhodium silylene is of fundamental interest. Following the isolation of donor-stabilized complexes of Ru and Fe,[7] synthetic methods were developed in order to access reactive silylenes for a host of transition metals.[8] Tilley and co-workers have shown that α-H migration from Si to a metal center (a 1,2-shift) can be promoted by abstraction of

either a methide ($CH_3^-$) or hydride ($H^-$) ligand with $B(C_6F_5)_3$, generating cationic silylenes from silyl complexes of Pt and Ir (Scheme 4.4).[9,10]

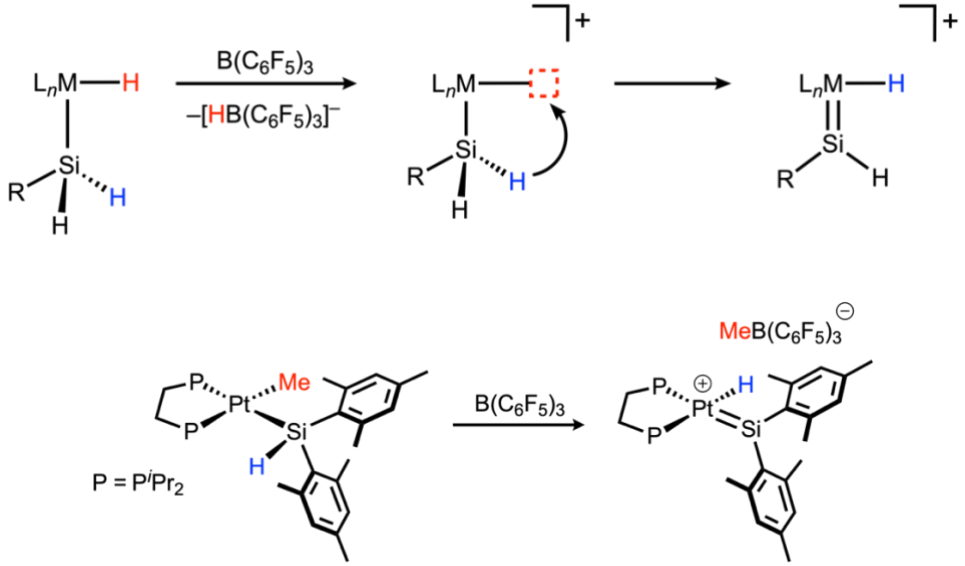


**Scheme 4.26. Generic route to** access transition metal silylenes by hydride ($H^-$), Si–H, or methide ($CH_3^-$) abstraction using $B(C_6F_5)_3$.[9]

Such α-H migration processes could serve as a promising route to rhodium silylenes, given the ubiquity of rhodium silyl hydride complexes that can be easily prepared by routine oxidative addition reactions of Si–H bonds.[1] Along these lines, Sadow and co-workers employed this strategy to generate the cationic Rh silylene [{κ$^3$-*N*,*Si*,*C*-PhB(OxMe$_2$)(OxMe$_2$SiHPh)ImMes}Rh(H)CO][HB(C$_6$F$_5$)$_3$] (OxMe$_2$ = 4,4-dimethyl-2-oxazoline; ImMes = 1-mesitylimidazole) from the addition of $B(C_6F_5)_3$ to the neutral rhodium silyl hydride {PhB(OxMe$_2$)$_2$ImMes}RhH(SiH$_2$Ph)CO (Scheme 4.5). Comprehensive NMR spectral data provided evidence for a silylene Si atom stabilized by coordination from a borate-linked oxazoline donor.[11] The NMR data corresponding to Sadow's rhodium silylene provided a useful reference point for the purpose of comparing $^{29}$Si chemical shifts (cf. δ 6.6) in this thesis work (*vide infra*). Furthermore, these results

showed that directed α-H migration and related strategies may lead to the isolation and structural characterization of catalytically important rhodium silylenes.

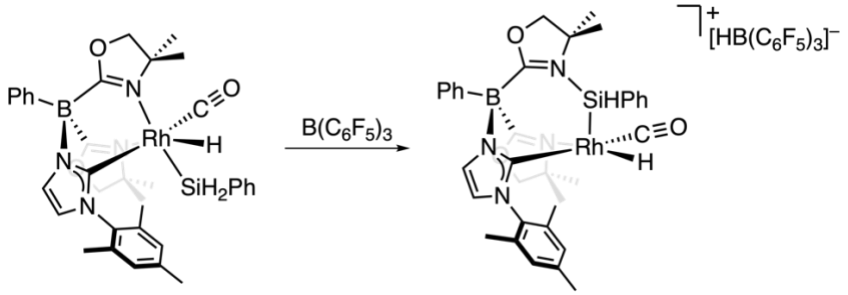


**Scheme 4.27.** Synthesis of an oxazoline-coordinated cationic Rh silylene by Sadow and co-workers (an oxazoline-component of the ligand was made transparent for clarity).[11]

Following a conceptually-related strategy, Huertos and co-workers employed a silyl-bridged pincer scaffold, and showed by NMR spectroscopy that a molecule of $PPh_3$ stabilizes the Si atom of a cationic dihydrido-Rh silylene complex $\{Rh(H)_2[Si(PPh_3)(o\text{-}C_6H_4SMe)_2](PPh_3)\}[BArF_{24}]$ (Scheme 4.6.).[12] Reactivity studies of this silylene showed that benzophenone was reduced to form the corresponding alkoxysilyl-Rh complex $\{Rh(H)[Si(OCHPh2)(o\text{-}C_6H_4SMe)_2](PPh_3)\}[BArF_{24}]$ in line with the proposed mechanism by Gade and Hofmann (Scheme 4.3).[4,5] This recent work emphasizes the ongoing interest in studying rhodium silylenes as elusive intermediates in hydrosilation over the past decade. Attempts to synthesize and characterize such species are herein disclosed.

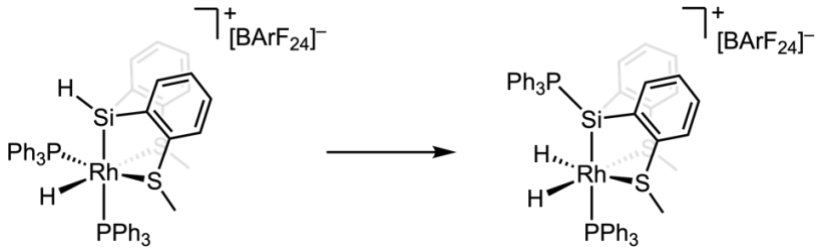


**Scheme 4.28.** Generation of a phosphine-stabilized Rh silylene by Huertos and co-workers (a portion of the ligand was made transparent for clarity).[12]

### 4.3. Results and Discussion

Rhodium complexes bearing phosphinimine donors as part of a monoanionic $^{R}$NNN ligand, ($^{R}$NNN = 2,5-[$R_2P$=N(4-$^{i}$Pr$C_6H_4$)]$_2$N($C_4H_2$)$^-$, R = Ph, $^{i}$Pr) have been shown to facilitate cooperative bond activation of $H_2$ and CO (Chapters 2 and 3, respectively).[13] The ylidic nature of the P−N bond results in strongly basic N donors capable of stabilizing electrophilic metals and main group functionalities.[14] Recognizing that transition metal silylenes are defined by the pronounced Lewis acidity of the Si atom,[8] precursor Rh silyl hydride complexes bearing a strongly-donating NNN ligand were targeted. A toluene solution of ($^{iPr}$NNN)Rh(COE) (**2-COE**) was combined with 1 equivalent of either $Ph_3SiH$, $Ph_2SiH_2$, or $PhSiH_3$ and stirred for 1 hour at ambient temperature leading to Si−H oxidative addition products along with the elimination of cyclooctene (Scheme 4.7).

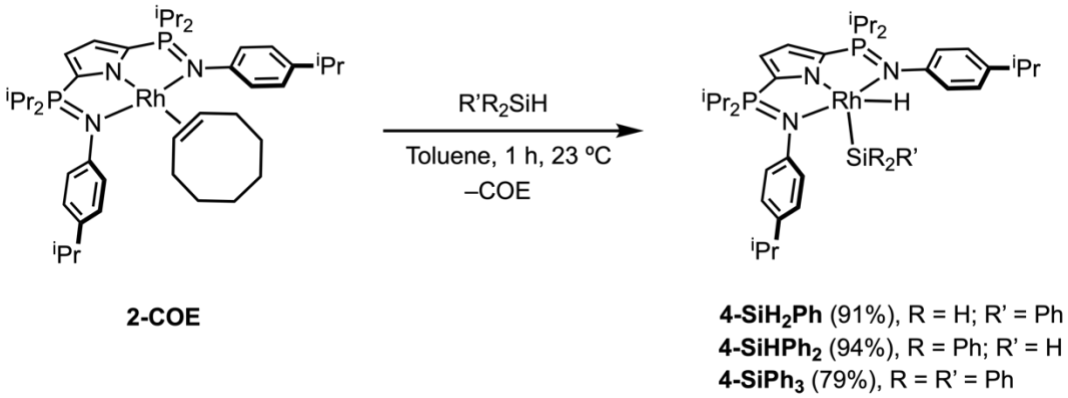


**Scheme 4.29.** Synthesis of rhodium silyl hydride complexes discussed in this chapter.

Recrystallization of the red-orange solids from pentane at −35 °C gave analytically pure rhodium silyl hydride complexes ($^{iPr}$NNN)Rh(H)$SiR_3$ in good to excellent yields (79-94%). The X-ray crystal structures of complexes **4-SiH$_2$Ph and 4-SiHPh$_2$** confirmed the presence of both rhodium hydride and silyl hydrogens (Figures 4.1 and 4.2). The crystallographic data show coordination of both phosphinimines to the Rh center, resulting

in elongation of the P–N bond distances relative to free phosphinimine (Table 4.1 and 4.2). In both **4-SiH$_2$Ph** (Si1---H1 = 1.93(3) Å) and **4-SiHPh$_2$** (Si1---H1 = 1.92(3) Å), the Rh–H ligand sits directly above the silyl Si atom forming acute angles with the Rh atom (Si1–Rh1–H1 = 57(1)º in **4-SiH$_2$Ph** and Si1–Rh1–H1 =58(1)º in **4-SiHPh$_2$**) suggesting that the complexes may contain some (Si–H)σ agostic character.[1] Nevertheless, hydride ligands for **4-SiH$_2$Ph** and **4-SiHPh$_2$** were characterized by $^1$H NMR spectroscopy as doublets centered at δ −14.3 ($^1J_{H–Rh}$ = 25.6 Hz) and δ −13.7 ($^1J_{H–Rh}$ = 26.1 Hz), respectively ($^{103}$Rh; $I$ = ½, 100%). The $^{29}$Si NMR spectrum of **4-SiH$_2$Ph** features two unique overlapping doublets ($^1J_{Si–Rh}$ = 27.5 Hz, $^1J_{Si–Rh}$ = 27.7 Hz) at δ −8.0 and δ −8.1, presumably the result of two rotomers that interconvert slowly on the NMR timescale *via* rotation about the Rh−Si bond.

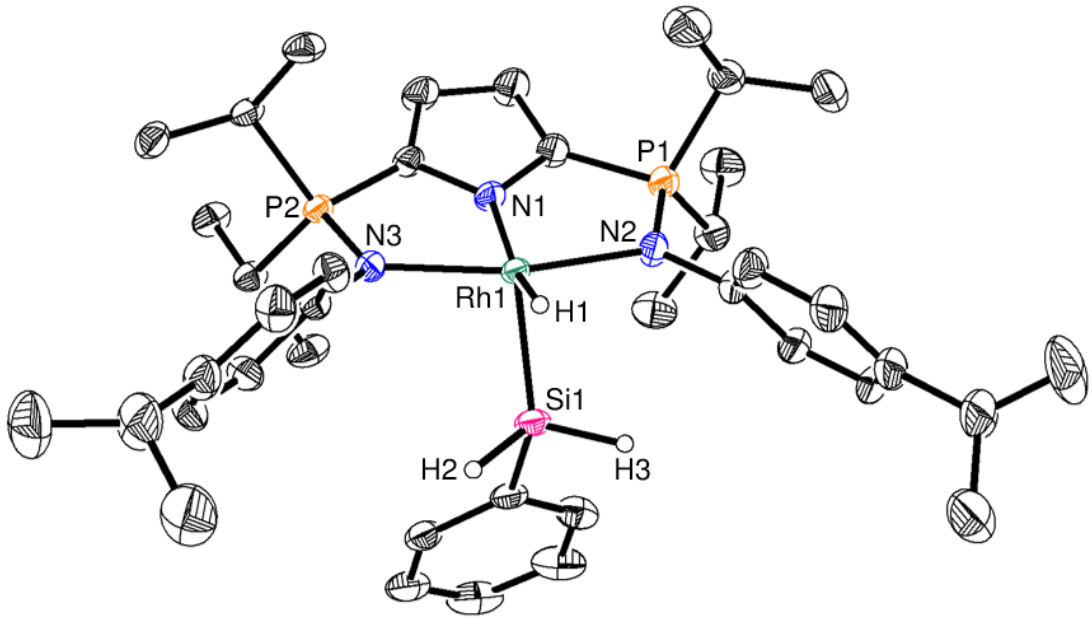


**Figure 4.1.** X-ray crystal structure of **4-SiH$_2$Ph** shown with 30% probability ellipsoids. Hydrogen atoms except for Rh–H and Si–H are omitted for clarity.

**Table 4.1.** Selected bond distances (Å) and angles (º) for **4-SiH$_2$Ph**.

| **Parameter** | **4-SiH$_2$Ph** |
|---|---|
| Bond distance (Å) | |
| P1–N2 | 1.627(2) |
| P2–N3 | 1.619(2) |
| Rh1–Si1 | 2.2466(7) |
| Rh1–N1 | 2.011(2) |
| Rh1–N2 | 2.087(2) |
| Rh1–N3 | 2.115(2) |
| Si1–H2 | 1.37(3) |
| Si1–H3 | 1.44(3) |
| Si1---H1 | 1.93(3) |
| Rh1–H1 | 1.60(4) |
| Bond angle (º) | |
| Si1–Rh1–H1 | 57(1) |
| N3–Rh1–N2 | 164.56(8) |

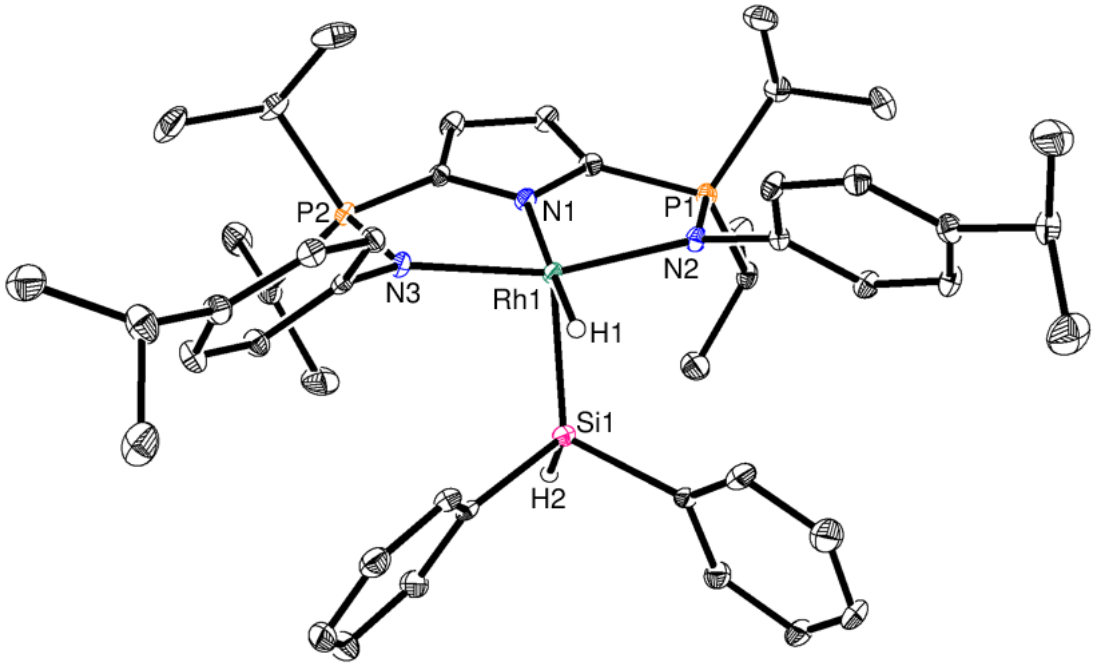


**Figure 4.2.** X-ray crystal structure of **4-SiHPh$_2$** shown with 30% probability ellipsoids. Hydrogen atoms except for Rh–H and Si–H are omitted for clarity.

**Table 4.2.** Selected bond distances (Å) and angles (º) for **4-SiHPh$_2$**.

| **Parameter** | **4-SiHPh$_2$** |
|---|---|
| Bond distance (Å) | |
| P1–N2 | 1.628(2) |
| P2–N3 | 1.632(2) |
| Rh1–Si1 | 2.2301(8) |
| Rh1–N1 | 2.005(2) |
| Rh1–N2 | 2.102(2) |
| Rh1–N3 | 2.088(2) |
| Si1–H2 | 1.49(2) |
| Si---H1 | 1.92(3) |
| Rh1–H1 | 1.55(3) |
| Bond angle (º) | |
| Si1–Rh1–H1 | 58(1) |
| N2–Rh1–N3 | 161.63(8) |

With silyl hydride complexes **4-SiH$_2$Ph** and **4-SiHPh$_2$** in hand, attempts to generate Rh silylenes *via* $H^-$ abstraction using $B(C_6F_5)_3$, in line with work by Tilley and Sadow, were conducted.[9,10,11] Specifically, a bromobenzene-$d_5$ solution of **4-SiH$_2$Ph** was combined with 1 equivalent of $B(C_6F_5)_3$, forming the anticipated hydridoborate anion $[HB(C_6F_5)_3]^-$, as confirmed by $^{11}B$ and $^{19}F$ NMR spectroscopy. However, the putative metal cation arising from α-H migration from Si to Rh could not be confidently assigned in the resulting mixture which contained multiple products according to $^1H$ and $^{31}P$ NMR spectra. Exhaustive efforts to isolate a Rh silylene species from this mixture by recrystallization proved unsuccessful. Moreover, monitoring the reaction by low-temperature (–80 ºC) NMR spectroscopy in either bromobenzene-$d_5$ or toluene-$d_8$ did not provide sufficient evidence to assign targeted Rh silylene.

Recognizing that the $^{iPr}$NNN ligand platform had previously demonstrated cooperative activity with Rh toward small molecules,[13] a strategy was conceived by which silylene formation could be mediated by a hemilabile phosphinimine donor. With this goal in mind, and the knowledge that the previously-reported dicarbonyl complex ($^{iPr}$NNN)Rh(CO)$_2$, **3-(CO)$_2$** exhibits a $\kappa^2$-*N*,*N* bound $^{iPr}$NNN ligand, it was postulated that combinations of **3-CO** and/or **3-(CO)$_2$** with silanes might lead to oxidative addition products featuring a pendant phosphinimine donor capable of stabilizing a Lewis acidic silylene Si.

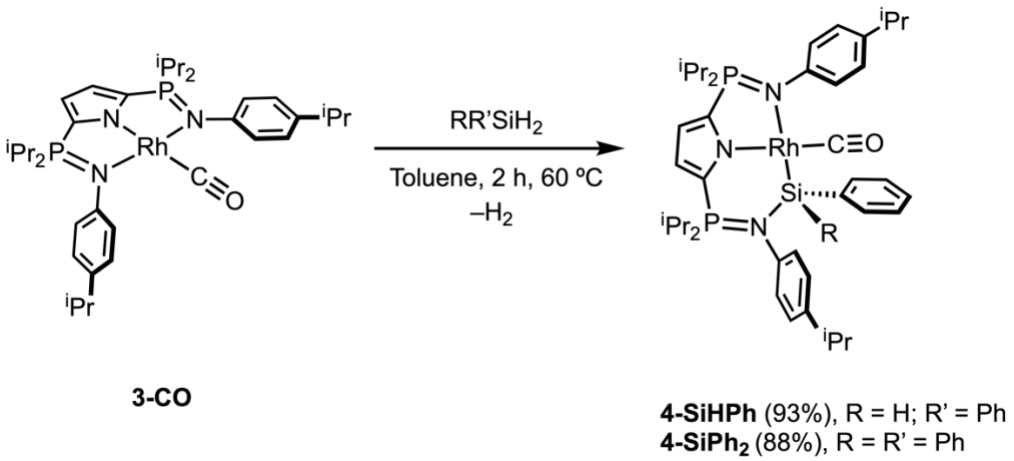


**Scheme 4.30.** Synthesis of rhodium silylene complexes discussed in this chapter by dehydrogenation of hydrosilanes.

Reaction of **3-CO** and $PhSiH_3$ in benzene-$d_6$ at 50 °C for 3 hours afforded a product showing two equal intensity peaks at δ 53.0 and δ 43.5 in its $^{31}P$ NMR spectrum.[15] The latter resonance was not consistent with a free phosphinimine but was similar to the $^{31}P$ NMR spectrum of **3-(CO)$_2$·BCF**.[13a] Examination of the $^{1}H$ NMR spectrum revealed a sharp singlet at δ 4.47 ppm, which disappeared upon exposure to reduced pressure, suggesting the evolution of $H_2$ gas. Cases in which silylene formation occurs with spontaneous $H_2$ loss are rare;[16] an example from Djukic and co-workers highlighted the role of an exogeneous donor (THF) in promoting such $H_2$ elimination at well-defined complexes of iridium.[17] A diagnostic silicon-bound hydrogen was identified as a doublet of doublets ($^{2}J_{H–Rh}$ = 5.4 Hz, $^{3}J_{H–P}$ = 5.8 Hz) at δ 5.90. When decoupled from $^{31}P$, this resonance collapses into a doublet with well-resolved $^{29}Si$ satellites ($^{1}J_{H–Si}$ = 183 Hz) ($^{29}Si$: $I$ = ½; 14%). A polarization transfer experiment ($^{1}H \rightarrow ^{29}Si$) indicated a single $^{29}Si$ environment as a doublet of doublet of doublets (ddd) centered at δ 54.6 ppm (Figure 4.3), a marked downfield shift compared to both **4-SiH$_2$Ph** (δ −8.3 ppm) and the previously reported Rh silylene described by Sadow (*vide supra*) (δ 6.6).[11] The $^{29}Si$ nucleus is coupled

to two chemically-unique $^{31}$P nuclei ($^{2}J_{Si-P}$ = 10 Hz and $^{3}J_{Si-P}$ = 2.6 Hz), consistent with a phosphinimine-stabilized Rh silylene. Notably, the observed $^{29}$Si chemical shift is comparable to base-stabilized Ru silylenes [Cp*(P$^{i}$Pr$_3$)RuH$_2$(SiPh$_2$·DMAP)]$^+$ (DMAP = 4-dimethylaminopyridine) (δ 68.5 ppm) and [Cp*(P$^{i}$Pr$_3$)RuH$_2$(SiPh$_2$·NHMePh)]$^+$ (δ 55.7 ppm) reported by Fasulo and Tilley (Chart 4.1).[18] Base-free, or terminal metal silylenes of the type L$_n$M=SiRR' typically exhibit $^{29}$Si chemical shifts in the range δ 200–370. The synthetic development of these silylenes has been reviewed by Waterman, Hayes, and Tilley.[8]

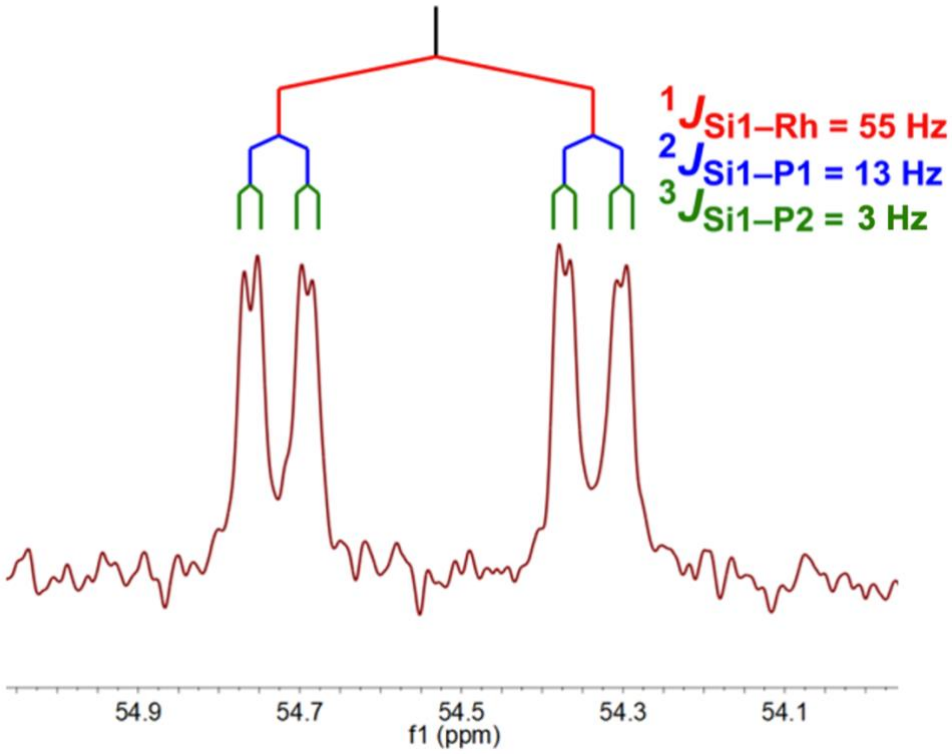


**Figure 4.3.** $^{29}$Si{$^{1}$H} NMR (INEPT) (139 MHz) spectrum of **4-SiHPh** in benzene-$d_6$ at 23 $^{o}$C.

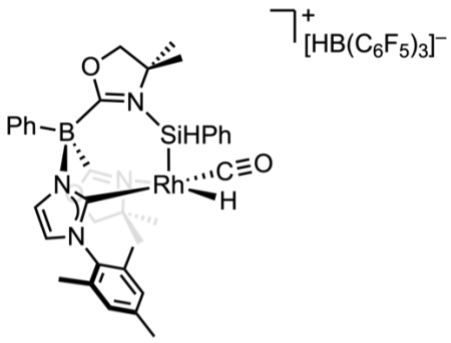


δ 6.6 (reference 11)

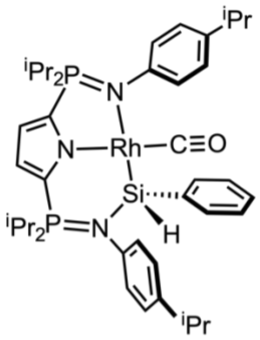


δ 54.6 (this work)

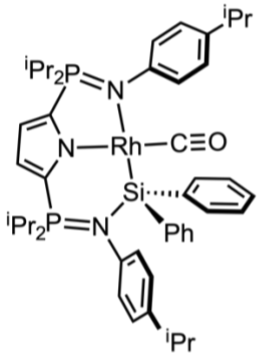


δ 51.4 (this work)

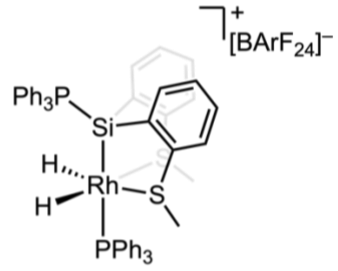


δ 95.0 (reference 12)

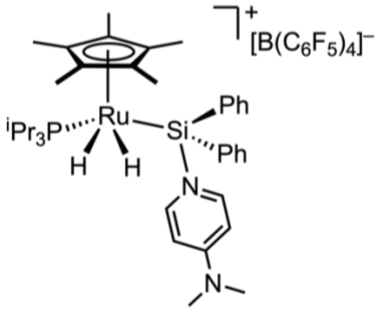


δ 68.5 (reference 18)

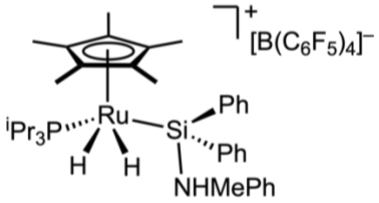


δ 55.7 (reference 18)

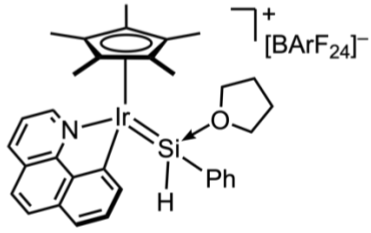


δ 73.1 (reference 17)

**Chart 4.1.** Selected examples of base-stabilized silylenes with corresponding $^{29}$Si chemical shifts.

Recrystallization of the purported silylene complex in pentane at −35 °C provided single yellow crystals suitable for X-ray diffraction analysis. The solid-state structure (Figure 4.4) confirmed the identity of **4-SiHPh** as $\kappa^2$-*N*,*N*($^{iPr}$NNN)(CO)RhSiHPh, an H-substituted Rh silylene,[19] and was, to the best of our knowledge, the first example of an isolated Rh silylene derived from a hydrosilane. The Rh−Si bond distance of 2.262(1) Å was the shortest observed at the time of publication. The N−Si contact between the phosphinimine N atom and the Lewis acidic silylene Si is 1.834(3) Å, 0.12 Å longer than N−Si bonds reported for stable N-heterocyclic silylene complexes of rhodium [1.711(2)–1.714(3) Å].[20]

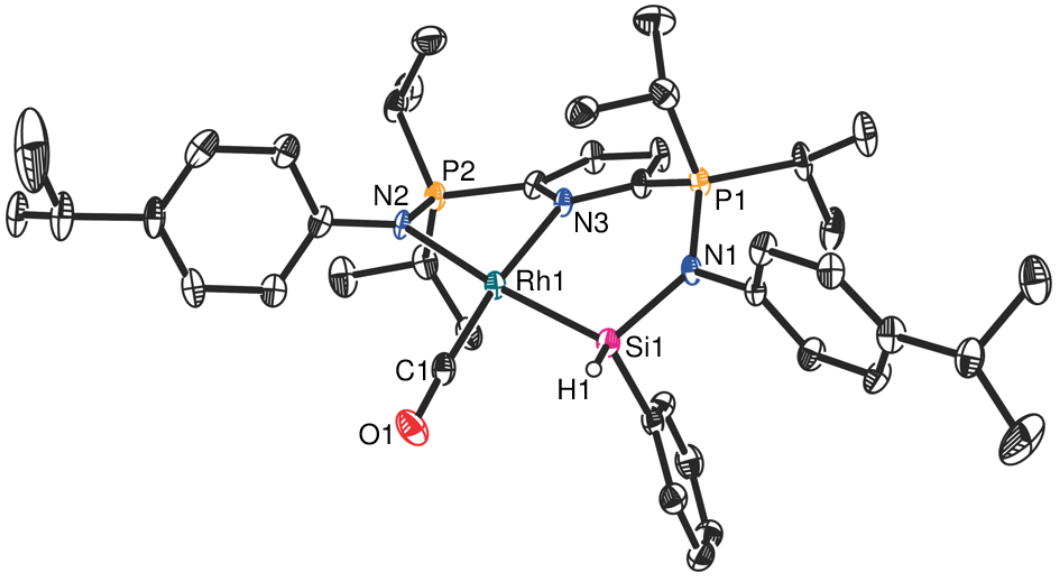


**Figure 4.4.** X-ray crystal structure of **4-SiHPh** shown with 30% probability ellipsoids. Hydrogen atoms except Si–H have been omitted for clarity.

**Table 4.3.** Selected bond distances (Å) and angles (º) for **4-SiHPh**.

| Parameter | 4-SiHPh |
|---|---|
| **Bond distance (Å)** | |
| P1–N1 | 1.647(3) |
| P2–N2 | 1.597(3) |
| C1–O1 | 1.165(6) |
| Rh1–Si1 | 2.269(2) |
| Rh1–C1 | 1.785(5) |
| Rh1–N2 | 2.200(4) |
| Rh1–N3 | 2.089(3) |
| N1–Si1 | 1.824(4) |
| **Bond angle (º)** | |
| N1–Si1–Rh1 | 113.8(1) |
| N2–Rh1–Si1 | 171.5(1) |
| N3–Rh1–C1 | 172.3(2) |

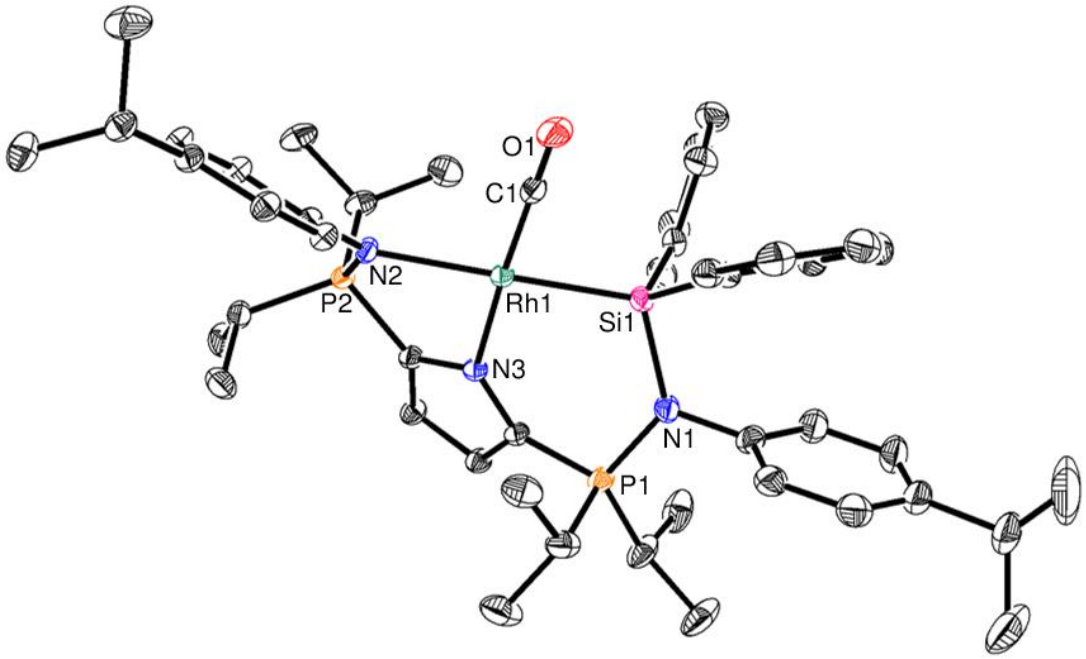


**Figure 4.5.** X-ray crystal structure of **4-SiPh$_2$** shown with 30% probability ellipsoids. All hydrogen atoms have been omitted for clarity.

**Table 4.4.** Selected bond distances (Å) and angles (º) for **4-SiPh$_2$**.

| Parameter | 4-SiPh$_2$ |
|---|---|
| **Bond distance (Å)** | |
| P1–N1 | 1.636(2) |
| P2–N2 | 1.607(2) |
| C1–O1 | 1.149(4) |
| Rh1–Si1 | 2.2702(7) |
| Rh1–C1 | 1.807(3) |
| Rh1–N2 | 2.224(2) |
| Rh1–N3 | 2.096(2) |
| N1–Si1 | 1.842(2) |
| **Bond angle (º)** | |
| N1–Si1–Rh1 | 113.55(8) |
| N2–Rh1–Si1 | 167.10(6) |
| N3–Rh1–C1 | 176.2(1) |

In order to ascertain the generality of the above reaction, $Ph_2SiH_2$ was combined with **3-CO** to give the anticipated diphenylsilylene $\kappa^2$-*N*,*N*-($^{iPr}$NNN)(CO)RhSiPh$_2$ (**4-SiPh$_2$**) and $H_2$. The X-ray crystal structure of **4-SiPh$_2$** (Figure 4.5) is isostructural with **4-SiHPh** with only minor geometrical deviations (Rh−Si = 2.2702(7), N−Si = 1.842(2) Å) (Table 4.4). For both **4-SiHPh** ($\tau_4$ = 1.0) and **4-SiPh$_2$** ($\tau_4$ = 0.97) the geometry at Si is tetrahedral according to equation 4.1.

$$\tau_4 = (360^o - (\alpha + \beta))/(360^o - 2\theta) \quad (\mathbf{4.1})$$

$\alpha$ and $\beta$ are the largest valence angles of the coordination center

$$\theta \approx 109.5^o$$

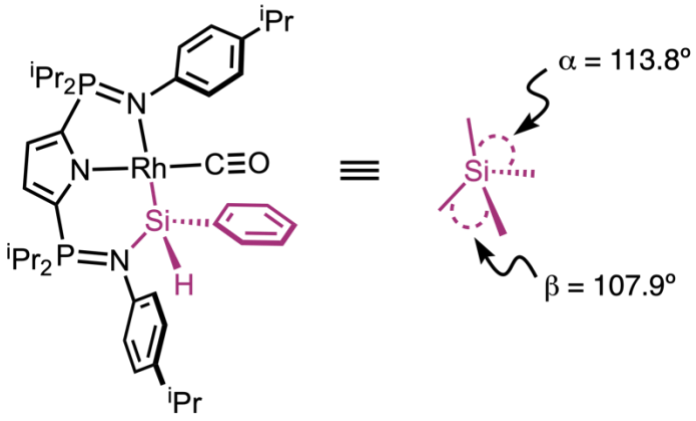


The $^{29}$Si NMR spectrum of **4-SiPh$_2$** revealed one resonance centered at $\delta$ 51.4 (dd), consistent with the connectivity established by X-ray diffraction analysis. Deuterium labelling experiments conducted with $Ph_2SiD_2$ exclusively produced $D_2$ gas, which was detected by $^2$H NMR spectroscopy, thus confirming that the silane is the source of liberated $H_2$. When the reaction was repeated using a 1:1 mixture of $Ph_2SiH_2$ and $Ph_2SiD_2$, no HD gas was observed, thus implying $H_2$ loss occurs *via* an irreversible, intramolecular process through a short-lived rhodium hydride that does not exchange with $Ph_2SiD_2$.

In an effort to understand the nature of the Rh−Si interactions in complexes **4-SiHPh** and **4-SiPh$_2$**, a DFT study was conducted at the BP3LYP/aug-cc-pVDZ level of theory using effective core potentials (ECP) for Rh. Geometry optimizations reproduced Rh−Si and Si−N bond lengths within 0.02 and 0.07 Å, respectively. Inspection of the Kohn-Sham orbitals obtained for both **4-SiHPh** and **4-SiPh$_2$** show HOMOs corresponding to a nonbonding Rh orbital consistent with a $d^8$ square planar Rh(I) center. The LUMOs for both species are delocalized over the $^{iPr}$NNN scaffold. Examination of the localized natural bonding orbitals (NBOs) of **4-SiHPh** revealed a Si-based acceptor orbital of p-character (94.1%). Second-order perturbation theory analysis provided a measure of electron delocalization from donor NBOs to the Si-based acceptor NBO (Figure 4.6). The strongest delocalization ($E^{(2)}$ = 158.4 kcal mol$^{-1}$) originated from one of two hybrid (sp) lone pairs on the phosphinimine group (Figure 4.7). Delocalizations originating from a Rh-based NBO of $d_{x^2-y^2}$ parentage were observed, but were relatively small compared to those reported previously for iridium silylenes (Figure 4.8).[10] Djukic and co-workers found that coordination of a THF solvent molecule to an [Ir=SiHPh] moiety resulted in a 30% reduction of the π character in the Ir−Si interaction.[17] It is therefore reasoned that the stronger σ-donor abilities of the phosphinimine may account for the diminished metal-ligand multiple bond character in the present system. A comparison of the natural atomic charge on Si in **4-SiHPh**, with that in the base-free (PNP)(H)Ir=SiHMes (PNP = [N(2-P$^i$Pr$_2$-4-Me-C$_6$H$_3$)$_2$]$^-$), reported by Tilley,[10] indicated similar values (+1.19 *c.f.* +1.03, respectively), which is perhaps at odds with this hypothesis. Whereas strong delocalizations from phosphinimine lone pairs render rhodium silylenes sufficiently stable for isolation, the reactivity of these species is diminished relative to base-free silylenes.

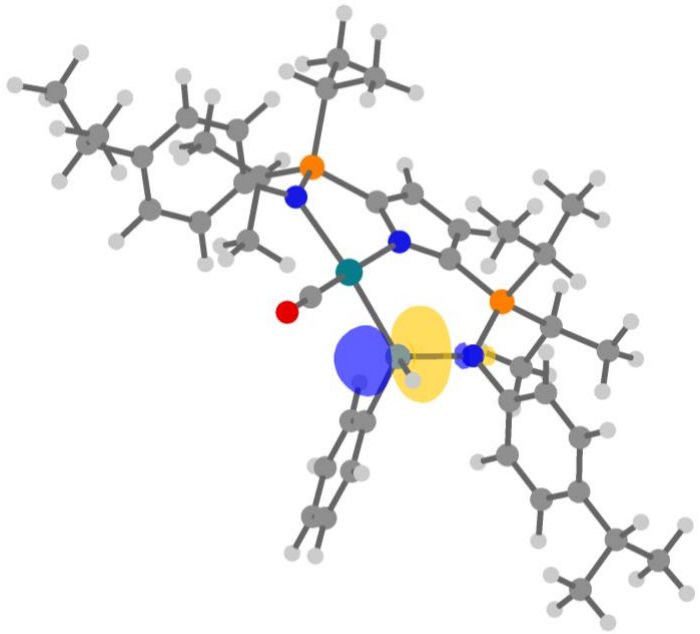

**Figure 4.6.** Graphical representation of the silicon-based acceptor (LP*) NBO in **4-SiHPh**. Orbital surfaces plotted with an isovalue of 0.08. Si LP*: s (5.49%) p (94.11%) d (0.40%).

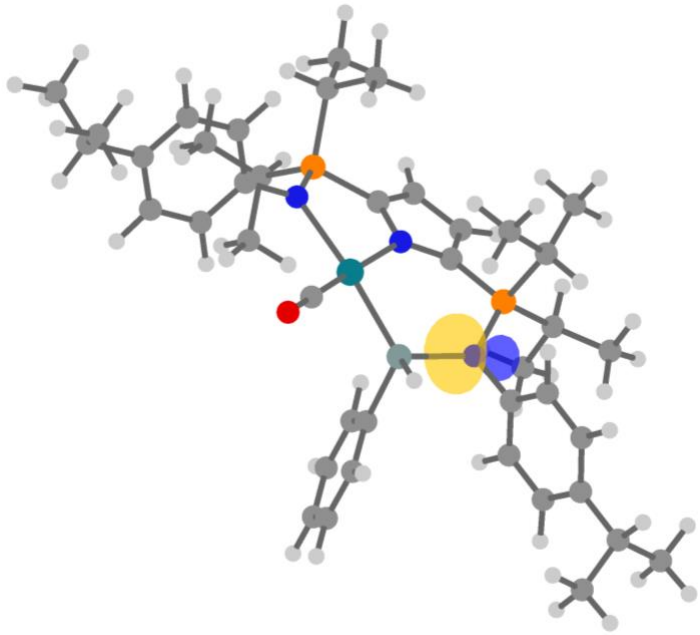

**Figure 4.7.** Graphical representation of the nitrogen-based lone pair (LP) donor NBO in **4-SiHPh**. Orbital surfaces plotted with an isovalue of 0.08. N LP (2): s (25.61%) p (74.35%).

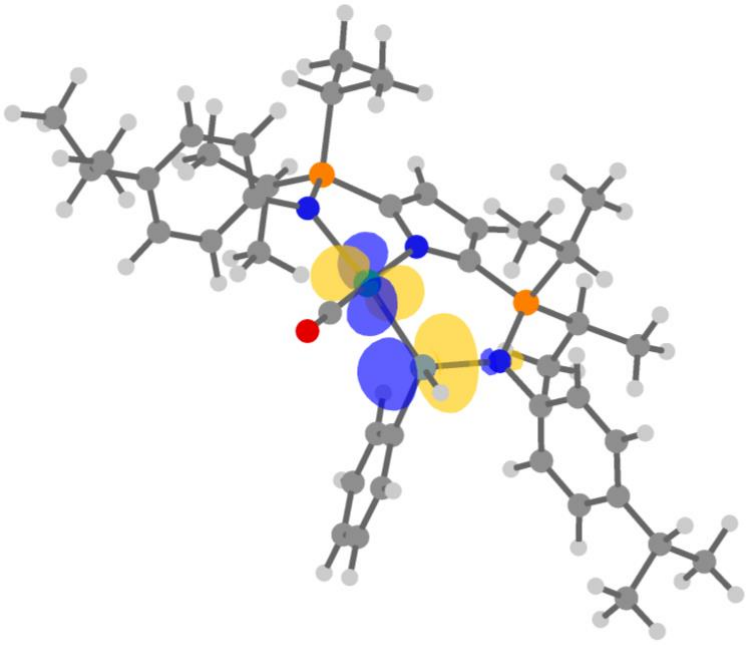

**Figure 4.8.** Orbital interaction between the rhodium-based donor NBO and Si-based acceptor NBO in **4-SiHPh** derived from second-order perturbation theory analysis. Orbital surfaces plotted with an isovalue of 0.08. Rh LP (3): s (0.14%) p (0.05%) d (99.73%), $d_{x^2-y^2}$.

In an effort to glean insight into the mechanism of silylene formation attempts were undertaken to generate **4-SiHPh** and **4-SiPh$_2$** following a complementary route. When either of the rhodium silyl hydrides **4-SiH$_2$Ph** or **4-SiHPh$_2$** were combined with excess CO gas, immediate formation of **3-(CO)$_2$** was observed, along with reductive elimination of the corresponding silane (Scheme 4.9).

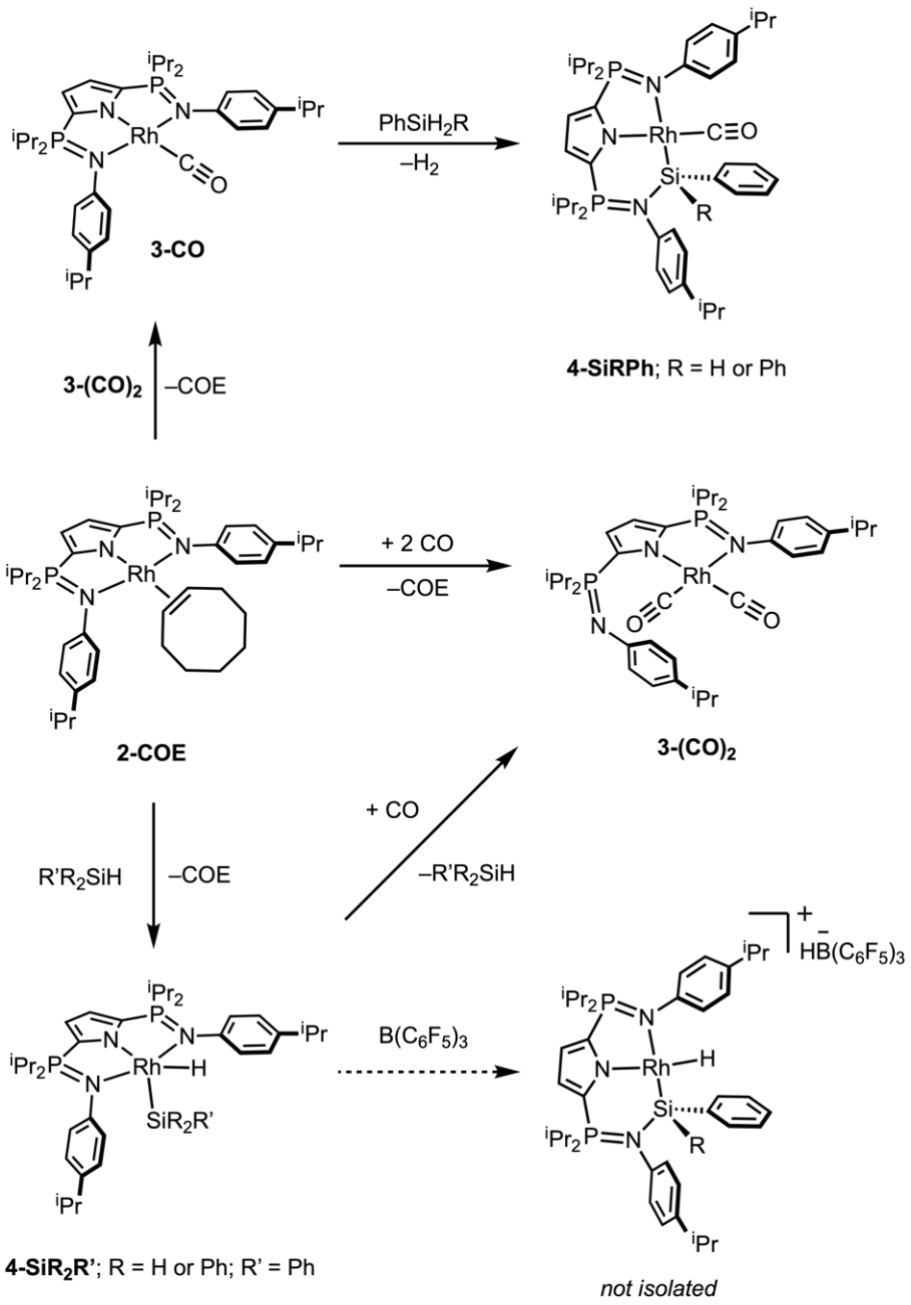


**Scheme 4.9.** Synthesis and interconversion of rhodium complexes relevant to Chapter 4.

Accordingly, the relative thermochemistry of **3-CO** and **3-(CO)$_2$** was investigated using DFT gas-phase calculations that demonstrated **3-CO** is destabilized by 13.8 kcal mol$^{-1}$ relative to **3-(CO)$_2$**. To further probe mechanistic questions, and to contrast the reactivity of **2-COE** and **3-CO**, each complex was also allowed to react with the tertiary silane

$Ph_3SiH$. Unsurprisingly, Si−H oxidative addition, along with concurrent elimination of cyclooctene, was observed in the former case, giving the rhodium silyl hydride ($^{iPr}$NNN)Rh(H)$SiPh_3$ (**4-SiPh$_3$**). In contrast, at elevated temperatures with $Ph_3SiH$ over multiple days, **3-CO** slowly transformed into an asymmetric product, characterized by equal intensity resonances in the $^{31}$P NMR spectrum (δ 76.2 and 42.9). A possible structure is the zwitterionic compound κ$^2$-*N*,*N*-(H-$^{iPr}$NNN)(CO)Rh$SiPh_3$, the result of deprotonation of the putative rhodium hydride in κ$^2$-*N*,*N*-($^{iPr}$NNN)(CO)Rh(H)$SiPh_3$ by the phosphinimine base (Scheme 4.10).[21] Notably, careful examination of the $^1$H NMR spectrum of the reaction mixture did not reveal any resonances attributable to a Rh–H ligand.

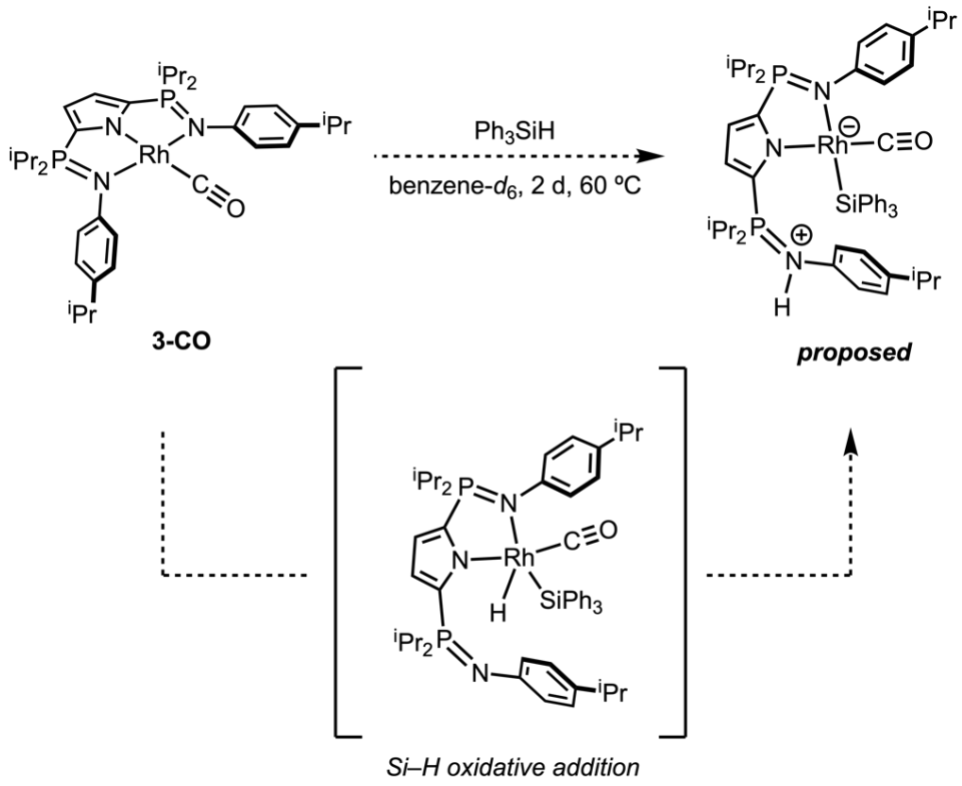


**Scheme 4.10.** Proposed formation of a zwitterionic complex following Si–H oxidative addition of $Ph_3SiH$ to **3-CO**.

Unfortunately, under all tested experimental conditions, this proposed complex decomposed at a rate that was competitive with its formation, thereby rendering further study impossible. Nonetheless, these data suggest that following Si−H oxidative addition, Rh−H deprotonation by the free phosphinimine, subsequent α-H migration from Si to Rh, and finally $H_2$ loss (NH and Rh−H)/phosphinimine coordination to Si, may be a plausible pathway for silylene formation (Scheme 4.11 A). A reasonable alternative is that direct phosphinimine coordination to Si would create a 5-coordinate hypervalent Si intermediate from which $H_2$ loss (from Rh−*H* and Si−*H*) is possible (Scheme 4.11 B).

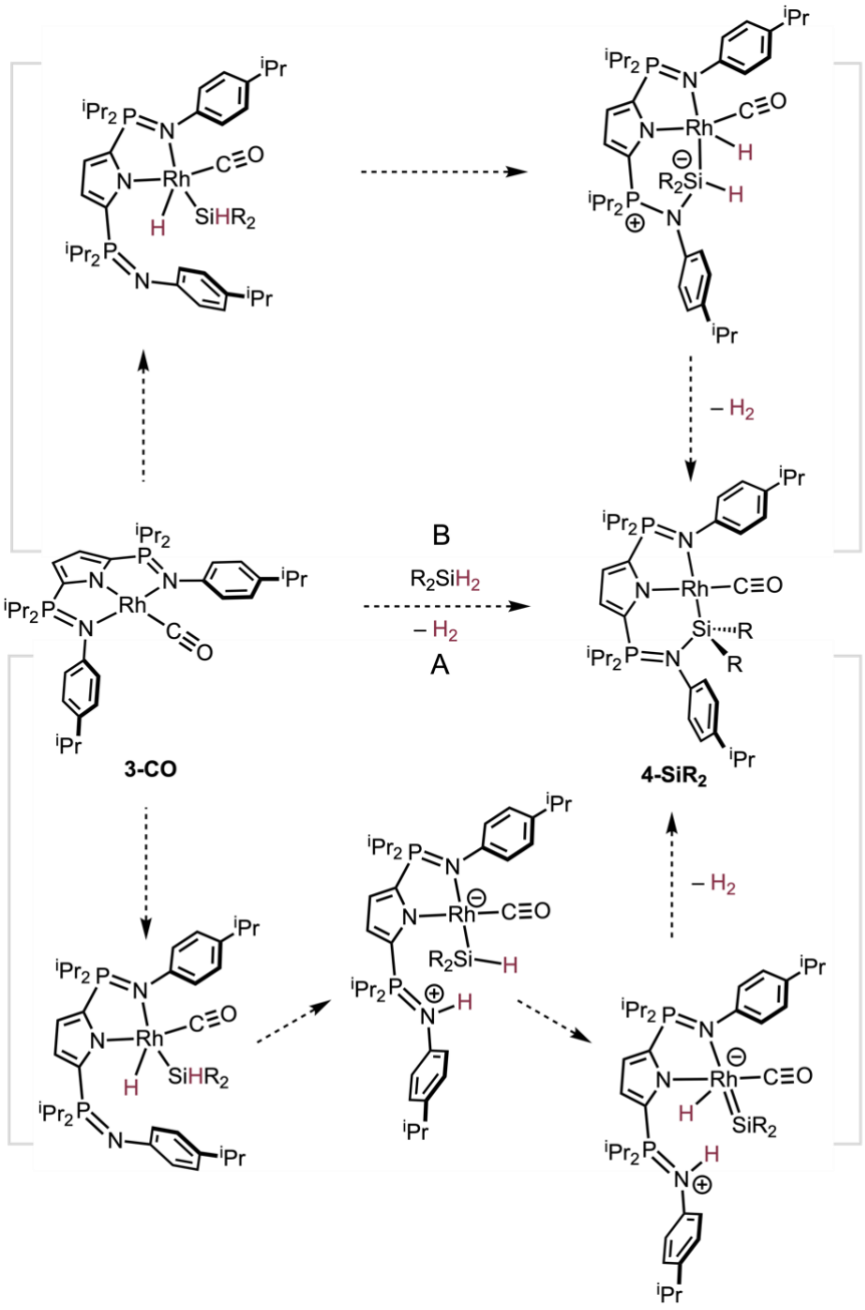


**Scheme 4.11.** Proposed mechanisms in the formation of neutral phosphinimine-stabilized rhodium silylenes.

## 4.4. Conclusions

By leveraging metal-ligand cooperation,[21] base-stabilized rhodium silylenes can be accessed directly from commercially available hydrosilanes *via* dehydrogenation. Thermochemical analysis using DFT suggests the observed reactivity stems from the energetic disparity of a hard nitrogen-donor ligand set and the soft rhodium center. The overall neutral, base-stabilized rhodium silylenes, which were synthesized on a preparative scale, allow for further studies into structure, bonding and reactivity. Cationic analogues could not be isolated by hydride abstraction using $B(C_6F_5)_3$, even at low temperatures. An alternate pathway to cationic rhodium silylenes was developed after the initial report on neutral silylenes and is described in Chapter 6 (Conclusions and Future Work).

## 4.5. References


**1.** Corey, J. Y. Reactions of Hydrosilanes with Transition Metal Complexes. *Chem. Rev.* **2016**, *116*, 11291–11435.

**2.** a) Chalk, A. J.; Harrod, J. F. Homogeneous Catalysis. II. The Mechanism of the Hydrosilation of Olefins Catalyzed by Group VIII Metal Complexes. *J. Am. Chem. Soc.* **1965**, *87*, 16–21; b) Ojima, I.; Kogure, T.; Kumagai, M.; Horiuchi, S.; Sato, T. Reduction of carbonyl compounds via hydrosilylation: II. Asymmetric reduction of ketones via hydrosilylation catalyzed by a rhodium(I) complex with chiral phosphine ligands. *J. Organomet. Chem.* **1976**, *122*, 83–97. c) Zheng, G. Z.; Chan, T. H. Regiocontrolled Hydrosilation of. alpha.,.beta.-Unsaturated Carbonyl Compounds Catalyzed by Hydridotetrakis(triphenylphosphine)rhodium(I). *Organometallics* **1995**, *14*, 70–79.

**3.** Ojima, I.; Nihonyanagi, M.; Kogure, T.; Kumagai, M.; Horiuchi, S.; Nakatsugawa, K.; Nagai, Y. Reduction of carbonyl compounds via hydrosilylation: I. Hydrosilylation of carbonyl compounds catalyzed by tris(triphenylphosphine)chlororhodium. *J. Organomet. Chem.* **1975**, *94*, 449–461.

**4.** Schneider, N.; Finger, M.; Haferkemper, C.; Bellemin-Laponnaz, S.; Hofmann, P.; Gade, L. H. Metal silylenes generated by double silicon-hydrogen activation: key intermediates in the rhodium-catalyzed hydrosilylation of ketones. *Angew. Chem. Int. Ed.* **2009**, *48*, 1609–1613; *Angew. Chem.* **2009**, *121*, 1637–1641.

**5.** Schneider, N.; Finger, M.; Haferkemper, C.; Bellemin-Laponnaz, S.; Hofmann, P.; Gade, L. H. Multiple Reaction Pathways in Rhodium-Catalyzed Hydrosilylations of Ketones. *Chem. Eur. J.* **2009**, *15*, 11515–11529.

**6.** Gigler, P.; Bechlars, B.; Herrmann, W. A.; Kühn, F. E. Hydrosilylation with Biscarbene Rh(I) Complexes: Experimental Evidence for a Silylene-Based Mechanism. *J. Am. Chem. Soc.* **2011**, *133*, 1589–1596.

**7.** a) Zybill, C.; Müller, G. Synthesis and Structure of $[(OC)_4Fe]Si(O\mathit{t}Bu)_2\cdot HMPT]$, a Donor-Stabilized Silanediyl ("Silylene") Complex. *Angew. Chem. Int. Ed. Engl.* **1987**, *26*, 669–670; *Angew. Chem.* **1987**, *99*, 683–684; b) Straus, D. A.; Tilley, T. D.; Rheingold, A. L.; Geib, S. J. Preparation, characterization, and X-ray crystal structure of an acetonitrile-complexed ruthenium silylene. *J. Am. Chem. Soc.* **1987**, *109*, 5872–5873; c) Ueno, K.; Tobita, H.; Shimoi, M.; Ogino, H. Synthesis, characterization, and x-ray crystal structure of a donor-stabilized bis(silylene)iron complex. *J. Am. Chem. Soc.* **1988**, *110*, 4092–4093.

**8.** Waterman, R.; Hayes, P. G.; Tilley, T. D. Synthetic Development and Chemical Reactivity of Transition-Metal Silylene Complexes. *Acc. Chem. Res.* **2007**, *40*, 712–719.

**9.** Mitchell, G. P.; Tilley, T. D. Generation of a Silylene Complex by the 1,2-Migration of Hydrogen from Silicon to Platinum. *Angew. Chem. Int. Ed.* **1998**, *37*, 2524–2526; *Angew. Chem.* **1998**, *110*, 2602–2605.

**10.** a) Calimano, E.; Tilley, T. D. Synthesis and Structure of PNP-Supported Iridium Silyl and Silylene Complexes: Catalytic Hydrosilation of Alkenes. *J. Am. Chem. Soc.* **2009**, *131*, 11161–11173; b) Calimano, E.; Tilley, T. D. Alkene Hydrosilation by a Cationic Hydrogen-Substituted Iridium Silylene Complex. *J. Am. Chem. Soc.* **2008**, *130*, 9226–9227.

**11.** Xu, S.; Boschen, J. S.; Biswas, A.; Kobayashi, T.; Pruski, M.; Windus, T. L.; Sadow, A. D. Mild partial deoxygenation of esters catalyzed by an oxazolinylborate-coordinated rhodium silylene. *Dalton Trans.* **2015**, *44*, 15897–15904.

**12.** Almenara, N.; Miranda, J. I.; Rodríguez-Diéguez, A.; Garralda, M. A.; Huertos, M. A. A phosphine-stabilized silylene rhodium complex. *Dalton Trans*. **2019**, *48*, 17179–17183.

**13.** a) MacNeil, C. S.; Glynn, K. E.; P. G. Hayes, P. G. Facile Activation and Deoxygenative Metathesis of CO. *Organometallics* **2018**, *37*, 3248–3252; b) Hänninen, M. M.; Zamora, M. T.; MacNeil, C. S.; Knott, J. P.; Hayes, P. G. Elucidation of the resting state of a rhodium *NNN*-pincer hydrogenation catalyst that features a remarkably upfield hydride $^{1}$H NMR chemical shift. *Chem. Commun.* **2016**, *52*, 586–589.

**14.** Hanson, S. S.; Richard, N. A.; Dyker, C. A. Powerful Bispyridinylidene Organic Reducing Agents with Iminophosphorano π-Donor Substituents. *Chem. Eur. J.* **2015**, *21*, 8052–8055.

**15.** For this work, an improved method of generating **3-CO** was employed, whereby **3-(CO)$_2$** and **2-COE** comproportionate to form 2 equivalents of **3-CO**. Refer to Chapter 3.

**16.** a) Lipke, M. C.; Tilley, T. D. Hypercoordinate Ketone Adducts of Electrophilic η3-$H_2SiRR'$ Ligands on Ruthenium as Key Intermediates for Efficient and Robust Catalytic Hydrosilation. *J. Am. Chem. Soc.* **2014**, *136*, 16387–16398; b) Gusev, D. G.; Fontaine, F.-G.; Lough, A. J.; Zargarian, D. Polyhydrido(silylene)osmium and Silyl(dinitrogen)ruthenium Products Through Redistribution of Phenylsilane with Osmium and Ruthenium Pincer Complexes. *Angew. Chem. Int. Ed.* **2003**, *42*, 216–219; *Angew. Chem.* 2003, *115*, 226–229; c) Price, J. S.; Emslie, D. J. H.; Britten, J. F. Manganese Silylene Hydride Complexes: Synthesis and Reactivity with Ethylene to Afford Silene Hydride Complexes. *Angew. Chem. Int. Ed.* **2017**, *56*, 6223–6227; *Angew. Chem.* **2017**, *129*, 6319–6323; d) Handwerker, H.; Leis, C.; Probst, R.; Bissinger, P.; Grohmann, A.; Kiprof, P.; Herdtweck, E.; Blümel, J.; Auner, M.; Zybill, C. Reversible intramolecular base-stabilization in silylene (silanediyl) complexes: surprising reactivity for silylene coordination compounds with a dynamic N···Si···N bond. *Organometallics* **1993**, *12*, 2162–2176; e) Corriu, R. J. P.; Lanneau, G. F.; Priou, C.; Chauhan, B. P. S.; Auner, N.; Handwerker, H.; Herdtweck, E. Lewis Base-Stabilized Transition Metal Complexes of Divalent Silicon Species. *Organometallics* **1995**, *14*, 1657–1666; f) Corriu, R. J. P.; Lanneau, G. F.; Priou, C.; Chauhan, B. P. S. Photochemical Reaction of 16-e Metal Species Generated from $Fe(CO)_5$, $Cr(CO)_6$, or $RCpMn(CO)_3$ (R = H, Me), with Primary and Secondary Arylsilanes in the Presence of Internal or External Electron Donors: Formation

of Functionally Stabilized Hydrosilanediyl-Transition Metal Complexes. *Organometallics* **1993**, *12*, 2001–2003; g) Dannappel, K.; Nienhaus, R.; Schürmann, M.; Costisella, B.; Jurkschat, K. The UV-Light Initiated Reaction of Organosilanes with Tungsten Hexacarbonyl: Formation of an Organosilylene Complex and Organosilylium Salts. *Z. Anorg. Allg. Chem.* **2009**, *635*, 2126–2134.

**17.** Binh, D. H.; Hamdaoui, M.; Fischer-Krauser, D.; Karmazin, L.; Bailly, C.; Djukic, J.-P. Entrapment of THF-Stabilized Iridacyclic $Ir^{III}$ Silylenes from Double H−Si Bond Activation and $H_2$ Elimination. *Chem. Eur. J.* **2018**, *24*, 17577–17589.

**18.** Fasulo, M. E.; Tilley, T. D. Stoichiometric Reaction Chemistry of Cationic Ruthenium Silylene Complexes toward Polar and Nonpolar Organic Substrates. *Organometallics* **2012**, *31*, 5049–5057.

**19.** A survey of the literature gave the following hydrogen-substituted transition metal silylenes: a) $[Cp^*(^iPr_3P)(H)_2Os{=}SiH(trip)][B(C_6F_5)_4]$ and b) $[Cp^*(^iPr_3P)(H)_2Ru{=}Si(H)Ph{\cdot}Et_2O][B(C_6F_5)_4]$ see: Glaser, P. B.; Tilley, T. D. Catalytic Hydrosilylation of Alkenes by a Ruthenium Silylene Complex. Evidence for a New Hydrosilylation Mechanism. *J. Am. Chem. Soc*. **2003**, *125*, 13640–13641; c) $Cp^*(^iPr_3P)(H)Os{=}SiH(trip\ or\ dmp)$ see: Hayes, P. G.; Beddie, C.; Hall, M. B.; Waterman, R.; Tilley, T. D. Hydrogen-Substituted Osmium Silylene Complexes: Effect of Charge Localization on Catalytic Hydrosilation. *J. Am. Chem. Soc.* **2006**, *128*, 428–429; d) $[(Et_3P)_3(H)_2Ir{=}Si(H)(dmp)][B(C_6F_5)_4]$ see: Simons, R. S.; Gallucci, J. C.; Tessier, C. A.; Youngs, W. J. Synthesis and characterization of the sterically hindered iridium(III)–silyl complex: $(Et_3P)_3(H)_2Ir[Si(H)Cl(C_6H_3\text{-}Mes_2\text{-}2,6)]$ and the generation of the cationic iridium(III)-silylene complex: $[(Et_3P)_3(H)_2Ir{=}Si(H)(C_6H_3\text{-}Mes_2\text{-}2,6)][B(C_6F_5)_4]$. *J. Organomet. Chem.* **2002**, *654*, 224–228; e) $[PhBP_3](H)_2Ir{=}SiH(trip)$ see: Feldman, J. D.; Peters, J. C.; Tilley, T. D. Activations of Silanes with $[PhB(CH_2PPh_2)_3]Ir(H)(\eta^3\text{-}C_8H_{13})$. Formation of Iridium Silylene Complexes via the Extrusion of Silylenes from Secondary Silanes $R_2SiH_2$. *Organometallics* **2002**, *21*, 4065–4075; f) $Cp^*(^iPr_2MeP)(H)Ru{=}SiH(trip\ or\ dmp)$ see: Hayes, P. G.; Waterman, R.; Glaser, P. B.; Tilley, T. D. Synthesis, Structure, and Reactivity of Neutral Hydrogen-Substituted Ruthenium Silylene and Germylene Complexes. *Organometallics* **2009**, *28*, 5082–5089; g) $Cp^*(CO)_2(H)W{=}Si(H)\{C(SiMe_3)_3\}$ see: Watanabe, T.; Hashimoto, H.; Tobita, H. Hydrido(hydrosilylene)tungsten Complexes with Strong Interactions between the Silylene and Hydrido Ligands. *Angew. Chem. Int. Ed.* **2004**, *43*, 218–221; *Angew. Chem.* **2004**, *116*, 220–223; h) $Cp^*(CO)_2(H)W{=}Si(H)\{C(SiMe_3)_3\}$; ($Cp^* = \eta^5\text{-}C_5Me_4Et$) see: Watanabe, T.; Hashimoto, H.; Tobita, H. Stoichiometric Hydrosilylation of Nitriles with Hydrido(hydrosilylene)tungsten Complexes: Formation of W−Si−N Three-Membered Ring Complexes and Their Unique Thermal Behaviors. *J. Am. Chem. Soc.* **2006**, *128*, 2176–2177; i) Cp*(CO)(H)Ru=Si(H){C(SiMe3)3} see: Ochiai, M.; Hashimoto, H; Tobita, H. Synthesis and Structure of a Hydrido(hydrosilylene)ruthenium Complex and Its Reactions with Nitriles. *Angew. Chem. Int. Ed.* **2007**, *46*, 8192–8194; *Angew. Chem.* **2007**, *119*, 8340–8342; j) $[Cp^*(^iPr_3P)(H)_2Ru{=}SiH(Mes)][CB_{11}H_6Br_6$ or $B(C_6F_5)_4]$ see: Fasulo, M. E.; Lipke, M. C.; Tilley, T. D. Structural and mechanistic investigation of a cationic hydrogen-substituted ruthenium silylene catalyst for alkene hydrosilation. *Chem. Sci.* **2013**,

*4*, 3882–3887, and Fasulo, M. E.; Glaser, P. B.; Tilley, T. D. Cp*(PiPr3)RuOTf: A Reagent for Access to Ruthenium Silylene Complexes. *Organometallics* **2011**, *30*, 5524–5531; k) [(PNP)(H)Ir=SiH(Mes)][B($C_6F_5$)$_4$]; see reference [10b]; l) [(PNP)(H)Ir=SiH(trip or dmp)][B($C_6F_5$)$_4$]; see reference [10a]; m) Cp*($^i$Pr$_2$MeP)Fe(H)Si=H(trip or dmp) see: Smith, P. W.; Tilley, T. D. Base-Free Iron Hydrosilylene Complexes via an α-Hydride Migration that Induces Spin Pairing. *J. Am. Chem. Soc.* **2018**, *140*, 3880–3883; n) Cp(CO)$_2$Mn=SiH(2-Me$_2$NCH$_2$C$_6$H$_4$), MeCp(CO)$_2$Mn=SiH(2-Me$_2$NCH$_2$C$_6$H$_4$), Cp(CO)$_4$Fe=SiH(2-Me$_2$NCH$_2$C$_6$H$_4$), and Cp(CO)$_5$Cr=SiH(2-Me$_2$NCH$_2$C$_6$H$_4$), see reference [15f]; o) Cp*(*m*-P,N-2-NMe$_2$-3-P$^i$Pr$_2$-indene)(H)$_2$Ru=SiHPh]$^+$X$^-$ (X = $SO_3CF_3$, B($C_6F_5$)$_4$), Cp*(μ-2-NMe$_2$-3-P$^i$Pr$_2$-indenide)(H)$_2$Ru=SiHPh, and [Cp*(μ-1-P$^i$Pr$_2$-2-NMe$_2$-indene)(H)$_2$Ru=SiHPh]$^+$X$^-$ (X = $SO_3CF_3$, B($C_6F_5$)$_4$; see: Rankin, M. A.; MacLean, D. F.; Schatte, G.; McDonald, R.; Stradiotto, M. Silylene Extrusion from Organosilanes via Double Geminal Si−H Bond Activation by a Cp*Ru(κ$^2$-*P*,*N*)$^+$ Complex: Observation of a Key Stoichiometric Step in the Glaser−Tilley Alkene Hydrosilylation Mechanism. *J. Am. Chem. Soc.* **2007**, *129*, 15855–15864.

**20.** a) Stoelzel, M.; Präsang, C.; Blom, B.; Driess, M. N-Heterocyclic Silylene (NHSi) Rhodium and Iridium Complexes: Synthesis, Structure, Reactivity, and Catalytic Ability. *Aust. J. Chem.* **2013**, *66*, 1163–1170; b) Neumann, E.; Pfaltz, A. Synthesis and Characterization of Cationic Rhodium Complexes with Stable Silylenes. *Organometallics* **2005**, *24*, 2008–2011; c) Al-Rafia, S. M. I.; Malcolm, A. C.; McDonald, R.; Ferguson, M. J.; Rivard, E. Efficient generation of stable adducts of Si(II) dihydride using a donor–acceptor approach. *Chem. Commun.* **2012**, *48*, 1308–1310.

**21.** Hu, Y.; Norton, J. R. Kinetics and Thermodynamics of H$^-$/H$^•$/H$^+$ Transfer from a Rhodium(III) Hydride. *J. Am. Chem. Soc.* **2014**, *136*, 5938–5948.

**22.** a) Karshtedt, D.; McBee, J. L.; Bell, A. T.; Tilley, T. D. Stoichiometric and Catalytic Arene Activations by Platinum Complexes Containing Bidentate Monoanionic Nitrogen-Based Ligands. *Organometallics* **2006**, *25*, 1801–1811; b) Fekl, U.; Goldberg, K. I. Homogeneous hydrocarbon CH bond activation and functionalization with platinum. *Adv. Inorg. Chem.* **2003**, *54*, 259–320; c) Fekl, U.; Goldberg, K. I. Five-coordinate platinum (IV) complex as a precursor to a novel Pt (II) olefin hydride complex for alkane activation. *J. Am. Chem. Soc.* **2002**, *124*, 6804–6805; d) Fekl, U.; Kaminsky, W.; Goldberg, K. I. β-Diiminate Platinum Complexes for Alkane Dehydrogenation. *J. Am. Chem. Soc.* **2003**, *125*, 15286–15287.

## Chapter 5: Metal-Ligand Cooperation Enables Reversible Dehydrogenation of a Primary Borane*

### 5.1. Abstract

The reversible activation and dehydrogenation of B–H bonds in primary aryl boranes [$H_2BAr$; Ar = 2,4,6-$(CH_3)_3C_6H_2$ (Mes), 3,5-$(CF_3)_2C_6H_3$ ($Ar^F$)] by the 16-electron rhodium(I) monocarbonyl complex, ($^{iPr}$NNN)Rh(CO) (**3-CO**; $^{iPr}$NNN = 2,5-[$^i$Pr$_2$P=N(4-$^i$PrC$_6$H$_4$)]$_2$N($C_4H_2$)$^-$) is described. Notably, the results of this chapter follow closely from observations made in the preceding chapter, to wit: the consecutive activation of Si–H bonds in primary and secondary silanes. A neutral, ligand-stabilized 'borylene' complex ($^{iPr}$NNN)(CO)RhBMes (**5-BMes**), the result of dehydrogenative {BMes} extrusion, was synthesized and isolated. Combined X-ray diffraction and computational (DFT/NBO) analyses revealed a trigonal planar boron atom stabilized by a lone pair from the adjacent ylidic phosphinimine nitrogen atom. Addition of $H_2$ gas to **5-BMes** resulted in the reformation of **3-CO** and $H_2$BMes. The trifluoromethylated aryl borane $H_2BAr^F$ reacted with **3-CO** to afford the B–H sigma complex **5-CO·$H_2$BAr$^F$**, stabilized by phosphinimine N→B and Rh→(B–H) agostic interactions. Variable temperature $^1$H NMR spectroscopy established dynamic B–H agostic interactions between the captured borane and the T-shaped 14-electron Rh center. Reactivity studies revealed that **5-BMes** promotes formal group transfer and that {BAr} fragments accessed by dehydrogenation are reactive entities.

*Adapted from: 'MacNeil, C. S.; Hsiang, S.-J.; Hayes, P. G. *Chem. Commun.* **2020**, *56*, 12323–12326.' with permission from The Royal Society of Chemistry.

## 5.2. Introduction

Metal-catalyzed hydroboration and C–H borylation are powerful methods for the conversion of feedstock hydrocarbons into value-added chemicals.[1] Organoboron compounds serve as intermediates in synthesis and are often critical lynchpins in late-stage transformations. The oxidative addition of a single B–H bond by an electron-rich metal center is well-precedented for boron electrophiles (*e.g.* 9-borabicyclo[3.3.1]nonane, pinacol-, catechol-, and alkylboranes).[2] Building on ground-breaking work by Alcaraz and Sabo-Etienne,[3] consecutive B–H activation has been observed in the formation of borylenes (Scheme 5.1. A) from dihydroboranes (Scheme 5.1. B),[4] boron-to-metal α-hydride migration from amineboranes,[5] and in the dehydropolymerization of ammonia-borane and primary amineboranes.[6] Taken together, these advances have established a framework for understanding the elementary steps involved in catalytic hydroboration, borylation, and more recently, the dehydrocoupling of amineboranes to form BN polymeric materials.

The concerted formation of a metal–boron multiple bond along with $H_2$ from a primary borane is an ideal, atom-economical route for the generation of transition metal borylenes [$L_nM$=BR; R = alkyl, aryl, amino)] from which group transfer methods may be developed (Scheme 5.1. C). Indeed, consecutive B–H and B–F activation has been used to access terminal borylenes at low valent metal centers in the cases of *fac*-$(PMe_3)_3Ir(BNR_2)(H)_2$ (R = $^i$Pr or Cy),[5] and more recently in $Fe(BF)(CO)_2(CNAr^{Tripp2})_2$, respectively.[7] Notably though, the complete separation of boron from hydrogen is exceedingly rare in transition metal systems. Partial dehydrogenation to give B–B coupled products has been reported by Braunschweig and co-workers at low-valent bis(phosphine) platinum.[8] Adjacent hydride ligands have

been shown to exert a stabilizing influence on the boron atom, as in $RuHCl(BMes)(PCy_3)_2$ where interactions between the borylene B atom and the hydride were investigated by NBO analysis.[4a] It was shown that the borylene B atom participates in (Ru–H)σ bonding despite the explicit characterization of :BR as a neutral CO analogue. The participation of the boron in the natural localized molecular orbital (NLMO) of (Ru–H)σ suggests a more nuanced account of the total bonding picture. By considering the two structural isomers of $RuHCl(BMes)(PCy_3)_2$ (square pyramid and trigonal bipyramidal), Sabo-Etienne and co-workers provided strong evidence that supports a coordination geometry where borylene and the π-donating Cl ligand are not trans-disposed as in $RuHCl(CO)(PCy_3)_2$. A complete understanding of the bonding in this Ru system was complicated by the fact that the hydride was not explicitly located in the Fourier difference map. A reversible, successive B–H activation sequence (Scheme 5.1. C) is challenging, given the fidelity of B···H interactions in transition metal complexes that contain hydride ligands.[9] While the treatment of borylenes (:BR) as π-accepting neutral ligands has allowed for useful comparisons between ubiquitous ligands in organometallic chemistry such as CO and $N_2$, further investigations into the coordination chemistry of transition metal borylenes *without* neighbouring hydride ligands is warranted.

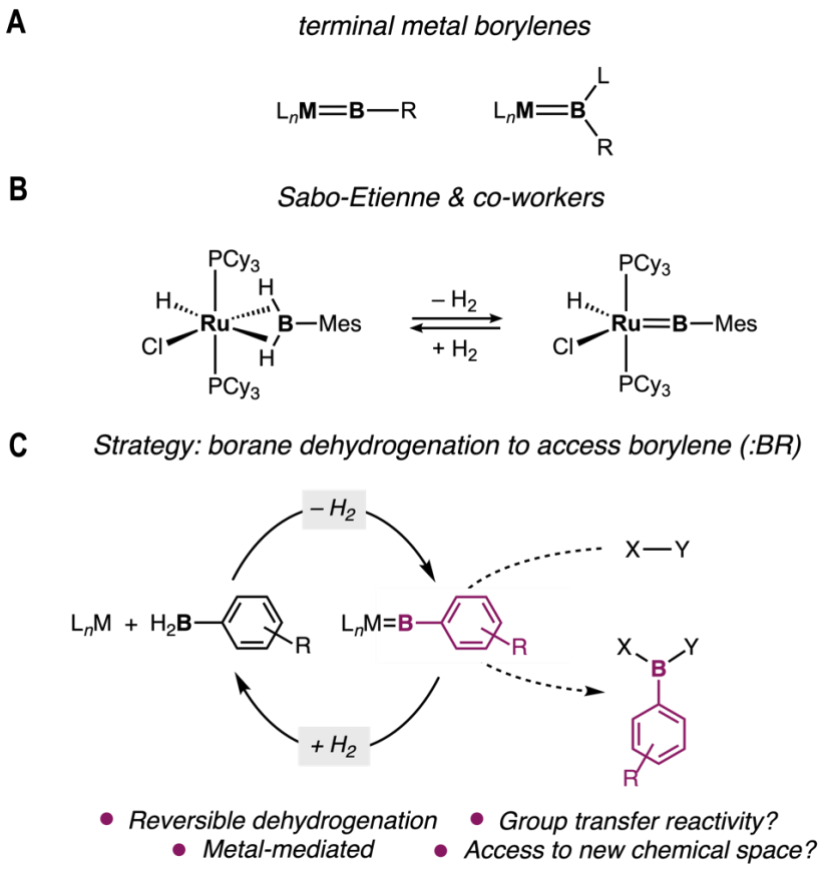


**Scheme 5.31.** A. Generic representations of terminal transition metal borylene complexes. B. Reported ruthenium complex that reversibly activates B–H bonds in mesityl borane. C. Reversible dehydrogenation of aryl borane to access aryl borylene for group transfer reactivity.

### 5.3. Results and Discussion

As outlined in the previous chapter, metal-ligand cooperative dehydrogenation of primary and secondary silanes has been demonstrated at a mononuclear rhodium(I) center and led to the isolation of the hydrogen-substituted silylene ($^{i\text{Pr}}$NNN)(CO)Rh=SiHPh.[10] Hence, a conceptually-diagonal approach was taken that combined an electron-rich rhodium complex ($^{i\text{Pr}}$NNN)Rh(CO) (**3-CO**) with a primary aryl borane. Dihydroarylboranes were prepared by reduction of the requisite dimethoxy precursor $(MeO)_2BAr$, or by lithium-halogen exchange with the

corresponding aryl halide, followed by quenching with $BH_3{\cdot}SMe_2$ (Scheme 5.2). Mesitylborane ($H_2BMes$) was isolated as a colourless crystalline solid while the 3,5-trifluoromethylated analogue ($H_2BAr^F$; $Ar^F$ = 3,5-$(CF_3)_2$-$C_6H_3$) was stored as the diethylether solution (see Chapter 7.1.1 for experimental details and synthetic procedures).

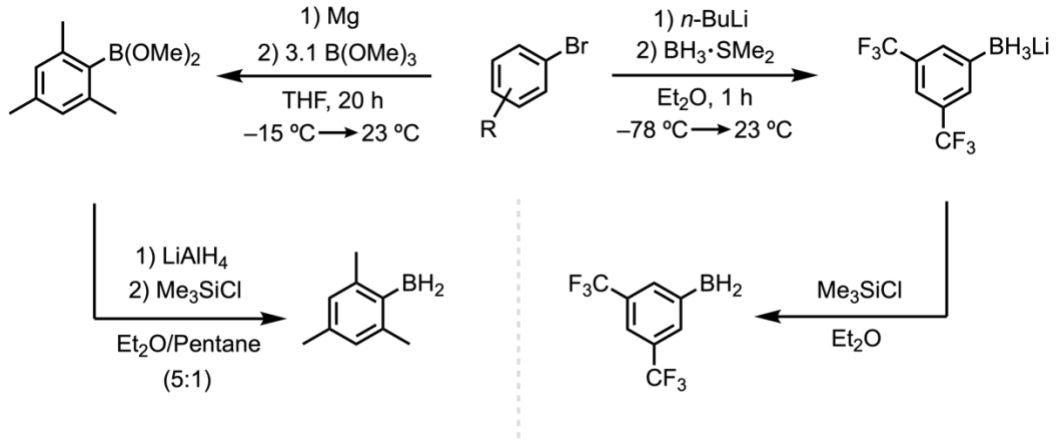


**Scheme 5.32.** Synthesis of dihydroarylboranes used in this chapter.

Analysis by $^1H$ and $^{31}P$ NMR spectroscopy revealed that treatment of **3-CO** with 1 equivalent of mesitylborane ($H_2BMes$) in benzene-$d_6$ gave a mixture of unreacted **3-CO** and a new, asymmetric product with $^{31}P$ resonances appearing at δ 52.7 and δ 37.9 (Figure 5.3). The apparent asymmetry of the resulting complex is consistent with chemically inequivalent phosphinimines, as in **3-$(CO)_2$·BCF** (Chapter 3) and **4-SiRR'** (Chapter 4). In these examples, the resonance associated with the phosphinimine bound to the main group element (C, Si) appears upfield relative to the phosphinimine bound to Rh, by Δδ = 4.5 and 9.7 ppm, respectively. Notably, when the reaction was carried out in a J. Young NMR tube in benzene-$d_6$, a resonance with a chemical shift consistent with $H_2$ gas in solution (δ 4.47) was visible by $^1H$ NMR

spectroscopy. Sabo-Etienne has demonstrated that isolated ruthenium borylenes can react with excess $H_2$, forming bis(σ-borane) complexes. Thus, it was reasoned that a rhodium borylene complex might react with evolved hydrogen gas, resulting in an equilibrium between **3-CO** and $H_2$BMes. Accordingly, the procedure was repeated in a 1:1 mixture of pentane and toluene under reduced pressure; recrystallization from $Et_2O$ at –35 ºC provided a bright yellow crystalline solid identified as (($^{iPr}$NNN)(CO)RhBMes, **5-BMes**) in 22% yield (*vide infra*). Characterization of **5-BMes** by $^1$H NMR spectroscopy revealed a coordinated {BMes} fragment absent of B–H hydrogens in an overall low-symmetry complex (Figures 5.1 and 5.2).

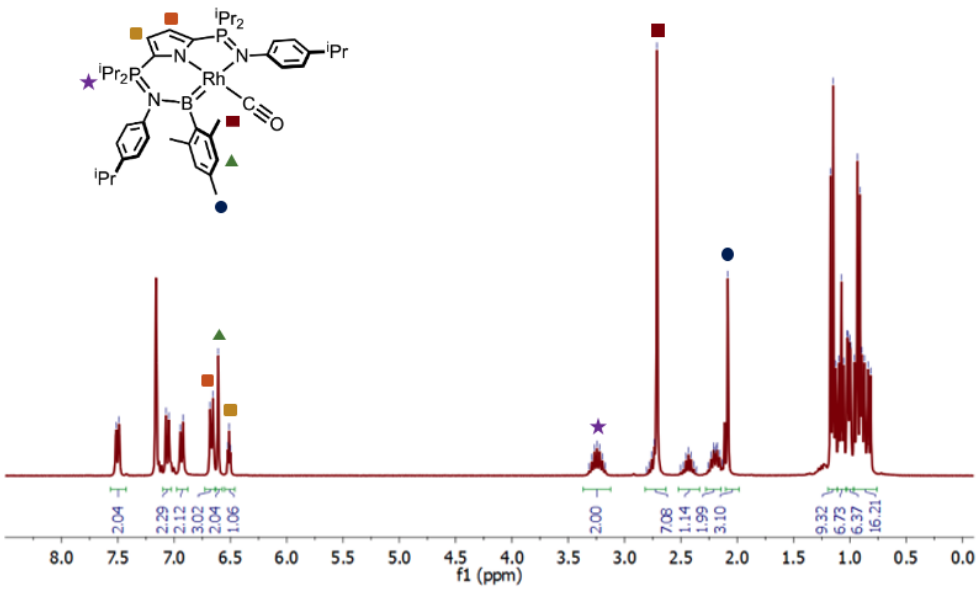


**Figure 5.1.** $^1$H NMR (300 MHz) spectrum of **5-BMes** in benzene-$d_6$ at 23 ºC.

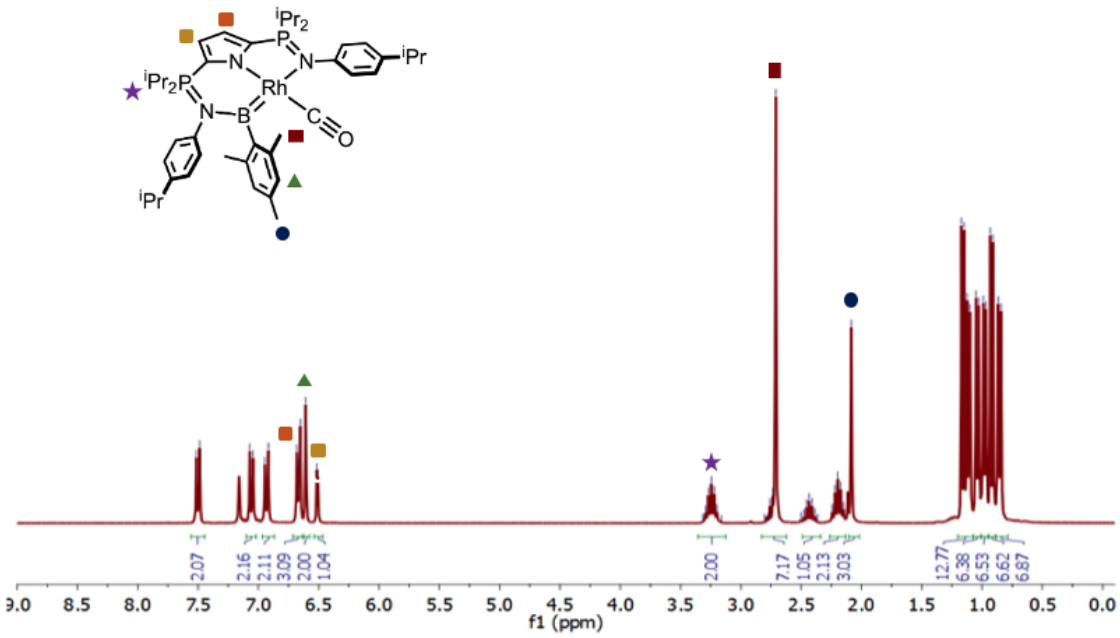


**Figure 5.2.** $^{1}H\{^{31}P\}$ NMR (300 MHz) spectrum of **5-BMes** in benzene-$d_6$ at 23 ºC.

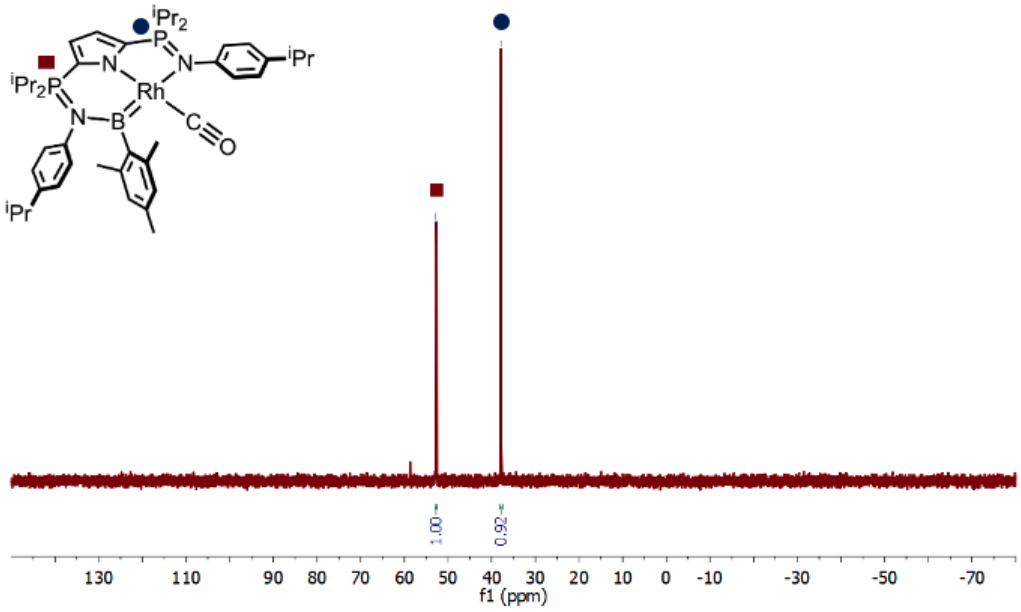


**Figure 5.3.** $^{31}P\{^{1}H\}$ NMR (121 MHz) spectrum of **5-BMes** in benzene-$d_6$ at 23 ºC.

Single-crystal X-ray diffraction studies confirmed the identity of **5-BMes** as a phosphinimine-stabilized rhodium borylene. The geometry at the 3-coordinate boron

atom ($\Sigma_{angles}$ = 359.8 º) is strictly trigonal planar. Careful examination of the Fourier difference map provided no indication of residual electron density from possible rhodium hydride or B–H atoms, which is consistent with the $^{1}$H NMR spectrum of isolated **5-BMes**. Mesityl *o*-$CH_3$ groups occupy the axial space above and below the equatorial plane defined by the phosphinimine nitrogen, mesityl *ipso*-carbon, and rhodium center. The rhodium-boron distance in **5-BMes** [Rh1–B1 = 2.024(5) Å] is shorter than the sum of the covalent radii for Rh and B (2.13 Å) and is comparable to that in the bridged dirhodium borylene complex [{($\eta^5$-$C_5H_5$)(CO)Rh}$_2${μ-BN($SiMe_3$)$_2$] reported by Braunschweig [Rh–B = 2.054(2) Å].[11] Further inspection of the unit cell revealed a secondary interaction between an oxygen atom of a CO ligand and pyrrolic C–H atom of a second molecule of **5-BMes** (Figure 5.5). In benzene-$d_6$, **5-BMes** features a broad $^{11}$B resonance at δ 32.6 ($\omega_{1/2}$ = 457 Hz). This signal is upfield compared to known rhodium aminoborylene (:B–$NX_2$) complexes (δ 75 to 120),[11,12] suggesting that π-donation from nitrogen to boron in **5-BMes** effectively shields the $^{11}$B nucleus. At the time of publication, **5-BMes** was the first example of a structurally characterized terminal rhodium borylene, prompting a comprehensive study of bonding by density functional theory (DFT), as well as NBO analysis.

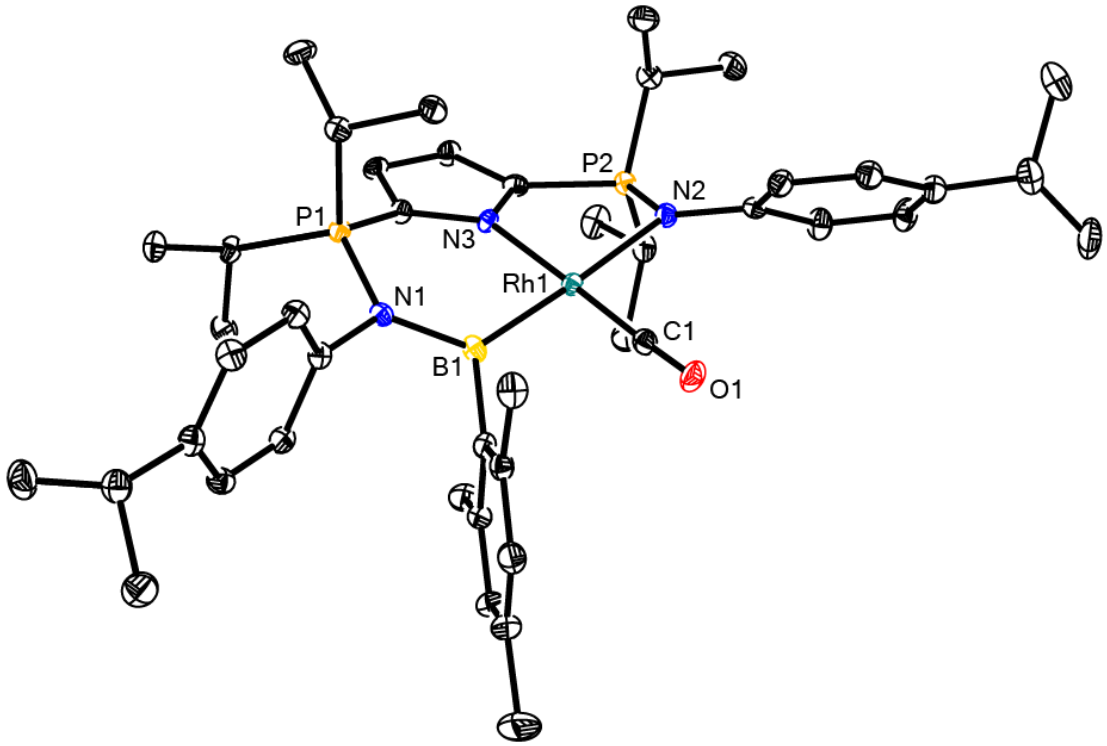


**Figure 5.4.** X-ray crystal structure of **5-BMes** illustrated using 30% probability ellipsoids. Hydrogen atoms have been omitted for clarity.

**Table 5.1.** Selected bond distances (Å) and angles (º) for **5-BMes**.

| **Parameter** | **5-BMes** |
|---|---|
| Bond distance (Å) | |
| Rh1–B1 | 2.024(5) |
| Rh1–N2 | 2.268(5) |
| Rh1–N3 | 2.068(5) |
| Rh–C1 | 1.797(6) |
| P1–N1 | 1.658(6) |
| P1–N2 | 1.584(5) |
| C1–O1 | 1.168(8) |
| N1–B1 | 1.501(8) |
| Bond angle (º) | |
| P1–N1–B1 | 127.9(4) |
| P2–N2–Rh1 | 114.2(2) |
| N3–Rh1–C1 | 177.9(2) |

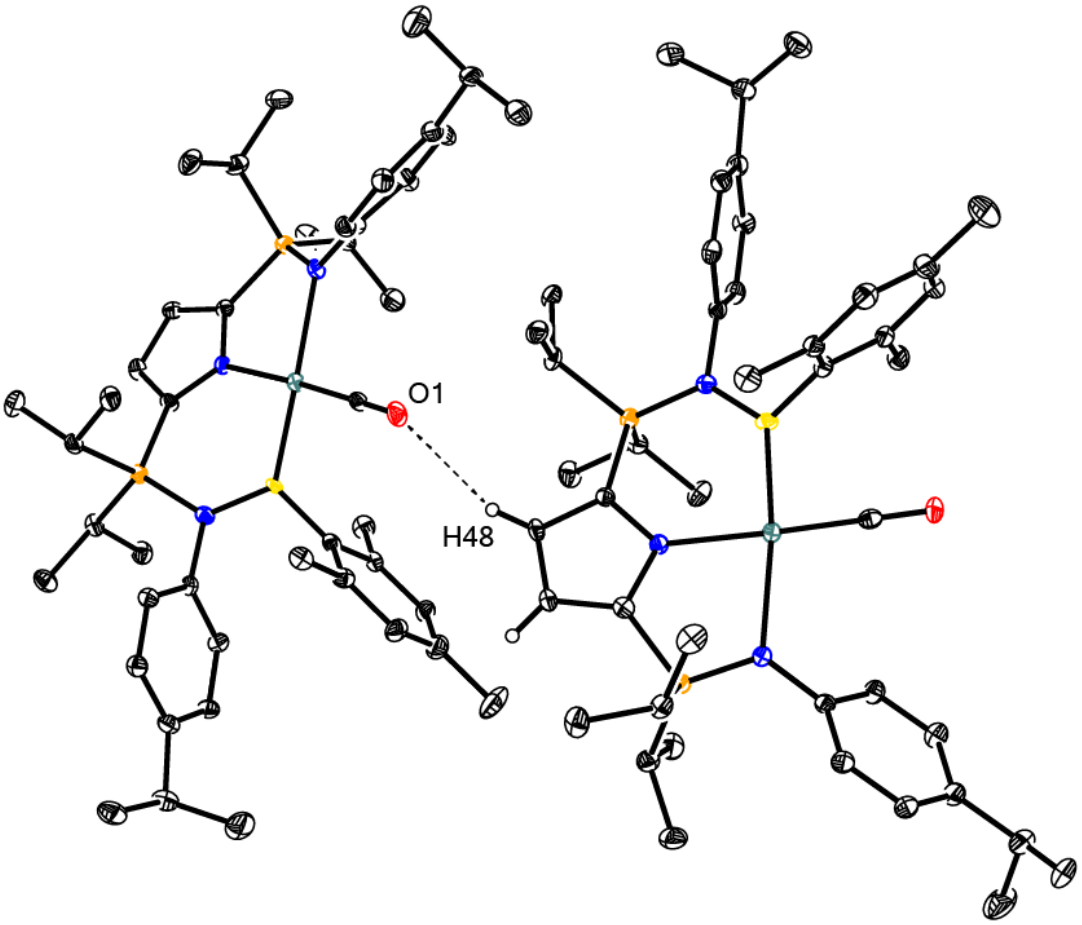


**Figure 5.5.** Depiction of a secondary interaction in the unit cell of **5-BMes** illustrated at 30% probability ellipsoids. Short contact (2.193 Å) between O1 and H48 is shown. Hydrogen atoms, except those of one pyrrole ring, have been omitted for clarity.

The gas-phase structure of **5-BMes** was optimized at the B3LYP/aug-cc-pVDZ level of theory with associated pseudopotentials for Rh (see Chapter 7 for details). Metrical parameters were reproduced in good agreement with experiment (Tables 5.1 and 5.2). The P1–N1 bond is elongated in the DFT-computed structure by +0.049 Å (%diff = 2.91%) and is consistent with single-bond P–N character in the phosphinimine bound to boron. X-ray diffraction studies from chapters 3 and 4 have emphasized the extent to which phosphinimines elongate when bound to a main group

element. It was reasoned that as contributions from the second lone pair on nitrogen increase, the P–N bond tends toward the ylidic (single-bond) extreme.

A natural bond orbital (NBO) calculation was performed on the optimized structure of 5-BMes to enhance understanding of the localized orbital interactions between rhodium, boron, and nitrogen. The B–Rh $\sigma$-bonding NBO is slightly polarized toward boron (Figure 5.6), suggesting a bonding model in which B→Rh $\sigma$-donation is the predominant interaction. Infrared (IR) spectroscopic analysis of **3-CO** (1930 $cm^{-1}$) and **5-BMes** (1909 $cm^{-1}$) revealed a redshift of the $\nu_{CO}$ stretch as a result of borylene formation, highlighting the $\sigma$-donor ability of borylene relative to phosphinimine. The B–Rh Wiberg bond index (WBI) of 0.93 falls slightly below the range established for terminal neutral borylene complexes of Co, Rh, and Ir [($\eta^5$-$C_5H_5$)(L)M=$BNX_2$), L = CO, $PMe_3$, X = Me, $SiH_3$, $SiMe_3$] (0.97-1.33).[13] Second order perturbation theory analysis indicated strong delocalization of the Lewis-type nitrogen lone pair donor orbital, N(lp) to a vacant acceptor orbital on boron, B(p) (Table 5.3). Notably, the N(lp)→B(p) interaction [$E^{(2)}$: 35.2 kcal $mol^{-1}$] was substantially stronger than the donor-acceptor π-interaction between rhodium and boron [$E^{(2)}$: 10.3 kcal $mol^{-1}$] (Figure 5.7). These data imply that phosphinimine (N) π-donation to Rh is important in **5-BMes**.

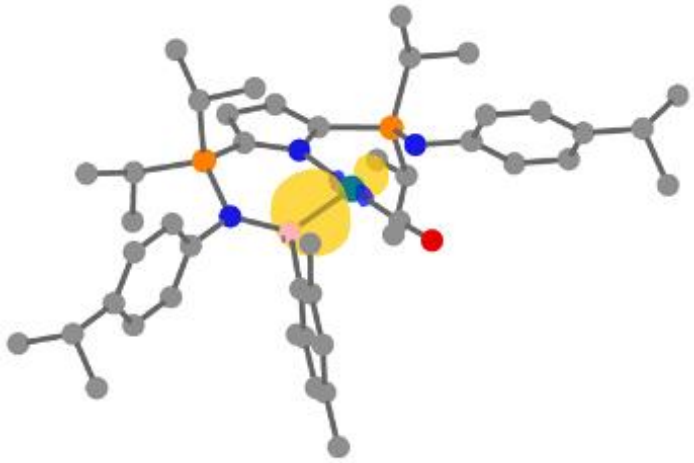

Rh–B σ NBO
Rh $d_{x2-y2}$ (46.9%)
B $p_x$ (53.0%)

**Figure 5.6.** NBO representation of the DFT-derived Rh–B bonding orbital (occupancy: 1.807 electrons). Orbital surfaces are plotted with an isovalue of 0.08 using Gaussview.

**Table 5.2.** Comparison of DFT-calculated (B3LYP/aug-cc-pVDZ) and experimental structural parameters in **5-BMes**.

| Parameter | Experimental | Calculated | % Difference |
|---|---|---|---|
| d(Rh1–B1) (Å) | 2.024(5) | 2.031 | 0.34% |
| d(P1–N1) (Å) | 1.658(6) | 1.707 | 2.91% |
| d(N1–B1) (Å) | 1.501(8) | 1.518 | 1.12% |
| d(Rh1–C1) (Å) | 1.797(6) | 1.824 | 1.49% |

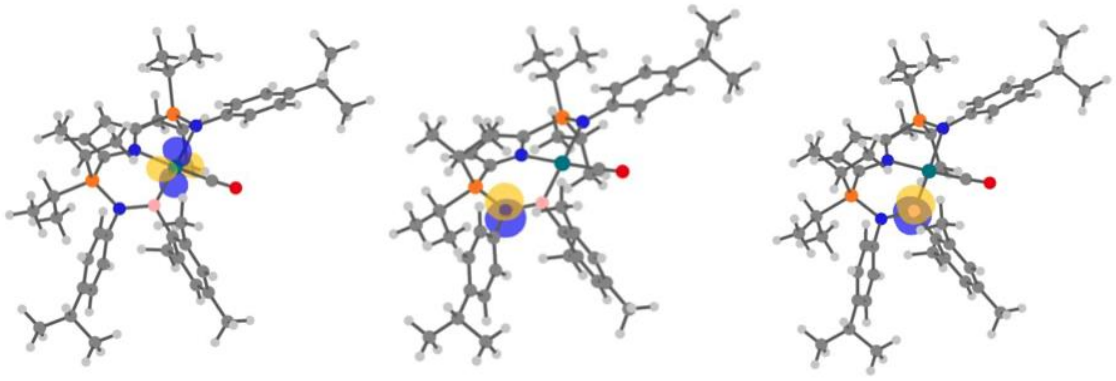

**Figure 5.7.** From left to right: representations of donor (Rh and N) and acceptor (B) NBOs for **5-BMes**.

**Table 5.3.** Selected second-order interactions involving the borylene boron atom in **5-BMes**.

| Donor | Acceptor | $E^{(2)}$ (kcal $mol^{-1}$) | $\varepsilon_i$-$\varepsilon_j$ | $F_{i,j}$ |
|---|---|---|---|---|
| 197. LP (4) Rh | 209. LP* (2) B | 1.89 | 0.21 | 0.018 |
| 202. LP (1) N | 209. LP* (2) B | 35.17 | 0.30 | 0.093 |
| 195. LP (2) Rh | 209. LP* (2) B | 10.35 | 0.21 | 0.044 |
| 196. LP (3) Rh | 209. LP* (2) B | 6.88 | 0.23 | 0.036 |

**Table 5.4.** NBO-derived Wiberg Bond Indices (WBI) of selected bonds in **5-BMes** at the B3LYP/aug-cc-pVDZ level of theory.

| Selected Bond | Wiberg Bond Index (WBI) |
|---|---|
| Rh1–B1 | 0.9308 |
| N1–B1 | 0.7026 |
| P1–N1 | 0.8570 |
| P2–N2 | 1.0606 |

The incorporation of a phosphine oxide moiety in ligand scaffolds has been shown to stabilize both primary and secondary boranes; work from the Stradiotto group highlights this strategy in the activation of both silanes and boranes in the same system.[14] Moreover, Drover, Schaefer, and Love have disclosed phosphoramidate-supported late metal systems for the activation of amino- and alkylboranes.[15] An obvious difference between phosphine oxide and phosphinimine in the present work is

the additional steric bulk surrounding the B atom, imposed by the N-aryl group. A space-filling model of **5-BMes** (Figure 5.8) illustrates the extent to which the boron atom is sterically confined. Close examination of the X-ray crystal structure revealed π–π interactions between the N- and B-aryl groups (centroid···centroid = 4.165 Å) that may hinder free rotation about the mesityl *ipso* C–B bond. Treatment of **5-BMes** with one equivalent of 4-dimethylaminopyridine yielded no evidence for adduct formation when analyzed by $^{1}H$ and $^{31}P$ NMR spectroscopy, even with prolonged heating at 50 $^{o}C$.

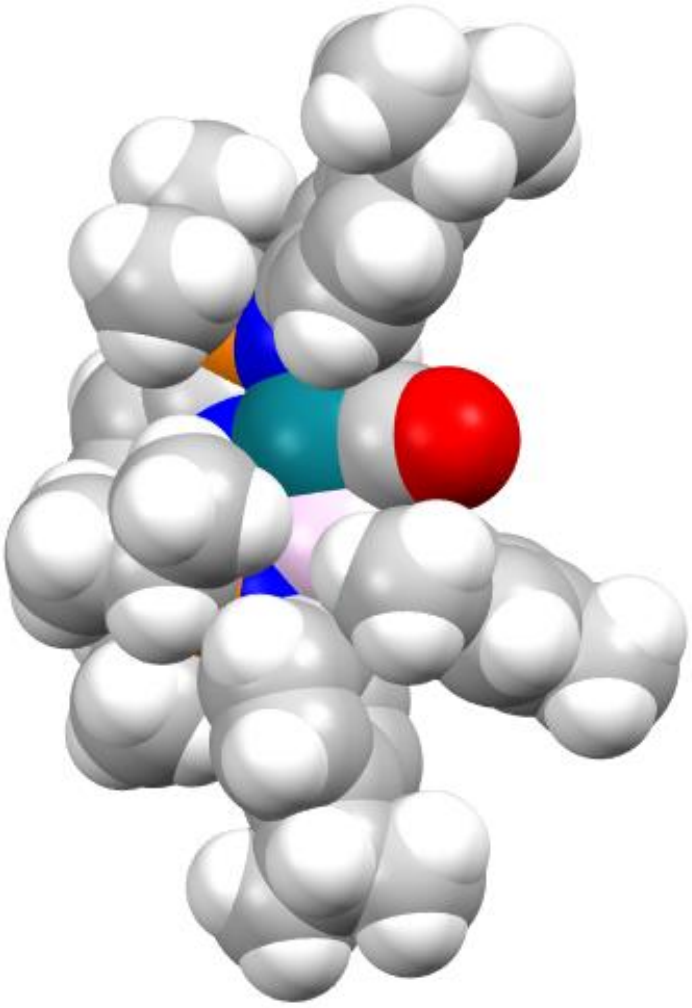

**Figure 5.8.** Space-filling model of **5-BMes** illustrating the steric shielding around the boron atom (pink).

To better understand the reversibility of B–H activation, the formation of **5-BMes** was reinvestigated in a series of isotopic-labelling experiments. Upon reaction of **3-CO** with a 1:1 mixture of 0.5 $H_2$BMes and 0.5 $D_2$BMes (1 total equivalent of borane), both $H_2$ and HD gas were identified in the $^{1}$H NMR spectrum (Figure 5.9). Examination of the $^{31}$P NMR spectrum revealed resonances corresponding to **3-CO**, **5-BMes** and some intermediate species (Figure 5.10).

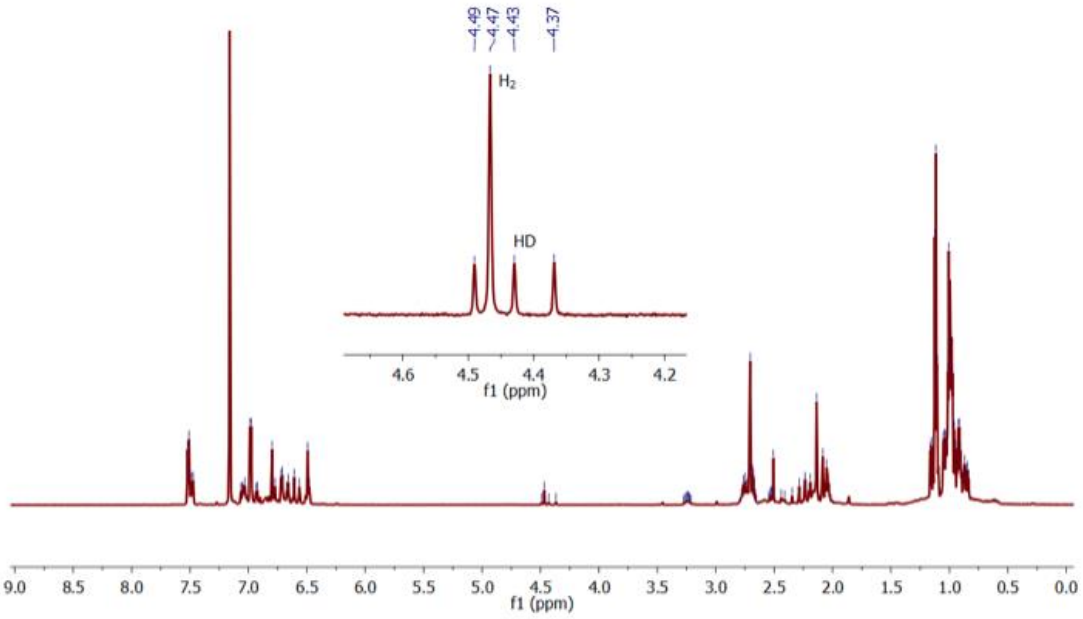


**Figure 5.9.** $^{1}$H NMR (700 MHz) spectrum of reaction between **3-CO** and a 1:1 mixture of mesitylborane and mesitylborane-$d_2$ in benzene-$d_6$. Inset: enlarged region showing $H_2$ and HD gas.

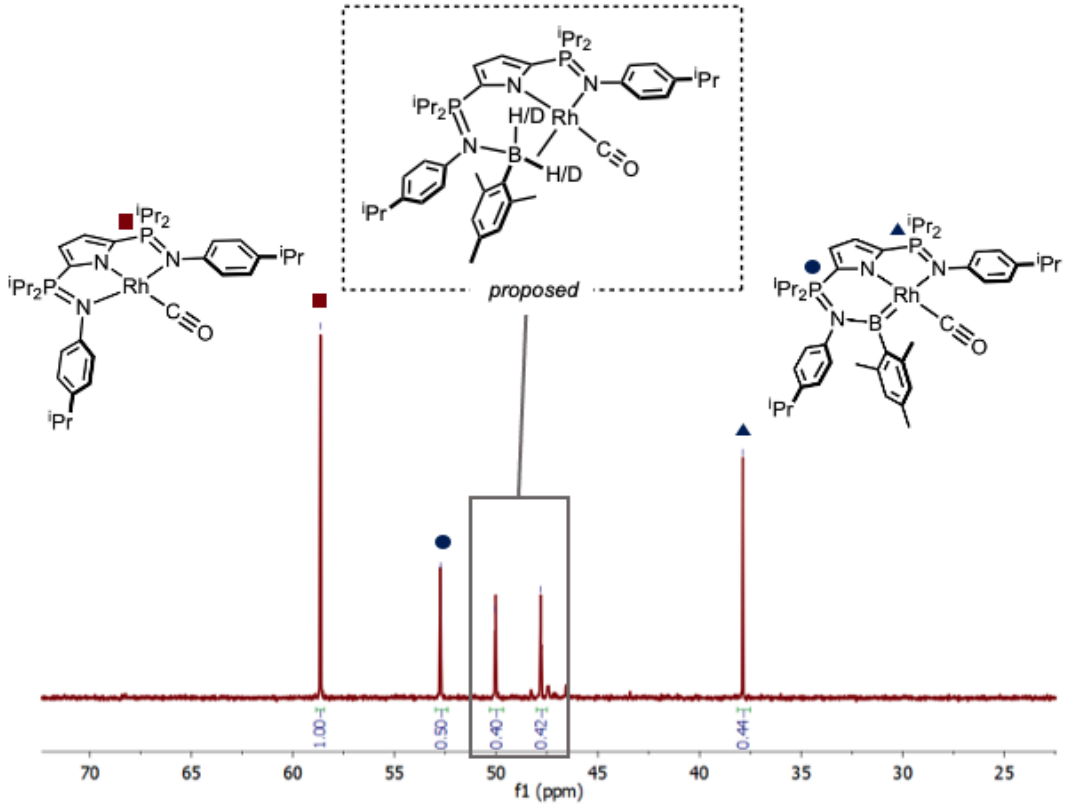


**Figure 5.10.** $^{31}P\{^{1}H\}$ NMR (283 MHz) spectrum of the reaction between **3-CO** and a 1:1 mixture of mesitylborane and mesitylborane-$d_2$ in benzene-$d_6$. Here, the proposed species "**5-CO·H$_2$BMes**" could be any of the isotopologues **5-CO·H$_2$BMes**/**5-CO·D$_2$BMes**/**5-CO·HDBMes**.

Isotope mixing supports the presence of a reactive boryl hydride,[5,16] capable of rapid Rh–H(D) and B–D(H) exchange at a rate that is competitive with the formation of **5-BMes**. Notably, the control reaction between $H_2$BMes and $D_2$BMes in the absence of **3-CO** showed no sign of H/D scrambling or evolution of HD gas. In an effort to corroborate the reversibility of borylene formation, a J. Young NMR tube containing **5-BMes** in benzene-$d_6$ was pressurized with 4 atmospheres of $H_2$ and monitored by $^{1}H$ and $^{31}P$ NMR spectroscopy. Rapid generation of mesitylborane and formation of **3-CO** (>80% in 10 minutes) was confirmed by comparing the product spectra of the

reaction to spectra of authentic samples. Examination of the $^{31}$P NMR spectrum after 1 week indicated that the equilibrium of **3-CO** + $H_2$BMes and **5-BMes** + $H_2$ was maintained under $H_2$ pressure (**5-BMes**:**3-CO** = 9:1). Hence, it was concluded that the poor yields obtained for reactions conducted at ambient temperature were likely the result of rapid re-uptake of hydrogen by **5-BMes**. Altering the original procedure by carrying out the reaction at low temperature under reduced pressure allowed the isolation of analytically pure **5-BMes** in substantially improved (53%) yield.[17]

To demonstrate the capacity for **5-BMes** to participate in group transfer chemistry beyond that already observed with $H_2$ gas, reactions that would release the {BMes} fragment from the rhodium(I) center were investigated. Complete borylene transfer was observed upon addition of pinacol to **5-BMes**, producing the boronate ester MesBpin, **3-CO**, and $H_2$ gas (Scheme 5.4). Monitoring the reaction by $^{31}$P NMR spectroscopy for ~1 week revealed gradual consumption of **5-BMes** with no evidence of any intermediate species (Figure 5.11) consistent with the formation of strong B–O bonds in a thermodynamically-favourable reaction.

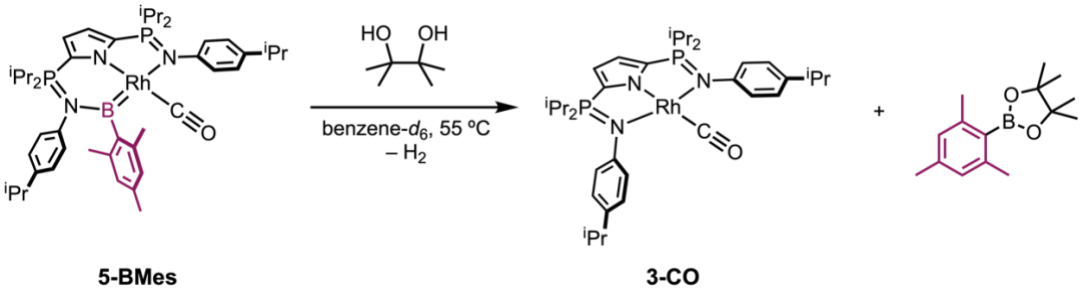


**Scheme 5.4.** Reaction of **5-BMes** with pinacol in benzene-$d_6$ monitored over 6 days at 55 °C.

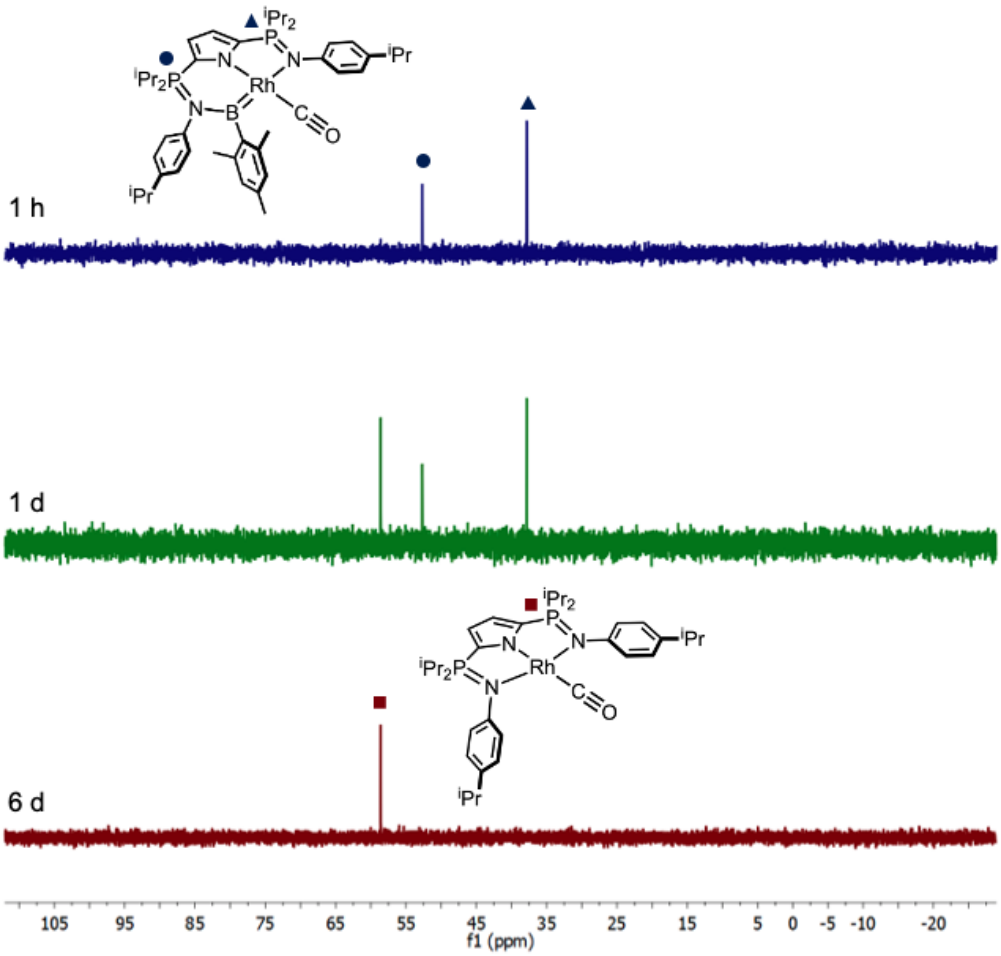


**Figure 5.11.** Stacked $^{31}P\{^{1}H\}$ NMR (283 MHz) spectra of the reaction between **5-BMes** and 1 equivalent of pinacol. Blue trace: 1 hour; Green trace: 1 day; Red trace: 6 days. The bottom (red) $^{31}P\{^{1}H\}$ spectrum is in accord with the $^{31}P\{^{1}H\}$ NMR spectrum of an authentic sample of **3-CO**.

Monitoring the reaction of **3-CO** and $H_2BMes$ by variable temperature NMR spectroscopy in toluene-$d_8$ at –40 ºC led to the observation of an intermediate species with $^{31}P$ resonances at δ 50.4 and δ 47.8 (*vide supra*). The accompanying $^{1}H$ NMR spectrum revealed a broad resonance centered at δ –2.7. Upon warming to 22 ºC, $^{1}H$ and $^{31}P$ peaks corresponding to the intermediate species were completely consumed while those attributed to **5-BMes** had grown in intensity. Notably, $H_2$ gas (δ 4.57) was

always visible in solution during the experiment. The intermediate species forms by dissociation of phosphinimine from rhodium, followed by coordination to the aryl borane to afford **5-CO·$H_2$BMes**. A B–H bond then undergoes oxidative addition, producing the Rh boryl hydride species ($^{iPr}$NNN)(CO)Rh(H)(BHMes). Finally, $H_2$ loss presumably occurs *via* either a 4-centered transition state involving Rh–H (δ+) and B–H (δ–), or a Brønsted pathway mediated by a free phosphinimine group (Scheme 5.3).[10]

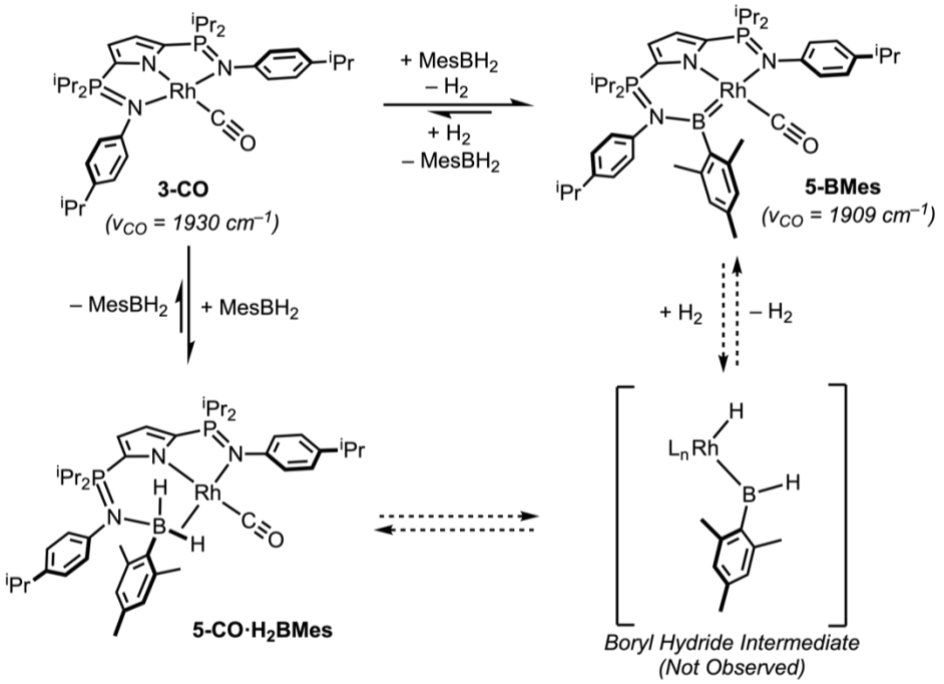


**Scheme 5.3.** Proposed formation of **5-BMes** via rhodium(III) boryl hydride.

The generality of aryl borane dehydrogenation was studied by reducing the steric profile about boron and altering the electronics of the aryl group. The trifluoromethylated borane $H_2BAr^F$ ($Ar^F$ = 3,5-$(CF_3)_2C_6H_3$) was combined with **3-CO** in benzene-$d_6$ leading to new $^{31}$P NMR resonances at δ 51.2 and δ 48.8, which closely resemble the intermediate observed in the low temperature reaction between **3-CO** and mesitylborane (δ 50.4 and δ 47.8, *vide supra*). In benzene-$d_6$, the $^{11}$B NMR spectrum

exhibits a single peak at δ –5.92 ($\omega_{1/2}$ = 11.1 Hz). In anticipation of unproductive back reaction with $H_2$, the experiment was repeated at –30 ºC in diethylether. A gradual colour change from orange to dark-yellow was accompanied by formation of a crystalline yellow solid which was isolated in 80% yield. Single crystals suitable for X-ray diffraction analysis were grown from a concentrated pentane/benzene (5:1) solution. The X-ray crystal structure of the isolated product **5-CO·$H_2$BAr$^F$** was confirmed as an encounter complex between **3-CO** and $H_2BAr^F$ (Figure 5.12), stabilized by phosphinimine coordination to boron [N1–B1 = 1.558(2) Å] and a B–H agostic interaction [H1–Rh1 = 1.61(2) Å] with the Rh center (Table 5.5).

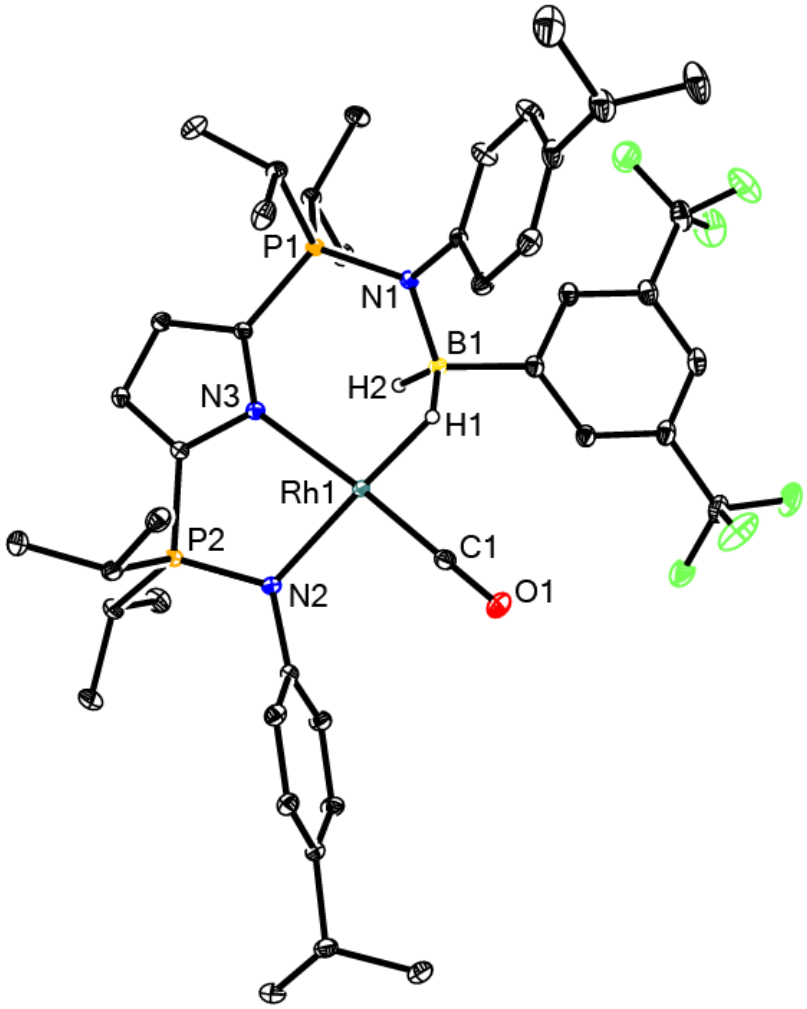


**Figure 5.12.** X-ray crystal structure of **5-CO·H$_2$BAr$^F$** illustrated using 30% probability ellipsoids. All hydrogen atoms (except H$_2$BArF) and one solvent molecule of benzene have been omitted for clarity.

**Table 5.5.** Selected bond distances (Å) and angles (º) for **5-CO·H$_2$BAr$^F$** ($^*$non-covalent interaction).

| Parameter | 5-CO·H$_2$BAr$^F$ |
|---|---|
| Bond distance (Å) | |
| Rh1–B1 | 2.482(2)$^*$ |
| Rh1–N2 | 2.094(1) |
| Rh1–N3 | 2.129(1) |
| Rh–C1 | 1.805(2) |
| P1–N1 | 1.642(1) |
| P1–N2 | 1.612(1) |
| C1–O1 | 1.155(2) |
| N1–B1 | 1.558(2) |
| Rh1–H1 | 1.61(2) |

| | |
|---|---|
| B1–H1 | 1.32(2) |
| B1–H2 | 1.11(2) |
| Bond angle (º) | |
| P1–N1–B1 | 119.0(1) |
| P2–N2–Rh1 | 116.90(7) |
| N3–Rh1–C1 | 172.95(7) |
| N2–Rh1–H1 | 175.6(7) |
| N1–B1–H1 | 110(1) |
| H1–B1–H2 | 115(1) |
| H2–B1–$C_{ipso}$ | 111(1) |
| H1–B1–$C_{ispo}$ | 105.9(9) |

The $\nu_{CO}$ stretching frequency (1950 $cm^{-1}$) in **5-CO·$H_2$BAr$^F$** is blue-shifted in the order **5-CO·$H_2$BAr$^F$** > **3-CO** > **5-BMes**, consistent with Nakazawa's report that strong delocalization of electron density from Rh to B is facilitated by a Rh···H–B linkage.[18] At 23 ºC, the $^1$H NMR spectrum of **5-CO·$H_2$BAr$^F$** contains a broad resonance at δ –3.8, tentatively assigned to the two rapidly exchanging B$H_2$. Upon cooling a toluene-$d_8$ solution of **5-CO·$H_2$BAr$^F$** to –80 ºC distinct resonances at δ 3.9 (B–*H*) and δ –9.8 (Rh–*H*–B) were observed. The coalescence temperature ($T_{coal}$) was determined by careful inspection of the $^1$H NMR spectra in toluene-$d_8$ at a range of temperatures (Figure 5.14). At –25 ºC, the peaks corresponding to the B–*H* and Rh–*H* protons vanished and the broad signal corresponding to the B$H_2$ moiety had not yet appeared. Here, Δν is the maximum peak separation in Hz. The $\Delta G^{\ddagger}$ was calculated using equation 5.1 at the coalescence temperature (–25 ºC). The two signals coalesce at –25 ºC ($\Delta G^{\ddagger}$ = 9.9(4) kcal $mol^{-1}$), reappearing as the original broad resonance (δ –3.8) near 0 ºC.

$$\Delta G^{\ddagger}_{coal}\,(\text{kcal mol}^{-1}) = \frac{1.914 \times 10^{-2}(T_{coal})[9.972 + \log\frac{T_{coal}}{\Delta\nu}]}{4.184} \qquad (\mathbf{5.1})$$

$T_{coal}$ = coalescence temperature (K)

$\Delta\nu$ = maximum peak separation (Hz)

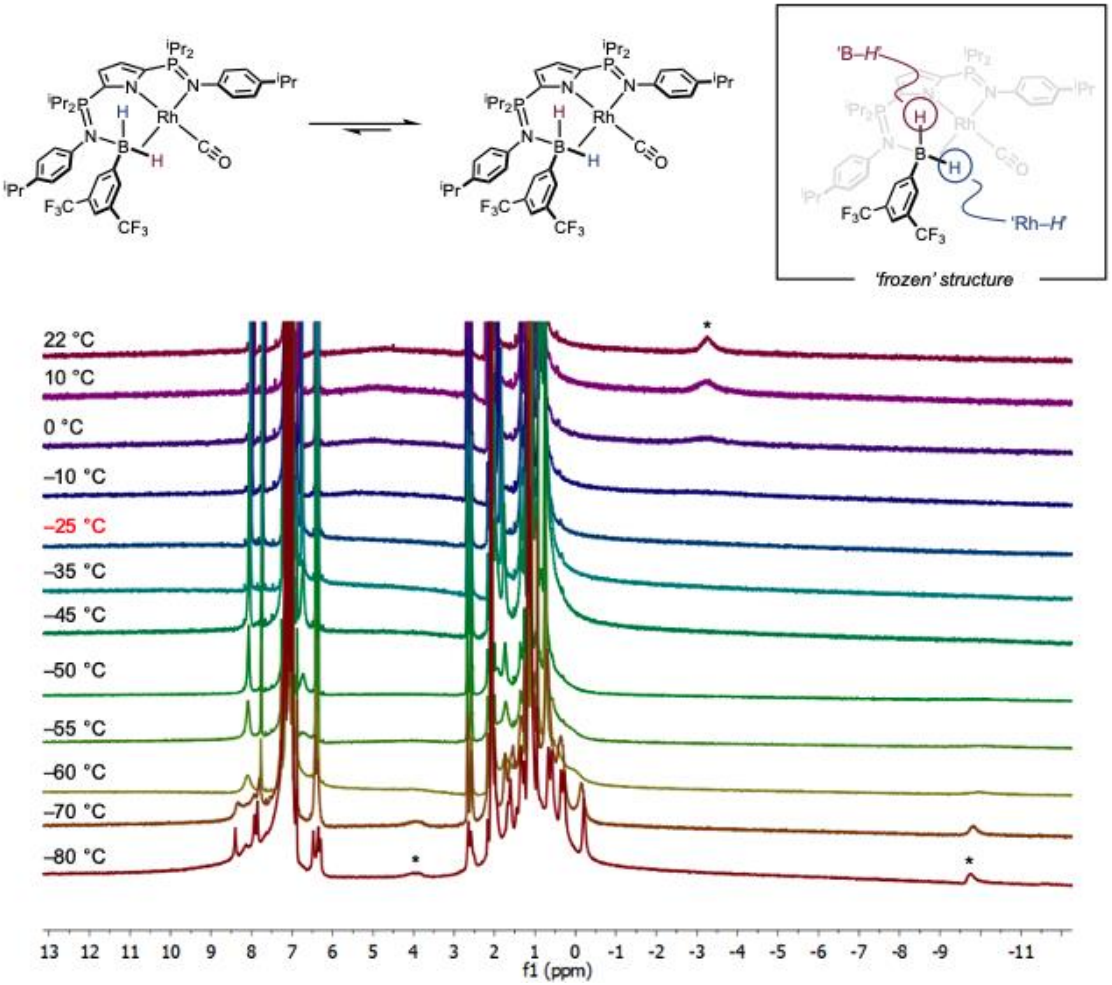


**Figure 5.13.** Stacked $^{1}$H NMR spectra of **5-CO·$H_2$BAr$^F$** in toluene-$d_8$. Coalescence temperature highlighted in red. Asterisks depict B–H chemical shifts of interest.

Despite the attenuated steric profile of $H_2BAr^F$, no evidence for borylene formation was observed, perhaps because the oxidative addition product, a Rh boryl hydride, is unstable to reductive elimination and reformation of **5-CO·$H_2$BAr$^F$**. These observations are in line with a recent contribution from Braunschweig detailing the steric and electronic parameters associated with borylene formation from $Ru(PCy_3)_2HCl(H_2)$ and various dihydroboranes.[19] For spontaneous dehydrogenation to occur from bis(σ)-borane complexes, aryl groups bearing *ortho*-substituents were

required. Aryl boranes containing only *meta*-substitution resulted in net endergonic reactions ($\Delta G$ between +0.98 and +2.40 kcal mol$^{-1}$), providing strong evidence that an *ortho-to-boron* effect is operative in the destabilization of ruthenium bis(σ)-borane complexes. Notably, the authors reported that attempts to prepare rhodium borylene complexes resulted in starting material decomposition.

Without a viable pathway for release of $H_2$, and consequently, borylene formation, reaction progress apparently stalls at **5-CO·H$_2$BAr$^F$**. While the interactions between **3-CO** and $H_2BAr^F$ render the complex stable for the purpose of isolation, dissolution of **5-CO·H$_2$BAr$^F$** in THF-$d_8$ immediately and exclusively gave **3-CO** and $H_2Ar^FB$·THF. Furthermore, when a sample of **5-CO·H$_2$BAr$^F$** was left at 23 ºC in benzene-$d_6$ for 48 h, a gradual change in the $^{31}$P NMR spectrum was accompanied by darkening of the solution and the appearance of rhodium black. A new asymmetric product formed, as judged by $^{31}$P peaks located at δ 52.0 and δ 10.6. The latter resonance is diagnostic of a dissociated phosphinimine,[10] implying that the new complex features a κ$^2$-bound $^{i\text{Pr}}$NNN ligand scaffold. A broad resonance at δ 4.7 in the $^1$H NMR spectrum sharpened considerably when decoupled from $^{11}$B. It is postulated that spontaneous decarbonylation of **5-CO·H$_2$BAr$^F$** afforded a new bis(σ-B–H) borane complex featuring $H_2BAr^F$ as a bis(σ-B–H) ligand (Scheme 5.5). Despite repeated efforts, an X-ray crystal structure supporting the formation of such a species has not been obtained, so the identity of the product remains tenuous. However, examination of the corresponding IR spectrum supported this hypothesis, as there were no distinguishable stretching frequencies corresponding to a CO ligand. Accordingly, the $^{13}$C-labelled complex **5-$^{13}$CO·H$_2$BAr$^F$** was prepared using **3-$^{13}$CO**. The $^{13}$C NMR

spectrum of **5-$^{13}$CO·H$_2$BAr$^F$** in benzene-$d_6$ exhibited a doublet ($^1J_{CRh}$ = 73.4 Hz) centered at δ 190.6 which completely disappeared after 12 h at 23 ºC. Given that the $^{13}$C label was not identified in any by-products, it is reasonable to conclude that $^{13}$CO elimination from **5-$^{13}$CO·H$_2$BAr$^F$** occurred with concomitant formation of the rhodium bis(σ)-borane complex **5-H$_2$BAr$^F$** (Scheme 5.5). While spontaneous decarbonylation from square-planar Rh is rare, Nakazawa showed that a B–H–Rh linkage can destabilize π-back-donation from Rh to CO.[18] Comparing $\nu_{CO}$ (IR) frequencies and $^1J_{CRh}$ coupling constants (Hz) suggests that the weakest Rh–C bond is present in **5-CO·H$_2$BAr$^F$** (1950 cm$^{-1}$, 73.5 Hz; c.f. 1930 cm$^{-1}$, 76.9 Hz for **5-BMes** and 1909 cm$^{-1}$, 87.9 Hz for **3-CO**). These spectroscopic data imply that of all the rhodium carbonyl complexes described in this chapter, **5-CO·H$_2$BAr$^F$** is most poised for decarbonylation.

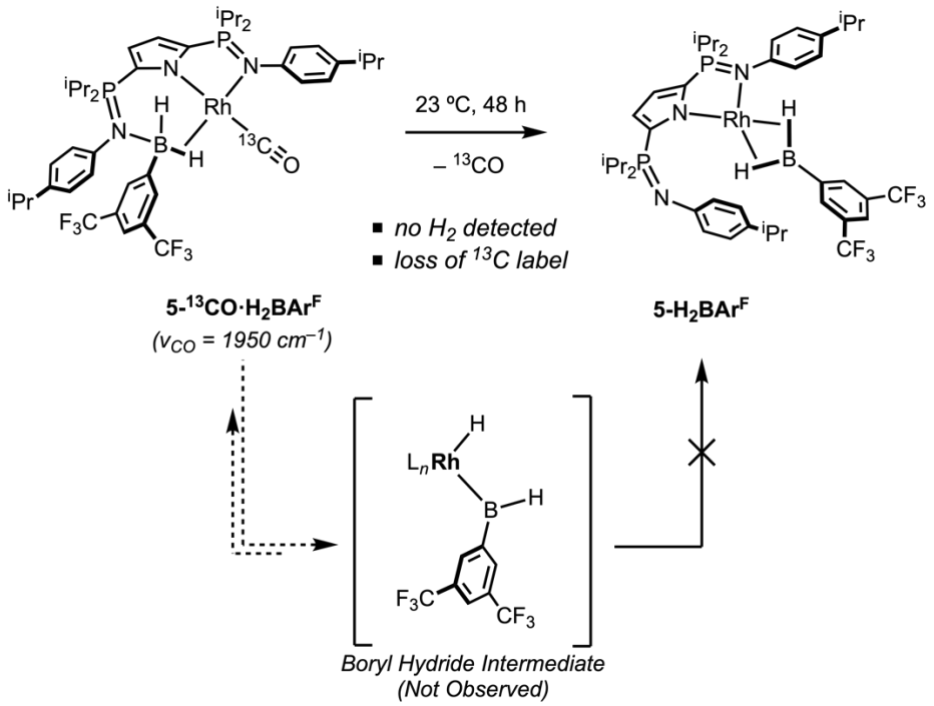


**Scheme 5.4.** Proposed formation of the borane complex **5-H$_2$BAr$^F$** by irreversible CO elimination.

## 5.4. Conclusions

The reversible dehydrogenation of an aryl dihydroborane has been demonstrated for the first time at rhodium. Complexation of the borane by a hemilabile phosphinimine led to spontaneous $H_2$ elimination in the case of mesitylborane. Group transfer reactivity of the {BMes} fragment was observed in reactions with $H_2$ and pinacol, where the latter generated the boronate ester MesBpin, along with $H_2$ gas. Entrapment of the electron-deficient borane $H_2B(3,5\text{-}(CF_3)_2C_6H_3)$ by **3-CO** highlights that subtle steric and electronic factors are involved in spontaneous dehydrogenation.[19] Ultimately, with the demonstration of formal borylene transfer, these results provide a method for interconversion of boranes and borylenes with hydrogen, from which new and more efficient routes to organoboranes may be developed.

## 5.5. References

**1.** (a) Waltz, K. M.; Hartwig, J. F. Selective functionalization of alkanes by transition-metal boryl complexes. *Science* **1997**, *277*, 211–213. (b) Mkhalid, I. A. I.; Barnard, J. H.; Marder, T. B.; Murphy, J. M.; Hartwig, J. F. C–H Activation for the Construction of C–B Bonds *Chem. Rev.* **2010**, *110*, 890–931. (c) Obligacion, J. V.; Semproni, S. P.; Chirik, P. J. Cobalt-Catalyzed C–H Borylation. *J. Am. Chem. Soc.* **2014**, *136*, 4133–4136. (d) Ros, A.; Fernández, R.; Lassaletta, J. M. Functional group directed C–H borylation. *Chem. Soc. Rev.* **2014**, *43*, 3229–3243.

**2.** (a) Westcott, S. A.; Blom, H. P.; Marder, T. B.; Baker, R. T. New homogeneous rhodium catalysts for the regioselective hydroboration of alkenes. *J. Am. Chem. Soc.* **1992**, *114*, 8863–8869. (b) Burgess, K.; van der Donk, W. A.; Westcott, S. A.; Marder, T. B.; Baker, R. T.; Calabrese, J. C. Reactions of catecholborane with Wilkinson's catalyst: implications for transition metal-catalyzed hydroborations of alkenes. *J. Am. Chem. Soc.* **1992**, *114*, 9350–9359. (c) Muhoro, C. N.; He, X.; Hartwig, J. F. Titanocene Borane σ-Complexes. *J. Am. Chem. Soc.* **1999**, *121*, 5033–5046. (d) Crudden, C. M.; Edwards, D. Catalytic Asymmetric Hydroboration: Recent Advances and Applications in Carbon−Carbon Bond-Forming Reactions. *Eur. J. Org. Chem.* **2003**, 4695–4712.

**3.** (a) Montiel-Palma, V.; Lumbierres, M.; Donnadieu, B.; Sabo-Etienne, S.; Chaudret, B. σ Borane and Dihydroborate Complexes of Ruthenium. *J. Am. Chem. Soc.* **2002**, *124*, 5624–5625. (b) Alcaraz, G.; Clot, E.; Helmstedt, U.; Vendier, L.; Sabo-Etienne, S. Mesitylborane as a Bis(σ-B–H) Ligand: An Unprecedented Bonding Mode to a Metal Center. *J. Am. Chem. Soc.* **2007**, *129*, 8704–8705. (c) Alcaraz, G.; Grellier, M.; Sabo-Etienne, S. Bis σ-Bond Dihydrogen and Borane Ruthenium Complexes: Bonding Nature, Catalytic Applications, and Reversible Hydrogen Release. *Acc. Chem. Res*. **2009**, *42*, 1640–1649. (d) Alcaraz, G.; Vendier, L.; Clot, E.; Sabo-Etienne, S. Ruthenium Bis(σ-B–H) Aminoborane Complexes from Dehydrogenation of Amine–Boranes: Trapping of $H_2B$–$NH_2$. *Angew. Chem. Int. Ed.* **2010**, *49*, 918–920.

**4.** (a) Alcaraz, G.; Helmstedt, U.; Clot, E.; Vendier, L.; Sabo-Etienne, S. A Terminal Borylene Ruthenium Complex: From B–H Activation to Reversible Hydrogen Release. *J. Am. Chem. Soc.* **2008**, *130*, 12878–12879. (b) Braunschweig, H.; Dewhurst, R. D. Reversible σ-Borane-to-Borylene Transformation: A Little Something For Everyone. *Angew. Chem. Int. Ed.* **2009**, *48*, 1893–1895.

**5.** O'Neill, M.; Addy, D. A.; Riddlestone, I.; Kelly, M.; Phillips, N.; Aldridge, S. Borane to Boryl Hydride to Borylene Dihydride: Explicit Demonstration of Boron-to-Metal α-Hydride Migration in Aminoborane Activation. *J. Am. Chem. Soc.* **2011**, *133*, 11500–11503.

**6.** (a) Jaska, C. A.; Temple, K.; Lough, A. J.; Manners, I. Transition Metal-Catalyzed Formation of Boron–Nitrogen Bonds: Catalytic Dehydrocoupling of Amine-Borane Adducts to Form Aminoboranes and Borazines. *J. Am. Chem. Soc.* **2003**, *125*, 9424–9434. (b) Baker, R. T.; Gordon, J. C.; Hamilton, C. W.; Henson, N. J.; Lin, P.-H.; Maguire, S.; Murugesu, M.; Scott, B. L.; Smythe, N. C. Iron Complex-Catalyzed Ammonia–Borane Dehydrogenation. A Potential Route toward B–N-Containing Polymer Motifs Using Earth-Abundant Metal Catalysts. *J. Am. Chem. Soc.* **2012**, *134*, 5598–5609. (c) Kumar, A.; Beattie, N. A.; Pike, S. D.; Macgregor, S. A.; Weller, A. S. The Simplest Amino-borane H2B=NH2 Trapped on a Rhodium Dimer: Pre-Catalysts for Amine–Borane Dehydropolymerization. *Angew. Chem. Int. Ed*. **2016**, *55*, 6651–6656. (d) Colebatch, A. L.; Weller, A. S. Amine–Borane Dehydropolymerization: Challenges and Opportunitoes. *Chem. Eur. J.* **2019**, *25*, 1379–1390.

**7.** Drance, M. J.; Sears, J. D.; Mrse, A. M.; Moore, C. E.; Rheingold, A. L.; Neidig, M. L.; Figueroa, J. S. Terminal coordination of diatomic boron monofluoride to iron. *Science* **2019**, *363*, 1203–1205.

**8.** N. Arnold, N.; H. Braunschweig, H.; R. D. Dewhurst, R. D.; W. C. Ewing, W. C. Unprecedented Borane, Diborane(3), Diborene, and Borylene Ligands via Pt-Mediated Borane Dehydrogenation. *J. Am. Chem. Soc.* **2016**, *138*, 76–79.

**9.** Parkin, G. A Simple Description of the Bonding in Transition-Metal Borane Complexes. *Organometallics* **2006**, *25*, 4744–4747.

**10**. MacNeil, C. S.; Hayes, P. G. An H-Substituted Rhodium Silylene. *Chem. Eur. J.* **2019**, *25*, 8203–8207.

**11.** Braunschweig, H.; Forster, M.; Kupfer, T.; Seeler, F. Borylene Transfer under Thermal Conditions for the Synthesis of Rhodium and Iridium Borylene Complexes. *Angew. Chem. Int. Ed.* **2008**, *47*, 5981–5983.

**12.** Braunschweig, H.; Forster, M.; Seeler, F. Synthesis and Structure of Heterodinuclear Rhodium and Iridium Borylene Complexes. *Chem. Eur. J.* **2008**, *15*, 469–473.

**13.** Pandey, K. K.; Musaev, D. G. Structure and Bonding Energy Analysis of Cobalt, Rhodium, and Iridium Borylene Complexes [($\eta^5$-$C_5H_5$)(CO)M($BNX_2$] (X = Me, $SiH_3$, $SiMe_3$) and [($\eta^5$-$C_5H_5$)($PMe_3$)M{$BN(SiH_3)_2$}] (M = Co, Rh, Ir) *Organometallics* **2010**, *29*, 142–148.

**14.** Rankin, M. A.; Hesp, K. D.; Schatte, G.; McDonald, R.; Stradiotto, M. Exploring the reactivity of a coordinatively unsaturated Cp*Ru($\kappa^2$-P,O) complex with small molecule substrates: application in E–H bond activation (E= H, B, and Si). *Dalton Trans.* **2009**, 4756–4765.

**15.** (a) Drover, M. W.; Schafer, L. L.; Love, J. A. Capturing $HBCy_2$: Using N,O-Chelated Complexes of Rhodium(I) and Iridium(I) for Chemoselective Hydroboration. *Angew. Chem. Int. Ed.* **2016**, *55*, 3181–3186. (b) Drover, M. W.; Bowes, E. G.; Schafer, L. L.; Love, J. A.; Weller, A. S. Phosphoramidate-Supported Cp*$Ir^{III}$ Aminoborane $H_2B{=}NR_2$ Complexes: Synthesis, Structure, and Solution Dynamics. *Chem. Eur. J.* **2016**, *22*, 6793–6797. (c) Drover, M. W.; Johnson, H. C.; Schafer, L. L.; Love, J. A.; Weller, A. S. Reactivity of an Unsaturated Iridium(III) Phosphoramidate Complex, [Cp*Ir{$\kappa^2$-*N,O*}][$BAr^F{}_4$] *Organometallics* **2015**, *34*, 3849–3856.

**16.** (a) Kawano, Y.; Yasue, T.; Shimoi, M. BH Bond Activation of Trimethylphosphineborane by Transition Metal Complexes: Synthesis of Metal Complexes Bearing Nonsubstituted Boryl–Trimethylphosphine, Cp*M$(CO)_3$($BH_2$·$PMe_3$) (M = Mo, W). *J. Am. Chem. Soc.* **1999**, *121*, 11744–11750. (b) Yasue, T.; Kawano, Y.; Shimoi, M. Proton-Induced Change of the Coordination Mode of a Boron Group: Boryl Complexes [$Mn(CO)_4(PR_3)(BH_2{\cdot}PMe_3)$] and Cationic Borane σ Complexes [$Mn(CO)_4(PR_3)(\eta^1$-$BH_3{\cdot}PMe_3)]^+$. *Angew. Chem. Int. Ed.* **2003**, *42*, 1727–1730. (c) Nakazawa, H.; Ohba, M.; Itazaki, M. Synthesis and Reactivity of a Phosphite−Boryl Complex of Molybdenum: Formation of ($\eta^5$-$C_5Me_5$)Mo$(CO)_3$($BH_2$·phosphite) and Its Mo−B, B−P, and B−H Bond Reactions. *Organometallics* **2006**, *25*, 2903–2905. (d) Braunschweig, H.; Matz, F.; Radacki, K.; Schneider, A. Reactivity of Platinum Iminoboryl

Complexes toward Covalent Element−Hydrogen Bonds of Opposing Polarity. *Organometallics* **2010**, *29*, 3457–3462. (e) Adams, G. M.; Colebatch, A. L.; Skornia, J. T.; McKay, A. I.; Johnson, H. C.; Lloyd-Jones, G. C.; Macgregor, S. A.; Beattie N. A.; Weller, A. S. *J. Am. Chem. Soc.* **2018**, *140*, 1481–1495. (f) Hui, Z.; Watanabe, T.; Tobita, H. Synthesis of Base-Stabilized Hydrido(hydroborylene)tungsten Complexes and Their Reactions with Terminal Alkynes To Give $\eta^3$-Boraallyl Complexes. *Organometallics* 2017, *36*, 4816–4824. (g) Johnson, H. C.; McMullin, C. L.; Pike, S. D.; Macgregor, S. A.; Weller, A. S. Dehydrogenative Boron Homocoupling of an Amine-Borane. *Angew. Chem. Int. Ed.* **2013**, *52*, 9776–9780. (h) Tang, C. Y.; Phillips, N.; Bates, J. I.; Thompson, A. L.; Gutmann, M. J.; Aldridge, S. Dimethylamine borane dehydrogenation chemistry: syntheses, X-ray and neutron diffraction studies of 18-electron aminoborane and 14-electron aminoboryl complexes. *Chem. Commun.* **2012**, *48*, 8096–8098.

**17.** Greb, L.; Oña-Burgos, P.; Schirmer, B.; Grimme, S.; Stephan, D. W.; Paradies, J. Metal-free Catalytic Olefin Hydrogenation: Low-Temperature $H_2$ Activation by Frustrated Lewis Pairs. *Angew. Chem. Int. Ed.* **2012**, *51*, 10164–10168.

**18.** Kameo, H.; Nakazawa, H. Synthesis of a Rhodium Complex Featuring the Rh–H–B Linkage via a Hydride Migration from Rhodium to Borane: Study on the Electronic Deviation Induced by the Presence of the Boron Moiety. *Organometallics* **2012**, *31*, 7476–7484.

**19.** Lenczyk, C.; Roy, D. K.; Nitsch, J.; Radacki, K.; Rauch, F.; Dewhurst, R. D.; Bickelhaupt, F. M.; Marder, T. B.; Braunschweig, H. Steric Effects Dictate the Formation of Terminal Arylborylene Complexes of Ruthenium from Dihydroboranes. *Chem. Eur. J.* **2019**, *25*, 13566–13571.

# Chapter 6: Conclusions and Future Work

## 6.1. Conclusions

The pairing of monoanionic bis(phosphinimine)pyrrolido ligands and rhodium(I) has led to the development of bond activation strategies enabled by metal-ligand cooperation. Beginning with the P-phenylated ligand $^{Ph}$NNN described in Chapter 2, alkene interconversion and catalytic hydrogenation was developed. The $^{Ph}$NNN ligand is instrumental in the stabilization of the catalyst resting state **2-Rh$_2$**, and to the heterolytic cleavage of $H_2$ across metal and ligand, as evidenced by the solution- and solid-state characterization of a protonated phosphinimine ($\delta$ 11.40; d, 1H, $^2J_{HP}$ = 2.5 Hz, P=N*H*). By all accounts, the isolation and characterization of **2-Rh$_2$** marked the beginning of the investigations that ultimately make up this thesis work insofar as highlighting a ligand platform which could be modified to exploit metal-ligand cooperation in the activation of small molecules.

In Chapter 3, a series of carbonylated rhodium(I) complexes bearing a modified bis(phosphinimine)pyrrolido ligand were prepared and characterized in solution and in the solid state. Replacement of the phenyl substituents on the phosphinimine P atom with isopropyl groups rendered the $^{iPr}$NNN ligand sufficiently electron-donating to stabilize either mono- or dicarbonylated Rh(I) metal centers, along with the activated CO complex **3-(CO)$_2$·BCF**. In combination with the Lewis acid B($C_6F_5$)$_3$, gradual deoxygenation of the CO ligand at ambient temperatures permitted an isotopic-labelling study using $^{13}$C-enriched **3-($^{13}$CO)$_2$·BCF**, prepared from the condensation of $^{13}$CO gas onto a solution of **2-COE**. Following the $^{13}$C-isotope label by $^{13}$C NMR spectroscopy revealed that deoxygenative metathesis was operative in the complete scission of the CO ligand.

Isolation of the relevant products, and their subsequent characterization by NMR spectroscopy and X-ray crystallography, provided a comprehensive summary of the reaction, and identified the fate of all reactive species.

Characterization of the so-called 'encounter complex' **3-(CO)$_2$·BCF** in the solid state by X-ray crystallography permitted a thorough investigation into the structure and bonding of the phosphinimine bound to CO. Notably, significant elongation of the P–N bond (1.693 Å) relative to both free phosphinimines and phosphinimines bound to rhodium(I) throughout this thesis, revealed an ylidic character in **3-(CO)$_2$·BCF** that places a formal positive charge on the P atom in the corresponding resonance form. Notably, this was a recurring feature in Chapters 3 and 4 and is likely a stabilizing influence that enables the activation of small molecules.

Divergent reactivity with Si–H bonds was demonstrated in Chapter 3 by substitution of the organometallic ligand in 16-electron Rh(I) complexes of the bis(phosphinimine)pyrrolido ligand $^{iPr}$NNN. Oxidative addition of the Si–H bonds in $PhSiH_3$, $Ph_2SiH_2$, and $Ph_3SiH$ to **2-COE** gave the corresponding Rh(III) silyl hydrides. Replacement of the alkene ligand in **2-COE** with CO resulted in distinct reactivity with $PhSiH_3$ and $Ph_2SiH_2$. The 16-electron monocarbonyl complex **3-CO** served as platform to study consecutive Si–H activation in formal dehydrogenative silylene extrusion. Neutral rhodium(I) silylenes stabilized by a hemilabile phosphinimine were fully characterized by multinuclear ($^1$H, $^{31}$P, $^{13}$C, $^{29}$Si) NMR spectroscopy and X-ray crystallography.

Finally, a conceptually related approach was taken in Chapter 5 to access neutral Rh(I) borylenes stabilized by a phosphinimine in $^{iPr}$NNN. Reversible activation of B–H bonds in arylboranes ($ArBH_2$) by **3-CO** was studied to better understand the implications

of metal-ligand cooperation in B–H activation and formal group transfer of the {BAr} fragment. Notably, for boranes substituted with electron-deficient arenes, formation of a base-stabilized borylene was not observed. Instead, a hemilabile phosphinimine coordinates to the borane which forms a B–H agostic complex with the Rh(I) center.

### 6.2. Future Work

Si–H and B–H bond activation strategies have emerged by exploiting metal-ligand cooperation and the hemilability of phosphinimine donors in Rh(I) complexes of bis(phosphinimine)pyrrolido ligands. Chapter 4 describes the consecutive activation of Si–H bonds leading to the isolation of neutral rhodium silylenes stabilized by phosphinimine donors with the loss of $H_2$. It was reasoned that this methodology could be extended to access cationic rhodium silylenes relevant in hydrosilation catalysis. Computational analysis of rhodium-catalyzed ketone hydrosilation by Gade and co-workers has shown that silylene formation occurs by oxidative addition of a Si–H bond to a rhodium complex followed by a second Si–H activation which delivers a hydride to the rhodium center *via* α–H migration (a 1,2-H shift).[1,2] Notably, the α–H migration proceeds spontaneously in the absence of an external activator (e.g. $B(C_6F_5)_3$ or $[CPh_3][B(C_6F_5)_4]$).

As described in Chapter 4, Sadow and co-workers have had success in generating a cationic rhodium silylene following an H-abstraction method.[3] Using the Lewis acid $B(C_6F_5)_3$, evidence was provided to support formation of the hydridoborate $[HB(C_6F_5)_3]^-$, along with a putative cationic oxazolinylborate-coordinated rhodium(III) silylene that catalyzed the partial deoxygenation of esters, aldehydes, amides, and ketones.[3] Through multinuclear ($^{29}Si$, $^{15}N$, $^{1}H$, $^{11}B$) NMR spectroscopy, the authors present a case where H-abstraction by $B(C_6F_5)_3$ is followed by rearrangement of the ligand to yield an unusual

oxazoline-coordinated silylene and coordinatively-unsaturated rhodium center. The preference for the oxazoline-silicon over oxazoline-rhodium coordination is rationalized by the enhanced electrophilicity of the silylene Si atom relative to the rhodium center.[3] It was therefore reasoned that electron-donating phosphinimines might be effective in stabilizing a cationic silylene.

### 6.2.1. Targeting a Cationic Rhodium Silylene

Following the work of Tilley and Sadow,[3,4] attempts to prepare cationic rhodium silylenes by H-abstraction from well-defined rhodium silyl hydrides with $B(C_6F_5)_3$ or $[CPh_3][BArF_{24}]$ generated intractable mixtures in bromobenzene. It was reasoned those combinations of the square planar rhodium monocarbonyl ($^{iPr}$NNN)Rh(CO) (**2-CO)** and $B(C_6F_5)_3$ with silanes could generate cationic rhodium silylenes following a similar consecutive Si–H activation pathway as described in Chapter 4. The key difference with the proposed method is the presence of $B(C_6F_5)_3$, used to intercept a transient Rh–H ligand by hydride abstraction, resulting in the formation of $[HB(C_6F_5)_3]^-$. Notably, for a cationic rhodium silylene to form, H-abstraction by $B(C_6F_5)_3$ would have to outcompete $H_2$ loss, and by extension, formation of **4-SiHPh** or **4-SiPh$_2$**.

First, interactions between **3-CO** and $B(C_6F_5)_3$ were probed by multinuclear NMR spectroscopy. In benzene-$d_6$, **3-CO** was combined with 1 equivalent of $B(C_6F_5)_3$ resulting in considerable broadening of the $^{31}$P NMR spectrum. The cause of spectral broadening was presumed to be a consequence of the borane interacting with either the carbonyl oxygen or a hemilabile phosphinimine donor. Crystallographic evidence of carbonyl *O*-coordination to $B(C_6F_5)_3$ was described in Chapter 3 in the isolation of **3-(CO)$_2$·BCF**. Additional precedent for carbonyl *O*-coordination was reported by Oestreich and co-

workers in the discovery of a novel Si–H activation pathway in hydrosilation catalysis.[5] Strong experimental evidence supports an outer-sphere mechanism for ketone hydrosilation by Bullock's cationic tungsten(II) catalyst[6] $[CpW(CO)_2(IMes)]^+[B(C_6F_5)_4]^-$, wherein tertiary silanes ($R_3SiH$) are heterolytically cleaved, forming a tungsten hydride and silylium cation ($R_3Si^+$). The silylium cation is stabilized by *O*-coordination of a CO ligand and was confirmed by X-ray crystallography.[5] Boranes and silylium cations are isoelectronic and contain a vacant p-orbital capable of productive overlap with the lone pair of a CO ligand. It is therefore reasonable to suggest that **3-CO** might interact with $B(C_6F_5)_3$ in a similar fashion. The alternative, *N*-coordination of a hemilabile phosphinimine donor, would result in the temporary formation of a 14-electron T-shaped rhodium center, poised for oxidative addition of an incipient Si–H bond. While this possibility has not been ruled out, it lacks obvious precedent. A thorough investigation into the fundamental coordination chemistry is therefore warranted.

The putative adduct of **3-CO** and $B(C_6F_5)_3$ was generated *in situ* and combined with 1 equivalent of $PhSiH_3$. Analysis by multinuclear NMR spectroscopy revealed formation of a new asymmetric product containing a rhodium hydride centered at δ –13.4 (d, $^1J_{HRh}$ = 27.1 Hz). In less than 1 hour, the product decomposed to an intractable mixture. Repeating the reaction with the secondary silane $Ph_2SiH_2$ in bromobenzene-$d_5$ led to quantitative formation of a product that was stable in solution for multiple days at ambient temperature. The $^{31}P$ NMR spectrum of the product revealed two equal intensity resonances at δ 60.0 and δ 56.1 (Figure 6.1), consistent with an asymmetrically bound $^{iPr}$NNN ligand, bearing resemblance to isolated neutral silylenes (cf. δ 53.0 and δ 43.5 for **4-SiHPh** in benzene-$d_6$).

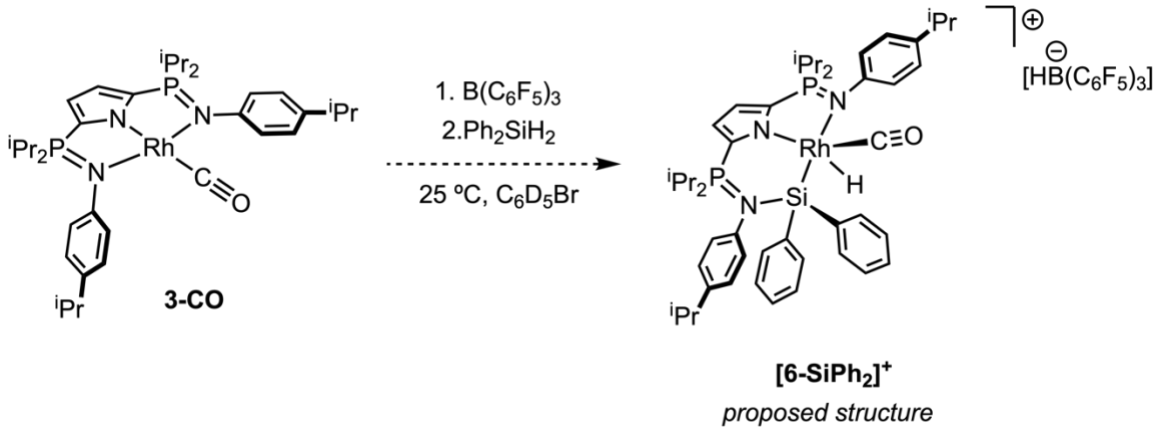


**Scheme 6.33.** Proposed formation of **[6-SiPh$_2$]$^+$** from the reaction of **3-CO** with B($C_6F_5$)$_3$ and $Ph_2SiH_2$.

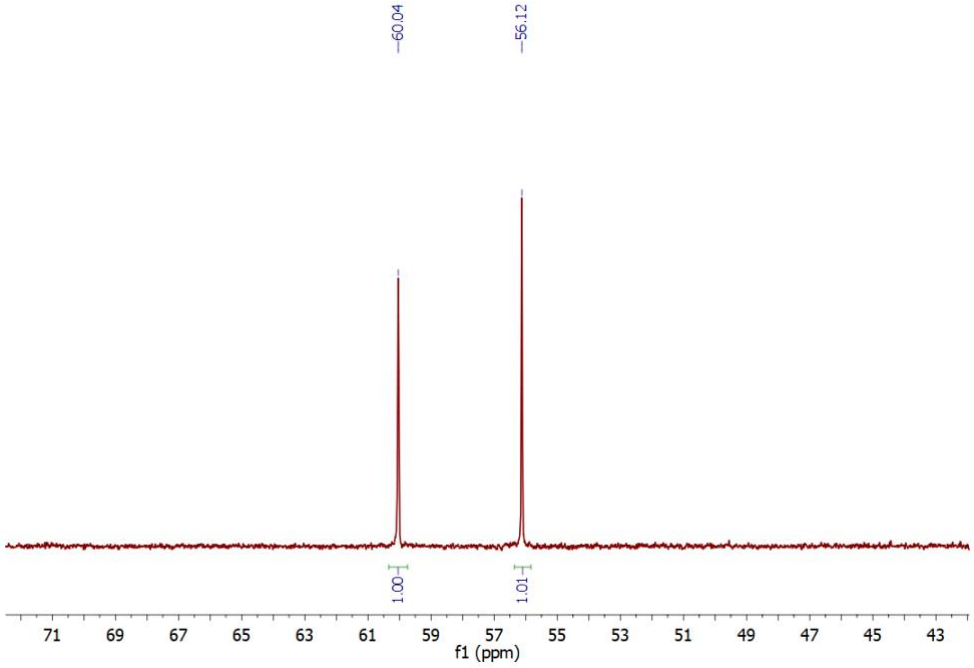


**Figure 6.1.** $^{31}P\{^1H\}$ NMR (283 MHz) spectrum of the reaction between **3-CO**, B($C_6F_5$)$_3$, and $Ph_2SiH_2$ in bromobenzene-$d_5$ at 25 ºC.

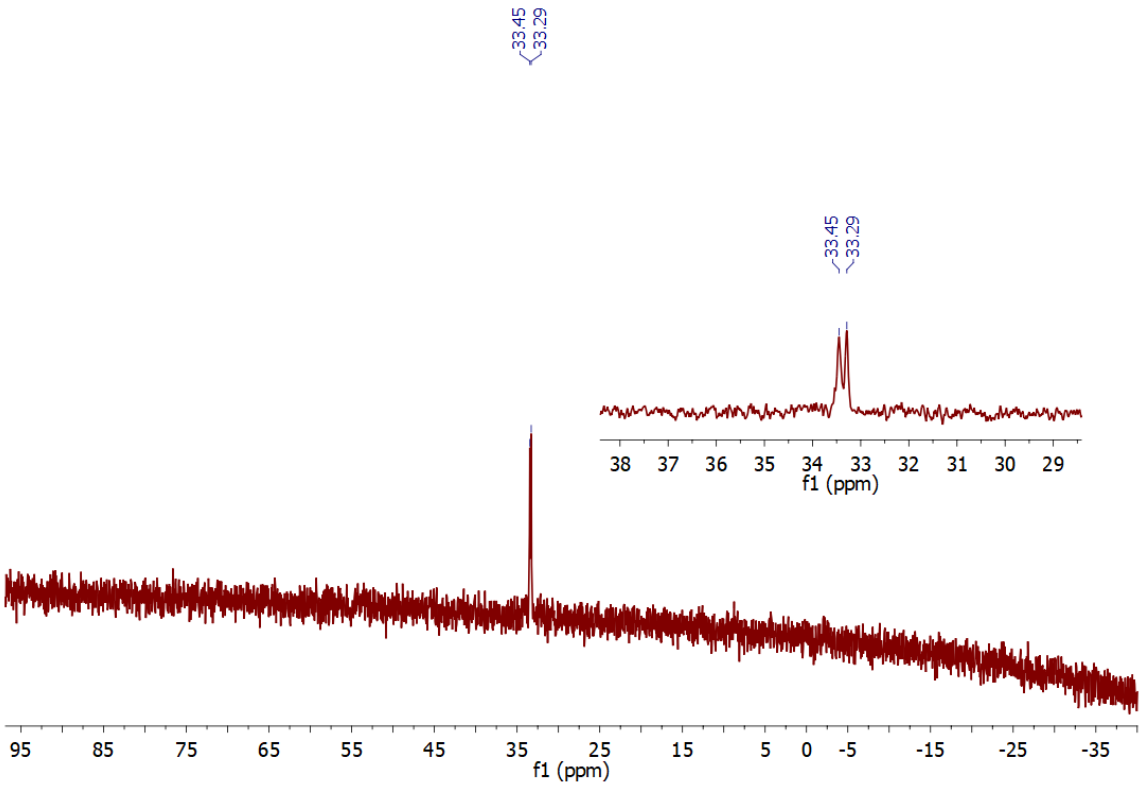


**Figure 6.2.** $^{29}Si\{^{1}H\}$ NMR (139 MHz) spectrum of the reaction between **3-CO**, $B(C_6F_5)_3$, and $Ph_2SiH_2$ in bromobenzene-$d_5$ at 25 ºC.

The $^{19}F$ NMR contained resonances consistent with an anionic 4-coordinate hydridoborate anion $[HB(C_6F_5)_3]^-$ ($\Delta\delta_{m,p}$ = 2.7 ppm), originating from either a Si–H or Rh–H bond. With the anion identified as the hydridoborate, the rhodium hydride cation would necessarily contain the $SiPh_2$ fragment trapped as a silylene coordinated by a hemilabile phosphinimine. Notably, a carbonyl ligand was identified by $^{13}C$ NMR spectroscopy as a doublet centered at δ 185.3 ($^{1}J_{CRh}$ = 68.0 Hz) which may impart a stabilizing effect on the cation, consistent with the report from Sadow.[3] The formation of the putative cationic rhodium silylene, $[(^{iPr}NNN)(CO)RhH(SiPh_2)]^+$ (**[6-SiPh$_2$]$^+$**) is the result of consecutive Si–H activation of $Ph_2SiH_2$. An upfield resonance corresponding to a Rh–H was observed at δ –13.8 in the $^{1}H$ NMR spectrum of **[6-SiPh$_2$]$^+$** in bromobenzene-$d_5$ along with a $^{29}Si$

resonance at δ 33.3 assigned to the putative phosphinimine-stabilized silylene (Figure 6.2). The prolonged stability of **[6-SiPh$_2$]$^+$**, relative to the hydrogen-substituted analogue **[6-SiHPh**]$^+$, is presumably the result of deleterious reactivity of the silylene Si–H bond, which is absent in **[6-SiPh$_2$]$^+$**, or from increased protection of the electrophilic Si center by an additional Ph group. Notably, when the order of addition was changed, and the combination of $Ph_2SiH_2$ and $B(C_6F_5)_3$ was added to **3-CO**, the same product formed in quantitative yield.

The apparent generation of **[6-SiPh$_2$]$^+$** is an encouraging result toward a more reactive class of rhodium silylenes stabilized bis(phosphinimine)pyrrolido ligands. Efforts should be made to isolate and characterize **[6-SiPh$_2$]$^+$** in the solid state, allowing for direct comparisons of structure and bonding with neutral phosphinimine-stabilized silylenes reported in Chapter 4. Beyond the fundamental studies into coordination chemistry, a reliable procedure to generate **[6-SiPh$_2$]$^+$** would aid in the evaluation of such a species in hydrosilation catalysis, as well as other reaction chemistry.

### 6.2.2. Photophysical Properties of Rhodium Carbonyls

The incorporation of visible light in organic reaction development has enabled novel C–C and C–heteroatom disconnection strategies by way of photoredox catalysis, with profound implications in medicinal chemistry.[7] The well-established photophysics of homoleptic ruthenium (e.g. $Ru(bpy)_3^{2+}$) and homo- and heteroleptic iridium complexes (e.g. $Ir(ppy)_3$) of polypyridyl ligands (bpy = 2,2′-bipyridine; ppy = 2-phenylpyridine) has laid the groundwork for exploiting the energy transfer (EnT) and single-electron transfer mechanisms that give rise to open-shell intermediates.[7a] Photo-initiated electron-transfer specifically, has been instrumental in generating organic radicals that can be intercepted by

organometallic complexes (e.g., $^{tBu}$bpyNi; $^{tBu}$bpy = 4,4′-Di-tert-butyl-2,2′-dipyridyl) which serve as platforms for C–C bond coupling by reductive elimination.[8]

While the emerging fields of photoredox and metallaphotoredox catalysis over the last few years have inspired fundamental studies in 'designer' photocatalysts for specific applications, a general interest in the interactions of visible and ultraviolet light with organometallic complexes has been pervasive in the chemical literature for decades. For example, the photochemistry of transition metal carbonyls was reviewed by Wrighton in the mid-70s and continues to be studied and exploited in many areas of chemistry, including catalysis outside of a photoredox manifold.[7a,9] In general, low valent transition metals tend to display a greater degree of covalency compared to higher valent species, which is why stable carbonyl complexes are often derived from low valent metals (e.g. $Fe(CO)_5$). Strong delocalization of electron density from metal to ligand should therefore translate to dramatic changes in bonding. Photophysical studies on the 16-electron rhodium(I) carbonyl complexes **3-(CO)$_2$** and **3-CO** described in Chapter 3 should be carried out to evaluate these complexes for use in photo-driven catalysis.

Generating 14-electron rhodium complexes by ligand dissociation is a proven method of promoting oxidative addition and was described in Chapter 4 for Si–H bonds. As a design principle, substitution of a labile alkene in **2-COE** for a CO ligand in **3-CO** resulted in two distinct pathways for Si–H activation, namely oxidative addition in the former case, and dehydrogenation by consecutive Si–H activation in the latter. Notably, phosphinimine-stabilized rhodium silylenes **4-SiHPh** and **4-SiPh$_2$** described in Chapter 4 each contain a CO ligand which would imply that a thermal CO dissociation is either reversible or not operative in the formation of **4-SiHPh** and **4-SiPh$_2$** from **3-CO**. More

likely is the dissociation of a phosphinimine, generating a carbonylated 14-electron species capable of oxidative addition. Evidence for this process appeared in Chapter 5 with the isolation of **5-CO·H$_2$BAr$^F$**, a (B–H)σ complex between **3-CO** and H$_2$BAr$^F$ (Ar$^F$ = 3,5-(CF$_3$)$_2$-C$_6$H$_3$) where a hemilabile phosphinimine coordinates to the boron atom.

The controlled photo-dissociation of CO ligands from well-defined organometallic complexes is an effective strategy to generate active catalysts for a host of chemical transformations, including the hydrogenation of alkenes described by Chirik and co-workers.[10] In that work, a bis(phosphine)cobalt dicarbonyl hydride operates by two distinct hydrogenation pathways under thermal and photochemical conditions, with hydrogen atom transfer (HAT) occurring at elevated temperatures. Under visible light irradiation, CO dissociation generates a highly active cobalt hydride capable of hydrogenating functionally rich alkenes by a 2-electron, coordination-insertion pathway. Following this strategy, the irradiation of **3-CO** by varying wavelengths of light might result in controlled CO photo-dissociation providing complementary reactivity to **3-CO** under thermal conditions where phosphinimine dissociation is operative. The ability to selectively activate **3-CO** by either phosphinimine or CO dissociation would allow for a myriad of bond activation reactions to be surveyed. Beyond hydrogenation, carbonylated rhodium complexes reported in this thesis include phosphinimine-stabilized silylenes and borylenes which might provide unique reaction chemistry under visible light irradiation. The photodissociation of CO from either **4-SiHPh** or **4-SiPh$_2$** may promote the migration of the {SiR$_2$} fragment from the phosphinimine to the metal, giving a terminal silylene complex with a κ$^3$-*N*,*N*,*N* ligand bonding arrangement. The generality of such a transformation could then be evaluated with **5-BMes**, providing a method of generating terminal main group fragments at rhodium.

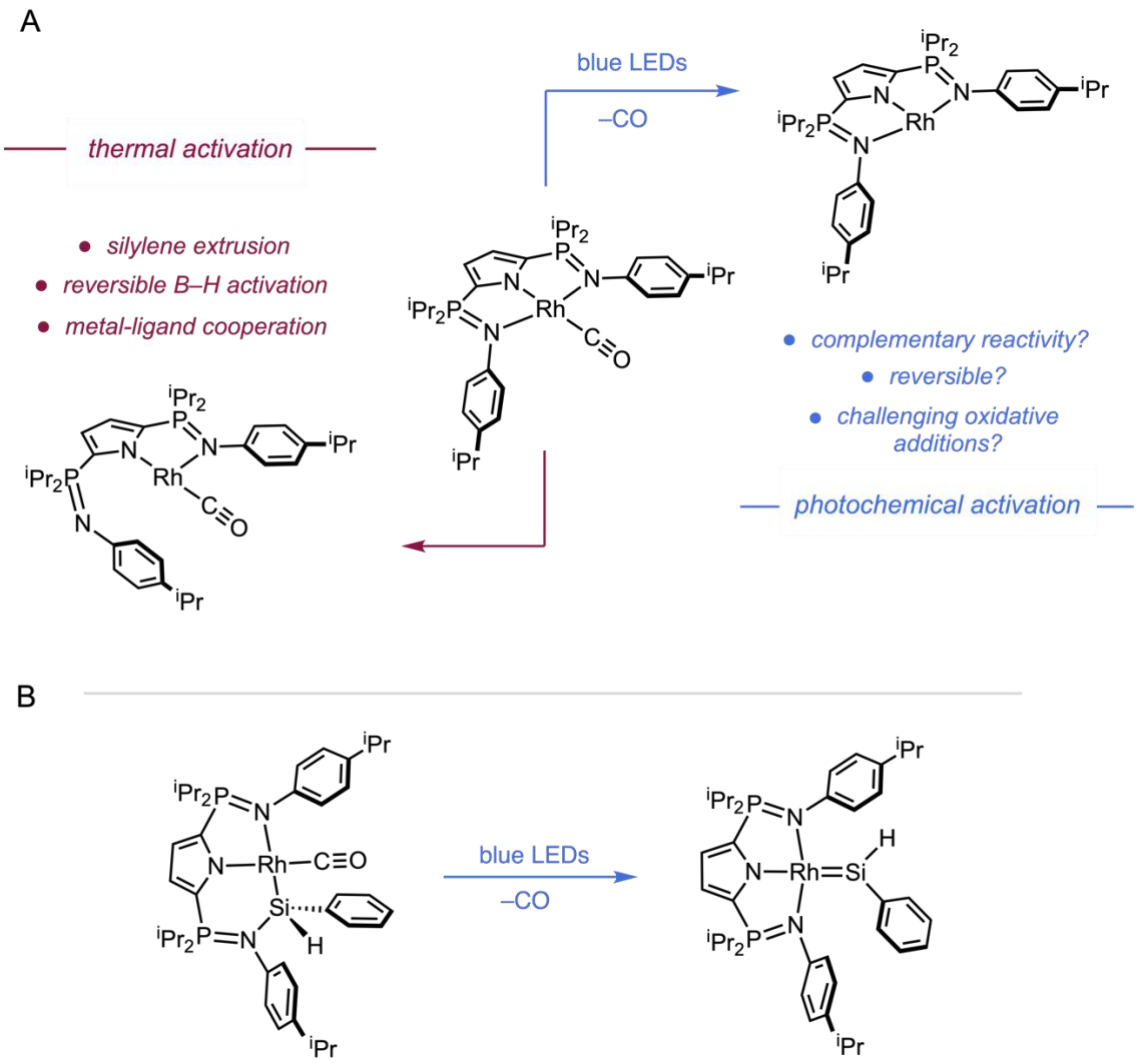


**Scheme 6.34.** A. Thermal and photochemical activation pathways for the generation of 14-electron rhodium complexes. B. Proposed formation of a terminal rhodium silylene by CO photodissociation.

### 6.2.3. Directed-Activation of C–F bonds by Rhodium Borylenes

After the realization of formal group transfer in Chapter 5, further exploration of this reactivity is warranted. The reaction of pinacol and **5-BMes** resulted in the generation of MesBpin and **3-CO** with loss of $H_2$. While the mechanism of this transformation is unclear, a reasonable pathway might involve coordination of a pinacol hydroxyl OH group to the boron atom as an initiating step. Transfer of the {BMes} fragment away from **5-**

**BMes** is likely driven by formation of a stable chelate containing two B–O bonds. Translating this reactivity in the activation of C–X bonds aided by an ortho directing group (e.g. –OH) might serve as a viable strategy. Of interest is the activation of C($sp^2$)– and C($sp^3$)–F bonds. Per- and polyfluoroalkyl substances (PFAS) are chemicals which persist in the ecological timeline, and by virtue of their inert C–F bonds, are difficult to sequester. A directed C–F activation might result in {BMes} group transfer, changing the fundamental properties of the PFAS to aid in removal.

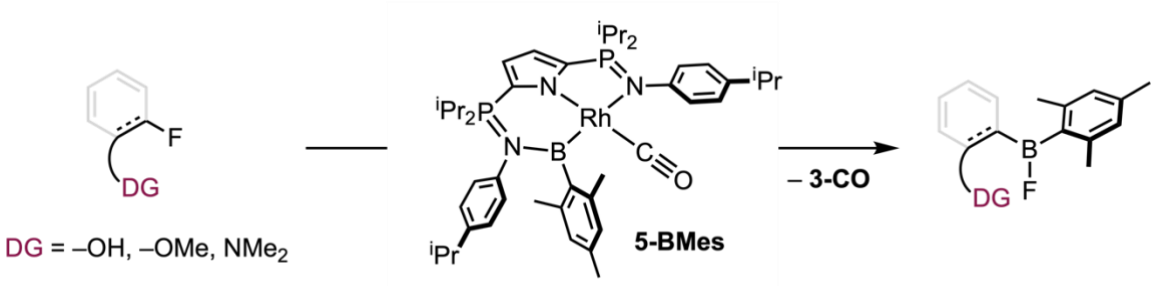


**Scheme 6.35.** Directed C–F activation by **5-BMes** by a proposed borylene insertion.

### 6.3. Outlook

Within the subset of monoanionic pincer ligands, *NNN* scaffolds are under-developed but offer a diversity of structure and function that should be explored in the design of new transition metal complexes. The incorporation of phosphinimine donors in the $^{R}$NNN (R = Ph, $^{i}$Pr) bis(phosphinimine)pyrrolido ligands described here places a unique ylidic structure in the primary coordination sphere of a metal which until this work, had been used to stabilize electrophilic rare earth metals,[11] along with divalent metal ions ($Ca^{2+}$, $Mg^{2+}$, and $Zn^{2+}$).[12] A central goal of this thesis work was to synthesize bis(phosphinimine)pyrrolido complexes of late transition metals for the purpose of developing new bond activation reactivity enabled by metal ligand cooperation. To this

end, a diversity of reactions has been successfully developed for complexes of rhodium, leading to a thorough understanding of H–H, C–O, Si–H, and B–H bond activation. While rhodium complexes served as a model system for this study, the reactivity observed here may translate onto other late transition metals. Moreover, first-row transition metals including Fe, Co, and Cu offer a high density of oxidation states and rich single-electron chemistry that could be exploited in the development of new chemical reactivity with these bis(phosphinimine)pyrrolido ligands.

### 6.4. References


**1.** Schneider, N.; Finger, M.; Haferkemper, C.; Bellemin-Laponnaz, S.; Hofmann, P.; Gade, L. H. Metal silylenes generated by double silicon-hydrogen activation: key intermediates in the rhodium-catalyzed hydrosilylation of ketones. *Angew. Chem. Int. Ed.* **2009**, *48*, 1609–1613; *Angew. Chem.* **2009**, *121*, 1637–1641.

**2.** Schneider, N.; Finger, M.; Haferkemper, C.; Bellemin-Laponnaz, S.; Hofmann, P.; Gade, L. H. Multiple Reaction Pathways in Rhodium-Catalyzed Hydrosilylations of Ketones. *Chem. Eur. J.* **2009**, *15*, 11515–11529.

**3.** Xu, S.; Boschen, J. S.; Biswas, A.; Kobayashi, T.; Pruski, M.; Windus, T. L.; Sadow, A. D. Mild partial deoxygenation of esters catalyzed by an oxazolinylborate-coordinated rhodium silylene. *Dalton Trans.* **2015**, *44*, 15897–15904.

**4.** Mitchell, G. P.; Tilley, T. D. Generation of a Silylene Complex by the 1,2-Migration of Hydrogen from Silicon to Platinum. *Angew. Chem. Int. Ed.* **1998**, *37*, 2524–2526; *Angew. Chem.* **1998**, *110*, 2602–2605.

**5.** Fuchs, J.; Irran, E.; Hrobárik, P.; Klare, H. F. T.; Oestreich, M. Si–H Bond Activation with Bullock's Cationic Tungsten(II) Catalyst: CO as Cooperating Ligand. *J. Am. Chem. Soc.* **2019**, 141, 18845–18850.

**6.** (a) Dioumaev, V. K.; Szalda, D. J.; Hanson, J.; Franz, J. A.; Bullock, R. M. An N-heterocyclic carbene as a bidentate hemilabile ligand: a synchrotron X-ray diffraction and density functional theory study. *Chem. Commun.* **2003**, 1670−1671. (b) Wu, F.; Dioumaev, V. K.; Szalda, D. J.; Hanson, J.; Bullock, R. M. A Tungsten Complex with a Bidentate, Hemilabile N-Heterocyclic Carbene Ligand, Facile Displacement of the Weakly Bound W−(C=C) Bond, and the Vulnerability of the NHC Ligand toward Catalyst Deactivation during Ketone Hydrogenation. *Organometallics* **2007**, *26*, 5079−5090.

**7.** (a) Prier, C. K.; Rankic, D. A.; MacMillan, D. W. C. Visible Light Photoredox Catalysis with Transition Metal Complexes: Applications in Organic Synthesis. *Chem. Rev.* **2013**, *113*, 5322–5363. (b) Romero, N. A.; Nicewicz, D. A. Organic Photoredox Catalysis. *Chem. Rev.* **2016**, *116*, 100075–10166.

**8.** Kariofillis, S. K.; Shields, B. J.; Tekle-Smith, M. A.; Zacuto, M. J.; Doyle, A. G. Nickel/Photoredox-Catalyzed Methylation of (Hetero)aryl Chlorides Using Trimethyl Orthoformate as a Methyl Radical Source. *J. Am. Chem. Soc.* **2020**, *142*, 7683–7689.

**9.** Wrighton, M. Photochemistry of metal carbonyls. *Chem. Rev.* **1974**, *74*, 401–430.

**10.** Mendelsohn, L. N.; MacNeil, C. S.; Tian, L.; Park, Y.; Scholes, G. D.; Chirik, P. J. Visible-Light-Enhanced Cobalt-Catalyzed Hydrogenation: Switchable Catalysis Enabled by Divergence between Thermal and Photochemical Pathways. *ACS Catal.* **2021**, *11*, 1351–1360.

**11.** Johnson, K. R. D.; Hannon, M. A.; Ritch, J. S.; Hayes, P. G. Thermally stable rare earth dialkyl complexes supported by a novel bis(phosphinimine)pyrrole ligand. *Dalton Trans.* **2012**, *41*, 7873–7875.

**12.** Wheaton, C. A.; Ireland, B. J.; Hayes, P. G. Activated Zinc Complexes Supported by a Neutral, Phosphinimine-Containing Ligand: Synthesis and Efficacy for the Polymerization of Lactide. *Organometallics* **2009**, *28*, 1282–1285.

# Chapter 7: Experimental Methods

## 7.1. General

### 7.1.1. Laboratory Equipment and Apparatus

An argon filled MBraun glove box was employed for manipulation and storage of all oxygen and moisture sensitive compounds. All thermally unstable compounds were stored in a –35 °C freezer within the glove box. All reactions were performed on a double manifold high vacuum line using standard techniques.[1] Commonly utilized specialty glassware includes the swivel frit assembly, needle valves, and thick walled (5 mm) glass bombs equipped with Kontes Teflon stopcocks.[1] All glassware was stored in a 110 °C oven for a minimum of 12 hours, or flame-dried before immediate transfer to the glove box antechamber or assembled on the vacuum line and evacuated while hot.

### 7.1.2. Solvents

Toluene, pentane, and tetrahydrofuran (THF) solvents were dried and purified using the Grubbs/Dow purification system and stored in evacuated 500 mL bombs over titanocene[2] (toluene and hexanes) or sodium/benzophenone ketal (THF).[3] Diethyl ether, pentane, heptane, benzene, benzene-$d_6$, toluene-$d_8$, and THF-$d_8$ were dried and stored over sodium/benzophenone ketal in glass bombs under vacuum. Bromobenzene and bromobenzene-$d_5$ were pre-dried over 4Å molecular sieves, stored over calcium hydride and distilled prior to use. Unless otherwise noted, solvents were introduced via vacuum transfer with condensation at –78 °C. Liquid nitrogen (–196 °C), liquid nitrogen/pentane (–130 °C), dry ice/acetone (–78 °C) dry ice/acetonitrile (–45 °C) and water/ice (0 °C) baths were used for cooling receiving flasks and to maintain low temperature conditions.

### 7.1.3. Instrumentation and details for NMR experiments

All NMR spectra were recorded at ambient temperature, except where noted, with a Bruker Avance II NMR spectrometer (300.13 MHz for $^{1}$H, 46.07 MHz for $^{2}$H, 96.29 MHz for $^{11}$B, 75.47 MHz for $^{13}$C, 282.40 MHz for $^{19}$F, 121.48 MHz for $^{31}$P, and 59.63 MHz for $^{29}$Si) or Avance III NMR spectrometer (700.13 MHz for $^{1}$H, 107.47 MHz for $^{2}$H, 224.63 MHz for $^{11}$B, 176.05 MHz for $^{13}$C, 658.78 MHz for $^{19}$F, 283.54 MHz for $^{31}$P, and 139.09 MHz for $^{29}$Si) NMR spectrometer. All $^{1}$H NMR spectra were referenced to $SiMe_4$ through the residual $^{1}$H resonance(s) of the employed solvent; benzene-$d_6$ (7.16 ppm), toluene-$d_8$ (2.09, 6.98, 7.02 and 7.09 ppm), THF-$d_8$ (1.73 and 3.58 ppm), or bromobenzene-$d_5$ (6.94, 7.02 and 7.30 ppm). $^{2}$H NMR spectra were referenced relative to an external standard of $Si(CD_3)_4$ (0.0 ppm) in benzene-$d_6$ prior to spectrum acquisition. $^{11}$B NMR spectra were referenced to an external standard of boron trifluoride diethyl etherate ($BF_3{\cdot}Et_2O$; δ 0.0 ppm) in benzene-$d_6$ prior to acquisition of the first spectrum. $^{13}$C NMR spectra were referenced relative to $SiMe_4$ through the resonance(s) of the employed solvent; benzene-$d_6$ (128.0 ppm), toluene-$d_8$ (20.4, 125.2, 128.0, 128.9, 137.5 ppm), THF-$d_8$ (25.4, 67.6 ppm), or bromobenzene-$d_5$ (122.3, 126.1, 129.3, 130.9 ppm). $^{19}$F NMR spectra were referenced externally to $C_6H_5F$ (δ –113.1 in benzene-$d_6$). Temperature calibration for NMR experiments was achieved by monitoring the $^{1}$H NMR spectrum of pure methanol (below room temperature) and pure ethylene glycol (above room temperature).[4] $^{1}$H NMR data for diamagnetic compounds are reported as follows: chemical shift, multiplicity (s = singlet, d = doublet, t = triplet, q = quartet, quint = quintet, sp = septet, br = broad, m = multiplet, app = apparent, obsc = obscured, ov = overlapping), coupling constants (Hz), integration, assignment. $^{13}$C NMR data for diamagnetic compounds are reported as follows: chemical

shift, assignment. Assignment of resonances were supported by $^{1}H–^{1}H$ COSY, $^{13}C\{^{1}H\}$ APT, $^{1}H–^{13}C\{^{1}H\}$, DEPT 135, DEPT 90, NOESY, and HSQC/HMBC experiments.

### 7.1.4. Crystallographic details

All structures were collected on a Rigaku SuperNova diffractometer equipped with a Dectris Pilatus 3R 200K-A hybrid-pixel-array detector, a four-circle κ goniometer, sealed graphite-monochromated Mo Kα (λ = 0.71073 Å) and Cu Kα (λ = 1.54178 Å) X-ray sources, and an Oxford cryostream-cooling device fixed at 100 K. Single crystals suitable for X-ray diffraction studies were mounted on a MiTiGen cryo-loop using desiccated Paratone–*N* oil stored in a glove box.

The structures were solved by the Intrinsic Phasing methods and refined by least-squares methods using SHELXT-2014 and SHELXL-2014 with the OLEX2 interface.[5-7] The program PLATON was employed to confirm the absence of higher symmetry space groups.[8] All non-H atoms were located in difference Fourier maps, and then refined anisotropically. Outlier reflections were omitted from refinement when appropriate. Hydrogen atoms on C atoms were placed at idealized positions and refined using a riding model. The isotropic displacement parameters of all hydrogen atoms were fixed to 1.2 times the atoms they are linked to (1.5 times for methyl groups). Crystallographic refinement details, including disorder modeling and software employed, have been delineated within each crystallographic information file (*.cif). Molecular graphics were generated using ORTEP. I performed all measurements at the University of Lethbridge. Data for **2-Rh$_2$** was collected by Dr. Mikko Hänninen. Further details on structures are noted below in the relevant chapter sections.

### 7.1.5. Computational Methods

Density Functional Theory (DFT) calculations were carried out on unmodified structures obtained from X-ray crystallography using the Gaussian 16 (revision B.01) computational suite.[9] Cartesian coordinates (*.xyz) were obtained from X-ray diffraction analysis. Gas-phase geometry optimization was performed using the B3LYP functional,[10] employing the aug-cc-pVDZ basis set with associated pseudopotentials (Rh) for non-C, H atoms (cc-pVDZ).[11] Visualization of optimized structures and rendering of molecular orbitals was performed using Gaussview.[12] Wiberg bond indices were determined using NBO 3.1,[13,14] also using the B3LYP/aug-cc-pVDZ level of theory.

### 7.1.6. Additional instrumentation

Elemental analyses (%CHN) were conducted at the University of Lethbridge by Jackson Knott or Dylan Webb on an Elementar Americas Vario MicroCube Analyzer (C, H, N, O, S capabilities) using bulk recrystallized compounds. Infrared spectroscopy was conducted on a Thermo-Nicolet iS10 FT-IR spectrometer using bulk recrystallized compounds.

### 7.1.7. Synthesis of ligands and starting materials

**Synthesis of Na-$^{Ph}$NNN:**

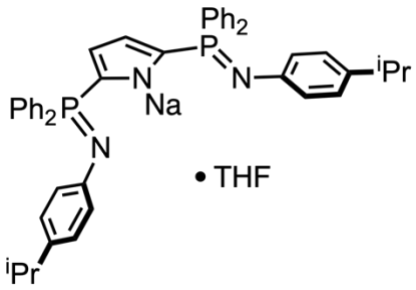


A mixture of $^{Ph}$NNN (from literature[15] procedure) (0.398 g, 0.567 mmol) and NaH (0.016 g, 0.65 mmol) was added to a 100 mL round-bottomed flask attached to a double manifold vacuum line and dissolved in THF (50 mL) to afford a cloudy, white, effervescent slurry. The reaction mixture was stirred at ambient temperature for 18 h to generate a clear, colourless solution. The solvent was removed *in vacuo* to afford a white powder which was washed with pentane (3 × 20 mL) and dried *in vacuo*, resulting in a white powder (0.366 g, 81.1%). $^{1}$H NMR (benzene-$d_6$, 300.13 MHz): 7.84 (dd, 8H, $^{3}J_{HP}$ = 11.5 Hz, $^{3}J_{HH}$ = 7.3 Hz, Ph C*H*), 6.98 (dd, 4H, $^{3}J_{HH}$ = 7.3 Hz, 4$J_{HP}$ = 1.5 Hz, Pipp C*H*), 6.86 (ov m, 12H, Ph C*H*), 6.77 (dd, 2H, $^{3}J_{HP}$ = 2.0 Hz, $^{4}J_{HP}$ = 2.0 Hz, 3,4-pyrrole C*H*), 6.66 (d, 4H, $^{3}J_{HH}$ = 7.3 Hz, C*H*(CH$_3$)$_2$), 3.44 (m, 4H, OC*H*$_2$C*H*$_2$), 2.66 (sp, 2H, $^{3}J_{HH}$ = 6.7 Hz, C*H*(CH$_3$)$_2$), 1.34 (m, 4H, OC*H*$_2$C*H*$_2$), 1.14 (d, 12H, $^{3}J_{HH}$ = 6.7 Hz, CH(C*H*$_3$)$_2$). $^{13}$C{1H} NMR (benzene-$d_6$, 75.47 MHz): 150.3 (d, $^{2}J_{CP}$ = 5.1 Hz, Pipp *C*), 137.8 (s, Pipp *C*), 135.8 (d, $^{1}J_{CP}$ = 20.4 Hz, 2,5-pyrrole *C*), 133.7 (d, $^{1}J_{CP}$ = 85.9 Hz, Ph *C*), 133.7 (d, $^{2}J_{CP}$ = 9.2 Hz, Ph *C*H), 131.3 (s, Pipp *C*H), 128.7 (d, $^{3}J_{CP}$ = 11.6 Hz, Ph *C*H), 127.6 (s, Pipp *C*H), 123.9 (d, $^{4}J_{CP}$ = 17.2 Hz, Ph *C*H), 121.5 (dd, $^{2}J_{CP}$ = 32.0 Hz, $^{3}J_{CP}$ = 12.9 Hz, 3,4-pyrrole *C*H), 68.1 (s, O*C*H$_2$*C*H$_2$), 34.0 (s, *C*H(CH$_3$)$_2$), 26.1 (s, O*C*H$_2$*C*H$_2$), 25.0 (s, CH(*C*H$_3$)$_2$). $^{31}$P{$^{1}$H} NMR (benzene-$d_6$, 121.49 MHz): 8.8 (s, 2P, *P*=N). Anal. Calcd. (%) for C$_{50}$H$_{52}$N$_3$NaOP$_2$: C: 75.45; H: 6.59; N: 5.28. Found C: 75.75; H: 6.94; N: 5.33.

**Chemical warning –** *Caution!* The handling of organic azides should be conducted in a fume hood behind a blast shield. Under no circumstances should reactions involving azides be conducted in a closed system. Addition of organic azides to phosphines results in the rapid evolution of $N_2$ gas.

**Synthesis of $^{iPr}$NNN:**

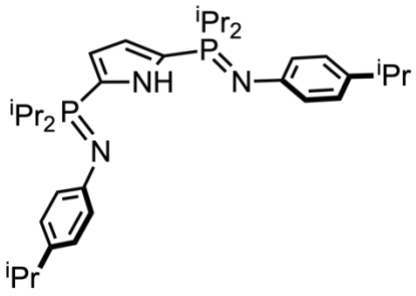


In a 250 mL round bottom flask, 2,5-bis(diisopropylphosphino)-*N*-H-pyrrole (0.990 g, 3.29 mmol) was dissolved in toluene (100 mL) to give a bright orange solution. 4- isopropylphenyl azide (1.06 g, 6.58 mmol) was added dropwise *via* syringe over 15 min at ambient temperature. Upon addition of the azide, the solution immediately began evolving $N_2$ gas. The reaction mixture was stirred for 18 h, after which, all volatiles were removed *in vacuo* and revealed an amber-coloured oil. Following pentane washes (3 × 15 mL), a waxy, bright yellow solid was produced. Yield: 1.68 g (90.2%). $^1$H NMR (benzene-$d_6$): δ 10.4 (br s, 1H, N–*H*), 7.10 (ov m, 8H, 4-$^i$PrC$_6$*H*$_4$), 6.40 (s, 2H, pyrrole-*H*), 2.82 (sp, $^3J_{HH}$ = 7.0 Hz, 2H, C*H*(CH$_3$)$_2$), 2.08 (sp, $^3J_{HH}$ = 7.0 Hz, 4H, C*H*(CH$_3$)$_2$), 1.26 (d, $^3J_{HH}$ = 7.0 Hz, 12H, CH(C*H*$_3$)$_2$), 1.01 (dd, $^3J_{HP}$ = 13.4 Hz, $^3J_{HH}$ = 7.0 Hz, 12H, CH(C*H*$_3$)$_2$), 0.99 (dd, $^3J_{HP}$ = 13.4 Hz, $^3J_{HH}$ = 7.0 Hz, 12H, CH(C*H*$_3$)$_2$). $^{13}$C{$^1$H} NMR (benzene-$d_6$): δ 149.5 (s, aromatic *ipso*-*C*), 138.2 (s, aromatic *ipso*-*C*), 127.4 (s, aromatic *C*H), 124.4 (dd, $^1J_{CP}$ = 108.2 Hz, $^3J_{CP}$ = 5.7 Hz, 2,5-pyrrole *C*), 124.0 (d, $^3J_{CP}$ = 14.2 Hz, aromatic *C*H), 117.5 (dd, $^2J_{CP}$ = 17.4 Hz, $^3J_{CP}$ = 11.6 Hz, 3,4-pyrrole *C*H), 34.2 (s, *C*H(CH$_3$)$_2$), 27.1 (d, $^1J_{CP}$ = 62.7 Hz, *C*H(CH$_3$)$_2$), 25.0 (s, CH(*C*H$_3$)$_2$), 16.9 (s, CH(*C*H$_3$)$_2$), 16.3 (s, CH(*C*H$_3$)$_2$). $^{31}$P{$^1$H}

NMR (benzene-$d_6$): δ 13.5. Anal. Calcd. (%) for $C_{34}H_{53}N_3P_2$: C, 72.18; H, 9.44; N, 7.43. Found: C, 71.86; H, 9.93; N, 7.88.

**Synthesis of Na-$^{iPr}$NNN**

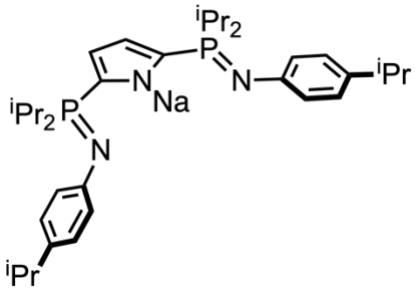


A round bottom flask was charged with $^{iPr}$NNN (1.08 g, 1.91 mmol) and sodium hydride (0.0564 g, 2.20 mmol) and dissolved in THF (25 mL) at −78 °C. The bright yellow solution bubbled as gas evolved while becoming opaque and bright orange. The solution was allowed to warm to ambient temperature with stirring, and after 12 hours was clear and orange. THF was removed under reduced pressure providing a dark yellow solid. Yield: 1.04 g (82.6%) $^1$H NMR (benzene-$d_6$): δ 7.14 (d, $^3J_{HH}$ = 8.2 Hz, 4H, 4-$^i$PrC$_6$H$_4$), 7.02 (d, $^3J_{HH}$ = 8.2 Hz, 4H, 4-$^i$PrC$_6$H$_4$), 6.80 (s, 2H, 3,4-pyrrole), 2.77 (sp, $^3J_{HH}$ = 7.0 Hz, 2H, C*H*(CH$_3$)$_2$), 2.19 (br sp, 4H, *CH*(CH$_3$)$_2$), 1.23 (d, $^3J_{HH}$ = 7.0 Hz, 12H, CH(CH$_3$)$_2$), 1.00 (ov m, 24H, CH(C*H*$_3$)$_2$). $^{13}$C{$^1$H} NMR (benzene-$d_6$): δ 152.7 (s, aromatic *ipso-C*), 138.7 (s, aromatic *ipso-C*), 127.7 (s, aromatic *C*H), 125.2 (d, $^3J_{CP}$ = 10.9 Hz, aromatic *C*H), 116.8 (dd, $^2J_{CP}$ = 26.9 Hz, $^3J_{CP}$ = 9.8 Hz, 3,4-pyrrole *C*H), 34.0 (s, *C*H(CH$_3$)$_2$), 27.2 (d, $^1J_{CP}$ = 60.8 Hz, *C*H(CH$_3$)$_2$), 25.0 (s, CH(*C*H$_3$)$_2$), 17.6 (s, CH(*C*H$_3$)$_2$), 16.6 (s, CH(CH$_3$)$_2$). One aromatic carbon (2,5-pyrrole *C*) was not observed. $^{31}$P{$^1$H} NMR (benzene-$d_6$): δ 28.0. Anal. Calcd. (%) $C_{34}H_{52}N_3NaP_2$: C, 69.48; H, 8.92; N, 7.15. Found: C, 69.01; H, 8.95; N, 7.26.

Rhodium dicarbonyl chloride [Rh(Cl)CO$_2$]$_2$ was prepared by following a report by Wilkinson.[16] B(C$_6$F$_5$)$_3$ was purchased from Boulder Scientific and dried by stirring a dichloromethane solution with Me$_2$SiHCl for no more than 20 minutes.[17] This was

followed by sublimation under dynamic vacuum at 80 °C for 18 hours. Bis(phosphinimine)pyrrole derivatives were synthesized according to prior reports.[15] All other reagents were purchased from Sigma Aldrich and used as received.

### 7.1.8. Catalytic hydrogenation reactions

In an argon filled glove box, **2-COE** (0.041 g, 0.045 mmol) was dissolved in 1.5 mL of benzene-$d_6$, giving a 0.03 M pre-catalyst stock solution. For a typical catalytic run, 0.15 mL of the stock solution was taken and mixed with 0.3 mL of benzene-$d_6$ and 30 equiv of substrate in a J. Young NMR tube. For COE hydrogenation, this equates to 0.01 M of **2-COE** and 0.3 M of substrate. The J. Young NMR tube was attached to a double manifold vacuum line and the solution was degassed by three freeze–pump–thaw cycles. A hydrogen atmosphere (1 atm) was applied to the tube at ambient temperature, or at –196 °C (to provide approximately 4 atm of $H_2$ upon warming to ambient temperature). The J. Young NMR tube was continually inverted at 30 turns $min^{-1}$ to ensure adequate mass transfer. The tube was refilled to 4 atm of hydrogen every 2 hours to maintain the desired pressure. All catalytic runs were monitored periodically using $^1$H NMR spectroscopy. All reactions resulted in quantitative conversion of substrate into product (>95 %) at ambient temperature. Between 30 and 60 equiv of substrate were used in catalytic experiments.

### 7.1.9. NMR tube reactions

Unless otherwise noted NMR tube reactions were carried out by charging an NMR tube with the initial reagents and solvents in the glove box. Subsequent reagents were introduced by syringe to the septa sealed NMR tubes submerged in the appropriate cold bath. The tube was shaken once to ensure proper mixing prior to insertion into the NMR

probe. This mixing was performed very quickly (~ 2 seconds) to avoid warming and premature reaction. In situations where gases or low boiling liquids were to be introduced a J. Young NMR tube and vacuum line adaptor were used. Once attached to the vacuum line the J. Young NMR tube was evacuated and solution degassed using a freeze-pump-thaw routine. The solution was carefully frozen with the appropriate cooling bath for the solvent in use followed by evacuation for several minutes. The frozen solution was thawed whereby dissolved gases were released into the headspace. The solution was frozen again, and the tube evacuated for several minutes. This process was repeated thrice more to ensure full degassing.

## 7.2. Experimental Procedures Pertaining to Chapter 2

### 7.2.1. Synthetic Procedures

**Synthesis of 2-COE:**

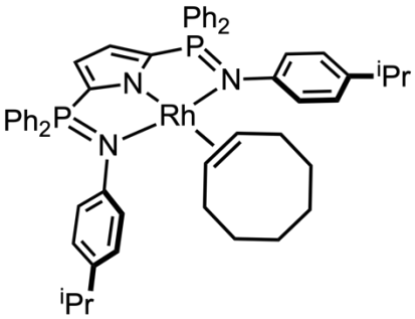


In an argon filled glove box, $[RhCl(COE)_2]_2$ (0.179 g, 0.249 mmol) and Na-$^{Ph}$NNN (0.417 g, 0.524 mmol) were added to a 50 mL round-bottomed flask and dissolved in toluene (15 mL). The reaction vessel was attached to a double manifold vacuum line and the mixture heated at 50 °C for 1.5 h under an argon atmosphere. Volatiles were removed under reduced pressure, resulting in a brown solid. The flask was taken into a glove box and the solid redissolved in toluene (5 mL). The solution was filtered to remove sodium chloride and the remaining solid was washed with benzene (5 × 2 mL) and toluene (1 × 2 mL). All volatiles were removed *in vacuo* to afford pure **2-COE** as an orange-red powder. Yield:

0.416 g (91.3%). $^{1}$H NMR (benzene-$d_6$, 300.13 MHz): δ 7.76 (dd, $J_{HP}$ = 12.0 Hz, $J_{HH}$ = 8.1 Hz, 8H, Ph C*H*), 7.12 (dd, $J_{HH}$ = 8.2 Hz, $J_{HP}$ = 2.4 Hz, 4H, Pipp C*H*), 6.97–6.88 33 (ov m, 12H, Ph C*H*), 6.74 (d, $J_{HH}$ = 8.2 Hz, 4H, Pipp C*H*), 6.72 (d, $J_{HP}$ =2.1 Hz, 2H, 3,4-pyrrole C*H*), 3.52 (d, $J_{HRh}$ = 7.8 Hz, 2H, COE C*H*), 2.59 (br s, 2H, COE $CH_2$), 2.54 (sp, $J_{HH}$ = 6.8 Hz, 2H, C*H*($CH_3$)$_2$), 1.73–1.51 (ov m, 8H, COE C*H*$_2$), 1.28 (br s, 2H, COE C*H*$_2$), 1.02 (d, 12H, $J_{HH}$ = 6.8 Hz, CH(C*H*$_3$)$_2$. $^{13}$C{$^{1}$H} NMR (benzene-$d_6$, 75.47 MHz): δ 147.3 (s, Ar *C*), 143.1 (d, $J_{CP}$ = 3.8 Hz, Ar *C*), 133.5 (d, $J_{CP}$ = 10.4 Hz, Ar *C*H), 132.4 (s, Ar *C*), 131.9 (ov d, $J_{CP}$ = 7.2 Hz, Ar *C*H), 131.9 (s, Ar *C*H), 131.1 (s, 2,5-pyrrole *C*), 128.6 (d, $J_{CP}$ = 12.7 Hz, Ar *C*H), 126.1 (s, Ar *C*H), 116.7 (dd, $J_{CP}$ = 26.9 Hz, $J_{CP}$ = 8.8 Hz, 3,4-pyrrole *C*H), 66.4 (d, $J_{CRh}$ = 14.9 Hz, COE *C*H), 34.1 (s, *C*H($CH_3$)$_2$), 31.5 (s, COE *C*$H_2$), 30.3 (s, COE *C*$H_2$), 27.6 (s, COE *C*$H_2$), 24.6 (s, CH(*C*$H_3$)$_2$). $^{31}$P{$^{1}$H} NMR (benzene-$d_6$, 121.49 MHz): δ 33.8 (d, 2P, $J_{PRh}$ = 6.0, P=N). Anal. Calcd. (%) for $C_{54}H_{58}N_3P_2Rh$: C, 70.97; H, 6.40; N, 4.60. Found: C, 70.73; H, 6.59; N, 4.81.

**Synthesis of 2-$C_2H_4$:**

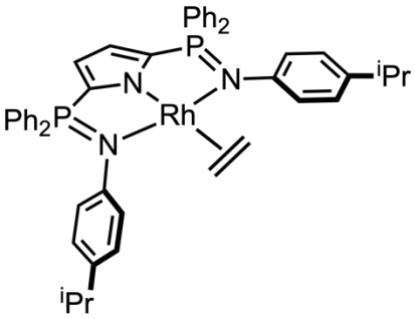


In an argon filled glove box, **2-COE** (0.051 g, 0.056 mmol) was added to a two-neck 25 mL round-bottomed flask and dissolved in toluene (5 mL). The reaction vessel was attached to a double manifold vacuum line and $C_2H_4$ gas was bubbled into solution (3 × 3 min). Between each addition of $C_2H_4$, the contents of the round-bottomed flask were evaporated to remove volatiles, including COE. The reaction mixture was stirred for a total of 1.5 h, and volatiles removed *in vacuo* to afford **2-$C_2H_4$** as an orange powder. The product was

recrystallized from a benzene/toluene/pentane (2:1:1) mixture at –35 ºC. Yield: 0.043 g (92%). $^{1}$H NMR (benzene-$d_6$, 300.13 MHz): δ 7.75 (dd, $J_{HH}$ = 7.2 Hz, $J_{HP}$ = 11.7 Hz, 8H, Ph C*H*), 7.03–6.88 (ov m, 16H, Ph C*H* + Pipp C*H*), 6.73 (ov m, 4H, Ph C*H* + Pipp C*H*), 6.68 (d, $J_{HP}$ = 1.8 Hz, 2H, 3,4-pyrrole C*H*), 3.14 (br s, 4H, $C_2H_4$), 2.54 (sp, $J_{HH}$ = 6.9 Hz, 2H, C*H*($CH_3$)$_2$), 0.97 (d, 12H, $J_{HH}$ = 6.9 Hz, CH(C*H*$_3$)$_2$). $^{13}$C{$^{1}$H} NMR (benzene-$d_6$, 75.47 MHz): δ 145.7 (s, Ar *C*), 142.6 (d, $J_{CP}$ = 3.3 Hz, Ar *C*), 133.4 (d, $J_{CP}$ = 9.9 Hz, Ar *C*H), 132.3 (s, Ar *C*), 132.0 (s, Ar *C*H), 131.1 (s, 2,5-pyrrole *C*), 130.6 (d, $J_{CP}$ = 6.6 Hz, Ar *C*H), 128.8 (d, $J_{CP}$ = 12.1 Hz, Ar *C*H), 126.5 (s, Ar *C*H), 116.8 (dd, $J_{CP}$ = 28.6 Hz, $J_{CP}$ = 8.8 Hz, 3,4-pyrrole *C*H), 51.8 (d, $J_{CRh}$ = 15.4 Hz, *C*$_2$H$_4$), 34.0 (s, *C*H($CH_3$)$_2$), 24.4 (s, CH(*C*H$_3$)$_2$)). $^{31}$P{$^{1}$H} NMR (benzene-$d_6$, 121.49 MHz): δ 33.9 (d, $J_{PRh}$ = 4.7 Hz, 2P, P=N). Anal. Calcd. (%) for $C_{48}H_{48}N_3P_2Rh$: C, 69.31; H, 5.82; N, 5.05. Found: C, 69.21; H, 5.81; N, 5.41.

**Synthesis of 2-Rh$_2$:**

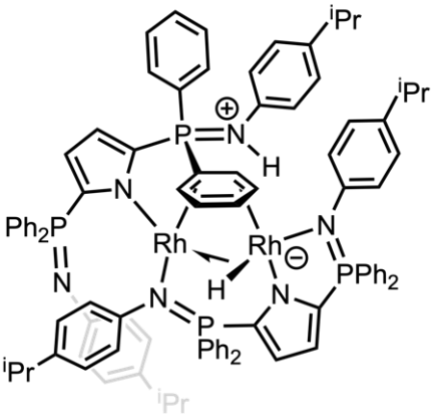


In an argon filled glove box, **2-COE** (0.047 g, 0.052 mmol) was added to a 25 mL round-bottomed flask and dissolved in toluene (5 mL). The reaction vessel was attached to a double manifold vacuum line and the solution was degassed by three freeze–pump–thaw cycles. A hydrogen atmosphere was applied to the flask and the solution was stirred at ambient temperature for 24 h. All volatiles were removed *in vacuo* to afford **2-Rh$_2$** as a dark brown powder. The product was recrystallized from a benzene/pentane (10:1) mixture at ambient temperature. Yield: 0.022 g (55%). $^{1}$H NMR (benzene-$d_6$, 700.39 MHz): δ 11.4 (d, 1H, $^{2}J_{HP}$ = 2.5 Hz, N*H*), 9.21 (dd, 2H, $^{3}J_{HP}$ =

11.3 Hz, $^{3}J_{HH}$ = 7.5 Hz, Ph C*H*), 8.07 (ddd, 2H, $^{3}J_{HP}$ = 11.6 Hz, $^{3}J_{HH}$ = 8.1 Hz, $^{4}J_{HH}$ = 1.2 Hz, Ph C*H*), 8.01 (m, 2H, Ph C*H*), 7.97 (ddd, 2H, $^{3}J_{HP}$ = 11.7 Hz, $^{3}J_{HH}$ = 8.4 Hz, $^{4}J_{HH}$ = 1.3 Hz, Ph C*H*), 7.95 (dd, 2H, $^{3}J_{HH}$ = 8.3 Hz, $^{4}J_{HP}$ = 1.9 Hz, Pipp C*H*), 7.82 (m, 2H, Pipp C*H*), 7.59 (m, 2H, Ph C*H*), 7.33 (ddd, 2H, $^{3}J_{HP}$ = 10.2 Hz, $^{3}J_{HH}$ = 8.2 Hz, $^{4}J_{HH}$ = 1.2 Hz, Ph C*H*), 7.29 (dd, 2H, $J_{HH}$ = 7.8 Hz, $J_{HP}$ = 3.3 Hz, Ph C*H*), 7.25–7.11 (ov m, 9H, Ar C*H*), 7.07 (t, 2H, $J_{HH}$ = 8.4 Hz, Ph C*H*), 7.06 (dd, 2H, $J_{HH}$ = 7.5 Hz, $J_{HP}$ = 2.0 Hz, Ph C*H*), 7.04 (dd, 2H, $J_{HH}$ = 7.5 Hz, $J_{HP}$ = 1.2 Hz, Ph C*H*), 7.01 (d, 2H, $J_{HH}$ = 8.4 Hz, Ph C*H*), 6.98 (m, 2H, Pipp C*H*), 6.97 (m, 3H, Ph C*H*), 6.91 (m, 5H, Ph C*H*), 6.86 (td, 2H, $J_{HH}$ = 7.8 Hz, $J_{HP}$ = 2.7 Hz, Ph C*H*), 6.81 (d, 2H, $^{3}J_{HH}$ = 8.1 Hz, Pipp C*H*), 6.68 (dd, 1H, $^{3}J_{HP}$ = 3.15 Hz, $^{3}J_{HH}$ = 3.15 Hz, 3,4-pyrrole C*H*), 6.50 (dd, 1H, $^{3}J_{HP}$ = 2.3 Hz, $^{3}J_{HH}$ = 1.6 Hz, 3,4-pyrrole C*H*), 6.49 (dd, 1H, $^{3}J_{HP}$ = 3.3 Hz, $^{3}J_{HH}$ = 3.3 Hz, 3,4-pyrrole C*H*), 6.34 (d, 2H, $^{3}J_{HH}$ = 8.0 Hz, Pipp C*H*), 6.30 (dd, 1H, $^{3}J_{HP}$ = 3.8 Hz, $^{3}J_{HH}$ = 3.8 Hz, 3,4-pyrrole C*H*), 6.23 (dd, 1H, $J_{HH}$ = 8.8 Hz, $^{3}J_{HH}$ = 5.9 Hz, Pipp C*H*), 5.65 (ddd, 1H, $^{3}J_{HH}$= 9.2 Hz, $^{4}J_{HH}$ = 5.2 Hz, $^{4}J_{HP}$ = 5.2 Hz, Pipp C*H*), 4.85 (dd, 1H, $J_{HP}$ = 10.1 Hz, $J_{HH}$ = 7.0 Hz, Pipp C*H*), 3.28 (ddd, 1H, $J_{HH}$ = 6.4 Hz, $J_{HH}$ = 6.2 Hz, $J_{HH}$ = 4.1 Hz, Pipp C*H*), 2.78 (sp, 2H, $^{3}J_{HH}$ = 6.9 Hz, $^{i}$Pr C*H*), 2.53 (sp, 1H, $^{3}J_{HH}$ = 6.9 Hz, $^{i}$Pr C*H*), 2.47 (sp, 1H, $^{3}J_{HH}$ = 6.9 Hz, $^{i}$Pr C*H*), 2.34 (dd, 1H, $J_{HP}$ = 12.6 Hz, $J_{HH}$ = 5.9 Hz, Ph C*H*), 1.25 (d, 3H, $^{3}J_{HH}$ = 6.9 Hz, $^{i}$Pr C$H_3$), 1.24 (d, 3H, $^{3}J_{HH}$ = 6.9 Hz, $^{i}$Pr C$H_3$), 1.19 (d, 3H, $^{3}J_{HH}$ = 6.9 Hz, $^{i}$Pr C$H_3$), 1.18 (d, 3H, $^{3}J_{HH}$ = 6.9 Hz, $^{i}$Pr C$H_3$), 1.03 (d, 3H, $^{3}J_{HH}$ = 6.9 Hz, $^{i}$Pr C$H_3$), 1.01 (d, 3H, $^{3}J_{HH}$ = 6.9 Hz, $^{i}$Pr C$H_3$), 0.97 (d, 3H, $^{3}J_{HH}$ = 6.9 Hz, $^{i}$Pr C$H_3$), 0.95 (d, 3H, $^{3}J_{HH}$ = 6.9 Hz, $^{i}$Pr C$H_3$), –35.8 (dd, 1H, $^{1}J_{HRh}$ = 19.8 Hz, $^{1}J_{HRh}$ = 19.8 Hz, Rh–*H*–Rh). $^{13}$C{$^{1}$H} NMR (benzene-$d_6$, 176.05 MHz): δ 151.6 (d, $^{2}J_{CP}$ = 1.8 Hz, Pipp *ipso*-C), 149.2 (d, $^{2}J_{CP}$ = 4.2 Hz, Pipp *ipso*-C), 144.0 (d, $^{2}J_{CP}$ = 2.0 Hz, Pipp *ipso*-C), 143.4 (d, $^{2}J_{CP}$ = 3.6 Hz, Pipp *ipso*-C), 141.7 (s, Pipp *C*), 141.4 (d, $^{1}J_{CP}$ = 14.0 Hz, 2,5-

pyrrole *C*), 141.1 (s, Pipp *C*), 141.1 (s, Pipp *C*), 141.1 (d, $^{1}J_{CP}$ = 18.5 Hz, 2,5-pyrrole *C*), 140.7 (d, $^{1}J_{CP}$ = 14.2 Hz, 2,5-pyrrole *C*), 140.6 (s, Pipp *C*), 140.1 (d, 2,5-pyrrole), 135.9 (d, $^{1}J_{CP}$ = 90.2 Hz, Ph *ipso*-C), 135.7 (d, $J_{CP}$ = 9.6 Hz, Ph *C*H), 134.5 (d, $J_{CP}$ = 8.2 Hz, Ph *C*H), 133.9 (d, $J_{CP}$ = 10.4 Hz; Ph *C*H), 133.8 (dd, $J_{CP}$ = 10.2 Hz, $J_{CRh}$ = 4.6 Hz, Ph *C*H), 133.8 (d, $^{1}J_{CP}$ = 80.6 Hz, Ph *ipso-C*), 133.5 (d, $J_{CP}$ = 9.0 Hz, Ph C*H*), 132.7 (d, $^{3}J_{CP}$ = 2.2 Hz, Pipp *C*H), 132.6 (d, $J_{CP}$ = 10.5 Hz, Ph *C*H), 132.2 (d, $^{3}J_{CP}$ = 1.9 Hz, Pipp *C*H), 132.2 (d, $^{1}J_{CP}$ = 91.3 Hz, Pipp *C*H), 132.1 (s, Pipp *C*H), 131.8 (d, $^{3}J_{CP}$ = 2.4 Hz, Pipp *C*H), 131.6 (s, Pipp *C*H), 131.1 (d, $J_{CP}$ = 12.4 Hz, Ph *C*H), 131.0 (dd, $J_{CRh}$ = 10.3 Hz, $J_{CP}$ = 1.8 Hz, Ph *C*H), 130.6 (d, $J_{CP}$ = 7.6 Hz, Ph *C*H), 129.5 (d, $J_{CP}$ = 11.7 Hz, Ph *C*H), 129.0 (d, $J_{CP}$ = 11.9 Hz, Ph *C*H), 128.9 (s, Pipp *C*H), 128.9 (d, $J_{CP}$ = 11.6 Hz, Ph CH), 127.8 (d, $J_{CP}$ = 10.9 Hz, Ph CH), 126.8 (s, Pipp CH), 125.9 (d, $^{3}J_{CP}$ = 1.7 Hz, Pipp CH), 125.2 (d, $^{1}J_{CP}$ = 83.8 Hz, Ph *ipso*-C), 125.2 (dd, $^{2}J_{CP}$ = 21.3 Hz, $^{3}J_{CP}$ = 11.4 Hz, 3,4-pyrrole *C*H), 124.5 (dd, $^{2}J_{CP}$ = 31.1 Hz, $^{3}J_{CP}$ = 12.1 Hz, 3,4-pyrrole *C*H), 119.7 (dd, $^{2}J_{CP}$ = 28.2 Hz, $^{3}J_{CP}$ = 12.0 Hz, 3,4-pyrrole *C*H), 119.3 (d, $J_{CP}$ = 8.4 Hz, Ph *C*H), 115.9 (dd, $^{2}J_{CP}$ = 28.5 Hz, $^{3}J_{CP}$ = 10.0 Hz, 3,4-pyrrole), 57.6 (br m, Ph *C*H), 54.6 (br m, Ph *C*H), 48.3 (br m, Ph *C*H), 47.6 (br ddd, $^{1}J_{CP}$ = 113.28 Hz, $^{1}J_{CRh}$ = 8.8 Hz, $^{1}J_{CRh}$ = 1.8 Hz, Ph *C*H), 34.2 (s, $^{i}$Pr *C*H), 34.1 (s, $^{i}$Pr *C*H), 34.1 (s, $^{i}$Pr *C*H), 34.0 (s, $^{i}$Pr *C*H), 25.3 (s, $^{i}$Pr *C*H$_3$), 25.0 (s, $^{i}$Pr *C*H$_3$), 24.9 (s, $^{i}$Pr *C*H$_3$), 24.7 (s, $^{i}$Pr *C*H$_3$), 24.7 (s, $^{i}$Pr *C*H$_3$), 24.6 (s, $^{i}$Pr *C*H$_3$), 24.1 (s, $^{i}$Pr *C*H$_3$). $^{31}$P{$^{1}$H} NMR (benzene-$d_6$, 176.1 MHz): δ 31.1 (s, 1P, Ph$_2$*P*=NPipp), 23.5 (s, 1P, Ph$_2$*P*=NPipp), 11.8 (d, 1P, $^{2}J_{PRh}$ = 6.2 Hz, Ph$_2$*P*=NHPipp), –1.9 (s, 1P, Ph$_2$P=NPipp). Anal. Calcd. (%) for $C_{92}H_{90}N_6P_4Rh_2$: C, 68.66; H, 5.64; N, 5.22. Found: C, 68.71; H, 5.08; N, 5.93.

**Synthesis of 2-Rh$_2$-*d*$_2$:**

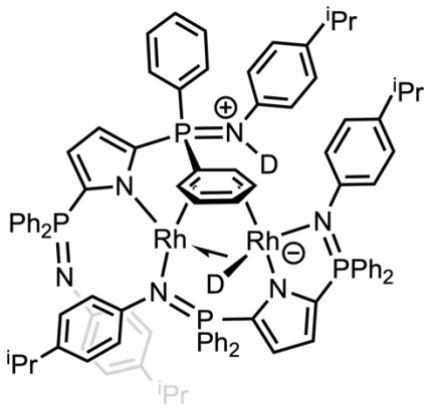


In an argon filled glove box, **2-COE** (0.088 g, 0.096 mmol) was added to a 25 mL round-bottomed flask equipped with a stir-bar and dissolved in toluene (7 mL). The reaction vessel was attached to a double manifold vacuum line and the solution was degassed by three freeze–pump–thaw cycles. A deuterium atmosphere was applied to the flask and the solution was stirred at ambient temperature for 18 h. All volatiles were removed *in vacuo* to afford **2-Rh$_2$-*d*$_2$** as a dark brown powder. Yield: 0.046 g (60%). $^1$H NMR (benzene-$d_6$, 300.13 MHz): δ 9.21 (dd, 2H, $^3J_{HP}$ = 11.9 Hz, $^3J_{HH}$ = 7.9 Hz, Ph C*H*), 8.46 (ddd, 2H, $^3J_{HP}$ = 10.9 Hz, $^3J_{HH}$ = 8.2 Hz, $^4J_{HH}$ = 1.7 Hz, Ph C*H*), 8.11 (m, 2H, Ph C*H*), 8.01 (m, 2H, Ph C*H*), 7.96 (dd, 2H, $^3J_{HH}$ = 7.3 Hz, $^4J_{HP}$ = 1.8 Hz, Pipp C*H*), 7.86 (m, 2H, Pipp C*H*), 7.69 (m, 2H, Ph C*H*), 7.35 (ddd, 2H, $^3J_{HP}$ = 11.3 Hz, $^3J_{HH}$ = 7.6 Hz, $^4J_{HH}$ = 1.7 Hz, Ph C*H*), 7.21 (dd, 2H, $J_{HH}$ = 7.8 Hz, $J_{HP}$ = 3.3 Hz, Ph C*H*), 7.19–7.11 (ov m, 9H, Ar C*H*), 7.06 (t, 2H, $J_{HH}$ = 8.4 Hz, Ph C*H*), 7.01 (dd, 2H, $J_{HH}$ = 7.5 Hz, $J_{HP}$ = 2.0 Hz, Ph C*H*), 6.98 (dd, 2H, $J_{HH}$ = 7.5 Hz, $J_{HP}$ = 1.2 Hz, Ph C*H*), 6.96 (d, 2H, $J_{HH}$ = 8.4 Hz, Ph C*H*), 6.94 (m, 10 H, Ph C*H*), 6.90 (td, 2H, $J_{HH}$ = 7.8 Hz, $J_{HP}$ = 2.7 Hz, Ph C*H*), 6.81 (d, 2H, $^3J_{HH}$ = 8.1 Hz, Pipp C*H*), 6.68 (dd, 1H, $^3J_{HP}$ = 4.6 Hz, $^3J_{HH}$ = 3.2 Hz, 3,4-pyrrole C*H*), 6.50 (dd, 1H, $^3J_{HP}$ = 2.3 Hz, $^3J_{HH}$ = 1.6 Hz, 3,4-pyrrole C*H*), 6.45 (dd, 1H, $^3J_{HP}$ = 3.3 Hz, $^3J_{HH}$ = 3.3 Hz, 3,4-pyrrole C*H*), 6.35 (d, 2H, $^3J_{HH}$ = 8.0 Hz, Pipp C*H*), 6.30 (dd, 1H, $^3J_{HP}$ = 3.5 Hz, $^3J_{HH}$ = 3.5 Hz, 3,4-pyrrole C*H*), 6.23 (dd, 1H, $J_{HH}$ = 8.4 Hz, $^3J_{HH}$ = 5.9 Hz, Pipp C*H*), 5.67 (ddd, 1H, $^3J_{HH}$= 8.5 Hz, $^4J_{HH}$ = 5.4 Hz, $^4J_{HP}$ = 5.0 Hz, Pipp

C*H*), 4.84 (dd, 1H, $J_{HP}$ = 10.4 Hz, $J_{HH}$ = 6.1 Hz, Pipp C*H*), 3.27 (ddd, 1H, $J_{HH}$ = 7.4 Hz, $J_{HH}$ = 5.8 Hz, $J_{HH}$ = 4.1 Hz, Pipp C*H*), 2.83 (sp, 2H, $^{3}J_{HH}$ = 6.4 Hz, $^{i}$Pr C*H*), 2.58 (sp, 1H, $^{3}J_{HH}$ = 7.0 Hz, $^{i}$Pr C*H*), 2.47 (sp, 1H, $^{3}J_{HH}$ = 7.2 Hz, $^{i}$Pr C*H*), 2.37 (dd, 1H, $J_{HP}$ = 12.6 Hz, $J_{HH}$ = 5.9 Hz, Ph C*H*), 1.26 (d, 3H, $^{3}J_{HH}$ = 7.4 Hz, $^{i}$Pr C*H*$_3$), 1.20 (d, 3H, $^{3}J_{HH}$ = 6.4 Hz, $^{i}$Pr C*H*$_3$), 1.19 (d, 3H, $^{3}J_{HH}$ = 6.4 Hz, $^{i}$Pr C*H*$_3$), 1.18 (d, 3H, $^{3}J_{HH}$ = 6.4 Hz, $^{i}$Pr C*H*$_3$), 1.03 (d, 3H, $^{3}J_{HH}$ = 6.4 Hz, $^{i}$Pr C*H*$_3$), 1.01 (d, 3H, $^{3}J_{HH}$ = 7.0 Hz, $^{i}$Pr C*H*$_3$), 0.97 (d, 3H, $^{3}J_{HH}$ = 6.4 Hz, $^{i}$Pr C*H*$_3$), 0.95 (d, 3H, $^{3}J_{HH}$ = 6.4 Hz, $^{i}$Pr C*H*$_3$). $^{31}$P{$^{1}$H} NMR (benzene-$d_6$, 121.49 MHz): δ 31.2 (s, 1P, Ph$_2$*P*=NPipp), 23.5 (s, 1P, Ph$_2$*P*=NPipp), 11.8 (d, 1P, $^{2}J_{PRh}$ = 7.3 Hz, Ph$_2$*P*=NHPipp), –1.8 (s, 1P, Ph$_2$P=NPipp). $^{13}$C{$^{1}$H} NMR spectra were consistent with that of **2-Rh$_2$**. $^{2}$H{$^{1}$H} NMR (benzene-$d_6$, 46.07 MHz): δ 11.2 (br s, 1D, N*D*), –35.3 (br s, 1D, Rh–*D*–Rh), coupling constants could not be ascertained due to the broadness of the observed resonances.

## 7.3. Experimental Procedures Pertaining to Chapter 3

### 7.3.1. Synthetic Procedures

**Chemical warning –** *Caution!* CO gas is deadly when inhaled. Experiments using CO gas were conducted in a double-manifold vacuum line equipped with inert gas (argon) inside a fume hood. CO and argon are condensable gases; caution should be taken when employing liquid nitrogen (–196 ºC) cooling baths.

**Synthesis of 2-COE:**

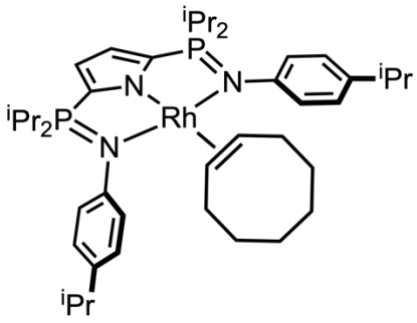


In a glove box, a 20 mL scintillation vial equipped with a magnetic stir bar was charged with 0.143 g (0.243 mmol) of Na-$^{iPr}$NNN dissolved in 8 mL of toluene. A separate toluene solution of $[RhCl(COE)_2]_2$ (0.087 g, 0.12 mmol, 0.5 equiv) was added to the rapidly stirring solution of Na-$^{iPr}$NNN. The reaction mixture became a deep red-orange colour after 5 minutes and was allowed to stir for 18 hours. The mixture was concentrated *in vacuo* and passed through a pad of Celite to remove sodium chloride. Volatiles were removed *in vacuo* to afford an oily residue that was washed with pentane (3 × 3 mL) followed by trituration with pentane (3 × 3 mL) affording **2-COE** as a bright orange powder. Yield: 0.164 g, 0.210 mmol, 86.7%. $^1$H NMR (benzene-$d_6$, 300.13 MHz): δ 7.21 (d, $^3J_{HH}$ = 7.5 Hz, 4H, N(4-$^i$PrC$_6H_4$)), 6.93 (d, $^3J_{HH}$ = 7.5 Hz, 4H, N(4-$^i$PrC$_6H_4$)), 6.60 (d, $^3J_{HP}$ = 1.59 Hz, 2H, pyrrole-H), 3.05 ($^3J_{HH}$ = 9.1 Hz, 2H, (HC=CH)C$H_2$), 2.68 (sp, $^3J_{HH}$ = 6.7 Hz, 2H, C$H$(CH$_3$)), 2.39 (dd, $^3J_{HRh}$ = 13.4 Hz, $^3J_{HH}$ = 2.4 Hz, 2H, ($H$C=C$H$), 1.97 (spd, $^3J_{HH}$ = 7.1 Hz, $^2J_{HP}$ = 1.8 Hz, C$H$(CH$_3$)), 1.69–1.22 (ov m, 10H, COE C$H_2$), 1.14 (d, $^3J_{HH}$ = 6.7 Hz, 12H CH(C$H_3$)$_2$), 1.04 (dd, $^3J_{HP}$ = 15.5 Hz, $^3J_{HH}$ = 7.2 Hz, 24H, CH(C$H_3$)$_2$). $^{31}$P{$^1$H} NMR (benzene-$d_6$, 121.49 MHz): δ 56.8 (d, $^2J_{PRh}$ = 3.2 Hz, 2P). $^{13}$C{$^1$H} NMR (benzene-$d_6$, 75.47 MHz): δ 147.9 (s, Ar *C*), 142.5 (s, Ar *C*), 130.9 (d, $^2J_{CP}$ = 6.4 Hz, Ar *C*), 125.5 (s, Ar *C*), 113.8 (dd, $^2J_{CP}$ = 24.5 Hz, $^3J_{CP}$ = 8.3 Hz, 3,4-pyrrole *C*H), 62.7 (d, $^1J_{CRh}$ = 15.1 Hz, COE *C*H), 33.7 (s, C), 30.9 (s, C), 29.4 (s, C), 27.0 (d, $^1J_{CP}$ = 14.5 Hz, *C*H(CH$_3$)$_2$), 26.4 (s, C), 24.1 (s, C), 16.1 (d, $^1J_{CP}$ = 17.1 Hz, *C*H(CH$_3$)$_2$). Anal. Calcd. (%) $C_{42}H_{66}N_3P_2Rh_1$: C, 64.85; H, 8.55; N, 5.40. Found: C, 64.59; H, 8.58; N, 5.46.

**Synthesis of 3-(CO)$_2$:**

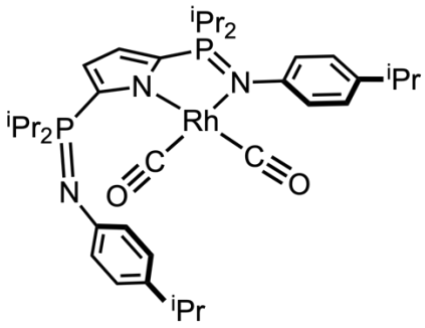

A 20 mL scintillation vial was charged with 0.067 g (0.171 mmol, 0.5 equiv) of [RhCl(CO)$_2$]$_2$, 0.201 g (1 equiv, 0.342 mmol) of Na-$^{iPr}$NNN, and a magnetic stir bar. The mixture was dissolved in 5 mL of toluene and stirred at ambient temperature for 18 hours. The reaction mixture was filtered through a thin pad of Celite to remove sodium chloride. Volatiles were removed under reduced pressure affording a yellow powder. The solid was washed with pentane (3 × 5 mL), giving a red filtrate, and then recrystallized from a mixture of pentane and toluene (3:1) at –35 °C. Yield: 0.235 g (94.9%). Note: In solution, **3-(CO)$_2$** slowly converts to **3-CO** as indicated by $^1$H and $^{31}$P NMR spectroscopy. Thus, although analytically pure samples of **3-(CO)$_2$** can be isolated in the solid state by washing a mixture of the two compounds with cold pentane, solution NMR spectra of **3-(CO)$_2$** were sometimes contaminated with a small quantity of **3-CO**. $^1$H NMR (benzene-$d_6$, 300.13 MHz): δ 7.54–7.04 (m, 6H, *aryl*), 7.01–6.97 (m, 2H, *aryl*), 6.66 (d, $^3J_{HH}$ = 3.3 Hz, 1H, pyrrole-*H*), 6.45 (d, $^3J_{HH}$ = 3.3 Hz, 1H, pyrrole-*H*), 2.95 (sp, $^3J_{HH}$ = 6.9 Hz, 1H, C*H*(CH$_3$)$_2$), 2.72 (sp, $^3J_{HH}$ = 7.2 Hz, 1H, C*H*(CH$_3$)$_2$), 2.44 (sp, $^3J_{HH}$ = 7.2 Hz, 2H, C*H*(CH$_3$)$_2$), 1.94 (sp, $^3J_{HH}$ = 6.9 Hz, 2H, C*H*(CH$_3$)$_2$), 1.36 (d, $^3J_{HH}$ = 6.9 Hz, 12H, CH(C*H*$_3$)$_2$), 1.16 (d, $^3J_{HH}$ = 6.9 Hz, 12H, CH(C*H*$_3$)$_2$), 0.88 (d, $^3J_{HH}$ = 6.9 Hz, 12H, CH(C*H*$_3$)$_2$). $^{31}$P{$^1$H} NMR (benzene-$d_6$, 121.49 MHz) 58.7 (s, 1P), 13.4 (s, 1P). $^{13}$C{1H} NMR (benzene-$d_6$, 75.47 MHz): δ 186.3 (dd, $^1J_{CRh}$ = 68.5 Hz, $^3J_{CC}$ = 9.5 Hz, 1C, Rh–*C*O), 184.6 (dd, $^1J_{CRh}$ = 69.3 Hz, $^3J_{CC}$ = 9.5 Hz, 1C, Rh–*C*O), 152.0 (d, $^1J_{CP}$ = 3.9 Hz, 1C), 150.0 (d, $^1J_{CP}$ = 1.5 Hz, 1C), 144.3 ($^1J_{CP}$ = 1.9 Hz, 1C), 136.5 (s, 1C), 128.3 (s, 1C), 127.4 (d, $^1J_{CP}$ = 6.6 Hz, 1C), 127.1 (d, $^1J_{CP}$ = 31.0

Hz 1C), 125.5 (d, $^{1}J_{CP}$ = 15.8 Hz, 1C), 119.3 (dd, $^{1}J_{CP}$ = 17.0 Hz, $^{1}J_{CP}$ = 11.4 Hz, 1C), 116.7 (dd, $^{1}J_{CP}$ = 24.9 Hz, $^{1}J_{CP}$ = 7.9 Hz, 1C), 34.1 (d, $^{1}J_{CP}$ = 17.9 Hz, 1C), 29.6 (d, $^{1}J_{CP}$ = 73.6 Hz 1C), 26.9 (d, $^{1}J_{CP}$ = 53.1 Hz, 1C), 24.9 (d, $^{1}J_{CP}$ = 49.0 Hz, 1C), 18.4 (d, $^{1}J_{CP}$ = 3.17 Hz, 1C), 17.0 (s, 1C), 16.4 (d, $^{1}J_{CP}$ = 2.87 Hz, 1C), 16.1 (d, $^{1}J_{CP}$ = 1.7 Hz, 1C). Anal. Calcd. (%) for $C_{36}H_{52}N_3O_2P_2Rh$: C, 59.75; H, 7.24; N, 5.81. Found: C, 59.35; H, 7.14; N, 6.14. IR $\nu_{CO}$ ($cm^{-1}$): 2071, 1994.

**Synthesis of 3-CO:**

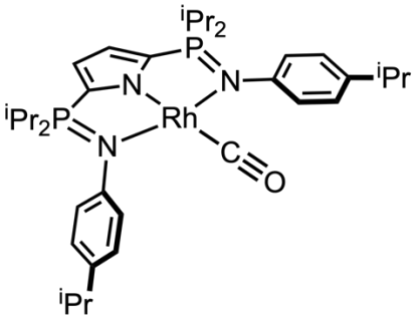


In an argon-filled glove box, a 20 mL scintillation vial equipped with a Teflon micro stir bar was charged with **3-(CO)$_2$** (0.193 g, 0.267 mmol) and 1 equiv of **2-COE** (0.207 g, 0.267 mmol) and dissolved in 4 mL of toluene. The mixture was stirred for 1 hour at ambient temperature at which point volatiles were removed under reduced pressure. The resulting red powder was recrystallized in minimal pentane at –35 °C producing large red crystals. Yield: 0.352 g (94.8%). All spectra were consistent with samples of **3-CO** prepared by a previous method which involved subjecting a toluene solution of **3-(CO)$_2$** to prolonged periods of reduced pressure. $^{1}$H NMR (benzene-$d_6$, 300.13 MHz): δ 7.52 (d, $^{3}J_{HH}$ = 8.2 Hz, 4H, *aryl*), 6.99 (d, $^{3}J_{HH}$ = 8.2 Hz, 4H, *aryl*), 6.49 (d, $^{3}J_{HP}$ = 1.8 Hz, 2H, pyrrole-*H*), 2.69 (sp, $^{3}J_{HH}$ = 6.9 Hz, 2H, C*H*$(CH_3)_2$), 2.06 (spd, $^{3}J_{HH}$ = 6.9 Hz, $^{3}J_{HP}$ = 1.8 Hz 4H, C*H*$(CH_3)_2$), 1.12 (d, $^{3}J_{HH}$ = 6.9 Hz, 12H, CH(C*H*$_3)_2$), 0.99 (dd, $^{2}J_{HP}$ = 19.4 Hz, $^{3}J_{HH}$ = 6.9 Hz, 24H, CH(C*H*$_3)_2$). $^{31}$P{$^{1}$H} NMR (benzene-$d_6$, 121.49 MHz) δ 60.9 (d, $^{2}J_{PRh}$ = 5.6 Hz, 2P). $^{13}$C{1H} NMR (benzene-$d_6$, 75.47 MHz): δ 195.7 (d, $^{1}J_{CRh}$ = 76.9 Hz, 1C), 152.3 (s, 1C),

142.2 (s, 1C), 128.6 (s, 1C), 128.2 (s, 1C), 126.6 (s, 1C), 115.7 (dd, $^{1}J_{CP}$ = 24.0 Hz, $^{1}J_{CP}$ = 8.7 Hz, 2C), 34.0 (s, 1C), 27.9 (d, $^{1}J_{CP}$ = 52.9 Hz, 1C), 24.7 (s, 1C), 16.7 (s, 1C), 16.6 (ov m, 1C). Anal. Calcd. (%) for $C_{35}H_{52}N_3O_1P_2Rh$: C, 60.43; H, 7.53; N, 6.04. Found: C, 60.26; H, 7.76; N, 6.00. IR $\nu_{CO}$ ($cm^{-1}$): 1930.

**Synthesis of 3-(CO)$_2$·BCF:**

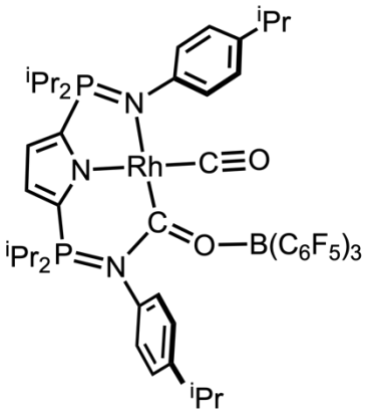


In a 20 mL scintillation vial, 0.058 g (0.08 mmol) of **3-(CO)$_2$** was dissolved in 5 mL of toluene. A toluene solution (5 mL) of $B(C_6F_5)_3$ (0.041 g, 0.08 mmol) was added dropwise at room temperature. The mixture was stirred for 15 minutes during which time a colour change from bright yellow to gold was observed. Volatiles were removed under reduced pressure giving a dark golden powder which was crystallized in a mixture of toluene and pentane (1:1) at –35° C. Yield: 0.088 g (89%). $^{1}$H NMR (benzene-$d_6$, 300.13 MHz): 7.14–6.87 (ov m, 8H, N(4-$^{i}$PrC$_6$*H*$_4$), 6.45 (dd, $^{3}J_{HH}$ = $^{3}J_{HP}$ = 3.5 Hz, 1H, pyrrole-*H*), 6.34 (dd, $^{3}J_{HH}$ = $^{3}J_{HP}$ = 3.3 Hz, 1H, pyrrole-*H*), 2.69 (spd, $^{3}J_{HH}$ = 6.9 Hz, $^{3}J_{HP}$ = 1.8, 2H, P(C*H*(CH$_3$)$_2$)$_2$, 1.84 (br sp, 2H, P(C*H*(CH$_3$)$_2$)$_2$, 1.23 (br sp, 2H, –N(4-$^{i}$PrC$_6$H$_4$), 1.12 (d, $^{3}J_{HH}$ = 6.9 Hz, 6H, CH(C*H*$_3$)$_2$), 1.01 (d, $^{3}J_{HH}$ = 6.9 Hz, 6H, CH(C*H*$_3$)$_2$), 0.89–0.78 (ov m, 12H, CH(C*H*$_3$)$_2$), 0.72 (br d, 6H), 0.47 (br d, 6H). Some ligand $^{13}$C resonances are obscured. $^{31}$P{$^{1}$H} NMR (benzene-$d_6$, 121.49 MHz) 58.8 (s, 1P), 54.2 (s, 1P). $^{13}$C{$^{1}$H} NMR (benzene-$d_6$, 75.47 MHz): δ 227.1 (dd, $^{1}J_{CRh}$ = 57.1 Hz, $^{3}J_{CP}$ = 17.2 Hz, 1C, Rh–*C*O–B(C$_6$F$_5$)$_3$), 190.4 (dd, $^{1}J_{CRh}$ = 79.9 Hz, $^{3}J_{CP}$ = 4.8 Hz, 1C, Rh–*C*O). $^{11}$B{$^{1}$H} NMR (benzene-$d_6$): –3.08 (br s, 1B). $^{19}$F{$^{1}$H} NMR (toluene-$d_8$, 243 K): δ –126.1 (br s, 1F, *o*-C$_6$F$_5$), –

128.8 (br s, 1F, *o*-$C_6F_5$), – 129.5 (br s, 1F, *o*-$C_6F_5$), – 130.9 (br s, 1F, *o*-$C_6F_5$), –134.2 (t, $^3J_{FF}$ = 17.2 Hz, 1F, *o*-$C_6F_5$), –135.4 (br s, 1F, *o*-$C_6F_5$), –158.5 (t, $^3J_{FF}$ = 19.3 Hz, 1F, *p*-$C_6F_5$), –158.8 (t, $^3J_{FF}$ = 21.5 Hz, 1F, *p*-$C_6F_5$), –159.4 (t, $^3J_{FF}$ = 21.5 Hz, 1F, *p*-$C_6F_5$), –161.8 (br s, 1F, *m*-$C_6F_5$), –163.3 (t, $^3J_{FF}$ = 19.3 Hz, 1F, *m*-$C_6F_5$), –164.3 (t, $^3J_{FF}$ = 21.5 Hz, 1F, *m*-$C_6F_5$), –164.9 (ov m, 1F, *m*-$C_6F_5$), –165.2 (ov m, 1F, *m*-$C_6F_5$), –166.1 (t, $^3J_{FF}$ = 19.3 Hz, 1F, *m*-$C_6F_5$). Anal. Calcd. (%) $C_{54}H_{52}BF_{15}N_3O_2P_2Rh \cdot C_7H_8$: C, 55.18; H, 4.55; N, 3.18. Found: C, 54.70; H, 4.91; N, 3.18. IR $\nu_{CO}$ ($cm^{-1}$): 1993.

**Synthesis of 3-$(CO)_2$PO·BCF:**

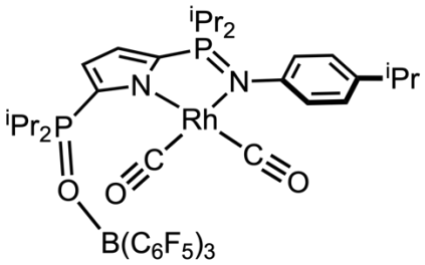


In an argon filled glove box, a 20 mL scintillation vial equipped with a magnetic stir bar was charged with 0.065 g of **3-$(CO)_2$·BCF** (0.053 mmol) and dissolved in 8 mL of toluene. The solution was stirred rapidly at 50 °C for 18 hours to ensure complete conversion to the product mixture. NMR experiments using isotopically labeled material established quantitative conversion to complexes **3-CO**, **3-$(CO)_2$PO·BCF**, and $(C_6F_5)_3B{\leftarrow}{:}C{\equiv}N(4\text{-}^{i}PrC_6H_4)$ in a 1:1:1 ratio. Single crystals suitable for X-ray diffraction were grown from a layered 1:1 solution of toluene and pentane. Yellow needles of complex **3-$(CO)_2$PO·BCF** were manually separated from the mixture. Analytically pure samples of **3-$(CO)_2$PO·BCF** could not be obtained from the complex mixture as both **3-CO** and $(C_6F_5)_3B{\leftarrow}{:}C{\equiv}N(4\text{-}^{i}PrC_6H_4)$ share similar solubility profiles and their crystals cannot be reliably distinguished by visual inspection. $^1$H NMR (benzene-$d_6$, 300.13 MHz): δ 6.98 (ov m, 4H, 4-$^{i}$PrC$_6$*H*$_4$), 6.43 (dd, $J_{HH} = J_{HP}$ = 3.8 Hz, 1H, pyrrole-*H*), 5.94 (dd, $J_{HH} = J_{HP}$ = 3.8 Hz, 1H, pyrrole-*H*), 3.16 (dsp,

$J_{HP}$ = 10.9 Hz, $J_{HH}$ = 7.2 Hz, 2H, C*H*($CH_3$)$_2$), 2.69 (sp, $J_{HH}$ = 6.9 Hz, 1H, C*H*($CH_3$)$_2$), 1.75 (dsp, $J_{HP}$ = 11.2 Hz, $J_{HH}$ = 7.2 Hz, 2H, C*H*($CH_3$)$_2$), 1.12 (d, $J_{HH}$ = 6.9 Hz, 6H, CH(C*H*$_3$)$_2$), 1.09 (dd, $J_{HP}$ = 11.7 Hz, $J_{HH}$ = 7.2 Hz, 6H, CH(C*H*$_3$)$_2$), (dd, $J_{HP}$ = 11.7 Hz, $J_{HH}$ = 7.2Hz, 6H, CH(C*H*$_3$)$_2$), 0.73 (dd, $J_{HP}$ = 16.5 Hz, $J_{HH}$ = 7.2 Hz, 6H, CH(C*H*$_3$)$_2$), 0.67 ($J_{HP}$ = 16.7 Hz, $J_{HH}$ = 7.2 Hz, 6H, CH(C*H*$_3$)$_2$). $^{31}$P{$^1$H} NMR (benzene-$d_6$, 121.49 MHz): δ 61.0 (s, 1P), 59.9 (s, 1P). $^{13}$C NMR (benzene-$d_6$, 75.47 MHz): δ 184.5 (dd, $J_{CRh}$ = 69.7 Hz, $J_{CC}$ = 9.2, Rh–*C*O), 183.6 (dd, $J_{CRh}$ = 66.5 Hz, $J_{CC}$ = 9.2, Rh–*C*O), 147.9 (s, aromatic *C*), 144.8 (s, aromatic *C*), 127.0 (s, aromatic *C*), 126.2 (d, $J_{CP}$ = 5.8 Hz, aromatic *C*), 33.5 (s, *C*H($CH_3$)$_2$), 25.8 (d, $J_{CP}$ = 52.0 Hz, *C*H($CH_3$)$_2$), 25.2 (d, $J_{CP}$ = 48.9 Hz, *C*H($CH_3$)$_2$), 23.9 (s, CH(*C*H$_3$)$_2$), 17.5 (s, CH(*C*H$_3$)$_2$), 16.2 (s, CH(*C*H$_3$)$_2$), 15.5 (s, CH(*C*H$_3$)$_2$), 15.1 (s, CH(*C*H$_3$)$_2$). Pyrrole carbon resonances were not observed; $C_6F_5$ resonances are not reported. $^{11}$B NMR (benzene-$d_6$): δ –21.3 (br s). $^{19}$F{$^1$H} NMR (benzene-$d_6$): –131.7 (br s, 2F, *o*-C$_6$*F*$_5$, –133.8 (d, $^3J_{FF}$ = 22.3 Hz, 2F, *o*-C$_6$*F*$_5$), –157.6 (t, $^3J_{FF}$ = 20.6 Hz, 1F, *p*-C$_6$*F*$_5$), –160.7 (t, $^3J_{FF}$ = 20.6 Hz, 1F, *p*-C$_6$*F*$_5$), –163.6 (t, $^3J_{FF}$ = 19.2 Hz, 2F, *m*-C$_6$*F*$_5$), –164.5 (t, $^3J_{FF}$ = 19.2 Hz, 2F, *m*-C$_6$*F*$_5$). IR $\nu_{CO}$ (cm$^{-1}$): 2074, 1990.

### 7.3.2. Crystallographic Details

**Table 7.3.1.** Crystallographic details for complexes discussed in Chapter 3.

| | **3-$(CO)_2$** | **3-CO** |
|---|---|---|
| CCDC Entry | 1822710 | 1822709 |
| Crystal Size (mm) | 0.20 × 0.10 × 0.05 | 0.25 × 0.25 × 0.25 |
| Moiety Formula | $C_{36}H_{52}N_3O_2P_2Rh$ | $C_{35}H_{52}N_3OP_2Rh$ |
| Formula weight (g/mol) | 723.65 | 695.64 |
| λ (nm) | 1.54178 | 1.54184 |
| T (K) | 100(2) | 100(2) |
| Crystal System | Triclinic | Tetragonal |
| Space group (*Z*) | P–1 (2) | P $4_1$ $2_1$ 2 (92) |
| *a* (Å) | 8.05860(10) | 10.84772(10) |
| *b* (Å) | 10.1052(2) | 10.84772(10) |
| *c* (Å) | 23.1513(5) | 29.6565(6) |
| *a* (deg) | 80.188(2) | 90 |
| b (deg) | 84.702(2) | 90 |
| g (deg) | 75.303(2) | 90 |
| Volume ($Å^3$) | 1794.55(6) | 3489.76(9) |
| Calc. *r* ($g\ cm^{-3}$) | 1.339 | 1.324 |
| μ ($mm^{-1}$) | 4.955 | 5.051 |
| Reflections | 7405 | 3572 |
| Completeness (to 2$\theta$) | 0.970 | 0.995 |
| C–C Bond Precision (Å) | 0.0047 | 0.0049 |
| $R_1$, $wR_2$ [$I > 2\sigma(I)$] | 0.0362, 0.0835 | 0.0256, 0.0657 |
| GoF on $F^2$ | 1.063 | 1.064 |

$R_1 = \Sigma||F_o| - |F_c||/\Sigma|F_o|$. $wR_2 = [\Sigma[w(F_o^2 - F_c^2)^2]/\Sigma w(F_o^4)]^{1/2}$.

**Table 7.3.2.** Crystallographic details for complexes discussed in Chapter 3.

| | **3-$(CO)_2$·BCF** | **3-$(CO)_2$PO·BCF** |
|---|---|---|
| CCDC Entry | 1822711 | 1822715 |
| Crystal Size (mm) | 0.15 × 0.20 × 0.32 | 0.25 × 0.20 × 0.05 |
| Moiety Formula | $C_{54}H_{52}BF_{15}N_3O_2P_2Rh$ | $C_{45}H_{41}BF_{15}N_2O_3P_2Rh$ |
| Formula weight (g/mol) | 1419.91 | 1118.46 |
| λ (nm) | 1.54184 | 1.54184 |
| T (K) | 100(2) | 100(2) |
| Crystal System | Monoclinic | Triclinic |
| Space group (*Z*) | P $2_1$/n (14) | P–1 (2) |
| *a* (Å) | 12.49908(8) | 13.7064(3) |
| *b* (Å) | 20.14166(13) | 14.1333(3) |
| *c* (Å) | 26.09610(18) | 14.2821(3) |
| *α* (deg) | 90 | 77.234(2) |
| β (deg) | 97.4055(6) | 80.940(2) |
| γ (deg) | 90 | 77.958(2) |
| Volume ($Å^3$) | 6514.95(7) | 2620.86(10) |
| Calc. $\rho$ (g $cm^{-3}$) | 1.448 | 1.417 |
| μ ($mm^{-1}$) | 3.368 | 4.037 |
| Reflections | 11593 | 11335 |
| Completeness (to $2\theta$) | 0.998 | 0.989 |
| C–C Bond Precision (Å) | 0.0042 | 0.0038 |
| $R_1$, $wR_2$ [$I > 2\sigma(I)$] | 0.0759, 0.2131 | 0.0354, 0.0906 |
| GoF on $F^2$ | 1.043 | 1.130 |

$R_1 = \Sigma||F_o| - |F_c||/\Sigma|F_o|$. $wR_2 = [\Sigma[w(F_o^2 - F_c^2)^2]/\Sigma w(F_o^4)]^{1/2}$.

## 7.4. Experimental Procedures Pertaining to Chapter 4

### 7.4.1. Synthetic Procedures

**Synthesis of $Ph_2SiD_2$.** To a stirring diethylether solution (10 mL) of $Ph_2SiCl_2$ (1.00 g, 4.59 mmol), $LiAlD_4$ (0.39 g, 9.3 mmol; 9.6 mL of a 1M $Et_2O$ solution) was added. The reaction mixture was stirred under argon for 16 hours and then added to a 1M aqueous solution (10

mL) of HCl. The organic phase was washed with a saturated NaCl solution (3 × 10 mL) and dried over $Na_2SO_4$. Residual solvent was removed *in vacuo* giving a clear, colourless liquid. Yield: 0.579 g (78%).

**Synthesis of 4-$SiH_2Ph$:**

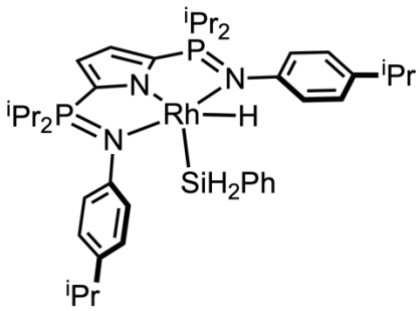


In an argon-filled glove box, a 20 mL scintillation vial equipped with a Teflon micro stir bar was charged with **2-COE** (0.250 g, 0.321 mmol) and dissolved in 4 mL of toluene. In a separate 5 mL vial, 1 equiv of $PhSiH_3$ (0.059 g, 0.32 mmol) was dissolved in 1 mL of toluene and added to the stirring solution of **2-COE**. The mixture was stirred for 1 hour at ambient temperature at which point volatiles were removed under reduced pressure. The resulting red powder was recrystallized in heptane at –35 °C affording bright red needle-like crystals. Yield: 0.24 g (96%). $^1$H NMR (benzene-$d_6$): δ 7.58 (ov m, 2H, Si-C$_6$*H*$_5$), 7.34 (d, $^3J_{HH}$ = 7.6 Hz, 4H, 4-$^i$PrC$_6$*H*$_4$), 7.11–6.99 (ov m, 3H, Si-C$_6$*H*$_5$), 6.87 (d, $^3J_{HH}$ = 7.6 Hz, 4H, 4-$^i$PrC$_6$*H*$_4$), 6.54 (d, $^3J_{HP}$ = 1.8 Hz, 2H, pyrrole-*H*), 5.49 (s, 2H, $^{29}$Si satellites (2.3%) $^1J_{HSi}$ = 183 Hz), 2.70 (sp, $^3J_{HH}$ = 7.3 Hz, 2H, C*H*(CH$_3$)$_2$), 2.06 (dsp, $^2J_{HP}$ = 6.9 Hz, $^3J_{HH}$ = 7.3 Hz, 2H, C*H*(CH$_3$)$_2$), 1.90 (dsp, $^2J_{HP}$ = 7.5 Hz, $^3J_{HH}$ = 7.3 Hz, 2H, C*H*(CH$_3$)$_2$), 1.28 (dd, $^3J_{HP}$ = 15.2 Hz, $^3J_{HH}$ = 7.3 Hz, 6H, CH(C*H*$_3$)$_2$), 1.17 (d, $^3J_{HH}$ = 7.3 Hz, 12H, CH(C*H*$_3$)$_2$), 0.99–0.90 (ov m,12H, CH(C*H*$_3$)$_2$), 0.62 (dd, $^3J_{HP}$ = 15.2 Hz, $^3J_{HH}$ = 7.3 Hz, 6H), –14.2 (d, $^1J_{HRh}$ = 25.6 Hz, 1H, Rh–*H*). $^{13}$C{$^1$H} NMR (benzene-$d_6$): δ 150.8 (s, aromatic *C*), 142.9 (s, aromatic *C*), 142.3 (s, aromatic *C*), 135.8 (s, aromatic *C*), 132.1 (s, aromatic *C*), 130.6 (s, aromatic *C*), 130.3 (dd, $^1J_{CP}$ = 147 Hz, $^4J_{CP}$ = 2.7 Hz, 2,5-pyrrole C), 127.2 (s, aromatic *C*), 126.2 (s, aromatic *C*), 115.9 (dd, $^2J_{CP}$ = 24.7 Hz, $^3J_{CP}$ = 8.7 Hz, 3,4-pyrrole *C*), 34.1 (s,

*C*H(CH$_3$)$_2$), 29.4 (d, $^1J_{CP}$ = 52.2 Hz, *C*H(CH$_3$)$_2$), 26.7 ($^1J_{CP}$ = 53.3 Hz, *C*H(CH$_3$)$_2$), 24.8 (s, CH(*C*H$_3$)$_2$), 16.9 (s, CH(*C*H$_3$)$_2$), 16.6–16.3 (ov m, CH(*C*H$_3$)$_2$). $^{31}$P{$^1$H} NMR (benzene-$d_6$): δ 64.1 (d, $^2J_{PRh}$ = 4.2 Hz, 2P). $^{29}$Si NMR (benzene-$d_6$): δ –7.65. Anal. Calcd. (%) for $C_{40}H_{60}N_3OP_2RhSi$: C, 61.92; H, 7.80; N, 5.42. Found: C, 61.92; H, 7.92; N, 5.42.

**Synthesis of 4-SiHPh$_2$:**

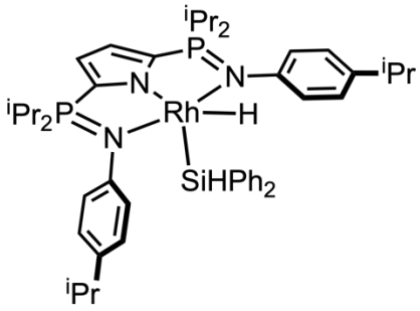


In an argon-filled glove box, a 20 mL scintillation vial equipped with a Teflon micro stir bar was charged with **2-COE** (0.250 g, 0.321 mmol) and dissolved in 4 mL of toluene. In a separate 5 mL vial, 1 equiv of Ph$_2$SiH$_2$ (0.321 mmol, 0.059 g) was dissolved in 1 mL of toluene and added to the stirring solution of **2-COE**. The mixture was stirred for 1 hour at ambient temperature at which point volatiles were removed under reduced pressure. The resulting bright orange powder was recrystallized in pentane at –35 °C. Yield: 0.251 g (92%). $^1$H NMR (benzene-$d_6$): δ 7.69–7.66 (ov m, 4H, Si–C$_6$*H*$_5$), 7.21 (d, $^3J_{HH}$ = 7.8 Hz, 4H, 4-$^i$PrC$_6$*H*$_4$), 7.05–6.94 (ov m, 6H, Si–C$_6$*H*$_5$), 6.76 (d, $^3J_{HH}$ = 7.8 Hz, 4H, 4-$^i$PrC$_6$*H*$_4$), 6.55 (d, $^3J_{HP}$ = 1.7 Hz, 2H, 3,4-pyrrole *H*), 6.39 (dd, $^2J_{HRh}$ = $^3J_{HH}$ = 4.1 Hz, 1H, Si–*H*), 2.71 (sp, $^3J_{HH}$ = 6.9 Hz, 2H, C*H*(CH$_3$)$_2$), 1.98–1.82 (ov sp, 4H, C*H*(CH$_3$)$_2$), 1.22 (d, $^3J_{HH}$ = 6.9 Hz, 12 H, CH(C*H*$_3$)$_2$), 1.19 (dd, $^3J_{HP}$ = 15.9 Hz, $^3J_{HH}$ = 7.1 Hz, 6H, CH(C*H*$_3$)$_2$), 1.00 (dd, $^3J_{HP}$ = 16.7 Hz, $^3J_{HH}$ = 6.9 Hz, 6H, CH(C*H*$_3$)$_2$), 0.89 (dd, $^3J_{HP}$ = 15.9 Hz, $^3J_{HH}$ = 6.9 Hz, 6H, CH(C*H*$_3$)$_2$), 0.58 (dd, $^3J_{HP}$ = 15.9 Hz, $^3J_{HH}$ = 7.1 Hz, 6H, CH(C*H*$_3$)$_2$), –13.6 ($^1J_{HRh}$ = 26.1 Hz, 1H, Rh–*H*). $^{13}$C{$^1$H} NMR: δ 150.5 (s, aromatic *C*), 144.5 (s, aromatic *C*), 141.9 (s, aromatic *C*), 135.4 (s, aromatic *C*), 130.5 (dd, $^1J_{CP}$ = 141 Hz, $^4J_{CP}$ = 9.9 Hz, 2,5-pyrrole *C*), 127.2 (s,

aromatic *C*), 126.9 (s, aromatic *C*), 125.9 (s, aromatic *C*), 116.1 (dd, $^{2}J_{CP}$ = 24.1 Hz, $^{3}J_{CP}$ = 8.2 Hz, 3,4-pyrrole *C*), 34.1 (s, *C*H(CH$_3$)$_2$), 29.6 (d, $^{1}J_{CP}$ = 54.3 Hz, *C*H(CH$_3$)$_2$), 26.6 (d, $^{1}J_{CP}$ = 53.1 Hz, *C*H(CH$_3$)$_2$), 24.9 (s, CH(*C*H$_3$)$_2$), 24.8 (s, CH(*C*H$_3$)$_2$), 17.0 (s, CH(*C*H$_3$)$_2$), 16.7 (s, CH(*C*H$_3$)$_2$), 16.4 (s, CH(*C*H$_3$)$_2$), 16.2 (s, CH(*C*H$_3$)$_2$). $^{31}$P{$^{1}$H}: δ 64.5 (d, $^{2}J_{HRh}$ = 4.4 Hz, 2P). $^{29}$Si NMR: δ 21.8 (d, $^{1}J_{SiRh}$ = 31.2 Hz). Anal. Calcd. (%) for C$_{46}$H$_{64}$N$_3$P$_2$RhSi: C, 64.85; H, 7.57; N, 4.93. Found: C, 63.79; H, 7.77; N, 4.78.

**Synthesis of 4-SiPh$_3$:**

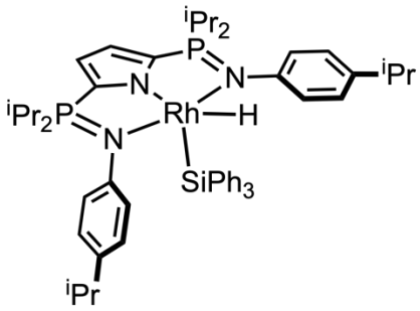


In an argon-filled glove box, a 20 mL scintillation vial equipped with a Teflon micro stir bar was charged with **2-COE** (0.069 g, 0.089 mmol), 4 mL of toluene and 1 equivalent of Ph$_3$SiH (0.023 g, 0.089 mmol). The reaction mixture was stirred for 18 hours at 60 °C. Volatiles were removed under reduced pressure to give a bright red powder. The product was recrystallized from pentane at –35 °C. Yield: 0.066 g (79%). $^{1}$H NMR (benzene-$d_6$): δ 7.72 (d, $J_{HH}$ = 6.6 Hz, 6H, C$_6$*H*$_5$), 7.28 (d, $J_{HH}$ = 8.2 Hz, 4H, 4-$^{i}$PrC$_6$*H*$_4$), 7.04 (ov m, 9H, C$_6$*H*$_5$), 6.75 (d, $J_{HH}$ = 8.2 Hz, 4H, 4-$^{i}$PrC$_6$*H*$_4$), 6.63 (d, $J_{HP}$ = 1.6 Hz, 2H, 3,4-pyrrole *H*), 2.72 (sp, $J_{HH}$ = 6.9 Hz, 2H, C*H*(CH$_3$)$_2$), 1.94–1.83 (ov m, 4H, C*H*(CH$_3$)$_2$), 1.23 (d, $J_{HH}$ = 6.9 Hz, 12H, CH(C*H*$_3$)$_2$), 0.95 (dd, $J_{HP}$ = 16.0 Hz, $J_{HH}$ = 7.0 Hz, 12H, CH(C*H*$_3$)$_2$), 0.89 (d, $J_{HH}$ = 7.0 Hz, 6H, CH(C*H*$_3$)$_2$), 0.56 (dd, $J_{HH}$ = 15.3 Hz, $J_{HH}$ = 7.0 Hz, 6H, CH(C*H*$_3$)$_2$), –13.5 (d, $J_{HRh}$ = 25.9 Hz, 1H, Rh–*H*). $^{13}$C{$^{1}$H} (benzene-$d_6$): δ 150.4 (s, aromatic *C*H), 143.9 (s, aromatic *C*H), 141.9 (s, aromatic *C*H), 137.5 (s, aromatic *C*H), 130.4 (dd, $J_{CP}$ = 140 Hz, $J_{CP}$ = 13.0 Hz, 2,5-pyrrole *C*), 128.9 (s, aromatic *C*H), 126.9 (s, aromatic *C*H), 126.8 (s,

aromatic *C*H), 125.9 (s, aromatic *C*H), 117.3 (dd, $J_{CP}$ = 24.2 Hz, $J_{CP}$ = 8.1 Hz, 3,4-pyrrole *C*H), 34.2 (s, *C*H($CH_3$)2), 28.8 (d, $J_{CP}$ = 54.9 Hz, *C*H($CH_3$)$_2$), 27.8 (d, $J_{CP}$ = 52.5 Hz, *C*H($CH_3$)$_2$), 25.0 (s, CH(*C*$H_3$)$_2$), 24.9 (s, CH(*C*$H_3$)$_2$), 17.4 (s, CH(*C*$H_3$)$_2$), 17.3 (s, CH(*C*$H_3$)$_2$), 16.4 (s, CH(*C*$H_3$)$_2$), 16.1 (s, CH(*C*$H_3$)$_2$). $^{31}P\{^1H\}$ NMR: δ 65.2 (d, $J_{PRh}$ = 4.2 Hz, 2P). $^{29}Si\{^1H\}$ NMR (benzene-$d_6$): δ 20.2 (d, $J_{SiRh}$ = 32.9 Hz), 20.1 (d, $J_{SiRh}$ = 32.9 Hz). Anal. Calcd. (%) for $C_{47}H_{62}N_3OP_2RhSi$: C, 67.30; H, 7.39; N, 4.53. Found: C, 67.38; H, 7.31; N, 4.58.

**Synthesis of 4-SiHPh:**

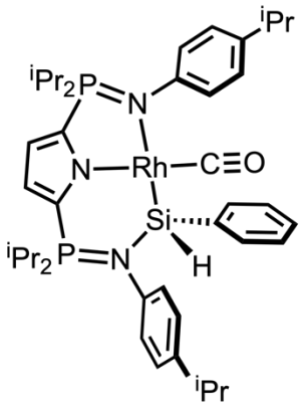


In an argon-filled glove box, a 50 mL high-pressure vessel equipped with a Teflon micro stir bar was charged with **3-CO** (0.151 g, 0.216 mmol) and dissolved in 8 mL of toluene. In a separate 5 mL vial, an excess of $Ph_3SiH$ (0.116 g, 1.07 mmol) was dissolved in 1 mL of toluene and combined with **3-CO**. The vessel was sealed with a Teflon tap and stirred for 2 hours at 363 K at which point the red-orange solution became bright yellow. Volatiles were removed under reduced pressure. The resulting yellow powder was recrystallized in pentane at –35 °C. Yield: 0.161 g (93%). $^1H$ NMR (benzene-$d_6$): δ 7.78 (d, $^3J_{HH}$ = 7.9 Hz, 2H, 4-$^i$PrC$_6$*H*$_4$), 7.58 (d, $^3J_{HH}$ = 7.9 Hz, 2H, 4-$^i$PrC$_6$*H*$_4$), 7.24–6.83 (ov m, 5H, Si–*C*$_6$H$_5$), 7.21 (d, $^3J_{HH}$ = 7.7 Hz, 2H, 4-$^i$PrC$_6$*H*$_4$), 7.12 (d, $^3J_{HH}$ = 7.7 Hz, 2H, 4-$^i$PrC$_6$*H*$_4$), 6.55 (dd, $^3J_{HP}$ = $^3J_{HH}$ = 3.6 Hz, 1H, pyrrole-*H*), 6.47 (dd, (dd, $^3J_{HP}$ = $^3J_{HH}$ = 3.6 Hz, 1H, pyrrole-*H*), 5.90 (dd, $^2J_{HRh}$ = 5.4 Hz, $^3J_{HP}$ = 5.8 Hz, 1H, Si–*H*), 2.78 (sp, $^3J_{HH}$ = 6.9 Hz, 1H, C*H*($CH_3$)$_2$), 2.62 (sp, $^3J_{HH}$ = 6.9 Hz, 1H, C*H*($CH_3$)$_2$), 2.31 (dsp, $^2J_{HP}$ = 11.7 Hz, $^3J_{HH}$ = 6.9 Hz, 1H, C*H*($CH_3$)$_2$), 2.24–2.11

(ov sp, 3H, C*H*($CH_3$)$_2$), 1.45 (dd, $^3J_{HP}$ = 16.1 Hz, $^3J_{HH}$ = 6.9 Hz, 3H, CH(C*H*$_3$)$_2$), 1.21–1.17 (ov m, 9H, C*H*($CH_3$)$_2$), 1.10–0.93 (ov m, 18H, CH(C*H*$_3$)$_2$), 0.58 (dd, $^2J_{HP}$ = 17.6 Hz, $^3J_{HH}$ = 6.9 Hz, 3H, CH(C*H*$_3$)$_2$), 0.38 (dd, $^2J_{HP}$ = 15.3 Hz, $^3J_{HH}$ = 7.3 Hz, 3H, CH(C*H*$_3$)$_2$). $^{13}$C (benzene-$d_6$): δ 194.6 (d, $^1J_{CRh}$ = 77.5 Hz, 1C, Rh–*C*O), 151.6 (s, aromatic *C*), 147.7 (s, aromatic C), 147.1 (d, $J_{CRh}$ = 2.3 Hz, aromatic *C*), 142.6 (s, aromatic *C*), 140.9 (d, $J_{CRh}$ = 2.1 Hz, aromatic *C*), 139.5 (d, $^1J_{CP}$ = 16.3 Hz, 2,5-pyrrole *C*), 137.6 (d, $^1J_{CP}$ = 15.5 Hz, 2,5-pyrrole *C*), 136.4 (s, aromatic *C*), 127.8 (s, aromatic *C*), 127.6 (s, aromatic *C*), 126.9 (s, aromatic *C*), 126.8 (s, aromatic *C*), 120.3 (dd, $^2J_{CRh}$ = 25.7 Hz, $^3J_{CRh}$ = 10.3 Hz, 3,4-pyrrole *C*H), 115. (dd, $^2J_{CRh}$ = 24.1 Hz, $^3J_{CRh}$ = 11.3 Hz, 3,4-pyrrole *C*H), 34.1 (d, *J* = 11.1 Hz, *C*H($CH_3$)$_2$), 18.1 (d, *J* = 3.4 Hz), 17.1 (d, *J* = 2.4 Hz), 17.0 (d, *J* = 2.0 Hz), 16.9 (s, *C*H($CH_3$)$_2$), 16.8 (d, *J* = 2.5 Hz), 16.6 (d, *J* = 2.3 Hz), 16.4 (*J* = 2.9 Hz), 15.5 (d, *J* = 3.1 Hz). $^{31}$P{$^1$H} NMR: δ 53.0 (s, 1P), 43.5 (s, 1P). $^{29}$Si NMR: δ 54.6 (ddd, $^1J_{SiRh}$ = 55 Hz, $^2J_{SiP}$ = 10 Hz, $^3J_{SiP}$ = 2.6 Hz, Rh–*Si*). Anal. Calcd. (%) for $C_{41}H_{58}N_3OP_2RhSi$: C, 61.41; H, 7.29; N, 5.24. Found: C, 62.01; H, 7.15; N, 5.52. IR $\nu_{CO}$ ($cm^{-1}$): 1962.

**Synthesis of 4-SiPh$_2$:**

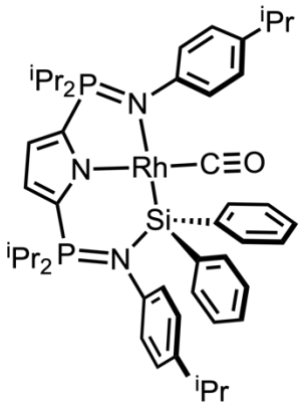

In an argon-filled glove box, a 25 mL high-pressure vessel equipped with Teflon micro stir bar was charged with **3-CO** (0.095 g, 0.138 mmol) and dissolved in 4 mL of toluene. In a separate 5 mL vial, an excess of $Ph_2SiH_2$ (0.150 g, 0.824 mmol) was dissolved in 1 mL of toluene and combined with **3-CO**. The vessel was sealed with a Teflon tap and stirred for 6 hours at 80 °C at which point the red-orange solution became bright yellow. Volatiles were removed under reduced pressure. The residue was triturated with cold pentane (3 × 5 mL) and recrystallized in pentane at –35 °C. Yield: 0.102 g (88%). $^1$H NMR (benzene-$d_6$): δ 7.89 (d, $^3J_{HH}$ = 6.7 Hz, 4H, 4-$^i$PrC$_6$*H*$_4$), 7.53 (d, $^3J_{HH}$ = 8.0 Hz, 3H, Si–C$_6$*H*$_5$), 7.14–7.10 (m, 6H, Si–C$_6$*H*$_5$), 6.64 (d, $^3J_{HH}$ = 8.1 Hz, 2H, 4-$^i$PrC$_6$*H*$_4$), 6.60 (d, $^3J_{HH}$ = 3.5 Hz, 1H, 3,4-pyrrole *H*), 6.52 (d, $^3J_{HH}$ = 8.1 Hz, 2H, 4-$^i$PrC$_6$*H*$_4$), 6.45 (d, *J* = 3.5 Hz, 1H, 1H, 3,4-pyrrole *H*), 2.77 (sp, $^3J_{HH}$ = 6.7 Hz, 1H, C*H*(CH$_3$)$_2$), 2.50 (sp, $^3J_{HH}$ = 6.7 Hz, 1H, CH(CH$_3$)$_2$), 2.26 (dsp, $^3J_{HH}$ = 7.3 Hz, 2H, CH(CH$_3$)$_2$), 2.14 (dsp, $^3J_{HH}$ = 7.1 Hz, 2H, CH(CH$_3$)$_2$), 1.19 (d, $^3J_{HH}$ = 6.7 Hz, 6H, CH(CH$_3$)$_2$), 1.02–0.92 (ov m, 24H, CH(CH$_3$)$_2$). $^{13}$C (benzene-$d_6$): δ 194.6 (d, $^1J_{CRh}$ = 76.9 Hz, 1C, Rh–*C*O), 151.5 (s, aromatic *C*H), 147.7 (s, aromatic *C*H), 147.1 (aromatic *C*H), 142.6 (s, aromatic *C*H), 141.0 (s, aromatic *C*H), 136.4 (s, aromatic *C*H). $^{31}$P{$^1$H} NMR: δ 53.1 (s, 1P), 43.1 (s, 1P). $^{29}$Si NMR: δ 51.4 (ddd, $^1J_{SiRh}$ = 60 Hz, $^2J_{SiP}$ = 11 Hz, $^3J_{SiP}$ coupling was not resolved). Anal. Calcd. (%) for $C_{47}H_{62}N_3OP_2RhSi$: C, 64.30; H, 7.12; N, 4.79. Found: C, 65.04; H, 7.16; N, 4.62. IR $\nu_{CO}$ (cm$^{-1}$): 1912.

### 7.4.2. Crystallographic Details

**Table 7.4.1.** Crystallographic details for complexes discussed in Chapter 4.

| | **4-SiH$_2$Ph** | **4-SiHPh$_2$** |
|---|---|---|
| CCDC Entry | 1901815 | 1901816 |
| Crystal Size (mm) | 0.41 × 0.23 × 0.19 | 0.31 × 0.28 × 0.23 |
| Moiety Formula | $C_{40}H_{59}N_3OP_2RhSi$ | $C_{46}H_{64}N_3P_2RhSi$ |
| Formula weight (g/mol) | 774.88 | 851.98 |
| λ (nm) | 1.54178 | 0.71073 |
| T (K) | 100(2) | 100(2) |
| Crystal System | Monoclinic | Monoclinic |
| Space group (*Z*) | P $2_1$/n (14) | P 2/c (13) |
| *a* (Å) | 11.7973(2) | 16.3088(6) |
| *b* (Å) | 29.6490(5) | 13.3859(6) |
| *c* (Å) | 12.8736(2) | 20.6448(9) |
| *α* (deg) | 90 | 90 |
| β (deg) | 100.662(2) | 91.889(4) |
| γ (deg) | 90 | 90 |
| Volume (Å$^3$) | 4425.16(13) | 4504.5(3) |
| Calc. $\rho$ (g cm$^{-3}$) | 1.163 | 1.256 |
| μ (mm$^{-1}$) | 4.265 | 0.510 |
| Reflections | 9662 | 9145 |
| Completeness (to 2$\theta$) | 0.996 | 0.991 |
| C–C Bond Precision (Å) | 0.0047 | 0.0041 |
| $R_1$, $wR_2$ [$I > 2\sigma(I)$] | 0.0359, 0.0956 | 0.0397, 0.0923 |
| GoF on F$^2$ | 1.031 | 1.031 |

$R_1 = \Sigma||F_o| - |F_c||/\Sigma|F_o|$. $wR_2 = [\Sigma[w(F_o^2 - F_c^2)^2]/\Sigma w(F_o^4)]^{1/2}$.

**Table 7.4.2.** Crystallographic details for complexes discussed in Chapter 4.

| | **4-SiHPh** | **4-SiPh$_2$** |
|---|---|---|

| | | |
|---|---|---|
| CCDC Entry | 1901814 | 1901817 |
| Crystal Size (mm) | 0.10 × 0.05 × 0.04 | 0.45 × 0.36 × 0.28 |
| Moiety Formula | $C_{41}H_{58}N_3OP_2RhSi$ | $C_{47}H_{62}N_3OP_2RhSi$ |
| Formula weight (g/mol) | 801.84 | 877.93 |
| λ (nm) | 1.54178 | 1.54184 |
| T (K) | 100(2) | 100(2) |
| Crystal System | Triclinic | Monoclinic |
| Space group (*Z*) | P–1 (2) | P $2_1$/n |
| *a* (Å) | 10.85145(14) | 11.7021(2) |
| *b* (Å) | 12.3015(2) | 20.8295(3) |
| *c* (Å) | 17.1913(2) | 18.8923(4) |
| *α* (deg) | 69.6255(15) | 90 |
| β (deg) | 71.8839(13) | 104.1354(17) |
| γ (deg) | 83.0832(13) | 90 |
| Volume ($Å^3$) | 2044.46(6) | 4465.54(15) |
| Calc. $\rho$ (g $cm^{-3}$) | 1.303 | 1.303 |
| μ ($mm^{-1}$) | 4.654 | 4.310 |
| Reflections | 8911 | 9228 |
| Completeness (to $2\theta$) | 0.988 | 0.939 |
| C–C Bond Precision (Å) | 0.0055 | 0.0056 |
| $R_1$, $wR_2$ [$I > 2\sigma(I)$] | 0.0392, 0.1014 | 0.0429, 0.1159 |
| GoF on $F^2$ | 1.113 | 1.112 |

$R_1 = \Sigma||F_o| - |F_c||/\Sigma|F_o|$. $wR_2 = [\Sigma[w(F_o^2 - F_c^2)^2]/\Sigma w(F_o^4)]^{1/2}$.

### 7.4.3. Computational Details Relevant to Chapter 4

**Sample Geometry Optimization and XYZ Coordinates and Details for 4 SiHPh and 4-$SiPh_2$**

**4-SiHPh**

Energy (SCF) = -2919.8338929 Ha
Zero-Point Energy = 0.879954 Ha
Lowest Frequency = 9 $cm^{-1}$
Coordinates:

| | | | |
|---|---|---|---|
| Rh | -0.80418100 | 0.30403700 | -0.53945100 |
| P | -3.06133800 | -1.80334200 | 0.55522400 |
| P | 2.40185300 | -1.84198400 | -0.16570100 |
| Si | 1.31114400 | 1.12507900 | -0.33625700 |
| H | 1.97286400 | 1.97886600 | -1.39473800 |
| O | -1.29269200 | 2.74626700 | -2.19751100 |
| N | -0.35790200 | -1.58192000 | 0.28611600 |
| N | 2.66630200 | -0.19585400 | -0.22821600 |
| N | -2.89975200 | -0.34497400 | -0.16485200 |
| C | 0.81545100 | -2.25107100 | 0.56576900 |
| C | -0.85299200 | -3.49666000 | 1.46051200 |
| H | -1.41333700 | -4.26420700 | 1.99439700 |
| C | 4.01081400 | 0.27770900 | -0.48219100 |
| C | -1.37023800 | -2.34485800 | 0.83001900 |
| C | 6.63697900 | 1.29383400 | -0.94831100 |
| C | 5.89856100 | 0.67951100 | -1.97855800 |
| H | 6.34052000 | 0.59724800 | -2.97889000 |
| C | -4.01964400 | 0.52096000 | -0.33281400 |
| C | -5.06400600 | 2.69960700 | 0.07413800 |
| H | -5.00664200 | 3.69768100 | 0.52622900 |
| C | 1.18400900 | 1.68412600 | 2.51954100 |
| H | 0.68700600 | 0.70837000 | 2.58959200 |
| C | -3.92138100 | -3.12732000 | -0.47123400 |
| H | -4.94901900 | -2.73379800 | -0.59561600 |
| C | -3.98964800 | 1.81531100 | 0.23800400 |
| H | -3.09471500 | 2.11272800 | 0.79472800 |
| C | 1.59931800 | 2.15639500 | 1.25051900 |
| C | -1.10554000 | 1.81003700 | -1.50258500 |
| C | 0.54403900 | -3.44257300 | 1.28910800 |
| H | 1.26453300 | -4.17488400 | 1.65268800 |
| C | 4.73210200 | 0.91486400 | 0.55128600 |
| H | 4.25839500 | 1.03595300 | 1.52932300 |
| C | 4.60205100 | 0.18947000 | -1.75969900 |
| H | 4.03308900 | -0.24120800 | -2.58939400 |
| C | 6.02198500 | 1.40975700 | 0.31703800 |
| H | 6.55605200 | 1.90017300 | 1.13910500 |
| C | 2.20176900 | 3.43485100 | 1.19323400 |
| H | 2.53303700 | 3.82930000 | 0.22480700 |
| C | -6.21515700 | 2.34242700 | -0.65756600 |
| C | 8.04250900 | 1.83228900 | -1.20258900 |
| H | 8.28501600 | 1.61739100 | -2.26171500 |

| | | | |
|---|---|---|---|
| C | 2.38446300 | 4.21047100 | 2.35157200 |
| H | 2.84768800 | 5.20135300 | 2.27953700 |
| C | -3.91556400 | -1.79830000 | 2.22427700 |
| H | -3.67968900 | -2.79668000 | 2.64538400 |
| C | -5.16308500 | 0.16830600 | -1.09078300 |
| H | -5.19493700 | -0.80190400 | -1.59724600 |
| C | 3.66361600 | -2.72312500 | 0.90061300 |
| H | 3.25144000 | -3.74929500 | 0.94819100 |
| C | 1.97730300 | 3.71453800 | 3.60025300 |
| H | 2.12037800 | 4.31577900 | 4.50513000 |
| C | -3.27640000 | -0.71995900 | 3.12052700 |
| H | -2.18270500 | -0.83911100 | 3.18364500 |
| H | -3.69285400 | -0.78929200 | 4.14079800 |
| H | -3.48662700 | 0.28831400 | 2.72925900 |
| C | 1.37710200 | 2.44543500 | 3.68273600 |
| H | 1.04852000 | 2.05705500 | 4.65391900 |
| C | 2.48663100 | -2.64097000 | -1.86281300 |
| H | 3.51565000 | -2.43320700 | -2.21568100 |
| C | -3.24877000 | -3.21406600 | -1.85431900 |
| H | -3.17313900 | -2.22468600 | -2.33355900 |
| H | -3.82734100 | -3.88319100 | -2.51511500 |
| H | -2.22803500 | -3.62382900 | -1.76358500 |
| C | 5.07672900 | -2.81431600 | 0.28736300 |
| H | 5.07312800 | -3.25712600 | -0.72200100 |
| H | 5.70068800 | -3.46017500 | 0.92978500 |
| H | 5.55954700 | -1.82752500 | 0.22829200 |
| C | 1.48249400 | -1.96760600 | -2.81770100 |
| H | 0.44516200 | -2.11068400 | -2.47384000 |
| H | 1.58438800 | -2.40637300 | -3.82613100 |
| H | 1.64182600 | -0.88010700 | -2.89068600 |
| C | 3.68736600 | -2.13646500 | 2.32577800 |
| H | 4.10093900 | -1.11646000 | 2.32270000 |
| H | 4.32956900 | -2.76289900 | 2.96905000 |
| H | 2.68098200 | -2.10020200 | 2.77105900 |
| C | 2.27790800 | -4.16612800 | -1.78699600 |
| H | 3.06030700 | -4.67424600 | -1.19844600 |
| H | 2.30197500 | -4.59097100 | -2.80562200 |
| H | 1.29907500 | -4.40911400 | -1.33992900 |
| C | -5.44676900 | -1.64024400 | 2.13394800 |
| H | -5.72305300 | -0.67284900 | 1.68520300 |
| H | -5.88128400 | -1.67981900 | 3.14858900 |
| H | -5.92098800 | -2.43917500 | 1.53971900 |
| C | -6.23708800 | 1.05836100 | -1.23895400 |
| H | -7.10174900 | 0.74548300 | -1.83686600 |
| C | 9.09677300 | 1.11693100 | -0.32834300 |
| H | 8.91534200 | 1.30115700 | 0.74518800 |

| | | | |
|---|---|---|---|
| H | 10.11169800 | 1.48284000 | -0.56253300 |
| H | 9.07871100 | 0.02588300 | -0.48928200 |
| C | -7.37375800 | 3.32103100 | -0.83215700 |
| H | -7.11957300 | 4.22868500 | -0.25029600 |
| C | -8.69683000 | 2.75935900 | -0.26568900 |
| H | -9.01168300 | 1.85416100 | -0.81466900 |
| H | -9.50977400 | 3.50162900 | -0.35436800 |
| H | -8.59398500 | 2.48691800 | 0.79826500 |
| C | -3.99791900 | -4.50389600 | 0.21587100 |
| H | -2.98949100 | -4.92386700 | 0.36913900 |
| H | -4.55554300 | -5.20905600 | -0.42579500 |
| H | -4.51240100 | -4.46753000 | 1.19075400 |
| C | 8.10995000 | 3.36396900 | -1.00997700 |
| H | 7.38377700 | 3.88154200 | -1.65839700 |
| H | 9.11894200 | 3.74283300 | -1.24921000 |
| H | 7.88619200 | 3.64468000 | 0.03429600 |
| C | -7.54301400 | 3.74799900 | -2.30802800 |
| H | -6.61267600 | 4.18702900 | -2.70484200 |
| H | -8.35087300 | 4.49400900 | -2.41260700 |
| H | -7.80166300 | 2.88268500 | -2.94372900 |

**4-SiPh$_2$**

Energy (SCF) = -3150.8847437 Ha
Zero-Point Energy = 0.960342 Ha
Lowest Frequency = 3 cm$^{-1}$
Coordinates:

| | | | |
|---|---|---|---|
| Rh | 1.00899000 | -0.17275500 | -0.36389800 |
| P | 3.37067200 | 2.03743900 | 0.17365800 |
| P | -2.12857800 | 2.12843900 | -0.22317300 |
| Si | -1.13976700 | -0.88740200 | -0.00972300 |
| O | 1.58532200 | -2.92617000 | -1.38303900 |
| N | 0.64763300 | 1.85359500 | 0.09903600 |
| N | -2.44549000 | 0.50553800 | 0.04127400 |
| N | 3.14408500 | 0.45137600 | -0.14748100 |
| C | -0.48847200 | 2.60399000 | 0.31887700 |
| C | 1.26155300 | 3.93637500 | 0.86148500 |
| H | 1.87376700 | 4.77003200 | 1.20572200 |
| C | -3.84208800 | 0.11071300 | -0.00525600 |
| C | 1.70927400 | 2.67030300 | 0.42912700 |
| C | -6.58234400 | -0.69207700 | -0.04923900 |
| C | -5.91006700 | -0.32412100 | -1.23081100 |
| H | -6.44763700 | -0.35617700 | -2.18601200 |
| C | 4.22733000 | -0.47185400 | -0.11413000 |

| | | | |
|---|---|---|---|
| C | 5.17185600 | -2.55760800 | 0.75898700 |
| H | 5.06409200 | -3.43680300 | 1.40637900 |
| C | -1.43822900 | -0.80974300 | 2.89411800 |
| H | -1.53943700 | 0.27462500 | 2.76216700 |
| C | 4.14801400 | 3.05030600 | -1.21138600 |
| H | 5.17687800 | 2.64827500 | -1.28915600 |
| C | 4.13394800 | -1.61825400 | 0.71043700 |
| H | 3.22094700 | -1.75557900 | 1.29931600 |
| C | -1.30778900 | -1.63468700 | 1.75034700 |
| C | 1.33328300 | -1.85569900 | -0.95383500 |
| C | -0.14392800 | 3.89929700 | 0.78856400 |
| H | -0.82204900 | 4.70993000 | 1.05378200 |
| C | -4.49761400 | -0.28565700 | 1.18094200 |
| H | -3.93334700 | -0.30473300 | 2.11755900 |
| C | -4.55988100 | 0.05659100 | -1.21769000 |
| H | -4.04813400 | 0.27942700 | -2.15818500 |
| C | -5.84325000 | -0.67762500 | 1.15319600 |
| H | -6.32432300 | -0.97888900 | 2.09100000 |
| C | -1.14709300 | -3.02417700 | 1.97169700 |
| H | -1.02704200 | -3.69786700 | 1.11516800 |
| C | 6.34948400 | -2.40440300 | -0.00115000 |
| C | -8.04945500 | -1.11321600 | -0.07916200 |
| H | -8.38603600 | -1.03547500 | -1.13137000 |
| C | -1.13489500 | -3.56489000 | 3.26866900 |
| H | -1.01179600 | -4.64525000 | 3.40666500 |
| C | 4.34001300 | 2.42541900 | 1.73111900 |
| H | 4.09427500 | 3.48808100 | 1.93245900 |
| C | 5.39965700 | -0.32624300 | -0.89632300 |
| H | 5.48507700 | 0.51920200 | -1.58706700 |
| C | -3.28139500 | 3.24824300 | 0.74196900 |
| H | -2.81713700 | 4.23842900 | 0.57180200 |
| C | -1.28154100 | -2.72617200 | 4.38517300 |
| H | -1.27375600 | -3.14596800 | 5.39713800 |
| C | 3.79681800 | 1.56396000 | 2.88816000 |
| H | 2.70434900 | 1.66365900 | 2.99240400 |
| H | 4.26699100 | 1.87710400 | 3.83685400 |
| H | 4.02628300 | 0.49903200 | 2.72282000 |
| C | -1.43162800 | -1.34208000 | 4.19334600 |
| H | -1.53806500 | -0.67682200 | 5.05838200 |
| C | -2.32054000 | 2.62261700 | -2.02509500 |
| H | -3.38206700 | 2.40918000 | -2.25576500 |
| C | 3.39801300 | 2.76551400 | -2.52651500 |
| H | 3.31220900 | 1.68440300 | -2.72154300 |
| H | 3.92648900 | 3.23786000 | -3.37311300 |
| H | 2.37658500 | 3.18115400 | -2.48744800 |
| C | -4.72899100 | 3.31962500 | 0.21387700 |

| | | | |
|---|---|---|---|
| H | -4.77712700 | 3.54786700 | -0.86324000 |
| H | -5.25920700 | 4.12841400 | 0.74703900 |
| H | -5.27569900 | 2.38169700 | 0.39146000 |
| C | -1.42626200 | 1.74422500 | -2.91976600 |
| H | -0.36194700 | 1.83921500 | -2.64539300 |
| H | -1.54861100 | 2.05173300 | -3.97354700 |
| H | -1.68621800 | 0.67689700 | -2.83927900 |
| C | -3.23260400 | 2.94197000 | 2.25129700 |
| H | -3.70692300 | 1.97281900 | 2.47021100 |
| H | -3.78775700 | 3.72235800 | 2.80053300 |
| H | -2.19953900 | 2.92149100 | 2.63241200 |
| C | -2.05289700 | 4.12574300 | -2.23945100 |
| H | -2.76199000 | 4.76829800 | -1.69092100 |
| H | -2.15474000 | 4.36438000 | -3.31250900 |
| H | -1.03068600 | 4.39647900 | -1.92651100 |
| C | 5.86777500 | 2.28889400 | 1.57260100 |
| H | 6.15390000 | 1.25673000 | 1.31569400 |
| H | 6.35992600 | 2.55171900 | 2.52574300 |
| H | 6.27308800 | 2.95887200 | 0.79581300 |
| C | 6.43743100 | -1.26794400 | -0.83051400 |
| H | 7.32607500 | -1.11759900 | -1.45567500 |
| C | -8.93393500 | -0.16866200 | 0.76529400 |
| H | -8.65001700 | -0.20437600 | 1.83190300 |
| H | -9.99628900 | -0.46014600 | 0.69328300 |
| H | -8.84089600 | 0.87741100 | 0.42807500 |
| C | 7.46918000 | -3.44026800 | 0.06190200 |
| H | 7.14714500 | -4.21876900 | 0.78105400 |
| C | 8.78712800 | -2.83269700 | 0.59260800 |
| H | 9.16461300 | -2.04777900 | -0.08679200 |
| H | 9.57189900 | -3.60522100 | 0.67756100 |
| H | 8.64547800 | -2.37497900 | 1.58619200 |
| C | 4.22470100 | 4.55894400 | -0.91017700 |
| H | 3.21405600 | 4.98959900 | -0.80878600 |
| H | 4.72677600 | 5.08071500 | -1.74416900 |
| H | 4.79152900 | 4.78376300 | 0.00912000 |
| C | -8.23096800 | -2.58288700 | 0.36195500 |
| H | -7.62722900 | -3.26445000 | -0.25961200 |
| H | -9.28925600 | -2.88677300 | 0.28056400 |
| H | -7.92249900 | -2.72483600 | 1.41260900 |
| C | 7.68981000 | -4.13064400 | -1.30281200 |
| H | 6.75903800 | -4.59413200 | -1.66961200 |
| H | 8.46243000 | -4.91635700 | -1.22681800 |
| H | 8.02502100 | -3.40502700 | -2.06505600 |
| C | -1.96939200 | -2.12954000 | -1.21718200 |
| C | -3.01341800 | -3.00772000 | -0.83779000 |
| C | -1.53646100 | -2.18117000 | -2.56447400 |

| | | | |
|---|---|---|---|
| C | -3.59618200 | -3.89464700 | -1.75759100 |
| H | -3.37538400 | -3.00117000 | 0.19631700 |
| C | -2.12109600 | -3.05743500 | -3.49365300 |
| H | -0.70640000 | -1.53594800 | -2.87811500 |
| C | -3.15356500 | -3.91927800 | -3.09031500 |
| H | -4.39646400 | -4.56974200 | -1.43314000 |
| H | -1.75908100 | -3.07955100 | -4.52790100 |
| H | -3.60524300 | -4.61319200 | -3.80827000 |

## 7.5. Experimental Procedures Pertaining to Chapter 5

### 7.5.1. Synthetic Procedures

**Synthesis of $(OMe)_2BMes$.** Adapting from a literature procedure,[18] an oven-dried 250 mL 3-neck round-bottomed flask was charged with a stir bar, 2.803 g of magnesium turnings, and a small crystal of iodine ($I_2$). The flask was evacuated on a double-manifold vacuum line and cooled to –78 ºC. Approximately 15 mL of THF was transferred under reduced pressure onto the magnesium turnings. A separate flask was charged with 18.2 g (91.3 mmol) of mesityl bromide which was degassed by three freeze–pump–thaw cycles. THF (70 mL) was added under reduced pressure. The THF solution was transferred *via* cannula into a 100 mL dropping funnel attached to the 250 mL flask containing the magnesium turnings. The mesityl bromide solution was added dropwise over 45 minutes, resulting in gentle bubbling and warming of the mixture. The dropping funnel was removed, and the reaction mixture was heated to reflux for 18 hours, at which point the solution was grey and opaque. The Grignard reagent was transferred *via* syringe to a 250 mL 2-neck round-bottomed flask containing 3.1 equivalents (283 mmol, 0.035 L) of $B(OMe)_3$ dissolved in 15 mL of cold (–15 ºC) diethylether. The reaction mixture became cloudy with a dense white precipitate that formed after several minutes. The mixture was warmed to ambient temperature, stirred for 20 hours and then diluted with 150 mL of pentane. The supernatant

was transferred *via* cannula into a 500 mL Teflon-sealed thick-walled flask. Volatiles were removed under reduced pressure to afford dimethoxymesitylborane as a colourless oil (10.5 g, 60% yield). NMR data ($^{1}$H, $^{11}$B) agreed well with literature data.[18]

**Synthesis $H_2BMes$.** A 100 mL round-bottomed flask was charged with a stir bar and 2.00 g (0.010 mol) of freshly distilled $(OMe)_2BMes$ dissolved in 60 mL of a 5:1 mixture of diethylether and pentane. The mixture was then cooled to 0 ºC. In a separate 50 mL round-bottomed flask 1.05 equivalents of $LiAlH_4$ (0.415 g) was suspended in diethylether (20 mL). The $LiAlH_4$ slurry was added dropwise to the cold (0 ºC) stirring $(OMe)_2BMes$ solution over 2 minutes. The mixture was allowed to gradually warm to ambient temperature whereupon it was stirred for 3 hours. The product was filtered through a pad of Celite and washed with a 1:1 mixture of pentane and diethylether (3 × 5 mL). Volatiles were removed under reduced pressure to afford $Li[H_3BMes]$ as a white solid (0.408 g, 28% yield). NMR data ($^{1}$H, $^{11}$B) agreed well with literature data.[18] One equivalent of $Me_3SiCl$ (0.232 g, 0.002 mol) was added to a diethylether solution of $Li[H_3BMes]$ (0.302 g, 0.002 mol) at ambient temperature. The reaction mixture was rapidly stirred for 3 hours during which a white precipitate formed. The solvent was removed under vacuum and the residue extracted with pentane (3 × 5 mL) to yield $H_2BMes$ as a crystalline white solid (0.358 g, 95% yield from $Li[H_3BMes]$). NMR data ($^{1}$H, $^{11}$B) agreed well with literature data.[18] Note: It is not necessary to isolate $Li[H_3BMes]$. It can be generated and used *in situ*.

**Synthesis of $H_2BAr^F$.** Following a literature procedure,[18] 150 mL Teflon-sealed thick-walled flask was charged with 3,5-bis(trifluoromethyl)bromobenzene (1.07 g, 3.62 mmol)

and 20 mL of diethylether. The solution was degassed by three freeze–pump–thaw cycles and cooled to –78 ºC. Under an atmosphere of argon, 1.45 mL (1 equivalent, 3.62 mmol) of *n*-butyl lithium (2.5 M in hexanes) was added dropwise *via* syringe over 10 minutes. The solution turned from colourless to yellow during 15 minutes of stirring. The mixture was quenched with 0.343 mL of $BH_3$•$SMe_2$ (1 equivalent, 3.62 mmol), added over 30 seconds *via* syringe. The reaction mixture was warmed to 23 ºC, becoming a pale-yellow colour. After 1 hour at 23 ºC, $Me_3SiCl$ (0.46 mL, 1 equivalent, 3.6 mmol) was added *via* syringe over 10 seconds, yielding $H_2BAr^F$ as a pale-orange solution. Since the product decomposes upon removal of the solvent, $H_2BAr^F$ was used as a diethylether solution of known concentration (e.g. 0.287 mol $L^{-1}$). $^1$H NMR (300.13 MHz, benzene-$d_6$): δ 8.01 (s, 2H, *m*-Ar *H*), 7.83 (s, 1H, *o*-Ar *H*), 2.85 (br s, 2H, B$H_2$). $^{11}$B NMR (96.29 MHz, benzene-$d_6$): δ –9.6 (br s). $^{19}$F NMR (282.23 MHz, benzene-$d_6$): δ –62.3 (s, 6F). NMR data ($^1$H, $^{11}$B, $^{19}$F) agreed well with literature data.[18]

**Synthesis of 5-BMes:**

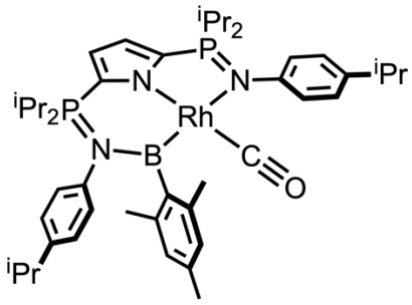


A 20 mL scintillation vial was charged with **3-CO** (0.045 g, 0.065 mmol), 1 equivalent of mesitylborane (9.1 mg, 0.066 mmol), and a Teflon-coated stir bar. The solids were dissolved in a mixture of pentane and toluene (5 mL, 5:1) giving a red-orange solution and the vial was placed in a cold well cooled with liquid nitrogen. The reaction mixture was rapidly stirred at low temperature for 1 h in the glove box with periodic sparging of the solution. The reaction solution became light-orange and was allowed to stand in the cold well for 18 h

producing a dark yellow crystalline solid. The solid was washed with cold pentane (3 × 5 mL) to yield 0.028 g (53% yield) of **5-BMes** as a bright yellow powder. $^{1}$H NMR (700.13 MHz, benzene-$d_6$): δ 7.51 (d, $^{3}J_{HH}$ = 7.7 Hz, 2H, 4-$^{i}$Pr-C$_6H_4$), 7.06 (d, $^{3}J_{HH}$ = 7.9 Hz, 2H, 4-$^{i}$Pr-C$_6H_4$), 6.93 (d, $^{3}J_{HH}$ = 7.7 Hz, 2H, 4-$^{i}$Pr-C$_6H_4$), 6.67 (d, $^{3}J_{HH}$ = 7.9 Hz, 2H, 4-$^{i}$Pr-C$_6H_4$), 6.66 (app t, $^{3}J_{HP}$ = $^{3}J_{HH}$ = 3.9 Hz, 1H, 3,4-pyrrole), 6.61 (s, 2H, Mes Ar *H*), 6.51 (dd, $^{3}J_{HP}$ = $^{3}J_{HH}$ = 3.9 Hz, 1H, 3,4-pyrrole), 3.26 (sp, $^{3}J_{HH}$ = 7.2 Hz, 2H, PC*H*(CH$_3$)$_2$), 2.73 (sp, $^{3}J_{HH}$ = 6.9 Hz, 1H, C*H*(CH$_3$)$_2$), 2.72 (s, 6H, Mes C*H*$_3$), 2.43 (sp, $^{3}J_{HH}$ = 6.9 Hz, 1H, C*H*(CH$_3$)$_2$), 2.19 (ov m, 2H, PC*H*(CH$_3$)$_2$), 2.09 (s, 3H, Mes C*H*$_3$), 1.16 (d, $^{3}J_{HH}$ = 6.9 Hz, 6H, CH(C*H*$_3$)$_2$), 1.11 (dd, $^{3}J_{HP}$ = 15.4 Hz, $J_{HH}$ = 7.2 Hz, 6H, PCH(C*H*$_3$)$_2$), 1.04 (dd, $^{3}J_{HP}$ = 15.7 Hz, $J_{HH}$ = 7.2 Hz, 6H, PCH(C*H*$_3$)$_2$), 0.97 (dd, $^{3}J_{HP}$ = 16.7 Hz, $J_{HH}$ = 7.2 Hz, 6H, PCH(C*H*$_3$)$_2$), 0.92 (d, $^{3}J_{HH}$ = 6.9 Hz, 6H, CH(C*H*$_3$)$_2$), 0.85 (dd, $^{3}J_{HP}$ = 16.2 Hz, $J_{HH}$ = 7.2 Hz, 6H, PCH(C*H*$_3$)$_2$). $^{11}$B NMR (224.63 MHz, benzene-$d_6$): δ 32.6 (br s, 1B). $^{13}$C{$^{1}$H} NMR (75.46 MHz, benzene-$d_6$): δ 196.6 (d, $^{1}J_{CRh}$ = 87.6 Hz, Rh–*C*O), 152.6 (br s, *ipso*-Mes *C*) 151.3 (s, *para*-Pipp *C*), 147.1 (s, *para*-Pipp *C*), 140.2 (d, $^{2}J_{CRh}$ = 2.4 Hz, *ipso*-Pipp *C*), 140.1 (m, $^{2}J_{CRh}$ = 3.4 Hz, *ipso*-Pipp *C*), 137.7 (dd, $^{1}J_{CP}$ = 145 Hz, $^{3}J_{CP}$ = 16.1 Hz, 2,5-pyrrole *C*), 133.6 (s, *ipso*-Mes *C*), 133.2 (s, *ipso*-Mes *C*), 129.1 (s, Ar *C*H), 127.1 (s, Ar *C*H), 126.6 (m, $^{3}J_{CRh}$ = 8.9 Hz, Pipp *C*H), 126.5 (s, Ar *C*H), 125.9 (s, Ar *C*H), 120.7 (ddd, $^{1}J_{CP}$ = 129 Hz, $^{3}J_{CP}$ = 13.5 Hz, $^{3}J_{CRh}$ = 3.4 Hz, 2,5-pyrrole *C*), 118.2 (dd, $^{2}J_{CP}$ = 24.6 Hz, $^{3}J_{CP}$ = 10.9 Hz, 3,4-pyrrole *C*H), 115.1 (dd, $^{2}J_{CP}$ = 24.8 Hz, $^{3}J_{CP}$ = 9.9 Hz, 3,4-pyrrole *C*H), 33.7 (s, *C*H(CH$_3$)$_2$), 33.6 (s, *C*H(CH$_3$)$_2$), 27.3 (s, CH(*C*H$_3$)$_2$), 26.6 (s, *C*H(CH$_3$)$_2$), 26.5 (s, *C*H(CH$_3$)$_2$), 24.1 (d, $^{1}J_{CP}$ = 54.9 Hz, P*C*H(CH$_3$)$_2$), 23.9 (s, 2,6-*C*H$_3$ Mes), 21.3 (s, 4-*C*H$_3$ Mes), 16.7 (m, CH(*C*H$_3$)$_2$), 16.6 (m, CH(*C*H$_3$)$_2$), 16.5 (m, CH(*C*H$_3$)$_2$), 16.4 (m, CH(*C*H$_3$)$_2$). $^{31}$P{$^{1}$H} NMR (283.42 MHz, benzene-$d_6$): δ 52.6 (d, $^{2}J_{PRh}$ = 7.3 Hz, 1P, *P*–N–Rh), 37.8 (s,

1P, *P*–N–B). Anal. Calcd. for $C_{44}H_{63}BN_3OP_2Rh$: C, 64.01; H, 7.69; N, 5.09. Found: C, 63.83; H, 7.96; N, 4.65. IR $\nu_{CO}$ ($cm^{-1}$): 1909.

**Synthesis of 5-CO•$H_2BAr^F$:**

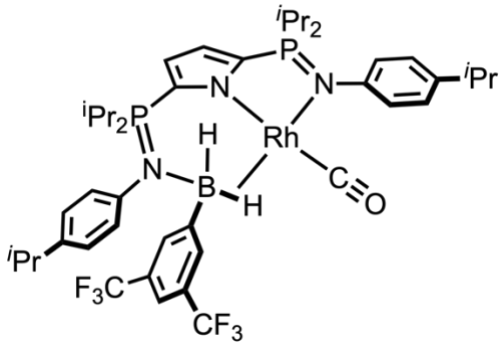


In a 20 mL scintillation vial, crystalline **3-CO** (0.025 g, 35.9 mmol) was dissolved in 5 mL of $Et_2O$ and chilled to –30 ºC. A solution of $H_2B(3,5\text{-}(CF_3)_2C_6H_3)$ in $Et_2O$ (0.125 mL, 37 mmol) was added *via* syringe over 10 seconds. The solution was stirred at –30 ºC for 2 hours becoming dark yellow in colour. The compound was dried under vacuum and washed with pentane (2 × 3 mL) giving 0.028 g of **5-CO•$H_2BAr^F$** as a bright yellow powder (84% yield). $^1$H NMR (700.13 MHz, benzene-$d_6$): δ 8.04 (s, 2H, *o*-$Ar^F$ *H*), 7.68 (s, 1H, *p*-$Ar^F$ *H*), 7.29 (d, $^3J_{HH}$ = 7.9 Hz, 2H, 4-$^i$Pr-$C_6H_4$), 7.21 (d, $^3J_{HH}$ = 7.9 Hz, 2H, 4-$^i$Pr-$C_6H_4$), 7.05 (d, $^3J_{HH}$ = 8.2 Hz, 2H, 4-$^i$Pr-$C_6H_4$), 6.83 (d, $^3J_{HH}$ = 8.2 Hz, 2H, 4-$^i$Pr-$C_6H_4$), 6.47 (app t, $^3J_{HP} = {}^3J_{HH}$ = 3.3 Hz, 1H, 3,4-pyrrole), 6.39 (ov dd, $^3J_{HP} = {}^3J_{HH}$ = 3.3 Hz, 1H, 3,4-pyrrole), 2.70 (sp, $^3J_{HH}$ = 6.9 Hz, 1H, C*H*$(CH_3)_2$), 2.60 (sp, $^3J_{HH}$ = 6.9 Hz, 1H, C*H*$(CH_3)_2$), 2.23 (m, 2H, PC*H*$(CH_3)_2$), 2.03 (m, 2H, PC*H*$(CH_3)_2$), 1.13 (d, $^3J_{HH}$ = 6.9 Hz, 6H, CH(C*H*$_3)_2$), 1.06 (d, $^3J_{HH}$ = 6.9 Hz, 6H, CH(C*H*$_3)_2$), 0.99 (dd, $^2J_{HP}$ = 15.5 Hz, $^3J_{HH}$ = 7.1 Hz, 6H, PCH(C*H*$_3)_2$), 0.90 (ov m, 12H, PCH(C*H*$_3)_2$), 0.84 (dd, $^2J_{HP}$ = 15.5 Hz, $^3J_{HH}$ = 7.1 Hz, 6H, PCH(C*H*$_3)_2$), –3.10 (br s, 2H, B*H*). $^{11}$B NMR (224.63 MHz, benzene-$d_6$): δ –5.9 (s, 1B). $^{13}$C{$^1$H} NMR (176 MHz, benzene-$d_6$): δ 190.6 (d, $^1J_{CRh}$ = 75.7 Hz, Rh–*C*O), 151.0 (s, Ar *C*), 146.9 (s, Ar *C*), 143.4 (s, Ar *C*), 142.9 (s, Ar *C*), 134.6 (br m, 2,5-pyrrole *C*), 129.9 (d, $^3J_{CF}$ = 4.0 Hz, Ar *C*H), 129.6 (d, $^2J_{CF}$ = 31.7 Hz, Ar *C*),

127.7 (s, Ar *C*H), 127.5 (s, Ar *C*H), 127.2 (s, Ar *C*H), 127.1 (d, $^{3}J_{CF}$ = 7.0 Hz, Ar *C*H), 126.6 (s, Ar *C*H), 124.6 (m, 2,5-pyrrole *C*), 118.4 (dd, $^{2}J_{CP}$ = 23.0 Hz, $^{3}J_{CP}$ = 10.4 Hz, 3,4-pyrrole *C*H), 115.2 (dd, $^{2}J_{CP}$ = 24.6 Hz, $^{3}J_{CP}$ = 11.2 Hz, 3,4-pyrrole *C*H), 33.9 (s, *C*H(CH$_3$)$_2$), 33.7 (s, *C*H(CH$_3$)$_2$), 26.8 (d, $^{1}J_{CP}$ = 52.8 Hz, P*C*H(CH$_3$)$_2$), 26.3 (d, $^{1}J_{CP}$ = 62.0 Hz, P*C*H(CH$_3$)$_2$), 24.3 (s, CH(*C*H$_3$)$_2$), 24.1 (s, CH(*C*H$_3$)$_2$), 17.0 (d, $^{2}J_{CP}$ = 2.7 Hz, PCH(*C*H$_3$)$_2$), 16.4 (d, $^{2}J_{CP}$ = 2.4 Hz, PCH(*C*H$_3$)$_2$), 16.2 (d, $^{2}J_{CP}$ = 2.7 Hz, PCH(*C*H$_3$)$_2$), 16.1 (d, $^{2}J_{CP}$ = 1.9 Hz, PCH(*C*H$_3$)$_2$), *ipso*-Ar$^{F}$ *C* and *C*F$_3$ signals could not be located. $^{19}$F{$^{1}$H} NMR (282 MHz, benzene-$d_6$): δ –62.1 (s, 6F, C*F*$_3$). $^{31}$P{$^{1}$H} NMR (283.42 MHz, benzene-$d_6$): δ 51.3 (s, 1P, *P*–N–Rh), 48.8 (s, 1P, *P*–N–B). Anal. Calcd. for C$_{44}$H$_{60}$BF$_6$N$_3$OP$_2$Rh: C, 56.04; H, 6.23; N, 4.56. Found: C, 56.16; H, 6.16; N, 4.33. IR $\nu_{CO}$ (cm$^{-1}$): 1950.

**Synthesis of 5-H$_2$BAr$^{F}$:**

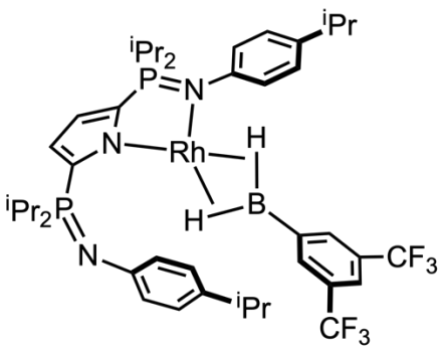


In a 20 mL scintillation vial, **5-CO·H$_2$BArF** (0.020 g, 0.022 mmol) was dissolved in 4 mL of toluene and stirred at 23 ºC for 48 h. The solvent was removed under vacuum and the product was extracted with 2 x 3 mL of pentane. The resulting solution was filtered through Celite and dried under reduced pressure to afford 0.010 g (51% yield) of **5-H$_2$BAr$^{F}$** as a dark brown solid. $^{1}$H NMR (700.13 MHz, benzene-$d_6$): δ 7.79 (s, 2H, *o*-Ar$^{F}$ *H*), 7.68 (s, 1H, *p*-Ar$^{F}$ *H*), 7.33 (br m, 1H, 3,4-pyrrole C*H*), 7.13 (obsc m, 4H, 4-$^{i}$Pr-C$_6$*H*$_4$), 6.89 (ov m, 4H, 4-$^{i}$Pr-C$_6$*H*$_4$), 6.32 (br m, 1H, 3,4-pyrrole C*H*), 4.69 (br s, 2H, B*H*$_2$), 2.83 (m, 1H, C*H*(CH$_3$)$_2$), 2.59 (m, 1H, C*H*(CH$_3$)$_2$), 2.37 (m, 1H, PC*H*(CH$_3$)$_2$), 1.81 (m, 1H, P*CH*(CH$_3$)$_2$), 1.72 (m, 1H, PC*H*(CH$_3$)$_2$), 1.55 (br m, 1H, PC*H*(CH$_3$)$_2$), 1.40-0.40 (ov m,

36H, CH(C$H_3$)$_2$). $^{11}$B NMR (224.63 MHz, benzene-$d_6$): δ 1.7 (br s, 1B). $^{13}$C{$^1$H} NMR (176 MHz, benzene-$d_6$, 23 ºC): δ 162.0 (s, Ar *C*), 145.1 (s, Ar *C*), 143.5 (s, Ar *C*), 142.4 (s, Ar *C*), 133.7 (br m, 2,5-pyrrole *C*), 130.0 (s, Ar *C*), 129.4 (s, Ar *C*H) 127.7 (s, Ar *C*H), 127.5 (s, Ar *C*H), 126.7 (br m, Ar *C*H), 125.7 (br m, Ar *C*H), 124.7 (br m, 2,5-pyrrole *C*), 124.3 (s, Ar *C*H), 123.3 (dd, $^2J_{CP}$ = 44.9 Hz, $^3J_{CP}$ = 14.3 Hz, 3,4-pyrrole *C*H), 117.7 (dd, $^2J_{CP}$ = 36.1 Hz, $^3J_{CP}$ = 14.1 Hz, 3,4-pyrrole *C*H), 33.9 (s, CH(CH$_3$)$_2$), 33.7 (s, CH(CH$_3$)$_2$), 27.2 (d, $^1J_{CP}$ = 53.6 Hz, PCH(CH$_3$)$_2$), 24.8 (br m, PCH(CH$_3$)$_2$), 24.1 (s, CH(CH$_3$)$_2$), 24.0 (s, CH(CH$_3$)$_2$), 16.4 (br s, PCH(CH$_3$)$_2$), 16.3 (br s, PCH(CH$_3$)$_2$), 15.9 (m, PCH(CH$_3$)$_2$), 15.3 (m, PCH(CH$_3$)$_2$), *ipso*-Ar$^F$ and CF$_3$ signals could not be located. $^{19}$F{$^1$H} NMR (282.40 MHz, benzene-$d_6$): δ –62.3 (s, 6F, C*F*$_3$). $^{31}$P{$^1$H} NMR (283.42 MHz, benzene-$d_6$): δ 51.7 (br s, 1P, *P*–N–Rh), 11.4 (br s, 1P, *P*–N). Anal. Calcd. for C$_{42}$H$_{57}$BF$_6$N$_3$P$_2$Rh: C, 56.45; H, 6.43; N, 4.70. Found: C, 55.88; H, 6.21; N, 4.41. IR $\nu_{CO}$ (cm$^{-1}$): not observed.

### 7.5.2. Crystallographic Details

**5-BMes.** The unit cell contained two unique molecules oriented in a head-to-tail arrangement. A short contact (2.193 Å) was located between the carbonyl oxygen atom of one molecule and the pyrrole C–H atom of another.

**Table 7.5.1.** Crystallographic details for complexes discussed in Chapter 5.

| | **5-BMes** | **5-CO•$H_2$B$Ar^F$** |
|---|---|---|
| CCDC Entry | 1985379 | 1985378 |
| Crystal Size (mm) | 0.20 × 0.10 × 0.05 | 0.25 × 0.25 × 0.25 |
| Moiety Formula | $C_{44}H_{63}BN_3OP_2Rh$ | $C_{43}H_{57}BF_6N_3OP_2Rh$ |
| Formula weight (g/mol) | 825.63 | 999.68 |
| λ (nm) | 1.54178 | 0.71073 |
| T (K) | 100(2) | 100(2) |
| Crystal System | Triclinic | Monoclinic |
| Space group (*Z*) | P–1 (4) | *I*2/*a* (8) |
| *a* (Å) | 14.5167(3) | 28.3648(5) |
| *b* (Å) | 18.5067(4) | 12.2130(1) |
| *c* (Å) | 19.7008(6) | 32.5843(5) |
| *α* (deg) | 65.627(2) | 90 |
| β (deg) | 88.777(2) | 111.394(2) |
| γ (deg) | 77.349(2) | 90 |
| Volume ($Å^3$) | 4689.8(2) | 10510.0(3) |
| Calc. $\rho$ (g $cm^{-3}$) | 1.169 | 1.264 |
| μ ($mm^{-1}$) | 3.831 | 0.443 |
| Reflections | 18596 | 11658 |
| Completeness (to 2$\theta$) | 0.960 | 0.995 |
| C–C Bond Precision (Å) | 0.0093 | 0.0025 |
| $R_1$, $wR_2$ [$I > 2\sigma(I)$] | 0.0759, 0.2131 | 0.0261, 0.0657 |
| GoF on $F^2$ | 1.080 | 1.035 |

$R_1 = \Sigma||F_o| - |F_c||/\Sigma|F_o|$. $wR_2 = [\Sigma[w(F_o^2 - F_c^2)^2]/\Sigma w(F_o^4)]^{1/2}$.

### 7.5.3. Computational Methods

**Sample Geometry Optimization and NBO Calculation Input File**

# B3LYP genecp guess=read pop=(full, nbo, savenbos) gfinput

5-BMes

0 1

| | | | |
|---|---|---|---|
| Rh | 0.79177806 | 0.14736201 | -0.11382101 |
| P | -2.00976614 | -2.17552716 | -0.60185805 |
| P | 3.23365523 | -1.84708013 | 0.82912706 |
| O | 1.25883109 | 3.05659622 | -0.58938804 |
| N | -2.29621916 | -0.53269104 | -0.23770302 |
| N | 0.59328604 | -1.90410414 | 0.21987502 |
| N | 3.00672121 | -0.42268603 | 0.05699600 |
| C | -0.47404803 | -2.74148419 | 0.10623201 |
| C | -0.11425501 | -4.06180529 | 0.45904503 |
| H | -0.74773405 | -4.94559135 | 0.45848003 |
| C | -3.69491326 | -0.13873801 | -0.32263802 |
| C | -1.98429014 | -2.46844418 | -2.45260318 |
| H | -3.00140122 | -2.20735216 | -2.78646520 |
| C | -3.29404824 | -3.32957724 | 0.11680901 |
| H | -2.80969420 | -4.30054731 | -0.08403901 |
| C | 1.64013612 | -2.66735919 | 0.65103905 |
| C | -4.43092032 | 0.14061901 | 0.83817806 |
| H | -3.94133928 | 0.07285101 | 1.80845913 |
| C | -1.80525413 | 1.90742314 | 0.44309103 |
| C | -2.16567515 | 2.91720821 | -0.47890803 |
| C | -5.76897342 | 0.52398204 | 0.75807705 |
| H | -6.30553147 | 0.74274405 | 1.68427712 |
| C | 1.24466709 | -4.00801629 | 0.81430006 |
| H | 1.86294414 | -4.84088035 | 1.14174608 |
| C | -4.33433431 | -0.00436300 | -1.56090411 |
| H | -3.77445927 | -0.17318801 | -2.48098718 |
| C | -1.88205714 | 2.21306316 | 1.82870313 |
| B | -1.20590609 | 0.49889804 | -0.00980600 |
| C | -3.41328325 | -3.17247423 | 1.64054512 |
| H | -2.43039517 | -3.15507023 | 2.13154115 |
| H | -3.98394529 | -4.02280229 | 2.04692715 |
| H | -3.95206829 | -2.25229116 | 1.90375714 |
| C | -5.68044641 | 0.37084103 | -1.63307412 |
| H | -6.15285442 | 0.46816003 | -2.61442719 |
| C | 4.49774933 | -2.99510821 | 0.05654800 |

| | | | |
|---|---|---|---|
| H | 4.26746531 | -3.97894528 | 0.50312904 |
| C | -4.66664133 | -3.34798224 | -0.57235104 |
| H | -5.23898738 | -2.43299217 | -0.37199703 |
| H | -5.24488338 | -4.20081630 | -0.18115601 |
| H | -4.59313733 | -3.47456025 | -1.66244312 |
| C | 4.14990430 | 0.96184207 | -1.57660512 |
| H | 3.39692425 | 0.64373005 | -2.30030416 |
| C | -1.42989710 | 1.20527409 | 2.86320421 |
| H | -2.03670015 | 0.28291002 | 2.84997120 |
| H | -1.48170411 | 1.62117712 | 3.88075828 |
| H | -0.39231003 | 0.88827406 | 2.66152219 |
| C | -6.42698945 | 0.64091105 | -0.47920903 |
| C | 4.06822629 | 0.45429503 | -0.26435302 |
| C | 1.03817107 | 1.93168414 | -0.39983303 |
| C | 6.12816544 | 2.29486216 | -1.03523108 |
| C | 5.15289037 | 1.85856813 | -1.94542214 |
| H | 5.17634837 | 2.23202216 | -2.97371621 |
| C | 4.25761230 | -3.07558522 | -1.45823710 |
| H | 3.21733123 | -3.34476924 | -1.69270012 |
| H | 4.91780835 | -3.84052328 | -1.89832913 |
| H | 4.47693832 | -2.11228915 | -1.94250814 |
| C | -0.97611907 | -1.54019411 | -3.14400023 |
| H | -1.16113108 | -0.48104003 | -2.92090021 |
| H | -1.04093307 | -1.68639412 | -4.23436330 |
| H | 0.05354000 | -1.75836213 | -2.82385521 |
| C | -2.61411619 | 4.16596930 | -0.02131600 |
| H | -2.87689021 | 4.93420535 | -0.75588205 |
| C | 3.63838826 | -1.76108213 | 2.66418119 |
| H | 4.65040534 | -1.32441210 | 2.70125119 |
| C | 6.04171942 | 1.79931113 | 0.27477402 |
| H | 6.76492951 | 2.12218815 | 1.02884607 |
| C | -1.71639312 | -3.94354228 | -2.78977320 |
| H | -0.73447805 | -4.26639531 | -2.41147318 |
| H | -1.71383112 | -4.06812229 | -3.88431628 |
| H | -2.48207818 | -4.62249633 | -2.38485317 |
| C | 3.67363726 | -3.14017722 | 3.33864324 |
| H | 3.94337629 | -3.02608122 | 4.40143032 |
| H | 4.41223632 | -3.81841828 | 2.88409921 |
| H | 2.68704519 | -3.62788426 | 3.29798924 |
| C | -2.05708015 | 2.68325819 | -1.96973014 |
| H | -2.01672015 | 3.63462426 | -2.52164918 |
| H | -2.92131521 | 2.11700315 | -2.35618417 |
| H | -1.15038508 | 2.10878015 | -2.21903116 |
| C | 5.03455436 | 0.90940707 | 0.65715205 |
| H | 4.98487936 | 0.58406504 | 1.69775012 |
| C | -2.71873520 | 4.46157932 | 1.34010010 |

| | | | |
|---|---|---|---|
| C | 5.95509141 | -2.63418919 | 0.38309903 |
| H | 6.22481845 | -1.64742812 | -0.02074200 |
| H | 6.62814349 | -3.38003824 | -0.07093801 |
| H | 6.15665545 | -2.62590619 | 1.46496910 |
| C | -2.33891717 | 3.46564925 | 2.25125816 |
| H | -2.38471917 | 3.67760227 | 3.32494524 |
| C | -7.88682158 | 1.06498808 | -0.57183904 |
| H | -8.14993956 | 1.06778308 | -1.64423312 |
| C | 2.66104919 | -0.80787906 | 3.36530124 |
| H | 1.63652012 | -1.21205709 | 3.35031024 |
| H | 2.63212219 | 0.17883001 | 2.88163721 |
| H | 2.96006421 | -0.67514605 | 4.41779732 |
| C | -8.09976356 | 2.49355618 | -0.03948600 |
| H | -9.14839765 | 2.80610820 | -0.17512001 |
| H | -7.45472756 | 3.21577323 | -0.56387204 |
| H | -7.86840055 | 2.55945719 | 1.03673907 |
| C | -8.82288962 | 0.06540400 | 0.13058401 |
| H | -8.62344361 | 0.02101600 | 1.21445409 |
| H | -8.70144963 | -0.95179407 | -0.27512502 |
| H | -9.87670674 | 0.36175003 | -0.00042600 |
| C | -3.18769223 | 5.81414341 | 1.82255713 |
| H | -2.37545517 | 6.36453744 | 2.32872617 |
| H | -4.01278329 | 5.72174239 | 2.54918718 |
| H | -3.54188425 | 6.43903845 | 0.98857007 |
| C | 7.21381353 | 3.27696824 | -1.45595410 |
| H | 7.05026950 | 3.49080525 | -2.52718018 |
| C | 7.10681151 | 4.61334833 | -0.69942705 |
| H | 6.11024142 | 5.06429037 | -0.82767406 |
| H | 7.86037859 | 5.33229239 | -1.06328508 |
| H | 7.27377852 | 4.47509132 | 0.38228403 |
| C | 8.62419965 | 2.67614719 | -1.31743310 |
| H | 8.86015766 | 2.44673018 | -0.26434302 |
| H | 9.38982668 | 3.38142124 | -1.68266812 |
| H | 8.71831461 | 1.74071813 | -1.89205213 |

C H 0
cc-pvdz
****
P N O B 0
aug-cc-pvdz
****
Rh 0
S 10 1.00
2.289320E+02 5.680000E-04
1.990870E+01 -4.680300E-02

1.244680E+01 2.723670E-01
7.778210E+00 -2.301680E-01
4.580060E+00 -5.095540E-01
1.290680E+00 8.098500E-01
5.934140E-01 4.978760E-01
1.491580E-01 3.315400E-02
7.195300E-02 -1.151300E-02
3.175200E-02 4.206000E-03
S 10 1.00
2.289320E+02 -1.860000E-04
1.990870E+01 1.518000E-02
1.244680E+01 -9.113000E-02
7.778210E+00 9.119900E-02
4.580060E+00 1.503790E-01
1.290680E+00 -3.344630E-01
5.934140E-01 -3.074430E-01
1.491580E-01 2.695540E-01
7.195300E-02 6.048640E-01
3.175200E-02 3.070670E-01
S 10 1.00
2.289320E+02 -2.440000E-04
1.990870E+01 7.929000E-03
1.244680E+01 -9.389300E-02
7.778210E+00 7.936000E-03
4.580060E+00 5.418830E-01
1.290680E+00 -1.497488E+00
5.934140E-01 4.948550E-01
1.491580E-01 1.990527E+00
7.195300E-02 -1.226037E+00
3.175200E-02 -5.093060E-01
S 10 1.00
2.289320E+02 -7.250000E-04
1.990870E+01 5.993000E-02
1.244680E+01 -3.549510E-01
7.778210E+00 3.902970E-01
4.580060E+00 5.857430E-01
1.290680E+00 -3.302856E+00
5.934140E-01 3.625717E+00
1.491580E-01 -1.236749E+00
7.195300E-02 -1.007047E+00
3.175200E-02 1.352346E+00
S 1 1.00
3.175200E-02 1.000000E+00
S 1 1.00
1.400000E-02 1.000000E+00
P 9 1.00

2.421170E+01 -1.579000E-03
1.513310E+01 2.719800E-02
6.447200E+00 -1.914630E-01
1.777760E+00 4.476580E-01
8.990200E-01 4.777240E-01
4.445220E-01 2.058190E-01
1.886740E-01 2.435200E-02
7.851400E-02 -5.800000E-05
3.219500E-02 3.330000E-04
P 9 1.00
2.421170E+01 -1.320000E-04
1.513310E+01 -6.532000E-03
6.447200E+00 5.644500E-02
1.777760E+00 -1.610630E-01
8.990200E-01 -1.842580E-01
4.445220E-01 -3.361000E-02
1.886740E-01 3.445440E-01
7.851400E-02 5.595730E-01
3.219500E-02 2.467510E-01
P 9 1.00
2.421170E+01 1.470000E-04
1.513310E+01 -1.335300E-02
6.447200E+00 1.094800E-01
1.777760E+00 -3.362590E-01
8.990200E-01 -3.686360E-01
4.445220E-01 2.138540E-01
1.886740E-01 6.803790E-01
7.851400E-02 3.077610E-01
3.219500E-02 1.258900E-02
P 9 1.00
2.421170E+01 2.304000E-03
1.513310E+01 -2.729700E-02
6.447200E+00 1.976470E-01
1.777760E+00 -8.063470E-01
8.990200E-01 -3.874520E-01
4.445220E-01 1.516827E+00
1.886740E-01 -1.135820E-01
7.851400E-02 -8.286130E-01
3.219500E-02 -2.446000E-02
P 1 1.00
3.219500E-02 1.000000E+00
P 1 1.00
1.320000E-02 1.000000E+00
D 8 1.00
2.949980E+01 1.677000E-03
7.404370E+00 -1.843900E-02

```
   3.059590E+00     1.050760E-01
   1.582050E+00     2.937700E-01
   7.748340E-01     3.641780E-01
   3.630560E-01     2.972650E-01
   1.610470E-01     1.599580E-01
   6.562000E-02     3.867900E-02
D 8 1.00
   2.949980E+01    -1.786000E-03
   7.404370E+00     2.013000E-02
   3.059590E+00    -1.279690E-01
   1.582050E+00    -3.807800E-01
   7.748340E-01    -2.708410E-01
   3.630560E-01     2.651630E-01
   1.610470E-01     5.378200E-01
   6.562000E-02     2.758530E-01
D 8 1.00
   2.949980E+01     3.029000E-03
   7.404370E+00    -3.628200E-02
   3.059590E+00     2.815510E-01
   1.582050E+00     6.384210E-01
   7.748340E-01    -3.871850E-01
   3.630560E-01    -7.962390E-01
   1.610470E-01     3.375180E-01
   6.562000E-02     5.715430E-01
D 1 1.00
   6.562000E-02     1.000000E+00
D 1 1.00
   2.670000E-02     1.000000E+00
F 1 1.00
   1.960600E+00     1.000000E+00
F 1 1.00
   5.553000E-01     1.000000E+00
F 1 1.00
   2.095000E-01     1.000000E+00
G 1 1.00
   1.190700E+00     1.000000E+00
G 1 1.00
   5.001000E-01     1.000000E+00
****

Rh 0
ECP28MDF 4 28
G-Komponente
1
2 1.000000 0.000000
S-G
```

2
2 12.194816 225.312054
2 5.405137 32.441582
P-G
4
2 11.280755 52.872826
2 10.927248 105.745526
2 5.090117 8.619344
2 4.851832 16.973459
D-G
4
2 9.136337 25.108501
2 8.964808 37.695731
2 3.643612 4.202584
2 3.636007 6.292790
F-G
2
2 8.616228 -9.673568
2 8.629435 -12.899847

$NBO bndidx $END

### 7.6. References


**1.** Burger, B. J.; Bercaw, J. E. *Experimental Organometallic Chemistry*; American Chemical Society: Washington, D.C., 1987.

**2.** Marvich, R. H.; Brintzinger, H. H. A Metastable Form of Titanocene. Formation from a Hydride Complex and Reactions with Hydrogen, Nitrogen, and Carbon Monoxide. *J. Am. Chem. Soc.* **1971**, *93*, 2046–2048.

**3.** Pangborn, A. B.; Giardello, M. A.; Grubbs, R. H.; Rosen, R. K.; Timmers, F. J. Safe and Convenient Procedure for Solvent Purification. *Organometallics* **1996**, *15*, 1518–1520.

**4.** Ammann, C.; Meier, P.; Merbach, A. E. A Simple Multinuclear NMR Thermometer. *J. Magn. Reson.* **1982**, *46*, 319–321.

**5.** Sheldrick, G. M. *SHELXT* – Integrated space-group and crystal-structure determination. *Acta Crystallogr. Sect. A* **2015**, *71*, 3–8.

**6.** Sheldrick, G. M. Crystal structure refinement with *SHELXL*. *Acta Crystallogr. Sect. C* **2015**, *71*, 3–8.

**7.** Dolomanov, O. V.; Bourhis, L. J.; Gildea, R. J.; Howard, J. A. K.; Puschmann, H. *OLEX2*: a complete structure solution, refinement and analysis program. *J. Appl. Crystallogr.* **2009**, *42*, 339–341.

**8.** Spek, A. L. Single-crystal structure validation with the program *PLATON*. *J. Appl. Crystallogr.* **2003**, *36*, 7–13.

**9.** Gaussian 16, Revision B.01, Frisch, M. J.; Trucks, G. W.; Schlegel, H. B.; Scuseria, G. E.; Robb, M. A.; Cheeseman, J. R.; Scalmani, G.; Barone, V.; Petersson, G. A.; Nakatsuji, H.; Li, X.; Caricato, M.; Marenich, A. V.; Bloino, J.; Janesko, B. G.; Gomperts, R.; Mennucci, B.; Hratchian, H. P.; Ortiz, J. V.; Izmaylov, A. F.; Sonnenberg, J. L.; Williams-Young, D.; Ding, F.; Lipparini, F.; Egidi, F.; Goings, J.; Peng, B.; Petrone, A.; Henderson, T.; Ranasinghe, D.; Zakrzewski, V. G.; Gao, J.; Rega, N.; Zheng, G.; Liang, W.; Hada, M.; Ehara, M.; Toyota, K.; Fukuda, R.; Hasegawa, J.; Ishida, M.; Nakajima, T.; Honda, Y.; Kitao, O.; Nakai, H.; Vreven, T.; Throssell, K.; Montgomery, J. A., Jr.; Peralta, J. E.; Ogliaro, F.; Bearpark, M. J.; Heyd, J. J.; Brothers, E. N.; Kudin, K. N.; Staroverov, V. N.; Keith, T. A.; Kobayashi, R.; Normand, J.; Raghavachari, K.; Rendell, A. P.; Burant, J. C.; Iyengar, S. S.; Tomasi, J.; Cossi, M.; Millam, J. M.; Klene, M.; Adamo, C.; Cammi, R.; Ochterski, J. W.; Martin, R. L.; Morokuma, K.; Farkas, O.; Foresman, J. B.; Fox, D. J. Gaussian, Inc., Wallingford CT, 2016.

**10.** Becke, A. D. Density-functional thermochemistry. III. The role of exact exchange. *J. Chem. Phys.* **1993**, *98*, 5648–5652.

**11.** Figgen, D.; Peterson, K. A.; Dolg, M.; Stoll, H. Energy-consistent pseudopotentials and correlation consistent basis sets for the 5*d* elements Hf–Pt. *J. Chem. Phys.* **2009**, *130*, 164108–164112.

**12.** GaussView, version 5.0 Gaussian, Inc., Wallingford, CT, 2016.

**13.** NBO, version 6.0. Glendening, E. D.; Badenhoop, J. K.; Reed, A. E.; Carpenter, J. E.; Bohmann, J. A.; Morales, C. M.; Landis, C. R.; Weinhold, F. Theoretical Chemistry Institute, University of Wisconsin, Madison, 2013.

**14.** Foster, J. P.; Weinhold, F. *J. Am. Chem. Soc.* **1980**, *102*, 7211–7218.

**15.** Johnson, K. R. D.; Hannon, M. A.; Ritch, J. S.; Hayes, P. G. Thermally stable rare earth dialkyl complexes supported by a novel bis(phosphinimine)pyrrole ligand. *Dalton Trans.* **2012**, *41*, 7873–7875.

**16.** Blackwell, J. M.; Foster, K. L.; Beck, V. H.; Piers, W. E. $B(C_6F_5)_3$-Catalyzed Silation of Alcohols: A Mild, General Method for Synthesis of Silyl Ethers. *J. Org. Chem.* **1999**, *64*, 4887–4892.

**17.** McCleverty, J. A.; Wilkinson, G. Dichlorotetracarbonyldirhodium. *Inorg. Synth.* **1966**, *8*, 211.

**18.** a) Mellerup, S. K.; Li, C.; Radtke, J.; Wang, X.; Li, Q.-S.; Wang, S. Photochemical Generation of Chiral N,B,X-Heterocycles by Heteroaromatic C−X Bond Scission (X = S, O) and Boron Insertion. *Angew. Chem. Int. Ed.* **2018**, *57*, 9634–9639. b) Samigullin, K.; Bolte, M; Lerner, H.-W.; Wagner, M. Facile Synthesis of (3,5-$(CF_3)_2C_6H_3)_2$BX (X = H, OMe, F, Cl, Br): Reagents for the Introduction of a Strong Boryl Acceptor Unit. *Organometallics* **2014**, *33*, 3564–3569.